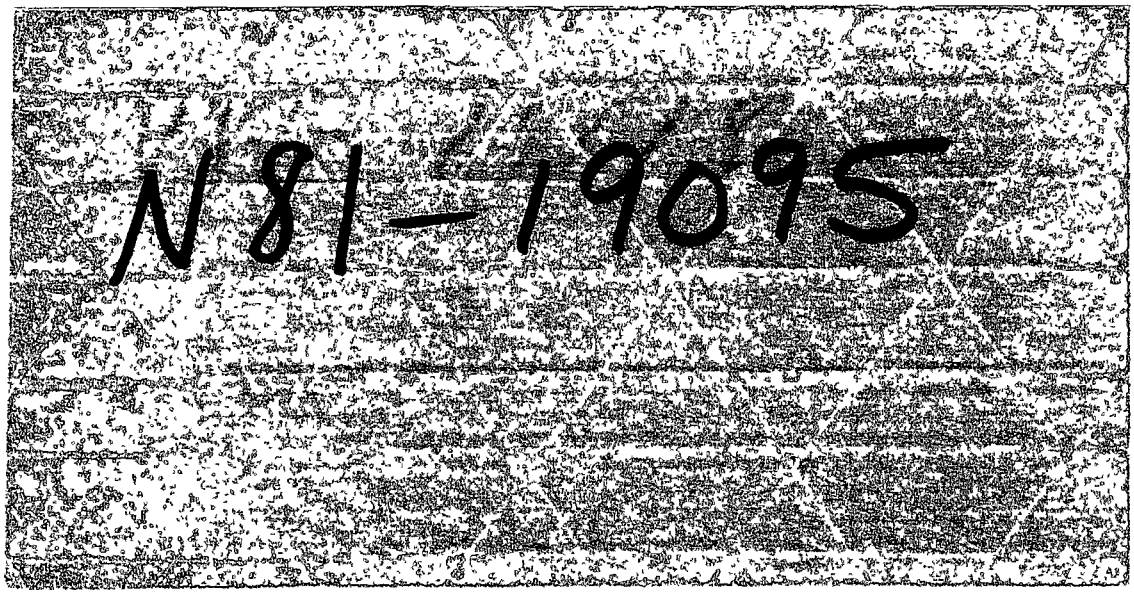

1 Report No	2 Government Accession No	3 Recipient's Catalog No
NASA CR 152 321		

4 Title and Subtitle	5 Report Date
VTOL IN GROUND EFFECT FLOWS FOR CLOSELY SPACED JETS	December 1979 /
	6 Performing Organization Code
7 Author(s)	8 Performing Organization Report No
David Migdal, William G. Hill, Jr. Richard C. Jenkins and Michael T. Siclari	
9 Performing Organization Name and Address	10 Work Unit No
Grumman Aerospace Corporation Bethpage, New York 11714	11 Contract or Grant No NAS 2-10097
12 Sponsoring Agency Name and Address	13 Type of Report and Period Covered Contractor Final Report
National Aeronautics and Space Administration Washington, D.C. 20546	14 Army Project No

15 Supplementary Notes

Final Report. Technical Monitor, David Koenig, Flight Systems Research Division, NASA Ames Research Center, Moffett Field, California

16 Abstract

Results of a series of in-ground-effect twin jet tests are presented along with flow models for closely spaced jets to help predict pressures and upwash forces on simulated aircraft surfaces. The experimental data used to develop the models consist of the effect of jet spacing and height above ground on the ground and upwash pressures, oil flow visualization pictures and the jet induced forces on a series of two and three dimensional bodies.

The isolated twin jet tests revealed unstable fountains (or upwash flow) over a range of spacings and jet heights, regions of below ambient pressure on the ground, and negative pressure differential in the upwash flow field. With the simulated fuselage surfaces placed between the jets, significant positive lift forces in-ground-effect were found to result from the addition of strakes and squaring the fuselage lower contour.

A separate computer code was developed for vertically oriented, incompressible jets which includes a jet impingement zone wall jet transition model. The model more accurately reflects fountain behavior without fully formed wall jets, as in the case of close jet spacing, and adequately predicts ground isobars, upwash dynamic pressure decay and fountain lift force variation with height above ground.

17 Key Words (Suggested by Author(s))		18 Distribution Statement
V/STOL	Wall jet	
In-Ground-Effect	Fountain	
Jet	Recirculation	
Ground Footprint		

19 Security Classif. (of this report)	20 Security Classif. (of this page)	21 No. of Pages	22 Price*
Unclassified	Unclassified		

*For sale by the National Technical Information Service, Springfield, Virginia 22161

NASA - Langley, 1979

CONTENTS

LIST OF ILLUSTRATIONS

LIST OF ILLUSTRATIONS (CONT)

LIST OF ILLUSTRATIONS (CONT)

LIST OF ILLUSTRATIONS (CONT)

VTOL IN GROUND EFFECT FLOWS FOR CLOSELY SPACED JETS

David Migdal, William G. Hill, Jr., Richard C. Jenkins and Michael J. Siclari

Grumman Aerospace Corporation
Bethpage, New York

1. SUMMARY

The primary purpose of this study was to obtain detailed pressure and velocity field data for twin jet configurations in-ground-effect and to develop flow models to aid in predicting pressures and upwash forces on aircraft surfaces. For the basic experiments 50.8 mm (2 in) diameter jets were used, oriented normal to a simulated ground plane, with pressurized air providing a jet velocity up to 90 m/sec. The experimental data consisted of (1) the effect of jet spacing and height, on the ground and upwash pressures (2) oil flow visualization photographs to identify streamline directions (3) the effect of simulated aircraft surfaces on the isolated flow field (4) the effects of adding a third jet on the two-jet upwash properties and (5) the jet induced forces on a series of two and three dimensional bodies with strakes and variations in fuselage cross section.

The isolated twin jet tests revealed regions where the fountain flow was unstable, below ambient pressure regions in the upwash, and the formation of ground stagnation lines (and upwash flow) even when the outer boundaries of the free jets have merged. With the simulated fuselage surfaces placed between the jets significant lift forces were obtained in-ground-effect with the addition of strakes and squaring the lower fuselage contour. Similar effects were not obtained with flat plate models.

A new flow model was developed for vertically oriented twin jets which accounts for the non-fully formed wall jets at close spacing. It includes a jet impingement zone wall jet transition model, the effects of fuselage cross section on fountain induced lift forces, and adequately predicts the effects of spacing and height above ground on flow field pressures and upwash forces.

It is concluded that (1) flow field instabilities can be present at low heights above ground; (2) in a twin jet configuration the onset of jet boundary merging does not

preclude the formation of fountains; (3) values over 20% lift/jet thrust can be obtained in-ground-effect due to fountains impinging on the underside of a simulated fuselage for a twin jet configuration, depending on the shape of the fuselage and dimensions of horizontal strakes and; (4) the use of a modified wall jet transition model adequately predicts the trends with height above ground and jet spacing on the ground and upwash pressures.

2. INTRODUCTION

Lift and control for V/STOL aircraft operating in-ground-effect presents a critical condition in sizing the propulsion system. Ground proximity effects can result in large jet induced lift losses, or produce positive fountain lift, depending on the aeropropulsion configuration. The complexity of the resulting flow field and the sensitivity to many design parameters gives rise to a large body of experimental data (Reference 1) which model various aspects of the flow field. References 2 to 6 describe the development of one technique to predict the pressure distributions and aerodynamic characteristics based on a modular approach to the various flow regions shown in Figure 2-1. The four major subregions consist of a free jet, impingement zone, wall jet and upwash flow. As shown in Figure 2-2, all of these major elements are present in the two jet ground impingement problem and the basic two-jet section can thus be used as a building block for multi-jet configurations.

The simplified modular approach utilizes basic mass, momentum and energy conservation principles along with empirical data describing entrainment of ambient air (e.g. maximum velocity decay and velocity profiles as described in References 2 to 4). A review of the basic experimental data regarding two-jet behavior indicates several limitations when the jet spacing is decreased. As reported in Reference 8, instabilities in the upwash flow were noted for some combinations of spacing and height. Also, as the jets are brought closer an upwash is formed prior to the establishment of a fully developed wall jet. For even closer spacings, the upwash can completely disappear when the two free jets merge as they grow in size due to entrainment of ambient air. The object of this study was to explore in more detail, the two-jet close spacing problems experimentally to help establish a more accurate model of the resulting flow field.

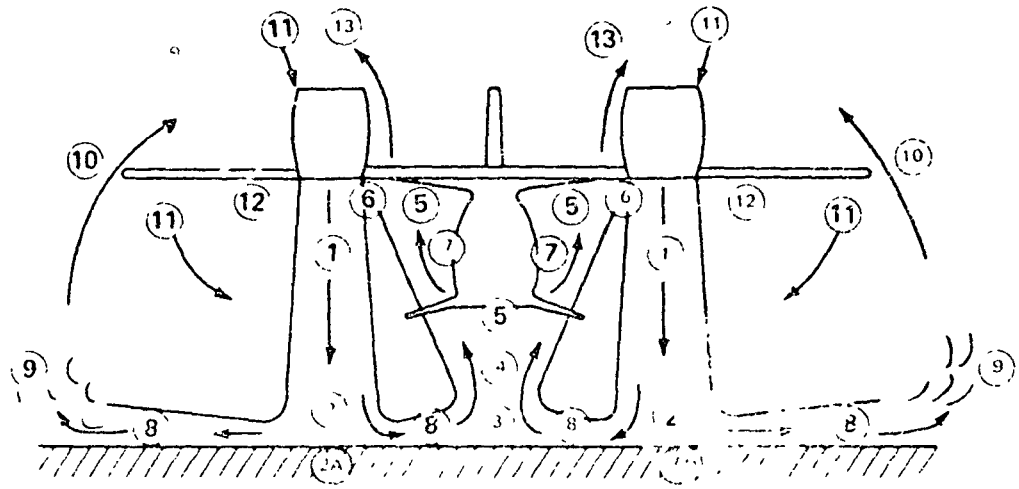

1	Jet Mixing and Mutual Interference
2	Jet Ground Impingement & Spreading
2A	Deck Heating
3	Fountain Formation
4	Fountain Flow and Mixing
5	Fountain Impingement on Aircraft
6	Spreading Fountain Effect on Inlet Jets
7	Fountain Flow Around Aircraft
8	Spreading Ground Jet Aircraft Impingement
9	Outer Stream Flow of Spreading Jet
10	Return Flow of Exhaust
11	Inflow Due to Entrainment and Recirculation
12	Pressures and Forces on Lower Surfaces of Aircraft Due to Inflow
13	Fountain Exhaust Products Sucked Into Inlets

Figure 2-1. Modular elements of modeling concept.

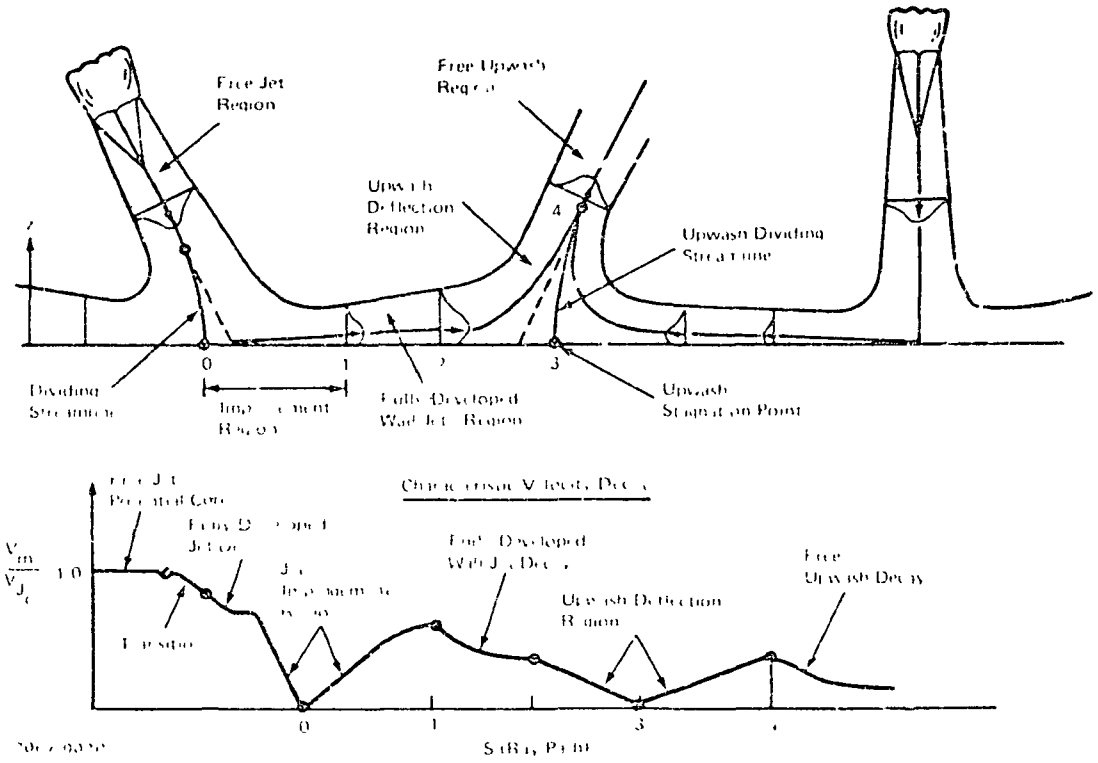

Figure 2-2. - Basic two-jet interaction flow field.

3. SYMBOLS

b	=	Boundary radius
ΔB	=	Body depth from nozzle exit
d, D	=	Nozzle diameter
δ (delta)	=	Boundary layer height
ΔF	=	Interference Force
h, H	=	Jet height above ground
L	=	Body length
M, $\dot{M}$	=	momentum
P_t	=	Total pressure
Δp	=	p - pa
p	=	Static pressure
$\overline{\Delta p}$	=	$\frac{p - pa}{p_o - pa}$
Q, q	=	Dynamic pressure
ρ (rho)	=	Density
r	=	Radius
S	=	Spacing between jet centerlines
σ	=	Strake depth
T	=	Jet thrust
V	=	Velocity
V_J	=	Jet exit velocity
W	=	Body width
W_s	=	Distance between strakes
X	=	Distance perpendicular to line joining jet centers
Y	=	Distance along line joining jet centers
Z	=	Probe height above ground
Z'	=	Distance from jet exit

SUBSCRIPTS

a	=	ambient
cs	=	stagnation line center conditions
g	=	ground plane
j, J	=	jet exit conditions
JH	=	jet half-width
m	=	maximum
n	=	nozzle
PC	=	potential core
s	=	static
0 (zero)	=	initial wall jet radius
.5	=	dimension at 1/2 maximum pressure
.25	=	dimension at 1/4 maximum pressure (1/2 maximum velocity)

4. MODELS AND APPARATUS

The experimental portions of this study were performed in the Grumman Research Department. Two similar air flow facilities were used, one for flow surveys (designated Facility 2) the other for vehicle force and pressure measurements (Facility 1). Sketches and photographs of these two facilities are shown in Figures 4-1 through 4-8. These facilities utilize centrifugal fans which are belt driven by 220 V/3 phase 7-1/2 HP motors. The flow rate and hence total pressure in the settling chamber is controlled by throttling the inlet to the fan. Experiments are usually conducted with a total pressure minus atmospheric pressure of 5004 Pa (20.1 inches of water) resulting in an exit velocity of 91 m/sec (300 ft/sec).

The flow from the fan into the settling chamber is non-uniform with higher velocities towards the outside of the fan (top). This flow is passed through a short constant area section where vanes redirect the flow for a more uniform distribution. The fan is connected to this section with a flexible material to avoid transmission of vibration from the fan to the settling chamber. The air then flows through a diffuser into the large settling chamber. To bring the length of the facility within the available space, large-angle segmented diffusers are used. These diffusers are an extension to the two dimensional work reported by Kline (Ref. 7). The diffuser of Facility 1 is approximately a 33° square pyramid filled for 2/3 of its length with 7° paper cones. The flow at its exit is almost completely attached and uniform.

The diffuser of Facility 2 is a 60° pyramid and filled with pyramidal sections of plexiglass (see Fig. 4-5) of approximately 7° angle. Flow into the settling chamber is then conditioned by honeycomb and screens and passes into the settling chamber. For the pairs of 50.8 mm (2 inch) diameter jets in most of the current experiments, a 610 mm (2 foot) square cross section leads to an area ratio of 92 (Facility 1) while Facility 2 has an area ratio of 20[illegible]. This produces a very uniform flow of low turbulence level (less than 1/2% RMS).

To facilitate changing the nozzle spacing, a pair of nozzles is mounted eccentrically on a pair of discs, which are clamped to the front face (Figure 4-6), providing continuous variation of nozzle spacing. The nozzles are spun aluminum with an entrance contour identical to an ASME long radius flow metering nozzle, but followed by a constant area section 5.5 diameters long. Alignment of nozzles in horizontal direction is done with reference to gravity by drop line and bubble level, and with reference

to other apparatus (traverse equipment primarily) by cross hair sightings. A check on the alignment is performed by traversing the free jets and tracking centerline (maximum q) locations using an electrically powered variable speed traversing mechanism.

Models

The models used for the upwash body impingement experiments include several classes. The initial experiments on the effect of jet spacing were conducted using the two-jet configuration shown in Figure 4-7. Cylindrical fuselage models (Figure 4-8) with a range of corner radii were used for the effect of body shape. These bodies were also instrumented for pressure distributions and were tested for various strake heights, in addition to the basic tests. The strakes are shown on a rectangular body (Figure 4-9) where the nozzles were contained within the planform. A third class of body is a large (12D x 12D) flat plate. Dimensional data for the various bodies are contained in Figure 4-10.

Instrumentation

The coordinate system for locating nozzles and probes is shown in Figure 4-11. The position of the ground plane and of the probes are measured by the voltage output of a 10-turn potentiometer for most data in this report (unless otherwise noted). For measurement of small dimensions, such as the boundary layer thickness, measurements were made with a linear potentiometer or a vernier caliper. For the traverse units, with screw thread drive or rack and pinion drive, (all probe movements and the ground plane motion on Facility 1) a rotary pot is used to measure cable motion connected to the moving apparatus. For the ground plane of Facility 2, a rotary pot was attached to a sprocket at one end of the chain loop. Since some hysteresis occurs for any of these systems, traverses were taken only in one direction, and a voltmeter was used to check an initial output at a starting location and periodically to check calibration.

The purpose of providing an electrical output for position is to produce a contiguous curve of the parameter being measured (vehicle forces, pressures, hot wire velocities, etc.) versus position, and to plot that curve on an X-Y Recorder. A real-time analog data reduction technique was used to protect against missing unusual behavior of the data or the development of problems during a test.

Pressures were measured with differential pressure transducers. For the pitot-static probe, the total and static pressure tubes were each connected to separate transducer referenced to the atmosphere (an undisturbed area of the room). Each of these pressure tubes also contained a "T", and a third transducer was connected to both pressures, thereby directly reading $P_t - P_s$ or q (another analog data reduction technique). The pressure transducers were calibrated and periodically checked by use of an oil manometer; vertical or inclined, depending on the transducer range.

Vehicle force measurements were made using a five-component strain gage balance, while force measurement on the ground plane utilized three separate force elements, spaced at a distance from the force center. Calibration of the force balance was achieved by placing weights from a laboratory scale, set on a special graduated body, and spot checks were done periodically on the model being tested.

During efforts to identify the cause of the measured large negative static pressure differentials, velocities were measured with a hot film system. This system is essentially the same as a hot wire system; our measurements involved a constant temperature anemometer, a signal linearizer, and a true RMS time-averaging voltmeter. Output from the traverses was plotted on the X-Y recorder.

Oil flows were used for both ground plane indications of the end of upwash formation with increasing jet interference and for qualitative flow description with a splitter plate. The oil base was 10W-30 motor oil and it was colored for identification and thickened by artist oil colors.

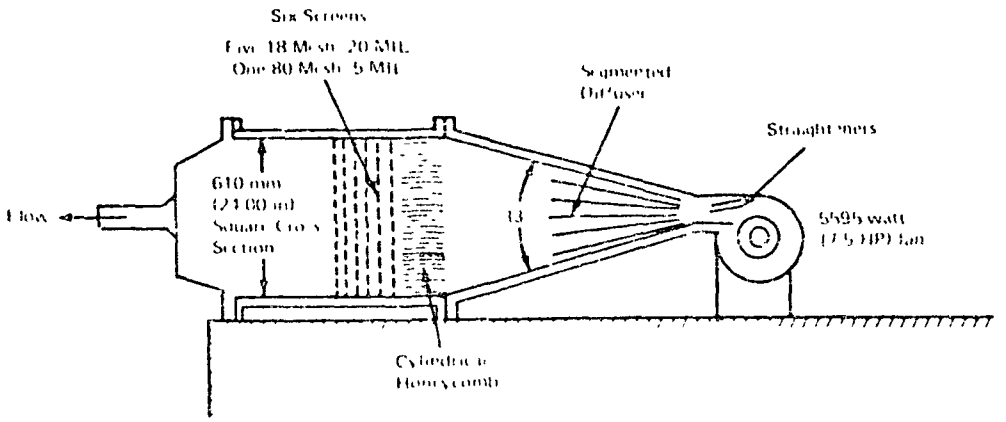

9067-003-P

Figure 1-1. - Facility 1 flow path.

Figure 1-2. Photograph of facility 1.

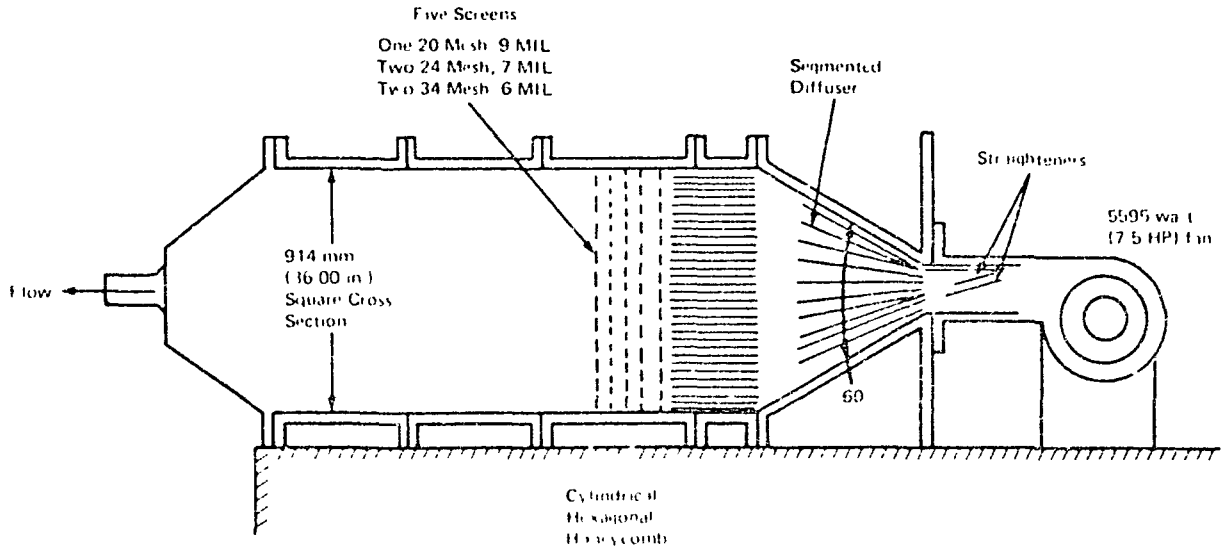

Figure 1-3. - Facility 2 flow path.

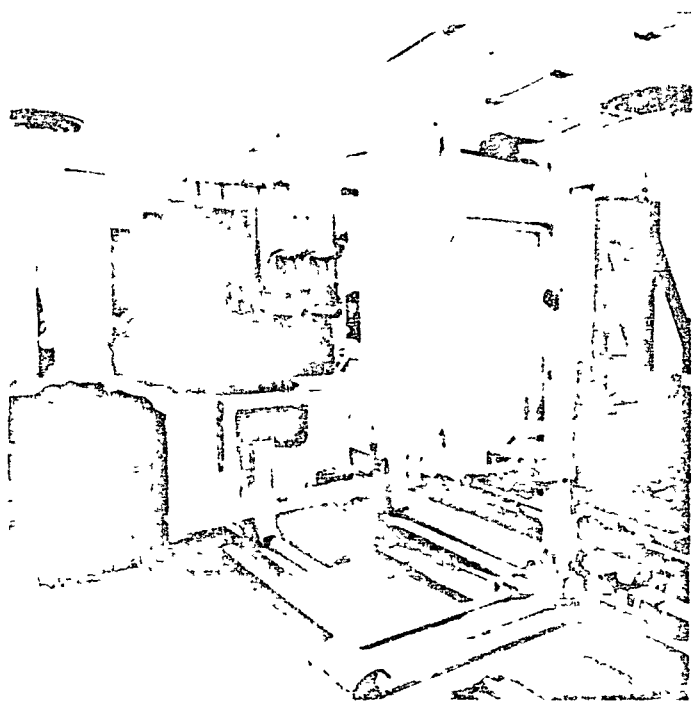

Figure 1-4 Photograph of facility 2.

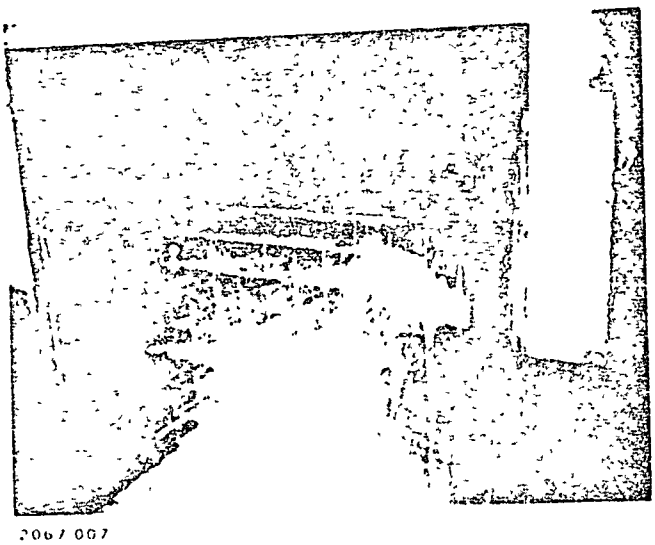

2067 007

Figure 1-5. Segmented diffuser.

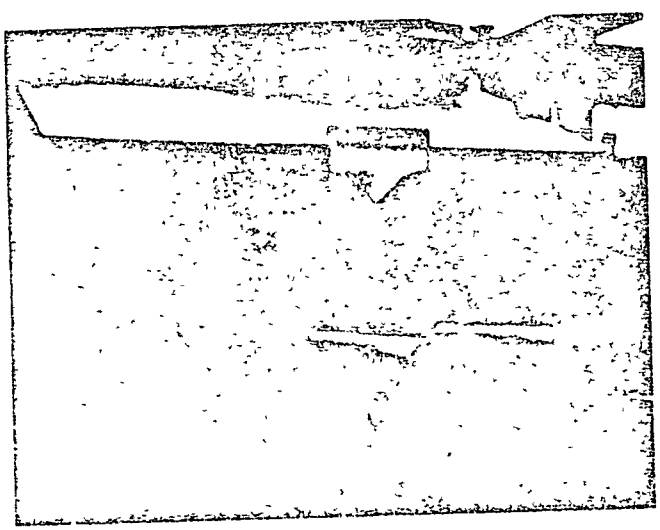

2067 008

Figure 1-6. Eccentric nozzle mounting.

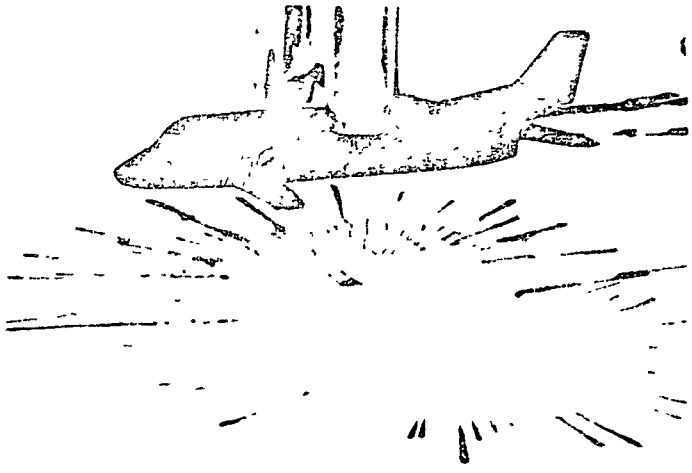

2067 009

Figure 4-7. Two-jet aircraft configuration (Ref. 5 & 6).

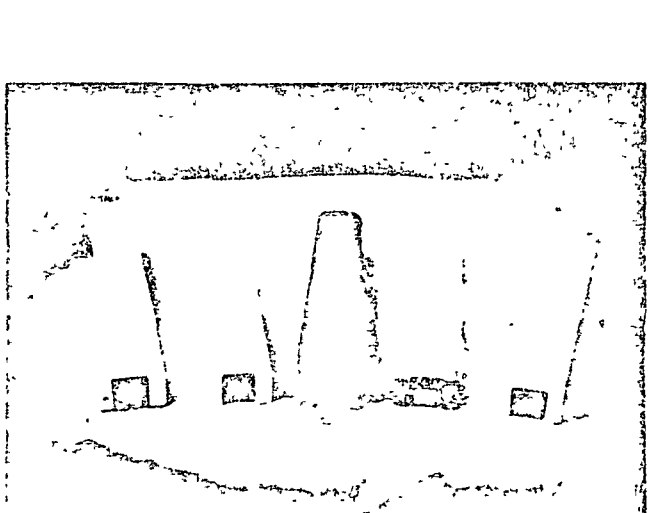

Figure 4-8. Cylindrical bodies with different corner radii.

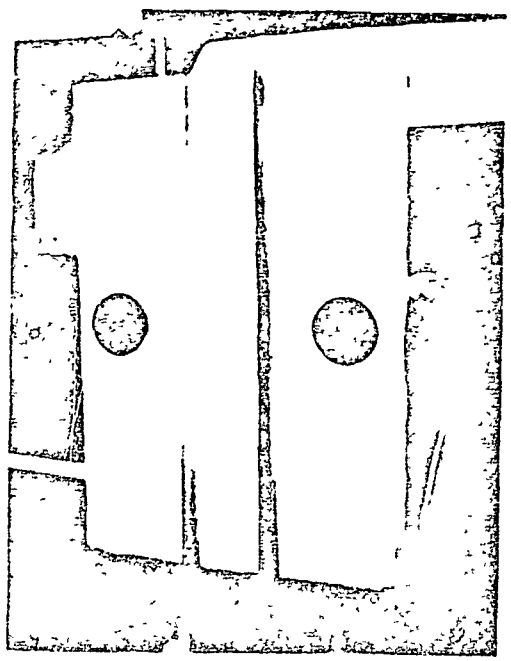

Figure 1-9. Rectangular body with strakes.

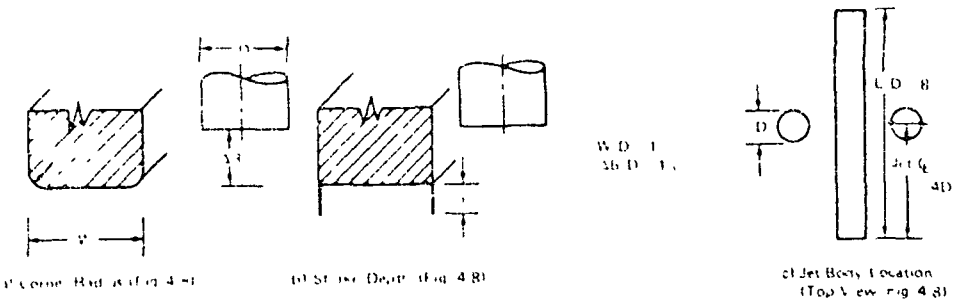

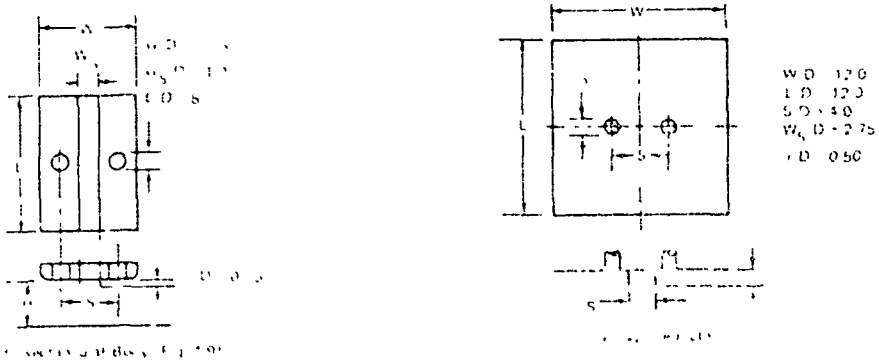

Figure 1-10. - Dimensional data and nomenclature for bodies placed in upwash flow field.

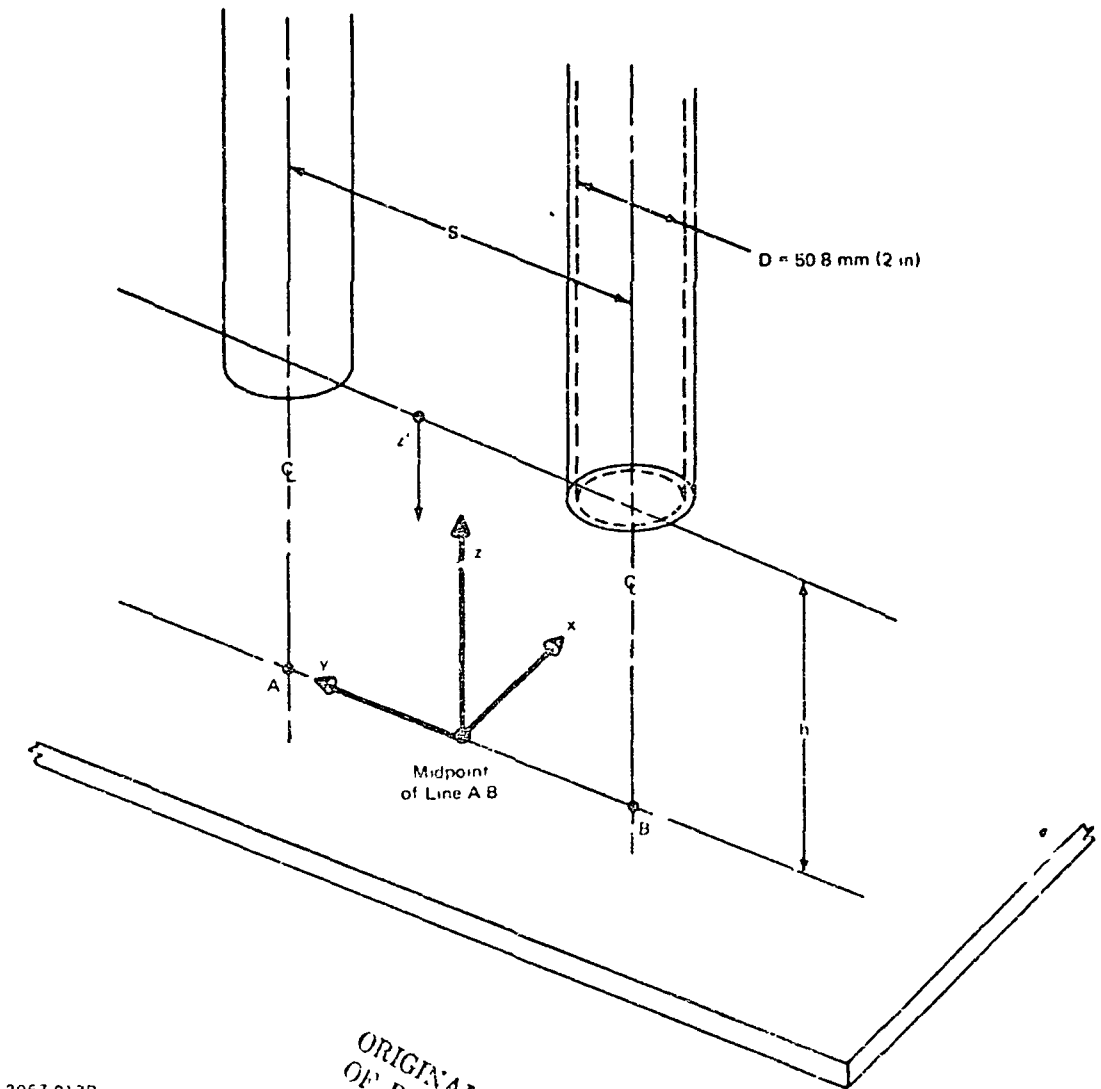

Figure 4-11. - Model coordinates and nomenclature.

5. JET PROPERTIES

Figures 5-1 and 5-2 contain the results of traversing the jet plumes with pitot pressure probes at various distances (Z') downstream of the nozzle exit plane, in the absence of a ground plane. The characteristics of the initial jet can be inferred from the data very close to the nozzle exit ($Z'/D = 1/16$). As shown in Figures 5-1 and 5-2, a relatively uniform (top hat) profile is available at the jet exit with the eccentric jet spacing mechanism and tapered settling chamber. The Figure 5-1 data indicates that for $S/D = 2$ the jets start to merge 4 diameters from the nozzle exit and that the merging is nearly complete at 20 diameters. Merging is considered to be complete when there are no distinct peaks in the profiles. These peaks distinguish the central region for each free jet. Thus while the jet outer boundaries spread at an equivalent angle B [$\tan B = (S/D - 1)/(2Z'/D)$], and for $S/D = 2$, $Z'/D = 4$, B is approximately 7°, the inner core region for each jet persists for a considerable distance downstream.

Static Pressure Inside Nozzle Near Exit

Static Pressures were measured inside of a nozzle at $Z'/D = -1/16$ (upstream of the exit) to investigate the effect of the upwash on nozzle exit conditions. Two pressure taps were used, located on opposite sides of the nozzle. The static pressure differential was less than 2% q_J for all cases.

Figure 5-3(a) shows the variation of nozzle exit pressure as the ground plane height was changed. The smooth curve shows the variation with ground height for single jet impingement, illustrating the influence of ground blockage when $h/d \leq 1.5$. The other two curves for dual jet impingement show that the effect of the presence of the ground plane on the nozzle exit flow are noticeable for $h/d < 4.5$ Data taken on the inner (towards the upwash) side of the nozzle illustrates an increasing pressure as the ground plane gets closer, which appears to be caused by interference between the incident flow and the upwash. The pressure rise with decreasing h/d is much less for slightly larger spacing (Figure 5-3(b)) and disappears for wide spacing (Figure 5-3(c

For a given nozzle spacing, decreasing h/d will decrease interference between upwash and incident flow, and at some value of h/d such interference should

disappear. Static pressure surveys showed that, in the absence of interference between upwash and incident flow, the static pressure on the upwash (inner) side of the nozzle should be slightly more negative than on the opposite side. Figure 5-3(a) shows that the inner tap pressure drops below outer tap pressure when h/d = 1.75, which should represent the ground height below which no interference between upwash and incident flow exists. Figures 5-3(b) and (c) show this value of h/d to be 3 for S/d = 3, and 4 for S/d = 5, 6.

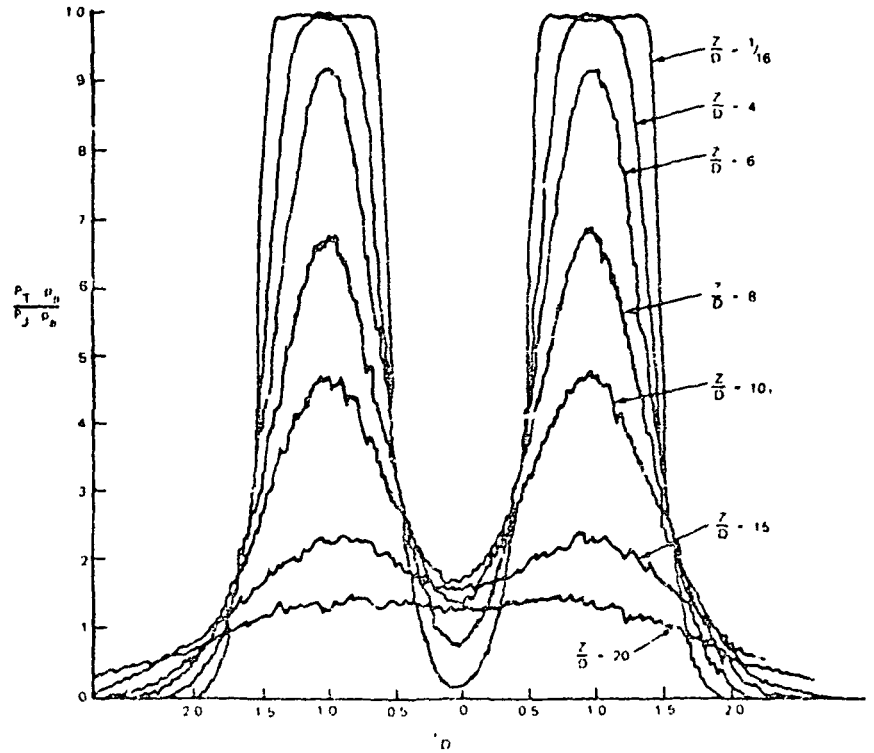

2067 014P

Figure 5-1. - Free jet profiles - S/D = 2.0.

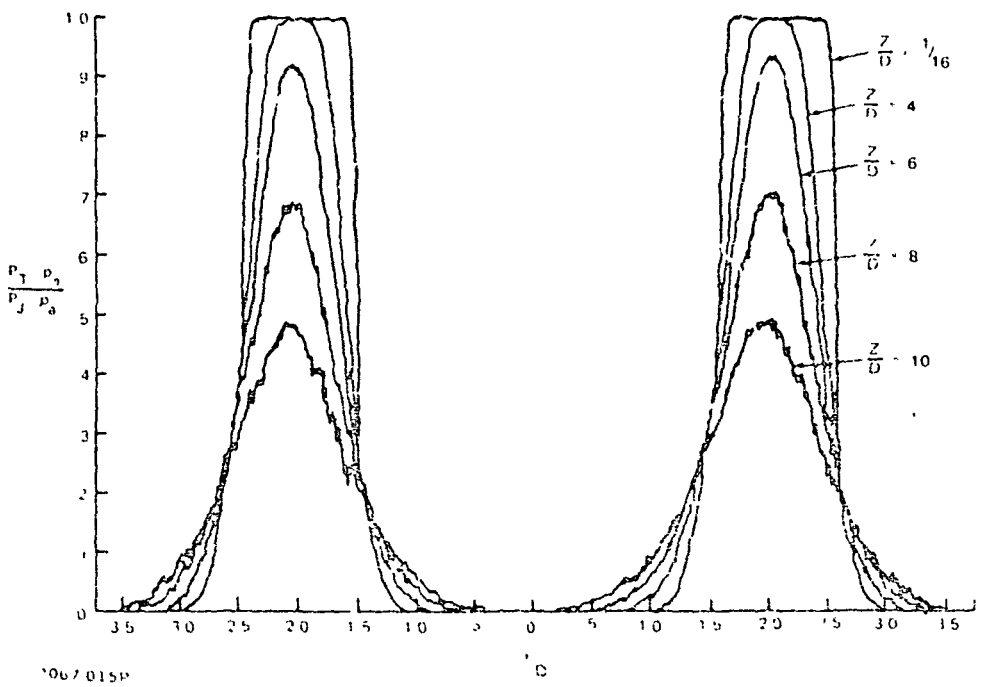

2067 015P

Figure 5-2. - Free-jet profiles - S/D = 1.

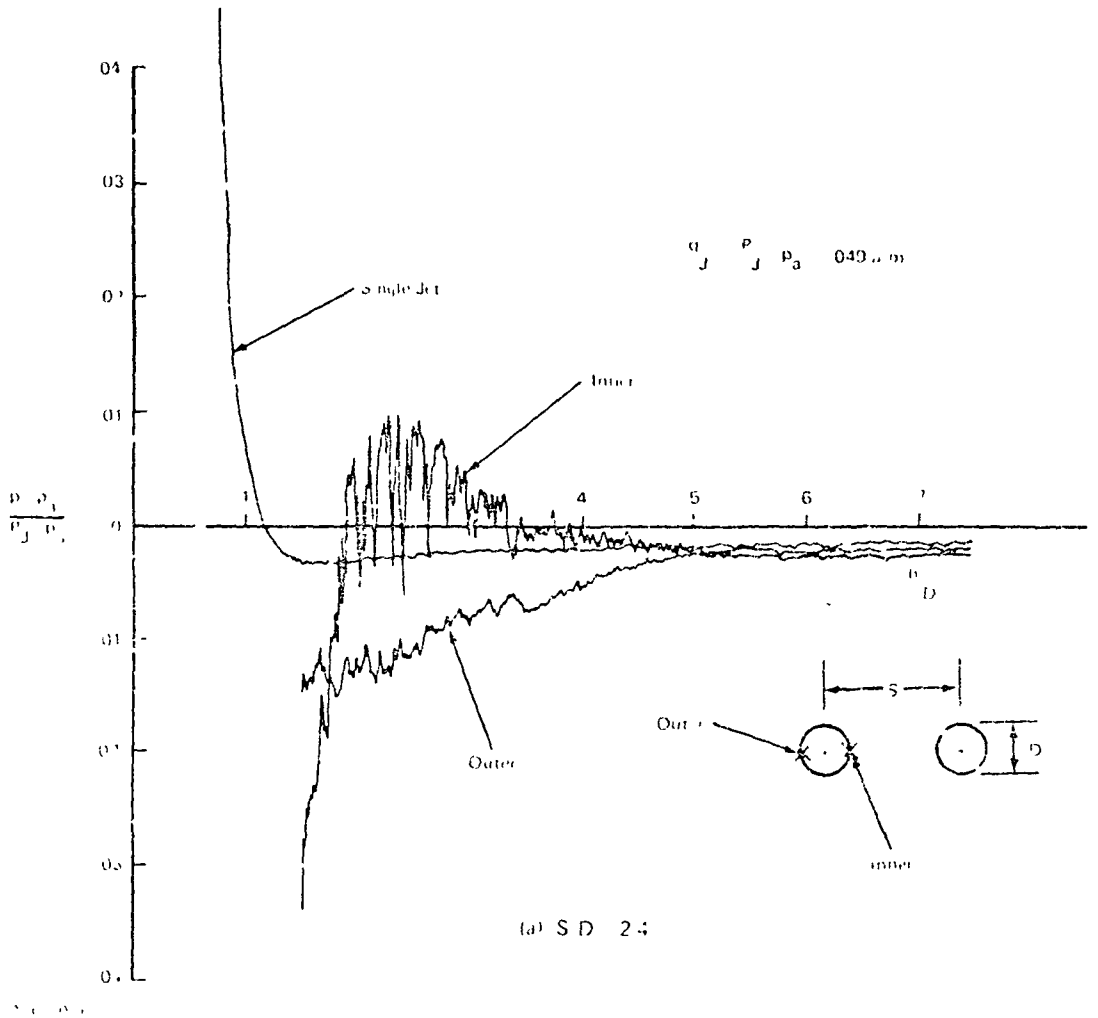

Figure 5-3. - Effect of ground plane on nozzle exit pressures.

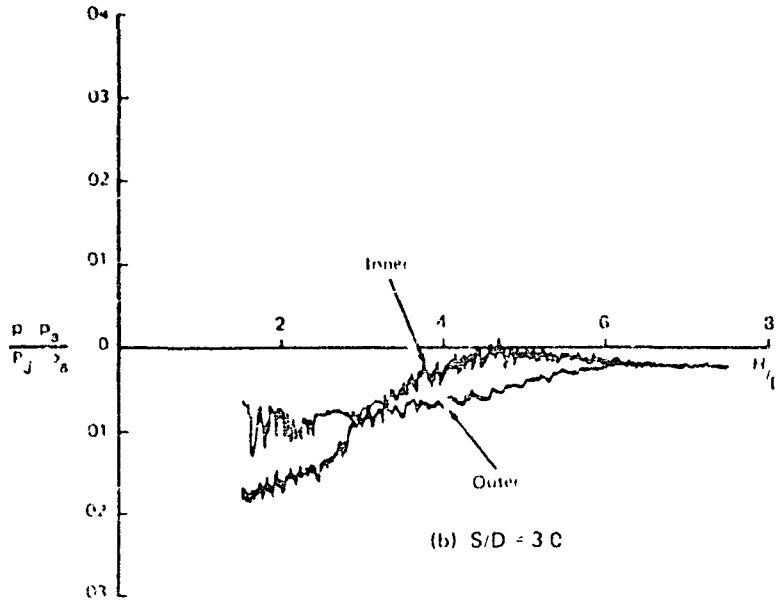

(b) S/D = 3.0

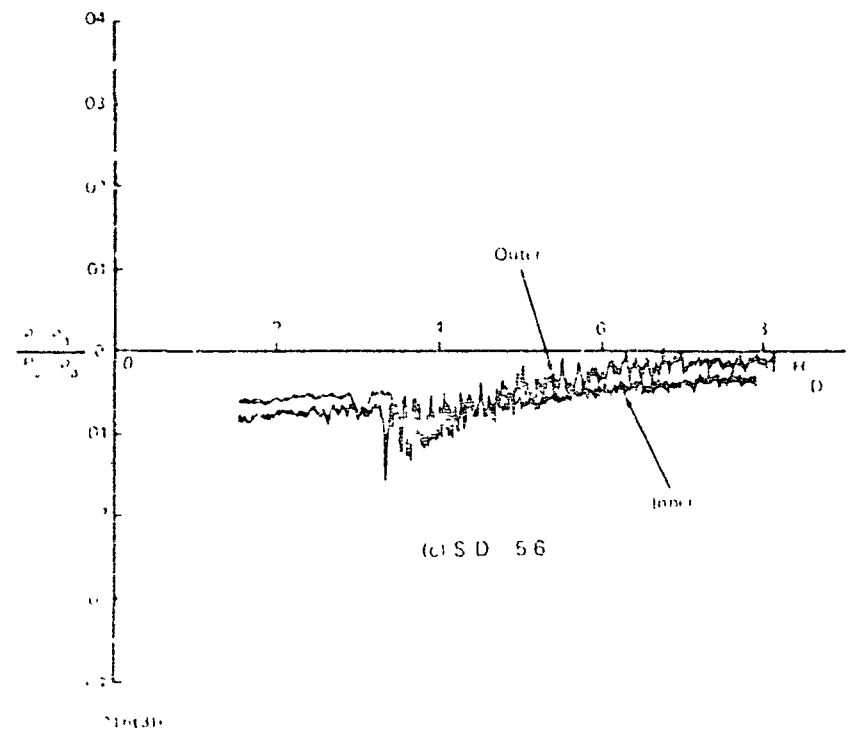

(c) S/D = 5.6

Figure 5-3. - Concluded.

6. GROUND PLANE PROPERTIES

The upwash formation region on the ground was investigated with oil flow patterns to aid in the identification of conditions where the upwash would no longer form because of jet/upwash interference. Several concentric rings of oil dots were placed around each jet impingement point and the flow was allowed to run for several minutes to develop a stable pattern. Figure 6-1(a) shows a typical radial flow from the jet impingement points meeting to form a straight stagnation line. For many cases, a double line was found. Further study showed this to be caused by a separation point. Oil drops placed within this bubble ran outwards along the outer line and towards the two oil lines (Figure 6-1(b)). Insufficient data exists at this time to determine the flow conditions that govern the formation of this separation bubble.

Figure 6-1 shows a series of oil flows for a spacing of S/D = 2.0 (closest available from eccentric nozzles). Starting at a height above ground of H/D = 1.5, a pattern of two separate radial spreading regions with a central stagnation region occurs until an H/D of about 20. This is generally above the region of interest for affecting airplane interference effects. Note that the separation region disappears at about H/d = 10 (Figure 6-1(d).

Stream surveys without the ground plane, taken by traversing a pitot probe across both jet centerlines, showed that the two jets had partially merged 10 diameters from the exit. Ground plane pressure profiles at H/D = 10 indicated a pressure rise corresponding to the stagnation line.

For H/D = 15, where the free stream survey showed two peaks, the ground oil flow pattern showed two distinct jet impingement points and a stagnation line also. At H/D = 20, where the free stream pitot survey showed no distinct peaks, the ground oil pattern also indicated that the two jets had merged.

It therefore seems reasonable to use the rule of thumb that: if separate peaks exist in the pitot pressure profiles of the free jets without a ground plane, separate impingement and stagnation line/upwash formation will occur on the ground plane.

Ground Plane Pressures

Ground pressures were obtained with a line of pressure taps perpendicular to the line connecting the jets and spaced one-half a jet diameter apart (along the x axis of Figures 4-11 and 6-2). The ground plane was moved slowly in a direction perpendicular to the line of taps and to the nozzle axis producing a continuous display of ground pressures. The ground coordinates x and y are oriented parallel to and perpendicular to the stagnation line, with the origin at the upwash center. Figure 6-3 contains a complete set of ground pressure data obtained with various jet spacings and heights above ground. Figure 6-3(a) contains the ground pressures for both the single and dual jets at S/D = 2, h/D = 3 and demonstrates that an upwash is formed (peak pressure at Y/D = 0) prior to the end of the impingement zone. The data implies an inboard shift of pressure peak and a distortion from axial symmetry when the second jet is turned on.

Figure 6-3(b) contains a complete data set for the closest spacing (S/D = 2) and varying nozzle height above ground. The general trend is that the peak values under the jet and at the stagnation point (Y/D = 0) decreases with increasing h/D while the profile broadens. Note that under the jet (Y/D = 1, Figure 6-3(b)) the impingement pressure is within 2% of the jet stagnation pressure for values of h/D up to 1. As h/D increases the jet impingement pressure decays in a manner similar to the free jet decay in maximum pressure (Figure 5-1). In general, the maximum wall pressure is higher than the corresponding value for the free jet at the same distance from the nozzle exit. Figure 6-3(c) contains the ground plane pressures for S/D = 2.5 and a range of nozzle h/D from 1.5 to 15. In this, as well as other cases to follow, sufficient data is provided to determine the maximum pressure on the center of the stagnation line P_{cs} (Figure 6-2). Note that P_{cs} increases with decreasing h/D until an h/D of 3.0. The data in Figure 6-3(a) is similar in that the value of P_{cs} does not continually increase with decreasing h/D. In addition at h/D = 2 (Figure 6-3(d)) it was not possible to obtain a stable profile and two peak values were exhibited. This instability was not observed at other spacings. At S/D = 3 and h/D = 1.5 to 2.0 the upwash would change from one side to the other with no apparent disturbance up to about 20 seconds. It could be switched from one side to the other with a temporary blockage near the nozzle exit plane.

This unstable behaviour at S/D = 3.0 is shown in Figure 6-3(d) with the actual pressure trace at h/D = 2.0. The large oscillations help to explain why in this case there is a drop in the maximum stagnation line pressure. Since the probe is reading a time-averaged value, and for a portion of the time there is not jet flow over the probe, the time-averaged value is lower.

Figures 6-3(e), (f) and (g) show the ground pressure variation with increased spacing. Note that as the spacing is increased (e.g., Figure 6-3(f) for S/D = 4.0) there is less effect of the fountain upwash (at Y/D = 0) on the impingement zone pressure distribution.

Summary Data of Maximum Ground Pressures

Figure 6-2 illustrates the ground pressure profile along a line passing through the two jet impact points and the center line of the upwash. The maximum pressure in the jet impingement region was always greater than the maximum pressure on the center of the stagnation line (P_{Cs}). The dimension $y_{.5}$ represents the half width of the pressure profile at half the maximum stagnation line pressure. Along the stagnation line the maximum ground pressure (P_m) decreases with distance (x) from the centerline.

Figure 6-4 shows the variation of centerline stagnation pressure with nozzle spacing for a nozzle height of three diameters above ground. The curve shown for comparison was predicted by assuming that the ground pressure on the center of the stagnation line is equal to the maximum pressure that would exist in a wall jet profile at the same radial location from one of the jets if the opposite jet were turned off. The predicted curve is given by the relation

$$\frac{P_{CS} - P_a}{P_j - P_a} = 13.78(S/D)^{-2.4} \qquad (1)$$

where P_j is the stagnation pressure at the nozzle exit and P_a is ambient pressure. The constants in this equation were derived from pitot probe measurements taken in the wall jet formed by impingement of a single 4 inch diameter jet. Figure 6-4 shows that this analysis provides an adequate prediction of the centerline ground pressure for jet spacings of about 4 diameters or greater. At closer nozzle spacings the measured values fall below the predicted curve. This deviation should be expected because

at S/D = 4 the stagnation line is two diameters from each jet impingement point, and this radial distance from a single impinging jet represents the beginning of the fully formed wall jet region. Hence the measured and predicted values begin to diverge, because at close jet spacings the ground flow approaching the stagnation line is not a fully formed wall jet. A modified wall jet analysis is needed to provide a better match.

For a given nozzle spacing, the ground pressure on the center of the stagnation line ($P_{cs} - P_a$) varied with nozzle height above ground as shown in Figure 6-5. For a nozzle spacing of 6 diameters above ground, increasing nozzle height above ground brought about a gradual decrease in ($P_{cs} - P_a$) that appears to be caused by interference between the edges of the upwash and the shear layers surrounding the incident jets close to the nozzle exit plane. At closer nozzle spacings, this variation of ($P_{cs} - P_a$) with height above ground was more extreme but followed the same trend. For nozzle spacings below 3 diameters, the effects of incident jet-upwash interference severely distorted the entire ground plane pressure profile at large H/D (see Figure 6-3(d)).

For each nozzle spacing the maximum value of ($P_{cs} - P_a$) occurred with H/D between 2 and 4. The decrease in ($P_{cs} - P_a$) at lower nozzle height appears to indicate the onset of instability conditions and may be caused by the presence of the ground affecting nozzle exit conditions. A severe instability was encountered at a nozzle spacing of 3 diameters for H/D less than 2-1/2. The ground pressure profile appeared to be temporarily stable in either of two unsymmetric shapes. This instability appeared to be peculiar to jet spacing of 3 diameters. For larger or smaller jet spacing, the ground plane pressure profile did not exhibit this bistable shape for nozzle heights down to 1-1/2 diameters.

The variation of maximum ground plane pressure ($P_m - P_a$) along the stagnation line is shown in Figure 6-6. Data taken at H/D = 3 at each jet spacing have been normalized by the corresponding centerline value and plotted versus X/D to illustrate the variation of this profile with jet spacing. When plotted versus X/S (Figure 6-7) the data for each nozzle spacing fall close to a profile which can be fitted by:

$$\frac{P_m - P_a}{P_{CS} - P_a} = \left[1 + \left(\frac{2X}{S}\right)^2\right]^{-2.2} \qquad (2)$$

Eq. (2) was derived by assuming that on the stagnation line only the components of wall jet velocity normal to the stagnation line contribute to the stagnation line pressure. The constants in Eq. (2) were obtained from wall jet measurements with a single impinging jet.

Figure 6-8 shows the shape of the ground pressure profiles taken across the center of the stagnation line for three nozzle heights above ground with a nozzle spacing of 4 diameters. For each ground height the pressures were normalized by the maximum value on the centerline and the distance y was normalized by the half-pressure dimension ($y_{.5}$). The data show that the profile shapes are essentially the same and can be represented by a Gaussian profile.

Integration of the ground pressure profile across the stagnation line provides a measure of the force exerted on the ground by the upwash, which can be related to the momentum flux of the upwash at ground level. Assume that the ground flow approaching the stagnation line from each of the impinging jets is an axisymmetric, radially expanding flow that exhibits constant momentum per radian in the wall jet. If flow momentum is conserved in the upwash formation region, the momentum flux per radian of the upwash flow normal to the ground at the stagnation line can be found by integrating the stagnation line pressure profile. Using a Gaussian equation to represent this profile, integration yields

$$\dot{M}_{\theta} = S/2 \sqrt{\frac{\pi}{0.6932}} (P_{CS} - P_a) y_{.5} \times \left[1 - \frac{y_{.5}}{S/2} \left(\frac{1}{\sqrt{.6932\pi}}\right)\right] \qquad (3)$$

Figure 6-9 shows the variation of maximum stagnation line pressure and half pressure width with nozzle height for S/D = 4. The maximum ground pressure decreases and the width increases as the ground height increases. This general trend appeared for all jet spacings. However, as seen in Figure 6-10, the centerline upwash momentum flux per radian computed from Eq. (3) using the data in Figure 6-9 is almost independent of nozzle height above ground. This result is important because it confirms one of the simplifying assumptions used in the prediction techniques.

The dashed line in Figure 6-10 represents twice the thrust per radian of one of the incident jets. Jet thrust was computed from velocity profiles that were taken at

the nozzle exit plane. We conclude that flow momentum is conserved in the upwash formation region, and that the upwash momentum at ground level can be computed from the nozzle exit conditions.

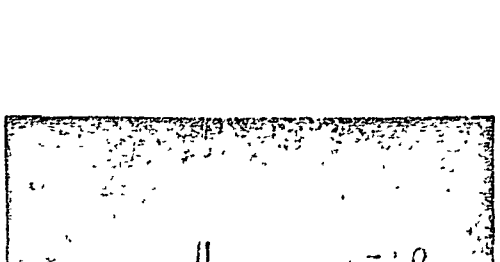

(a) H/D = 1.5

(b) H/D = 2.0

(c) H/D = 5.0

(d) H/D = 10

9067 017

Figure 6-1. Ground plane oil flow, S/D = 2.0.

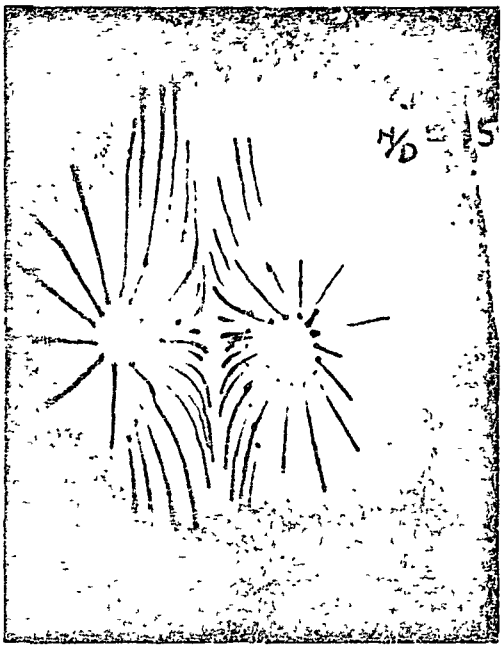

(e) H/D 15

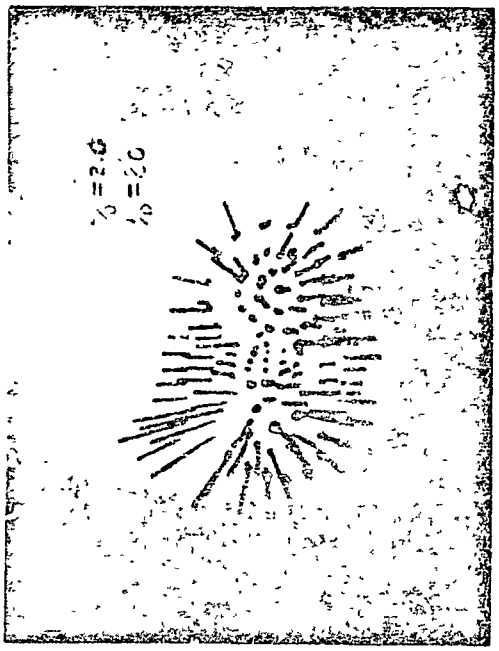

(f) H/D 20

Figure 6-1. Concluded.

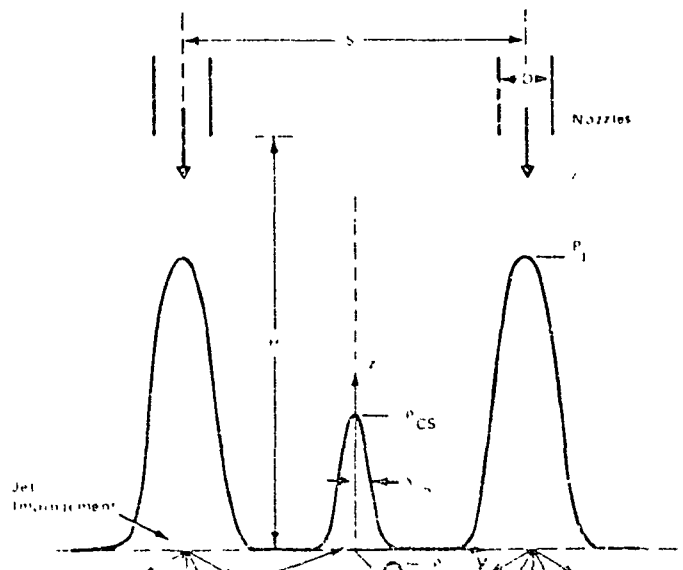

Figure 6-2. - Details of ground plane impingement and upwash.

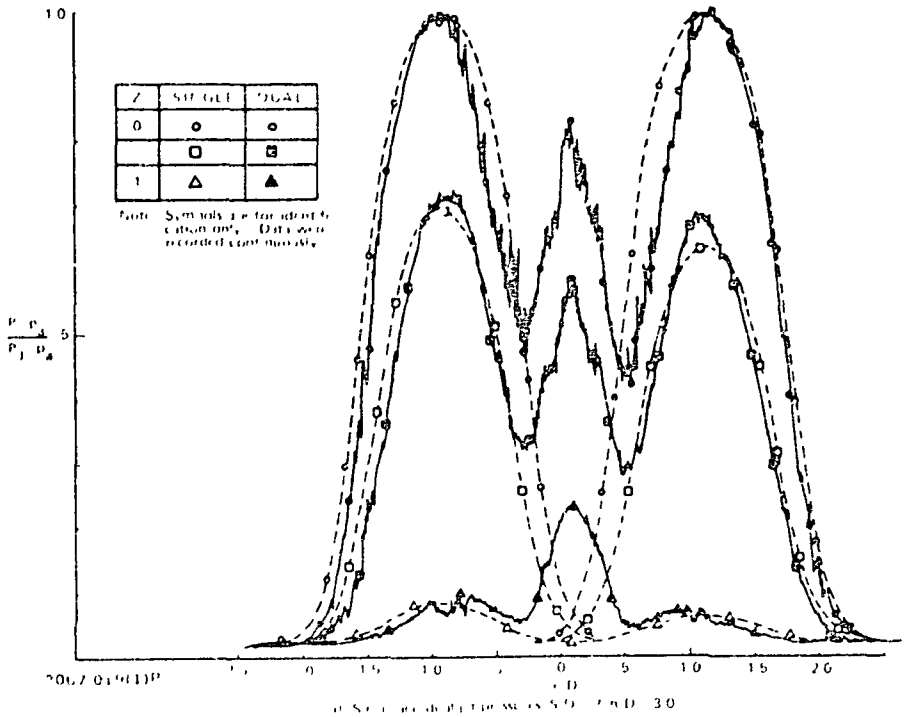

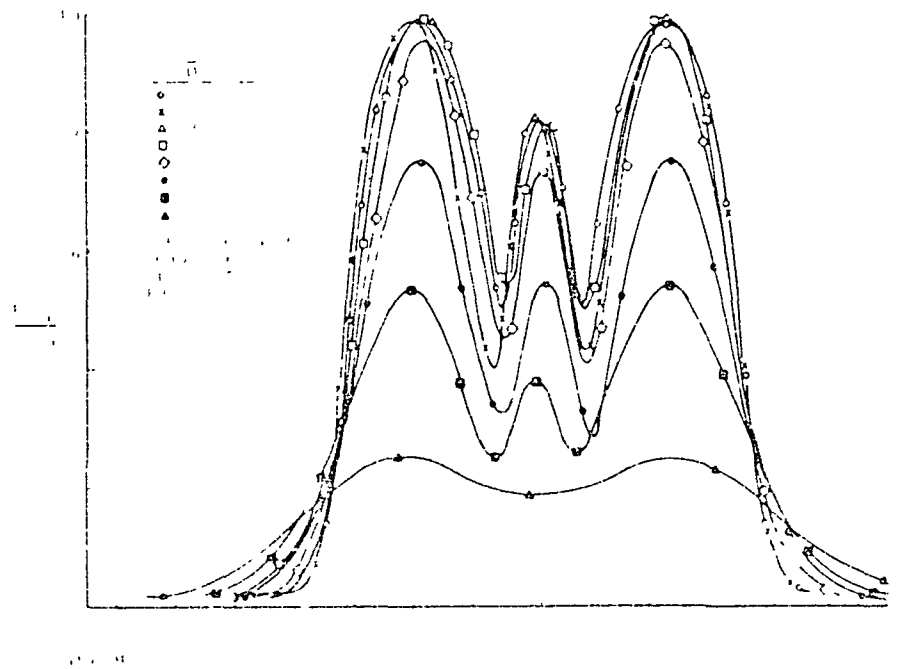

Figure 6-3. - Ground plane pressures.

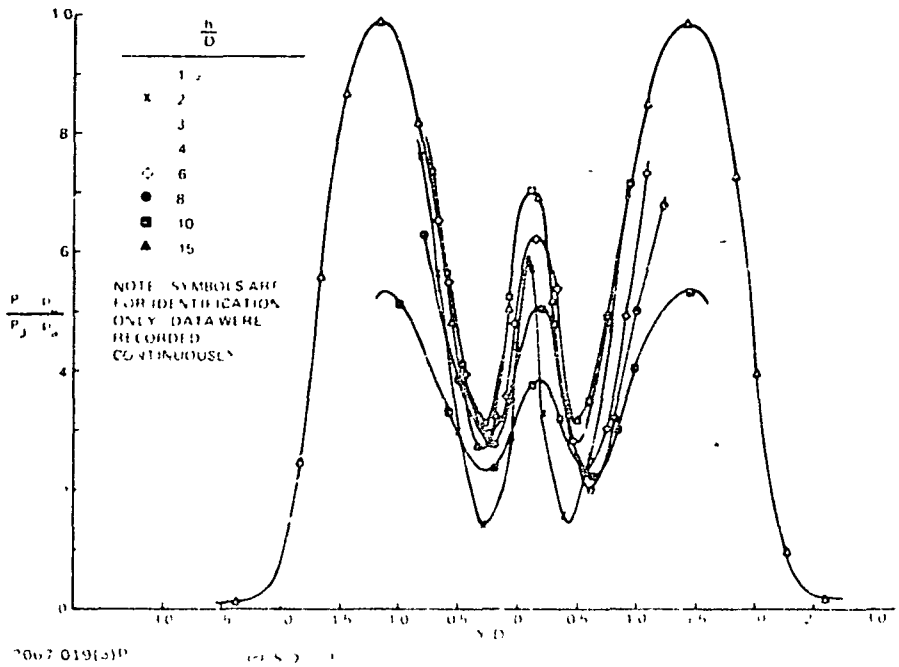

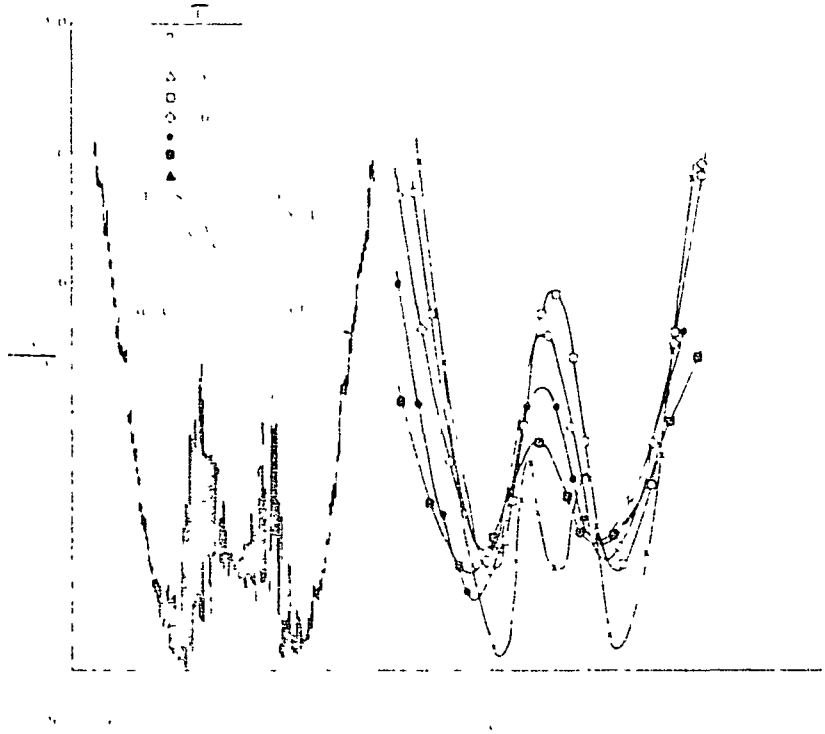

Figure 6-3. - Continued.

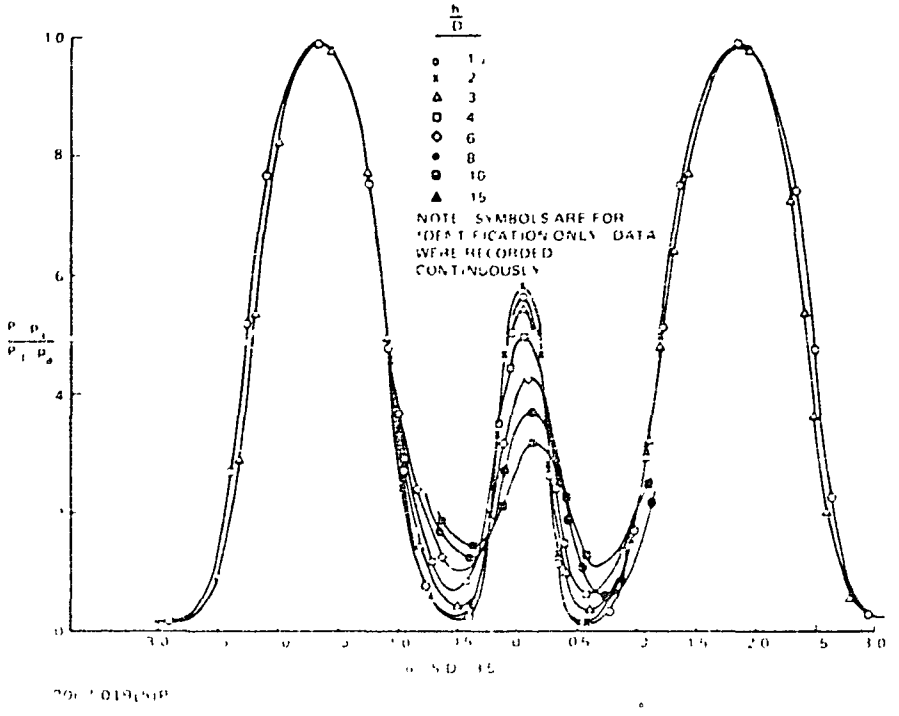

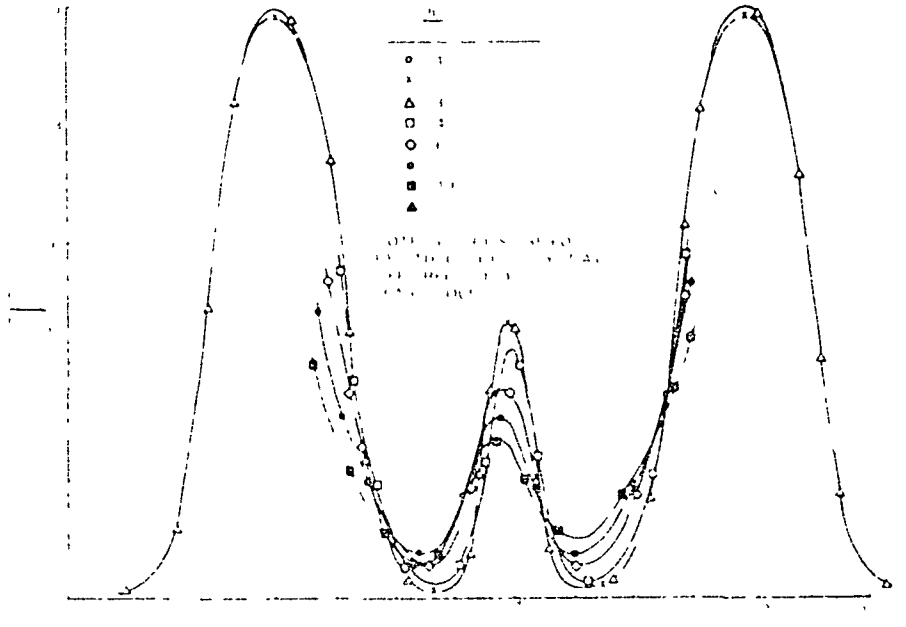

Figure 6-3. - Continued.

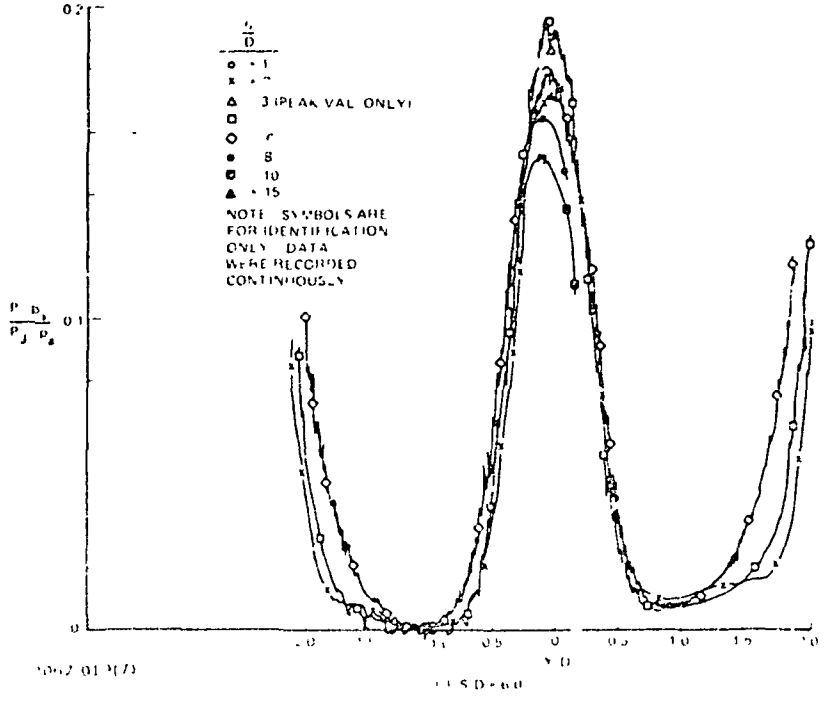

Figure 6-3. - Concluded.

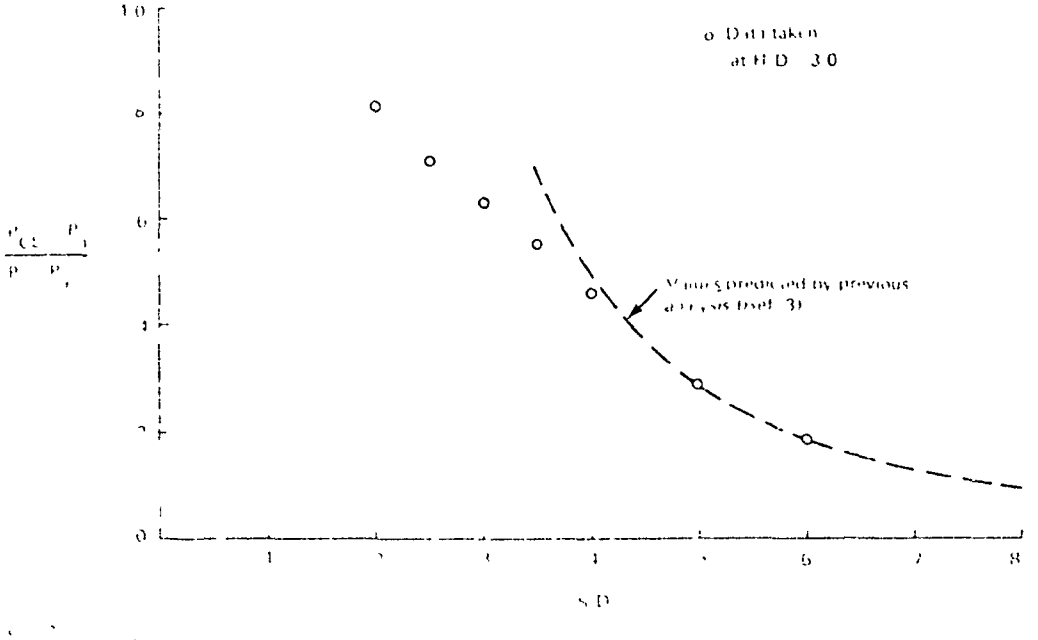

Figure 6-4. - Effect of jet spacing on maximum stagnation line ground pressure.

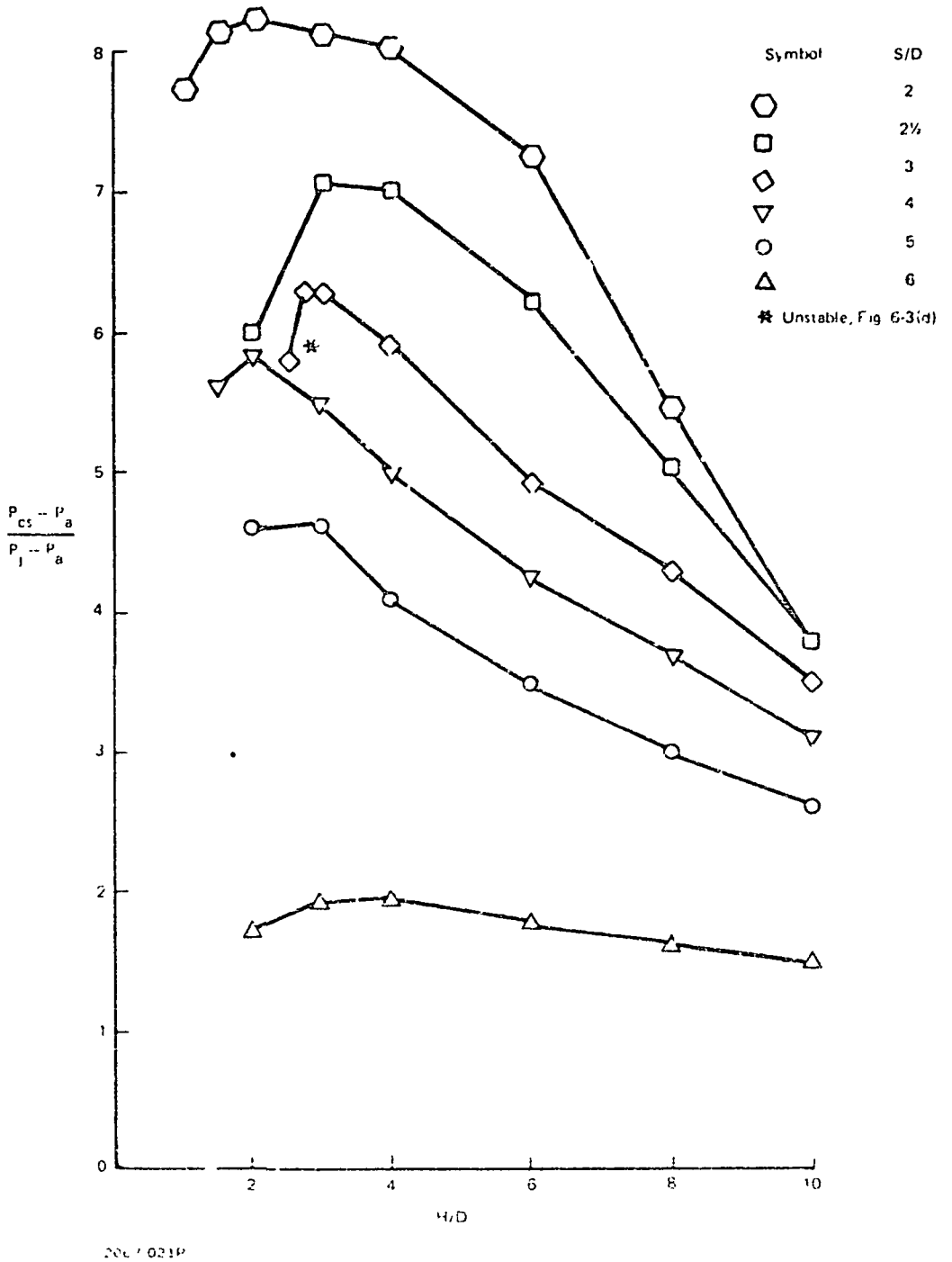

Figure 6-5. - Maximum ground pressure on center of stagnation line.

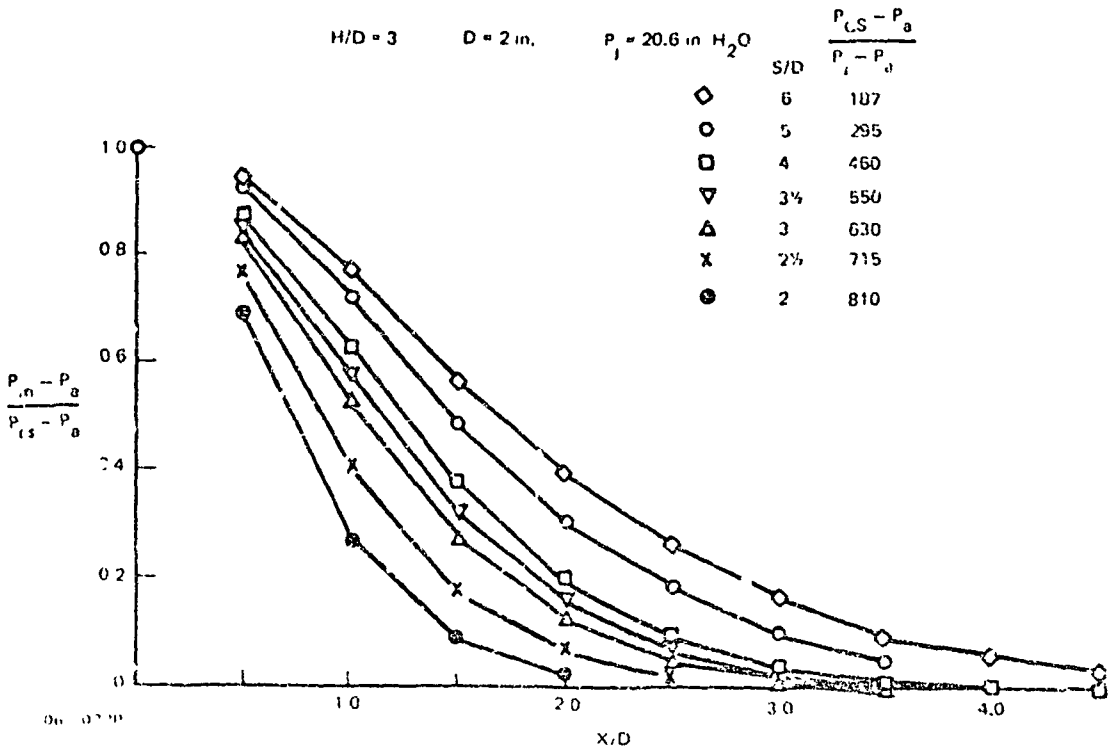

Figure 6-6. - Variation of maximum ground pressure along stagnation line.

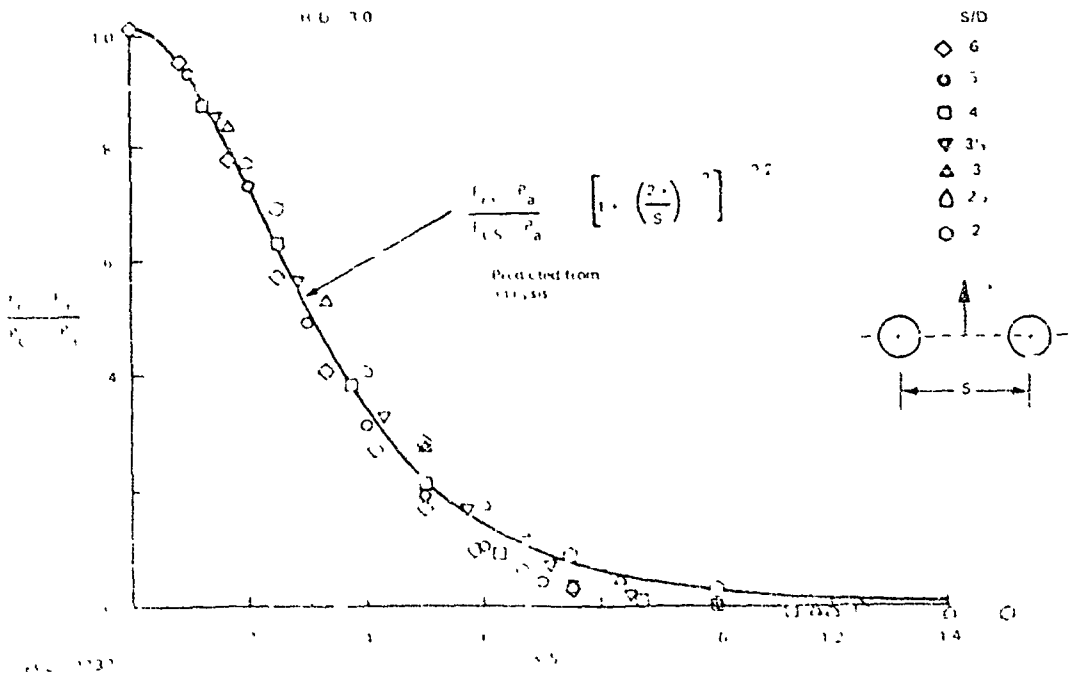

Figure 6-7. - Maximum ground pressure variation along stagnation line.

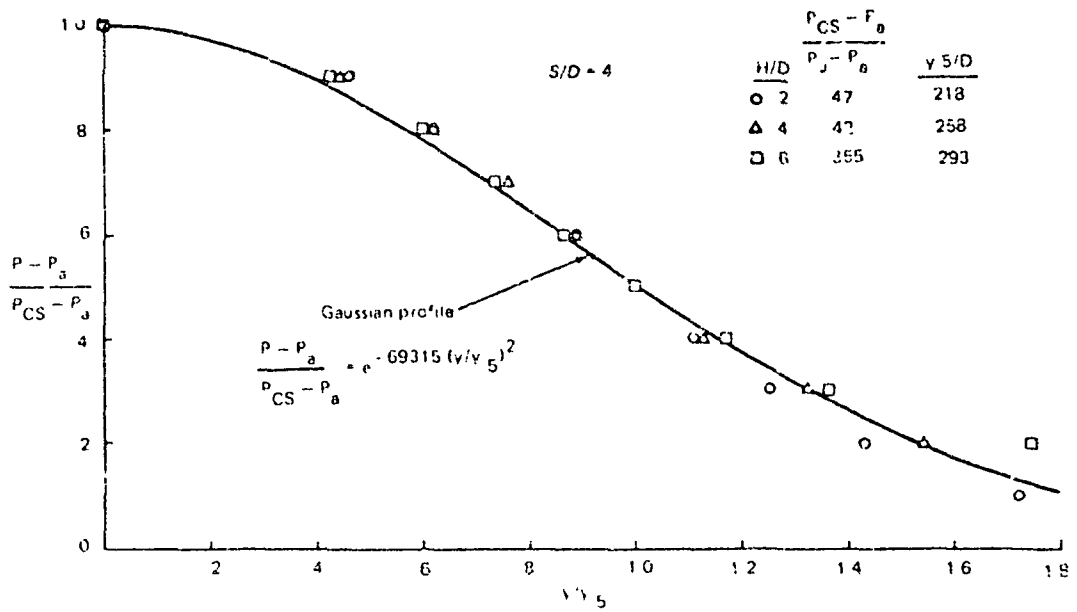

Figure 6-8. - Ground pressure variation across center of stagnation line.

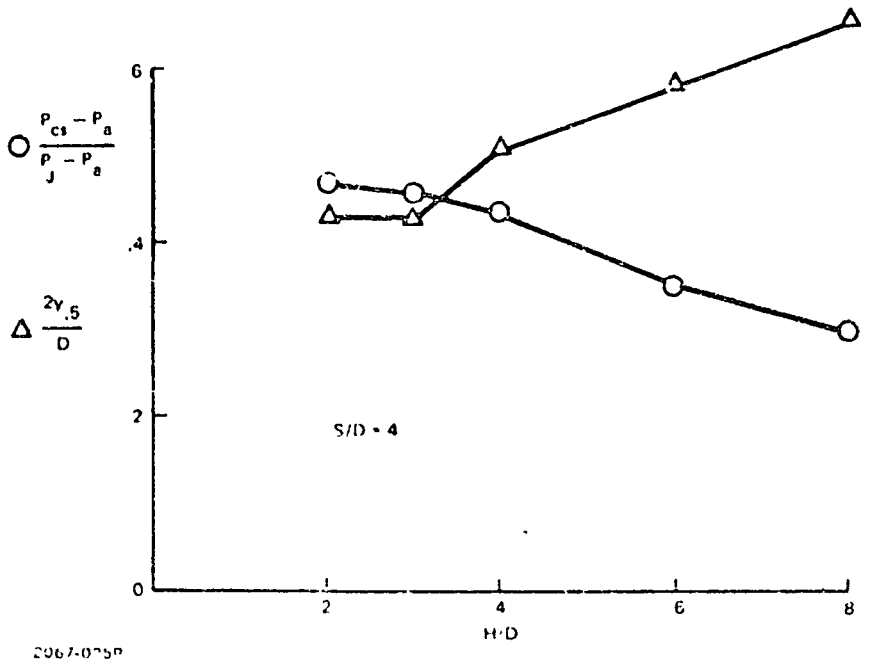

Figure 6-9. - Variation of ground stagnation line characteristics with nozzle height.

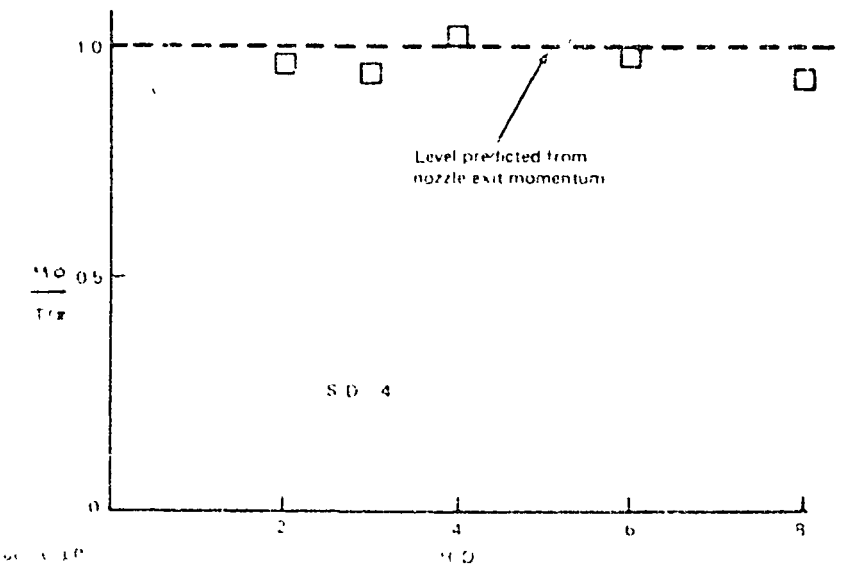

Figure 6-10. - Integrated ground pressure force.

7. UPWASH PROPERTIES

Oil flow techniques were used to qualitatively assess upwash flow behavior. A series of "splitter plates", (thin sheets of metal at right angles to the ground plane that split, or divide the flow) were used. In one series, the splitter plates were placed between the two jets along the centerline of the upwash (in the X-Z plane) looking at the radial spreading characteristics of the flow. In the second series, the splitter plate was placed along the line connecting the two nozzle centerlines (Y-Z plane) splitting each nozzle flow in half.

Oil Flow Results

The presence of the splitter plate will affect the upwash changing the flow both by damping the turbulent fluctuations normal to the flow direction and by developing a boundary layer of lower energy flow which can interfere when pressure gradients are encountered. We therefore sought primarily to look for the regions of jet/upwash interference with detailed probe surveys to follow.

For the splitter plate placed between the jets (X-Z plane), and a wide spacing (S/D = 6), a uniform spreading flow was found at heights of H/D = 2 and 6 (Figure 7-1(b)). For much closer spacings, beginning with S/D = 2 we find a similar situation at low heights. At H/D = 2, (Figure 7-1(c)), the flow spreading agrees well with our radial flow model. At a height of H/D = 6, streamlines along the center appear to be drawn in as if by entrainment from the jet (Figure 7-1(d)). At H/D = 8, a definite divergence of the center streamline occurs (7-1(a)) and going a little higher (H/D = 9, Figure 7-1(f)) a definite stagnation region is found where the oil in the upper center region is flowing downward. With another increase in height (H/D = 10, Figure 7-1(g)), the location of this stagnation point appears to remain the same, but the extent of its effect on the upwash is broadened

With the splitter plate/nozzle arrangement, we were able to go to a spacing of S/D = 1, i.e., nozzle edges touching. At this spacing, a similar effect is found at lower heights. At H/D = 2 (Figure 7-1(h)), a spreading in the upper-central region is noted and a clear stagnation region is seen at H/D = 1 (Figure 7-1(i)).

For the second set of splitter plate experiments (Plate in Y-Z plane), we again began at a wide spacing of S/D = 6. Results are shown in Figures 7-1 (j), (k), (l), beginning at an H/D of 2 and increasing to 6. At the height of H/D = 6, the dynamic pressure was so low that it was difficult to form the oil patterns. Note the large angle (about 30°) that appears to be the outer wall jet growth angle. We believe that this is due to the corner flow and is a warning on the qualitative accuracy of this method of visualization.

Another view of changes produced by the splitter plate is found in Figure 7-1(m) looking down on the ground plane. A conventional ground flow/stagnation line is formed, but the center of the jet stagnation region is displaced outward from the splitter plate. Again, this is believed to be due to the boundary layer formed between the jet plume and the plate.

Proceeding then to the closer spacing (S/D = 2) a similar series of heights was examined. At H/D = 2, a fairly clean jet plume and upwash picture was formed (Figure 7-1(n)). At an H/D = 4, the upwash curved into the jet on the right (Figure 7-1(o)). A slight movement of the splitter plate caused this to be reversed with the upwash veering to the left (Figure 7-1(p)). By careful movement of the splitter plate while observing the oil, it was possible to obtain an upwash flow up the center (Figure 7-1(q)). At larger H/D, Figures 7-1(r) and 7-1(s), this sensitivity did not appear to exist, but a stagnation region marked the end of the upwash.

Summary of Upwash Pressures

Flow properties in the upwash were found by traversing the Kiel and static probes in the y-direction at various heights (z) above ground. Figure 7-2 shows data obtained from a probe traverse across the upwash centerline. Note that the static pressure was below ambient throughout the upwash and beyond its edges. At the edges of the upwash (smallest value y for which dynamic pressure is zero) and outside the edges, the Kiel pressure and static pressure readings were equal, in spite of the different shapes and orientations of the pressure holes in the probes. Within the upwash the static pressure profile was only slightly dependent on the size of the static pressure probe. The static pressure was below ambient throughout the region between the nozzle exit plane and the ground except for a small zone less than 25 mm above the ground just above the stagnation line. This large region of low static pressure

appears to be a characteristic of multiple jet ground impingement flows, and was found at all values of H and S that were run.

The dynamic pressure profile showed a Gaussian shape except at jet spacings below S/D = 3 where it was distorted by a lack of symmetry. Figure 7-3 shows data obtained from probe traverses across the center of the upwash at various heights above ground for H/D = 2 and S/D = 4. For each height above ground (z) the profile was normalized by the maximum dynamic pressure on centerline (q_c), and the probe distance (y) relative to the centerline was normalized by $y_{.25}$. This plot shows that data taken at different heights above ground has the same profile shape, which closely matches the Gaussian profile

$$q/q_c = e^{-1.386(y/y_{.25})^2} \qquad (4)$$

Profiles of this shape were found for nozzle separation distances down to S/D = 3 providing the nozzle height above ground was not large enough to provide a significant interaction between the incident jets and the upwash. When the dynamic pressure profile shape is independent of height above ground, at any value of z the upwash properties on the centerline can be specified by the values of q_c/q_j and $y_{.25}$.

Figure 7-4 shows the dynamic pressure decay along the upwash centerline for H/D = 1 at different nozzle spacings. For each spacing the values of q_c were normalized by the corresponding maximum ground pressure at the center of the stagnation line. The data are plotted versus $\frac{S/2 + z}{S/2}$ to account for changes in the radial flow pattern in the upwash at different values of S. The data for S/D = 5 and 6 fall along a straight line, indicating that the dynamic pressure variation along the upwash centerline can be represented by a power law decay. As the spacing is decreased the data deviates from a straight line because of interference between the upwash and the incident jet flow at this nozzle height above ground.

Our modeling of the flow direction in the upwash assumes that the radial pattern of the wall jet flow on the ground continues into the upwash after the collision of wall jets at the stagnation line. The variation of dynamic pressure along the upwash at constant height above ground can be found from:

$$\frac{q_m}{q_c} = \frac{1}{1 + \left(\frac{x}{S/2 + z}\right)^2} \qquad (5)$$

if there is no interaction between upwash and impingement zone. Equation (5) is plotted in Figure 7-5 for S/D = 4 and Z/D = 2 for comparison with data taken at several different values of nozzle height above ground.

The variation of upwash properties on the centerline at the nozzle exit plane with jet spacing and jet height above ground is illustrated in Figure 7-6. Decreasing nozzle spacing increases the exit plane maximum dynamic pressure, with not much change in upwash width, until a maximum value is reach between 3 and 4 diameters. Further decreases in nozzle spacing results in a decrease in exit plane dynamic pressure.

At low ground heights we encountered instabilities in the upwash at a nozzle spacing of 3 diameters. Such instabilities appeared as abnormally large fluctuations in probe readings. Kiel probe fluctuations in the upwash were generally found to be in the range of 10 to 20 percent. Unstable upwash conditions increased the magnitude to over 50 percent. Such conditions were encountered for S/D = 3 when H/D was decreased to less than 2-1/2. Corresponding fluctuations in ground plane pressure were noted under the same impingement conditions, indicating that the entire upwash flow was affected. Further decrease in jet spacing provided more stable upwash conditions at low ground heights, but the pressure profiles at the exit plane were somewhat unsymmetric.

The flow properties on the upwash centerline at the nozzle exit plane are illustrated in Figure 7-7, which shows curves of constant dynamic pressure on a plot of H/D versus S/D. The boundaries on the left side of this curve, labeled 7° and 10° represent the conditions where the incident jets overlap shear layers before impinging on the ground. The difference in these two boundaries is the spreading angle assumed for the free jet plumes. The lower boundary corresponds to a stability limit illustrated on a similar plot presented by Hall and Rogers (Reference 8). We found that stable impingement flows existed at lower values of H/D than they indicated, however, an unstable region does appear to exist around S/D = 3 as illustrated by the dashed region sketched in Figure 7-7

At the closest nozzle spacing, S/D = 2, we found that the upwash was mildly unstable at H/D = 2-1/2 and 3, but not for lower or higher values of H/D. Such instabilities would disappear if the symmetry of the impingement flow was disturbed. Misalignment of the ground plane by a few degrees would smooth out the instability described above. In addition, excessive blockage by a probe support could stabilize this type of fluctuation.

Effect of Bodies on Upwash

Since the basic analytic procedures assume isolated upwash behavior, using the two-jets as a building block, a brief experimental study was undertaken to determine the effects of adding various surfaces. Figure 7-8 illustrates the effects of the presence of our aircraft model on flow properties in the upwash. The total and static pressure profiles along the upwash centerline are shown for H/D = 6 and S/D = 5 with and without the model in place. At this height above ground the change in centerline upwash profiles caused by the model is significant only at points closer than one nozzle diameter from the fuselage underside. The static pressures increased as the flow stagnated on the bottom of the model. Figure 7-9 shows the effect on the upwash of the models used in the force experiments at the exit plane for a lower height above ground (H/D = 3) and a closer nozzle spacing (S/D = 4). In this case the models altered the flow properties of the upwash by producing lowered static and total pressures. The greater the body area, the greater the effect, although it was not large for any cases. This effect does not appear to alter the general behavior of the flow but a correction for its effects on the general pressure level may be needed.

Effect of Adding a Third Jet

To determine the influence of a third jet on the properties of the upwash formed between two jets, probe surveys were taken across one of the upwash flows with and without the third jet in operation. The primary jet pair was spaced at S/D = 4. The third jet was located at either S/D = 3.86 and S/D = 5.69 with respect to the other two jets (3.3 and 5.3) with respect to the line connecting the first two jet centerlines (see sketch on Figure 7-10 and 7-11).

The impingement geometry is illustrated in Figure 7-10, which shows measurements for the closest spacing of the third jet. The maximum dynamic pressure in the fountain flow is quite close to the predicted fountain location. Note that the maximum

dynamic pressure in the upwash formed between the primary jets is lowered 10% by the presence of the third jet, even at points that are far from the fountain region. The direct influence of the fountain presence appears to extend into the upwash about .75D from the predicted location.

Figure 7-11 shows a similar plot of maximum dynamic pressure with the third jet located further from the primary pair, showing that the influence of the third jet on the primary upwash almost negligible. The direct fountain presence again appears to extend 1.75D. For this case, probe surveys were taken at several heights above ground to investigate the fountain flow. Figure 7-12 shows a comparison of the properties in the fountain with the properties on the centerline of a two jet upwash. The inclination of the location of maximum fountain dynamic pressure is illustrated in Figure 7-13.

(a) S/D 6 h/D 2

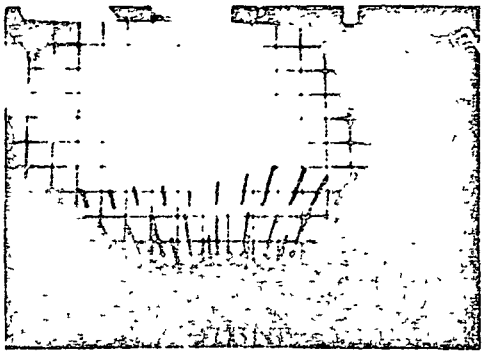

(b) S/D 6 h/D 6

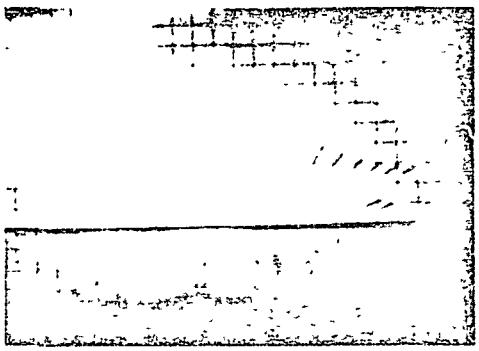

(c) S/D 2 h/D 2

(d) S/D 2 h/D 6

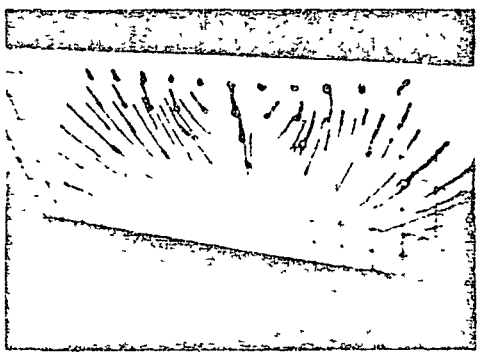

(e) S/D 6 h/D 9

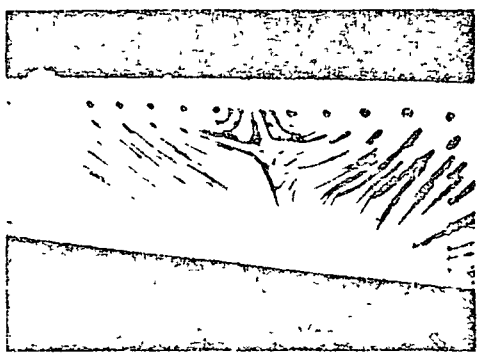

(f) S/D 2 h/D 9

Figure 7-1. Oil Flow Photographs.

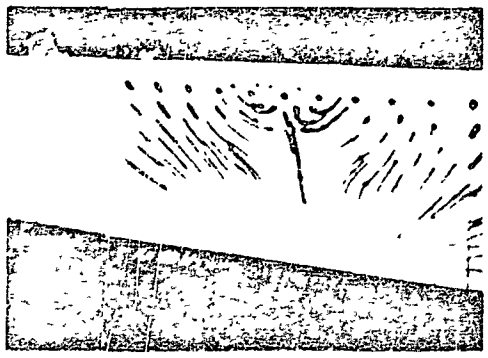

(g) S/D = 2 h/D = 10

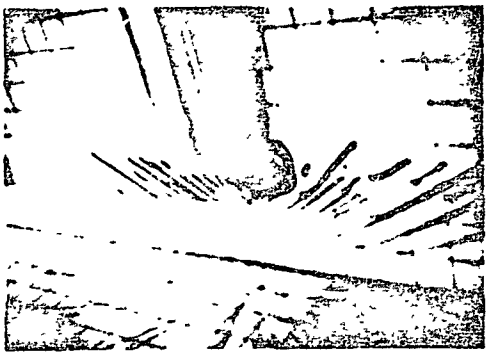

(h) S/D = 11 h/D = 2

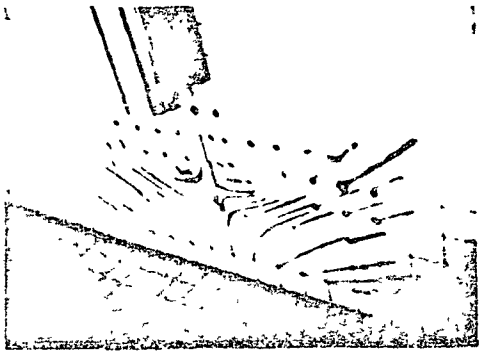

(i) S/D = 1 h/D = 4

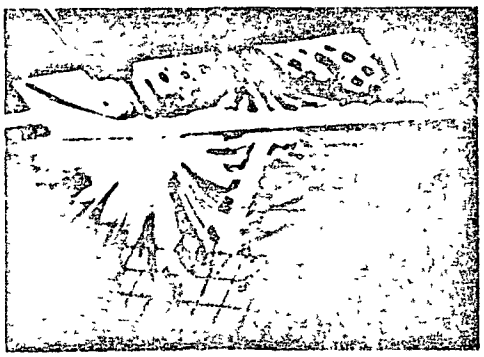

(j) S/D = 6 h/D = 2

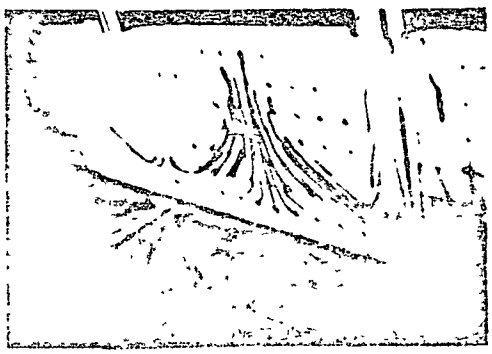

(k) S/D = 6 h/D = 1

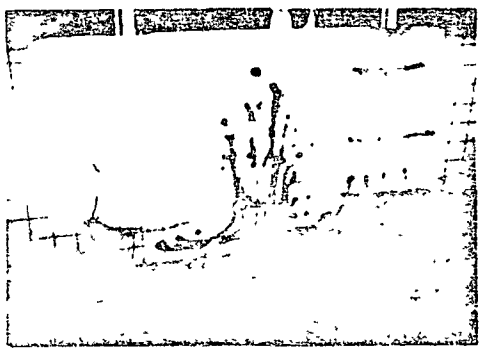

(l) S/D = 5 h/D = 6

Figure 7-1 Continued

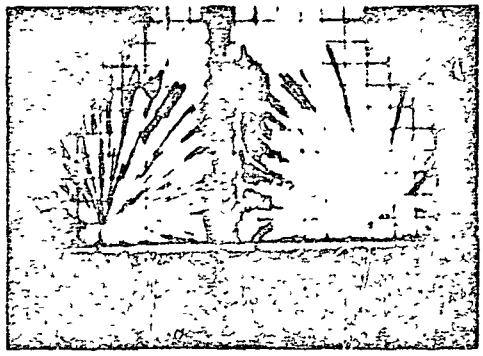

(m) VIEW LOOKING DOWN SPLITTER PLATE

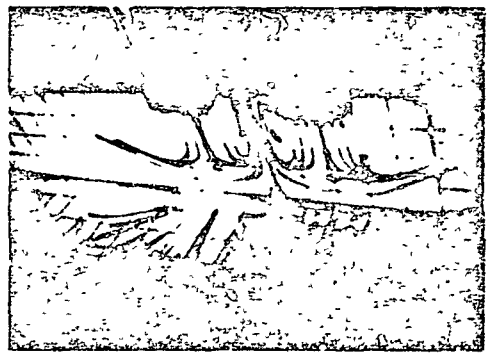

(n) S/D - 2 h/D - 2

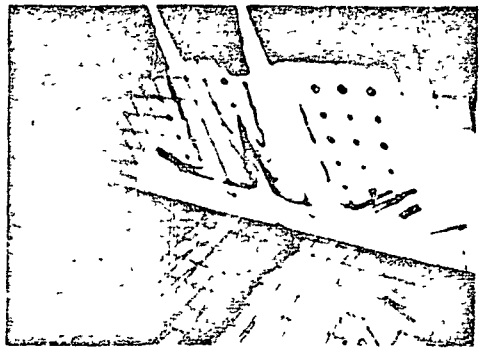

(o) S/D - 2 h/D - 4

(p) S/D - 2 h/D - 4

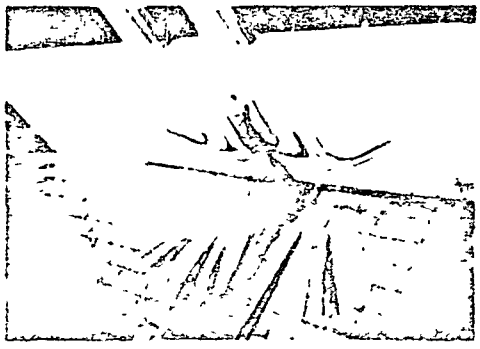

(q) S/D - 2 h/D - 4

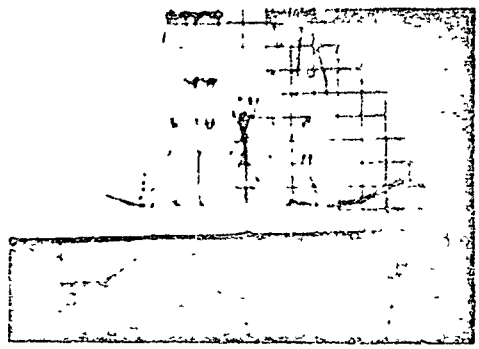

(r) S/D - 2 h/D - 6

206/027(3)

Figure 7-1 Continued.

ORIGINAL PAGE IS
OF POOR QUALITY

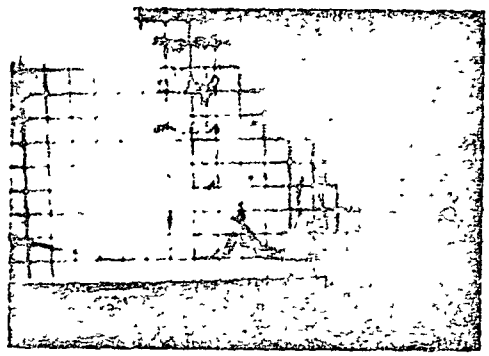

(s) S/D 2 h/D - 8

0267 027 (4)

Figure 7-1 Concluded.

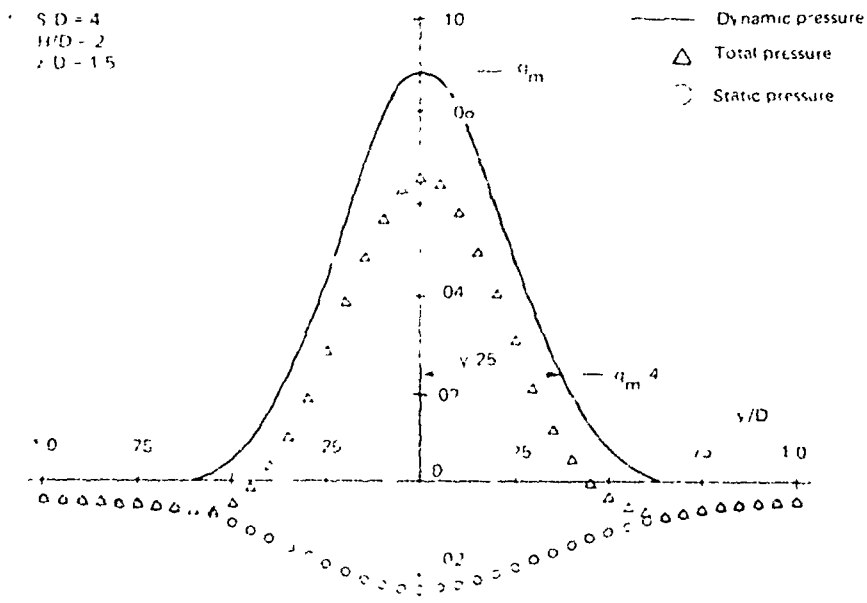

Figure 7-2. - Pressure profiles across wake centerline.

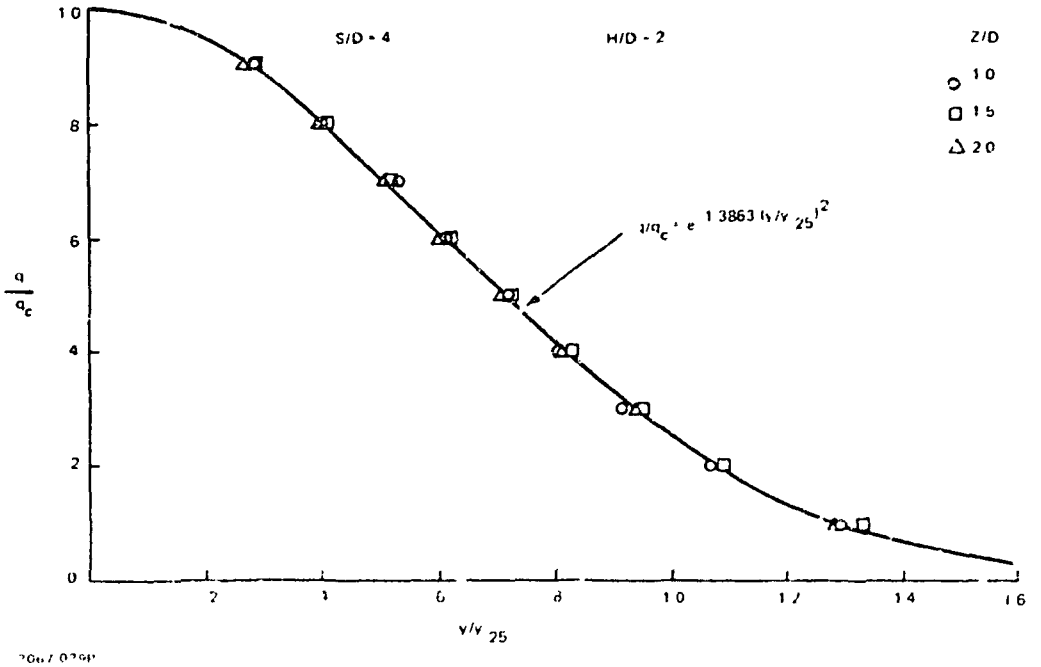

Figure 7-3. - Dynamic pressure profiles across upwash.

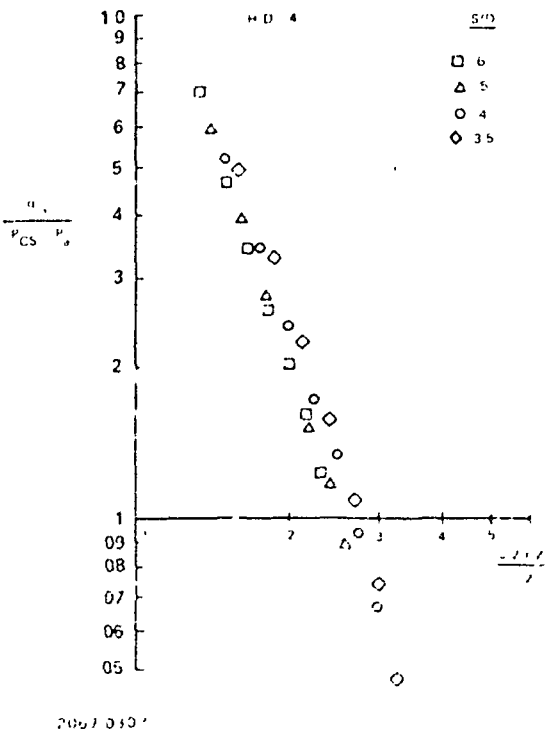

Figure 7-4. - Dynamic pressure decay along upwash centerline.

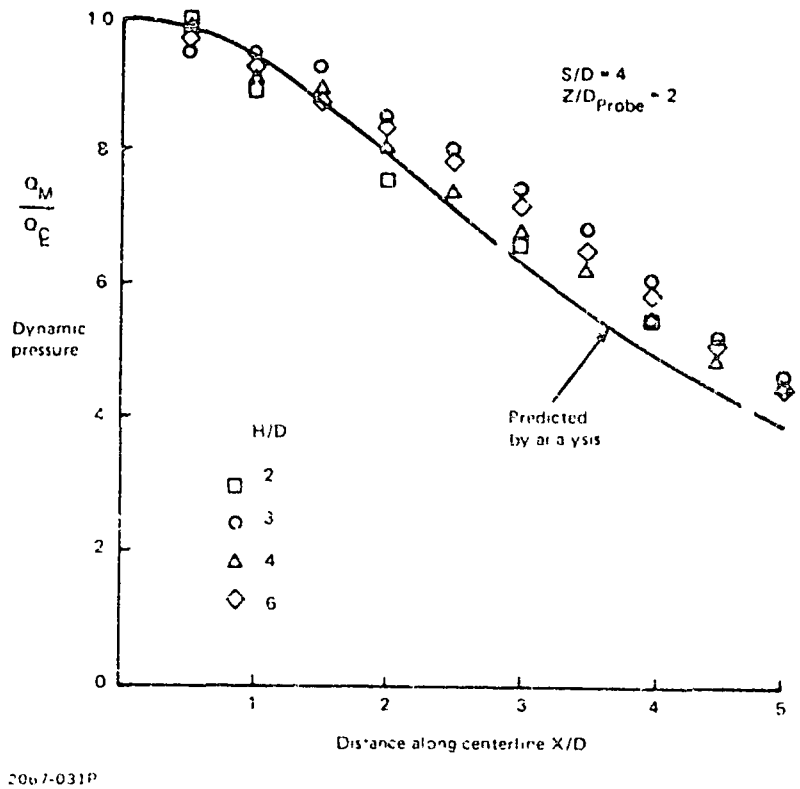

Figure 7-5. - Variation of dynamic pressure along upwash (X).

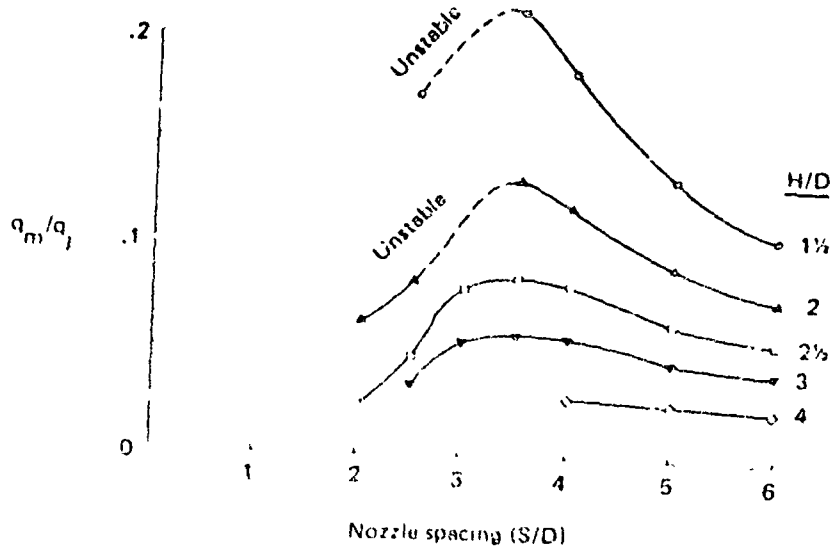

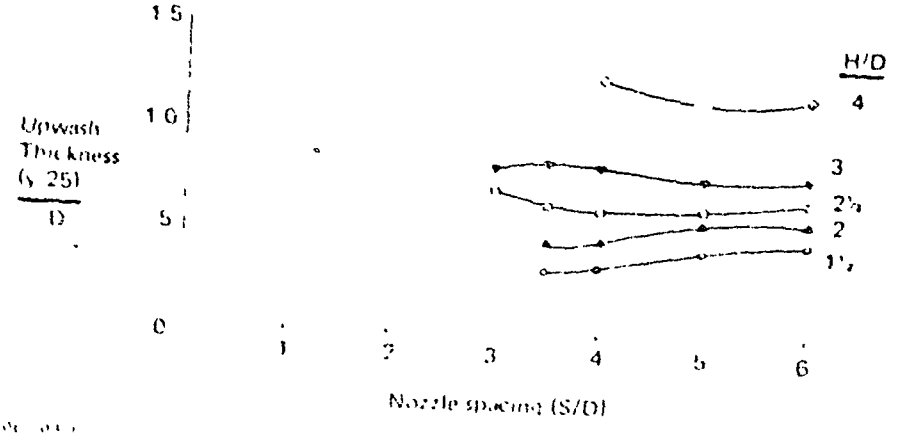

Figure 7-6. Upwash properties at nozzle exit plane.

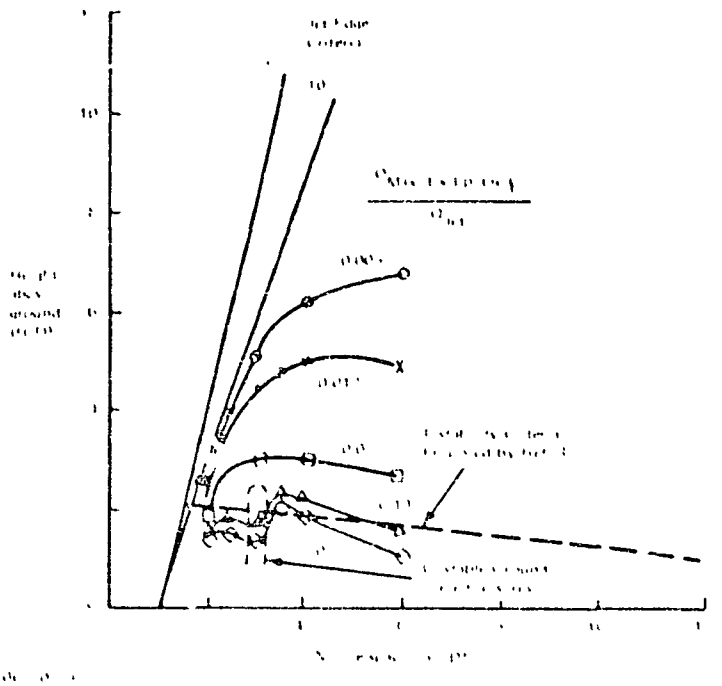

FIGURE 7-7. MAXIMUM DYNAMIC PRESSURE IN UPWASH AT NOZZLE EXIT HEIGHT.

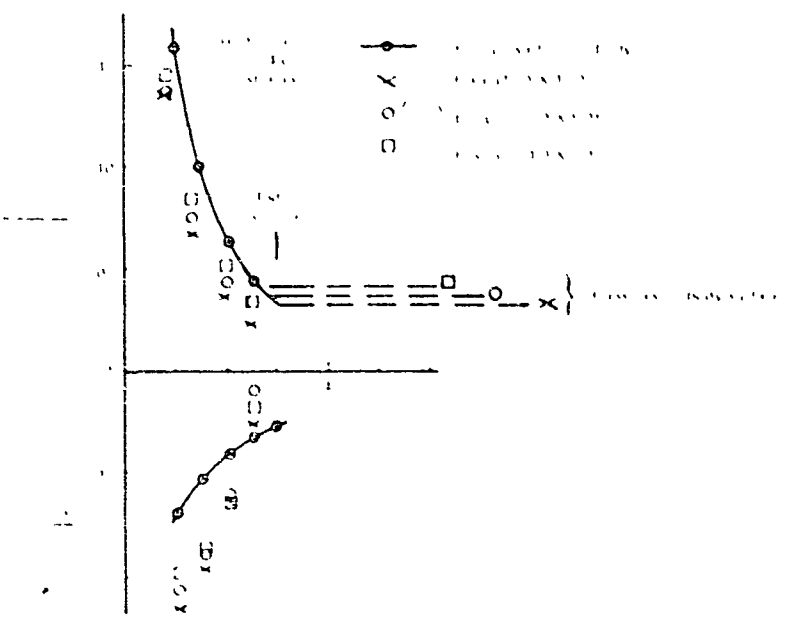

FIGURE 7-8. EFFECT OF THE THREE CLASSES OF BODIES ON THE UPWASH PROPERTIES.

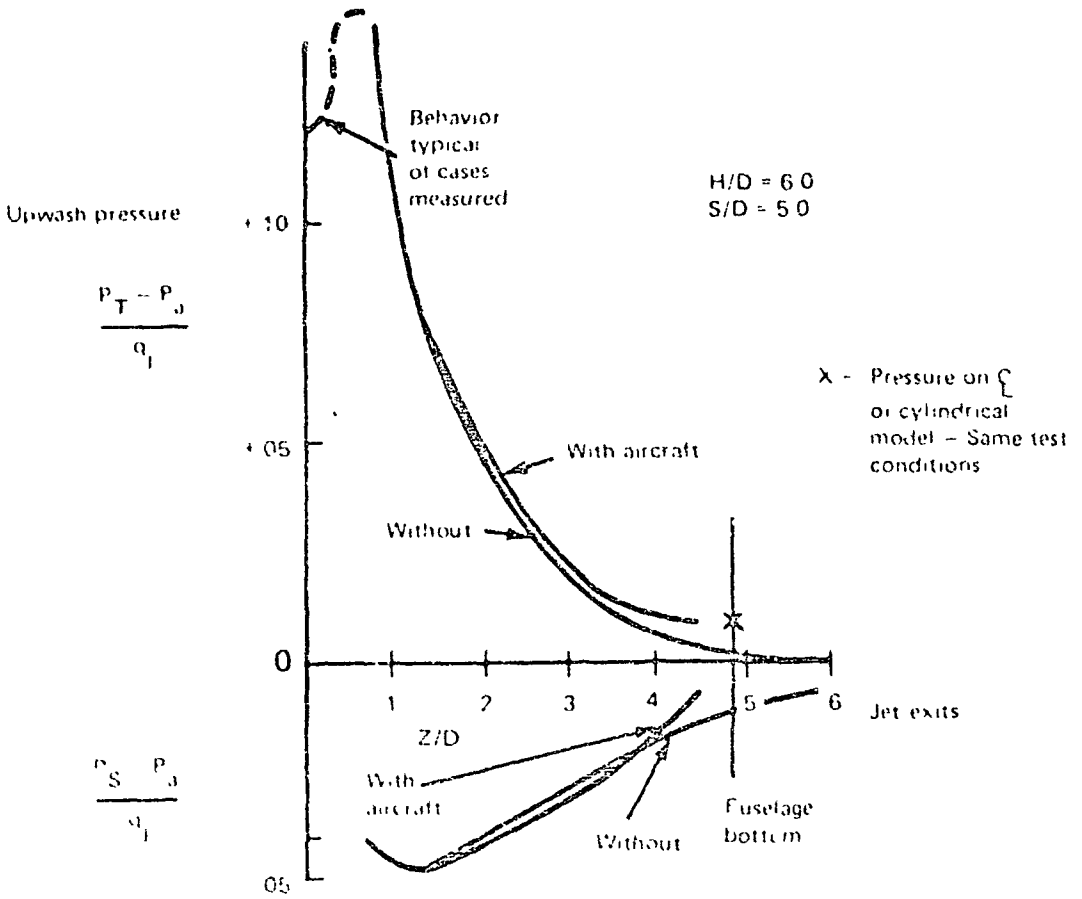

Figure 7-9. Effect of aircraft on upwash development.

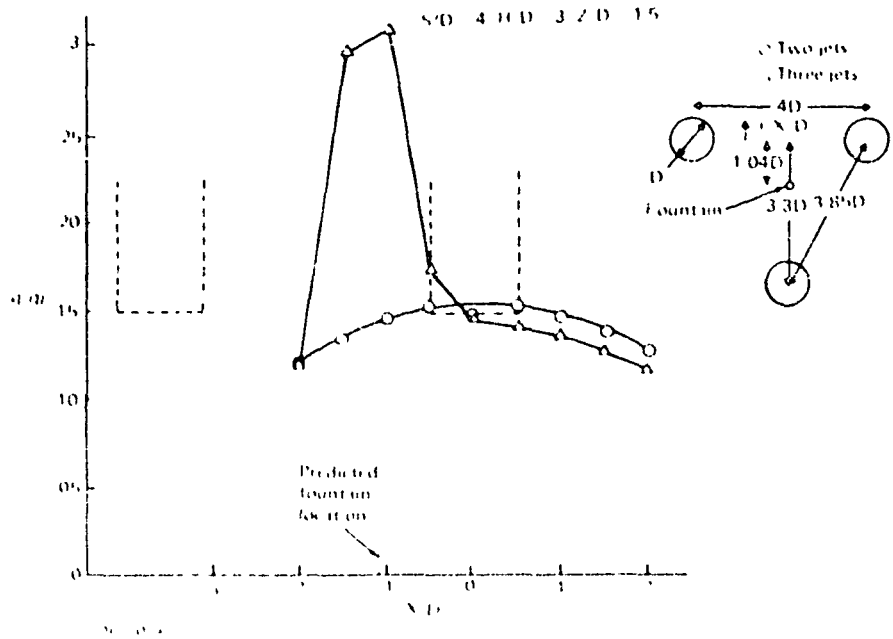

Figure 7-10. - Effect of third jet on maximum dynamic pressure along two-jet upwash. (Close spacing).

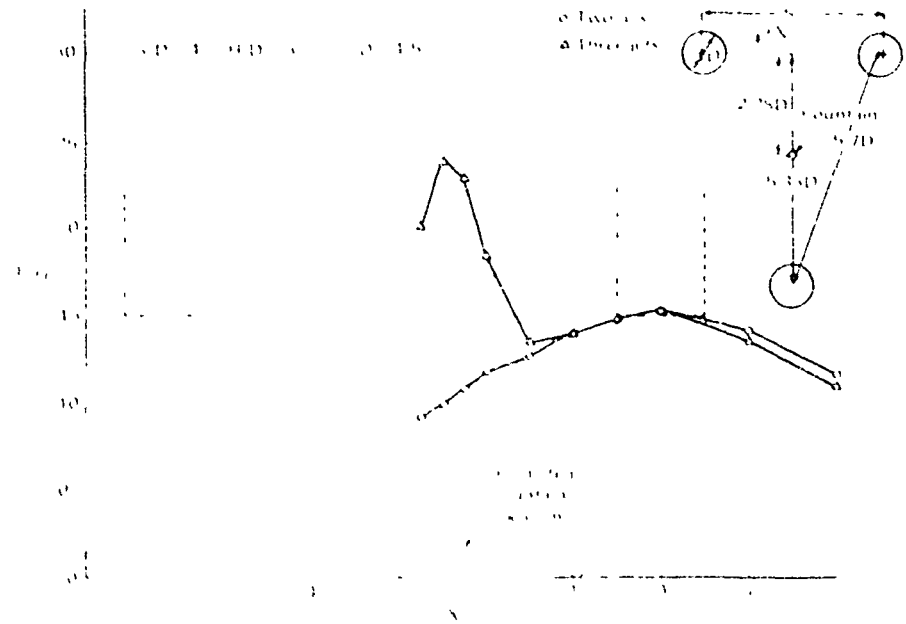

Figure 7-11. Effect of third jet on maximum dynamic pressure along two-jet upwash. (Wide spacing).

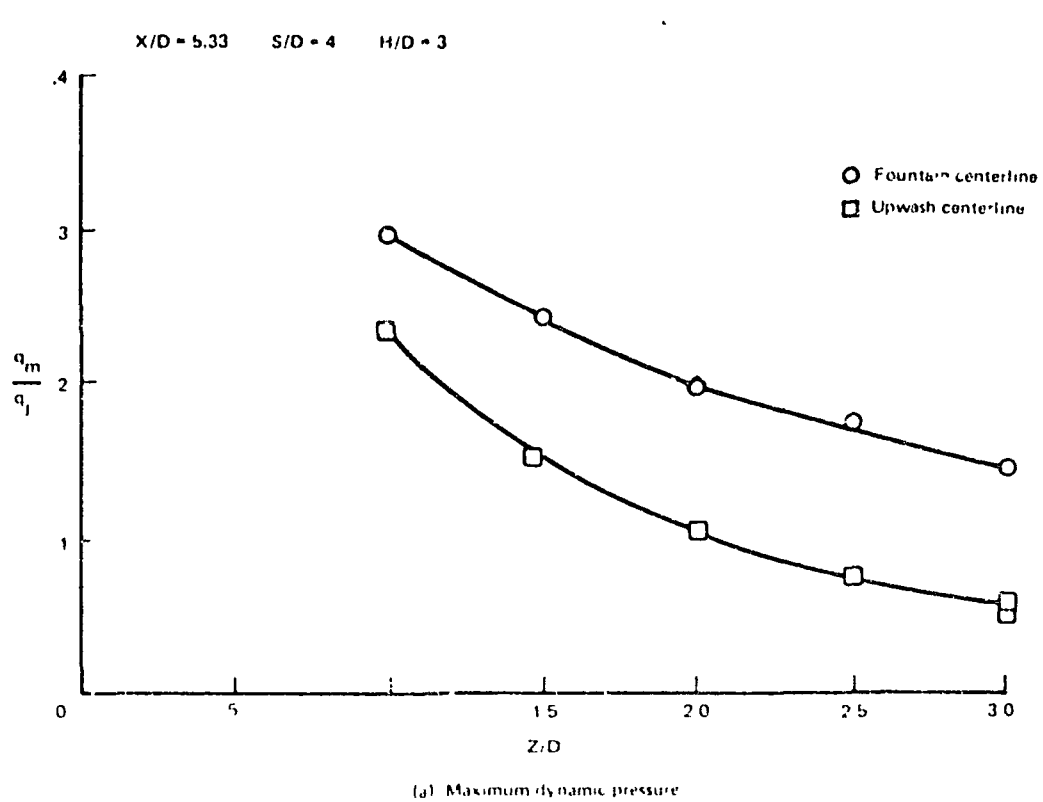

(a) Maximum dynamic pressure

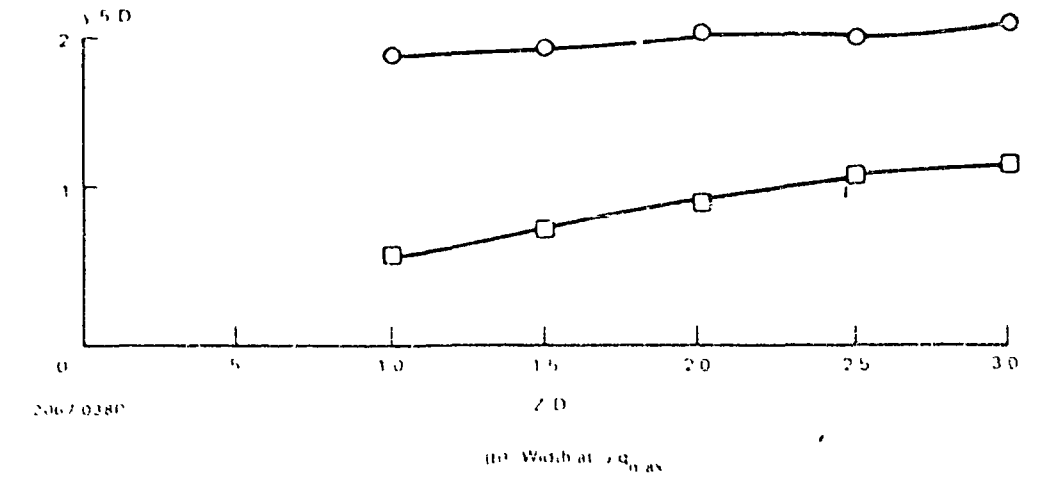

(b) Width at $q_{q_{max}}$

Figure 7-12. - Comparison of fountain and upwash properties.

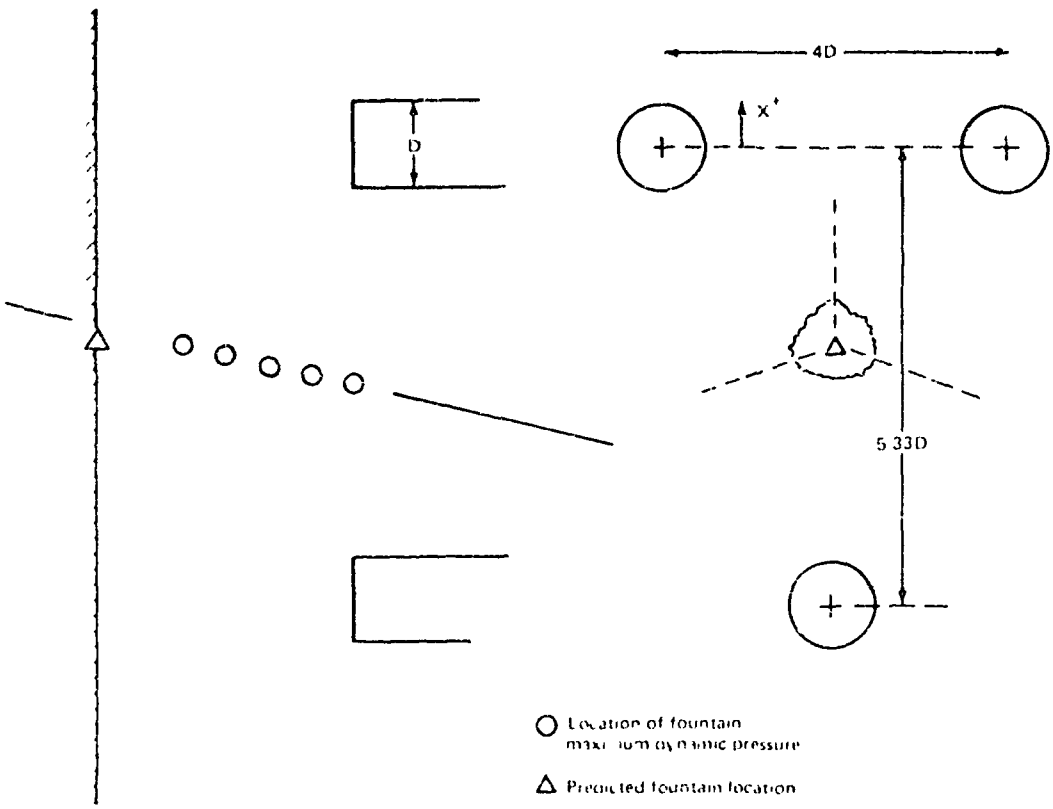

Figure 7-13. - Path of maximum fountain dynamic pressure.

8. JET INDUCED FORCES

Jet induced forces were obtained for two-jet configurations by using a strain gauge balance for the simulated aircraft surfaces (full aircraft model of Figure 4-1 and fuselages of Figure 4-8). For the flat plate (Figure 4-10) the force was measured with three separate strain gauge beams. In all cases, only the jet-induced forces were measured, and the jet thrust was not metric. Jet thrust was calculated from integrated total pressure profiles at the nozzle exit plane, including measurements through the boundary layer.

Forces on Aircraft Model

The aircraft design used in this study is shown in Figure 4-7. A series of experiments with the basic airplane (Figure 8-1) showed interference force levels becoming more negative as the jets were brought closer together, down to a nozzle spacing to diameter (S/D) ratio of 2.8. Below 2.8, down to 2.4 (the limit of our apparatus) the force curves stayed essentially constant. The only hint of any unusual behavior was the slightly more positive than expected force levels and the local positive deviation of the force curve for an S/D of 3.2 around a height of H/D = 1.6. (This curve is shown as a dashed line in Figure 8-1 for clarity.)

Strakes were then attached to the lower surface of the fuselage. These strake surfaces are shown in Figure 8-2. When strakes were added, a much more complicated situation developed. For aid in observing and understanding the behavior, these data are presented in a series of three graphs in Figure 8-3. Figure 8-3(a) shows that beginning at moderately wide spacings (S/D = 5.7) the interference forces ($\Delta F/_T$) are positive over the range of H/D investigated. As the jet spacing is decreased, the forces become larger up to a spacing of S/D = 4, and then stay approximately constant to S/D = 3.2. Figure 8-3(b) (carrying over the curve for S/D = 3.2) indicates that at a spacing of S/D = 3.1 the flow became very unsteady for heights between approximately H/D = 1.8 and 2.1. The force levels varied over the range indicated in the shaded area of the figure. As the spacing decreased still further, this unsteady behavior disappeared, but a region near these same H/D's occurred where the force fell from the S/D = 3.2 value to a much lower value. The width (in H/D values) of this region of lowered forces grew wider as S/D was decreased until for spacings less than S/D = 2.8 the higher force

region did not occur at all. After this point the general force level again showed a slight increase with closer spacings down to S/D = 2.4. For these close spacings another much smaller unsteady transition area occurred near a height of H/D = 5. This was a transition between the forces with strakes and the lower force levels (negative) without strakes.

The changes in general level and shape of these interference forces with strakes were found to be a property of the upwash flow itself, rather than its interaction with the aircraft, as noted in Section 7.

The above experiments were conducted with one specific aircraft design. Earlier work indicated that details of the body geometry could strongly affect the interference forces also (Reference 6). An example of this is the effect of the fuselage corner radius. Making the fuselage corner radius sharper produces positive interference forces.

To conduct a systematic investigation of the effects of body geometry we used a series of simplified bodies, as well as extensive measurements and modeling of the basic jet/upwash flows.

Two-Dimensional Body Forces

The first series of experiments involved cylindrical bodies (shown in Figure 1-8), similar to the aircraft fuselage in the previous section, with varying lower surface contour. In addition to confirming that a fuselage-type surface can experience large positive forces in-ground-effect it was found that there was a change between attached flow around the body and separation at the lower corner as the corner radius was changed. Flow visualization photos using tufts show this behavior clearly (Figure 8-4). The switch between attached and separated flow was found at a corner radius to body width (r/w) of 0.188. At this radius both flows could exist, and could be switched by disturbances of the flow.

The effect of corner radius on the interference forces is shown in Figure 8-5. Beginning from a sharp corner which results in a large positive interference force, the force decreases as the corner radius is increased. When the flow switches from separation at the corners to attached flow ($r/_{w}$ = 0.188), the force jumps upward to a larger value. Further increase in the radius results in a return to the trend of decreasing force with increasing radius.

The occurrence of a larger upward force (body "drag" in the upwash flow) for attached flow than for separated flow is understandable with reference to the pressure distributions of Figure 8-6. The pressures on the lower surface and the upper surface are affected by the change from separated to attached flow. The pressure on the upper surface is very near ambient when the flow is separated. When the flow is attached the upwash above the body acts as an ejector and produces a larger negative pressure which, in this particular case, is a positive interference, or lift. The pressure distributions of Figure 8-6 also show the reason for the sensitivity of the forces to the body geometry. The integrated pressures (forces) involve two areas on the bottom surface, one positive, one negative. The resulting force is therefore the small difference between two large numbers, and very sensitive to shifts in the curve.

Another study area was the effect of the strake depth on interference forces. Figure 8-7 shows a continuing increase in upwards forces with increased depth. The curve for r = 0, no strakes is a reference line. This was the curve of greatest interference force in Figure 8-5. Note that also a body with a corner radius and fitted with strakes which are level with the fuselage bottom section produces a higher interference force than the flat bottomed body.

With a strake depth of $^{C}/D = 0.125$ a series of experiments was conducted with three different body widths, W/D = 0.5, 1.0, and 1.5. Results of this series are shown in Figure 8-8. A progression of higher forces with greater body width is seen, but the thinnest body does not have as fast a drop off of force with height above ground as found for the other two. All three of these bodies are enveloped by the upwash for values of H/D down to 1.

Extending this investigation to other classes of bodies; a lower fineness ratio (L/D = 2.8 vice 16 for the fuselage type body) rectangular body was tested with and without strakes (Figure 4-9). Nozzle spacings between 2.4 and 1.0 result in nozzles contained within the planform.

Interference forces on these bodies with strakes (Figure 8-9) have much larger negative values than those for the preceding cases. This results because of the larger area for the lower surface pressures to affect. We found no significant effect of the corner radius or the upper surface corner geometry for this body. The addition of strakes again produced a large positive increment in forces, and a region of

unsteady flow developed for S/D = 3.0 and height above ground between S/D of 1.5 and 2.5 (Figure 8-9).

A survey of the effects of strake height and strake spacing were conducted at a nozzle spacing (S/D) of 4.0 (Figures 8-10, 8-11). Variation of the strake spacing produced some changes in the force curves, with an optimum at some intermediate spacing. In all cases significant positive forces resulted. The positive force increment due to the strakes (Figure 8-10) increased with increasing strake height up to about $\sigma/D = .25$. Doubling of that value produced very little change.

Also examined briefly was the flow with a very large plate at the nozzle exit plane, using a square plate 12D x 12D, with a nozzle spacing of S/D = 4.0. Large negative forces were found without strakes, but for this "vehicle" the large positive force increments with strakes did not occur (Figure 8-12). In fact, for some values of H/D the strakes resulted in more negative forces.

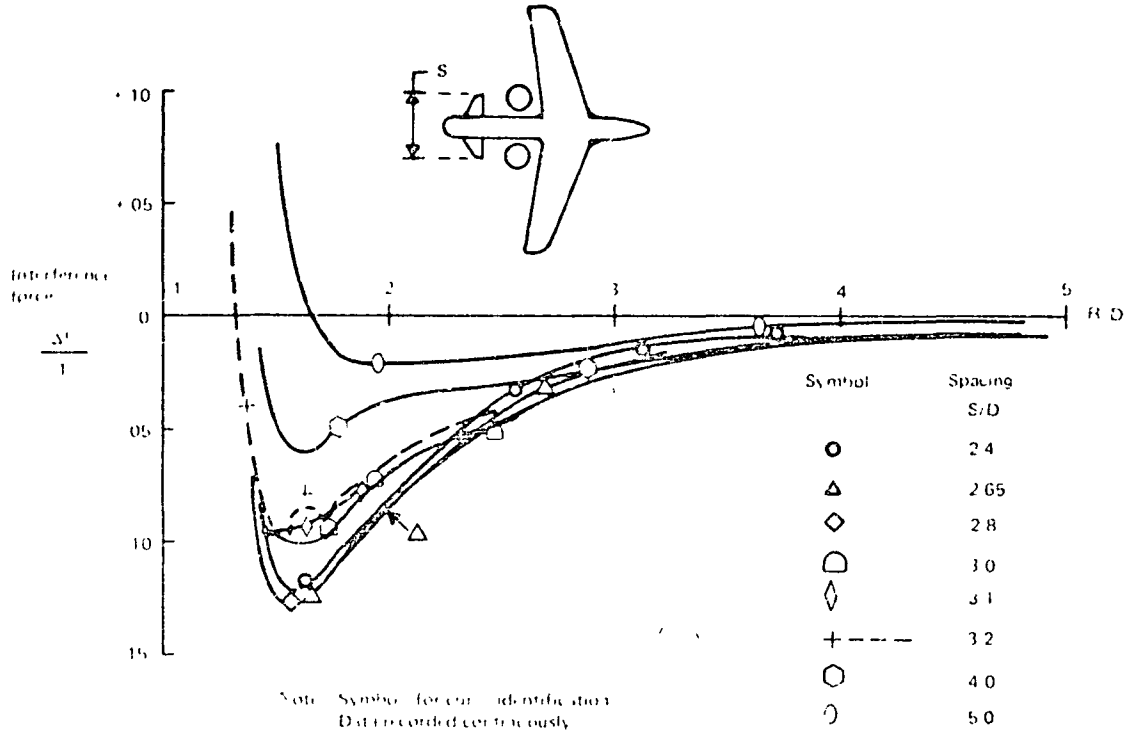

Figure 5-1. - Effect of jet spacing on aircraft forces.

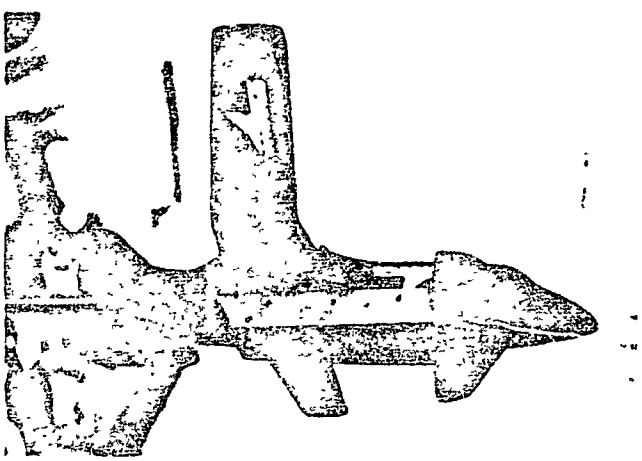

Figure 5-2. Strake used on the aircraft model.

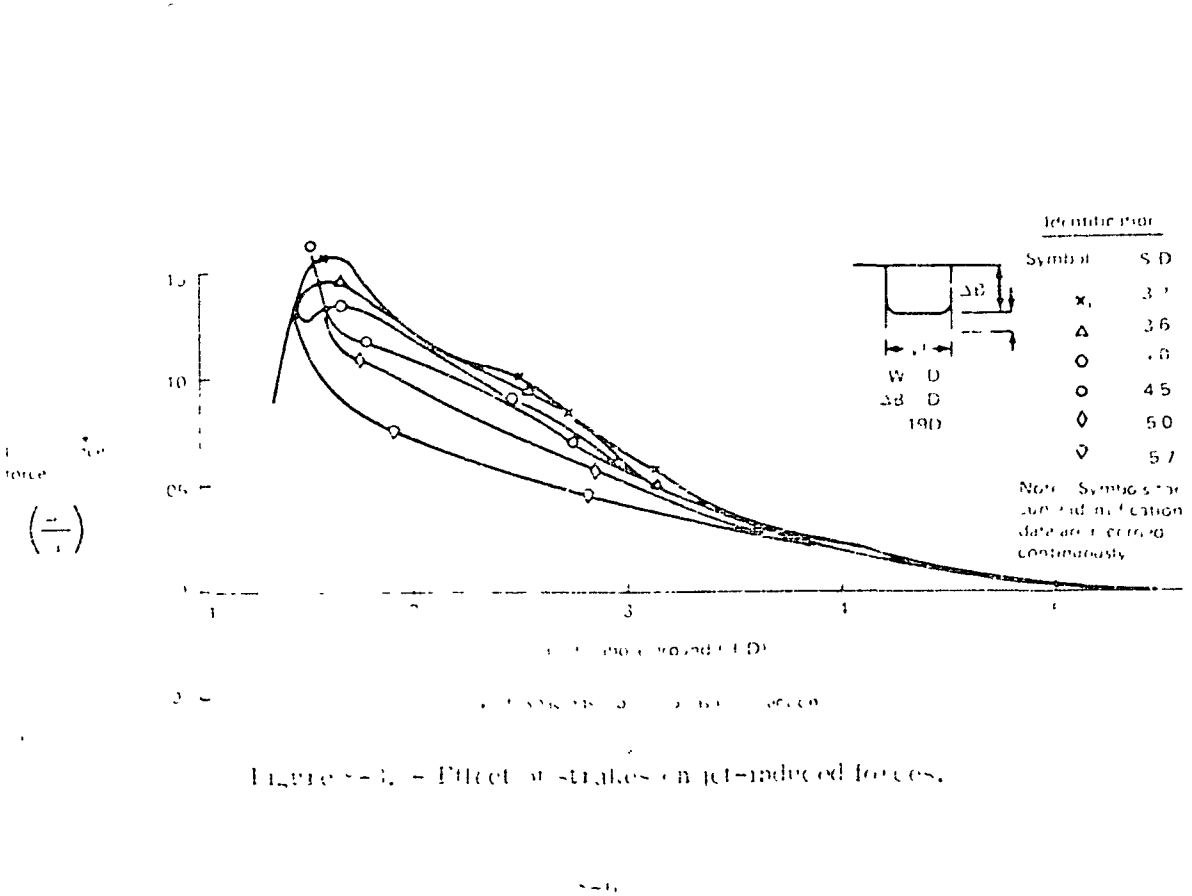

Figure 5-3. – Effect of strakes on jet-induced forces.

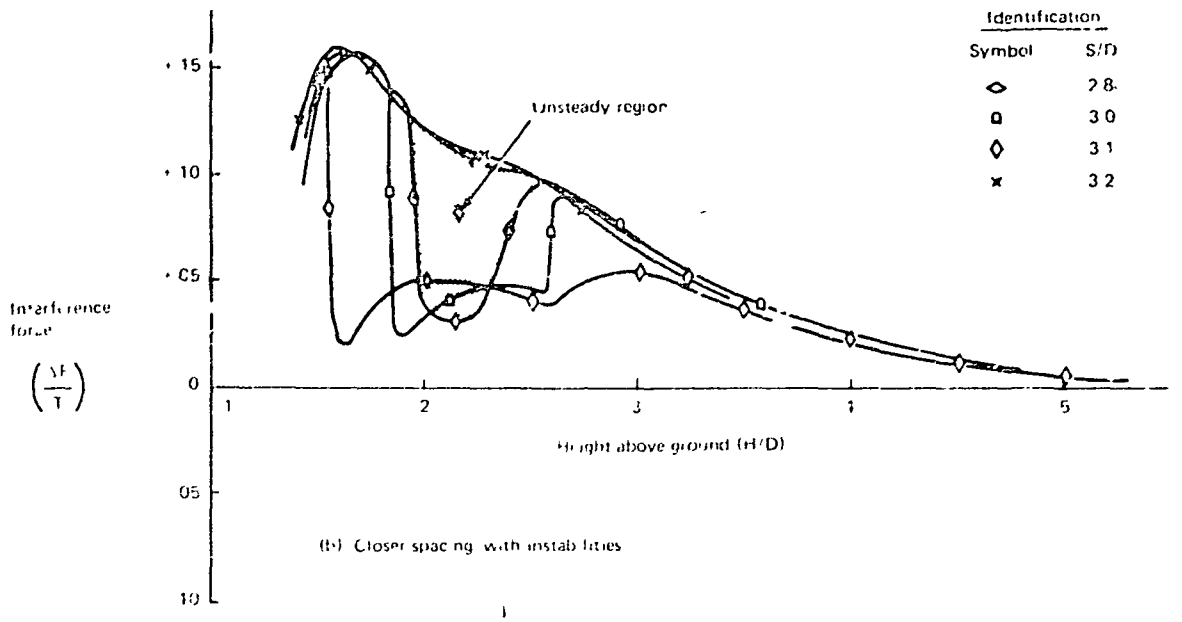

Figure 5-3. - Continued

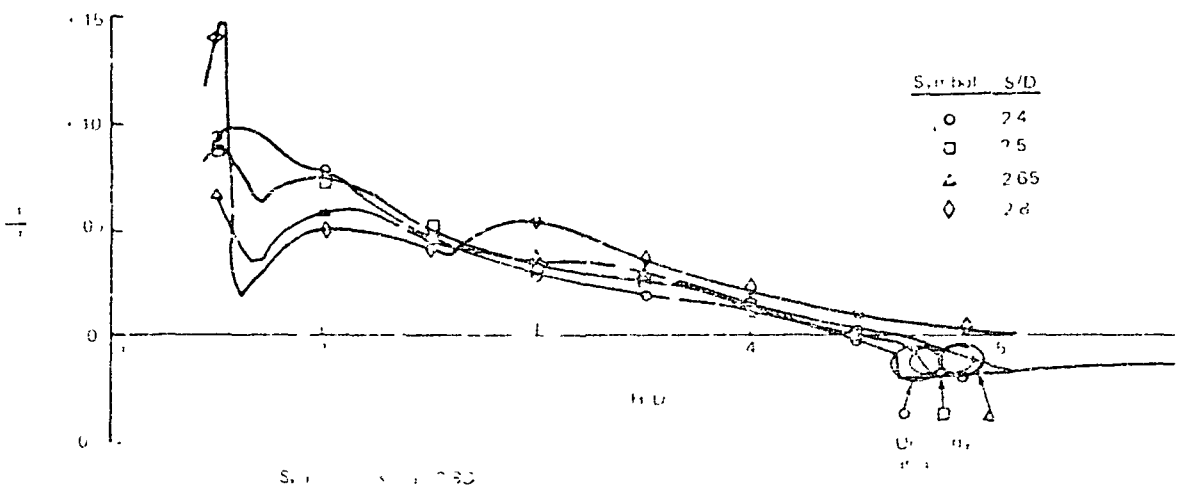

Figure 5-3. - Concluded

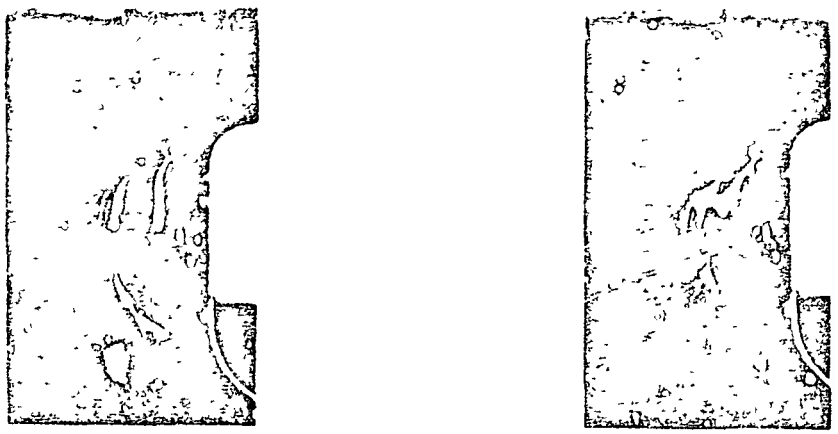

Figure 5-4. Flow visualization of upwash on fuselage.

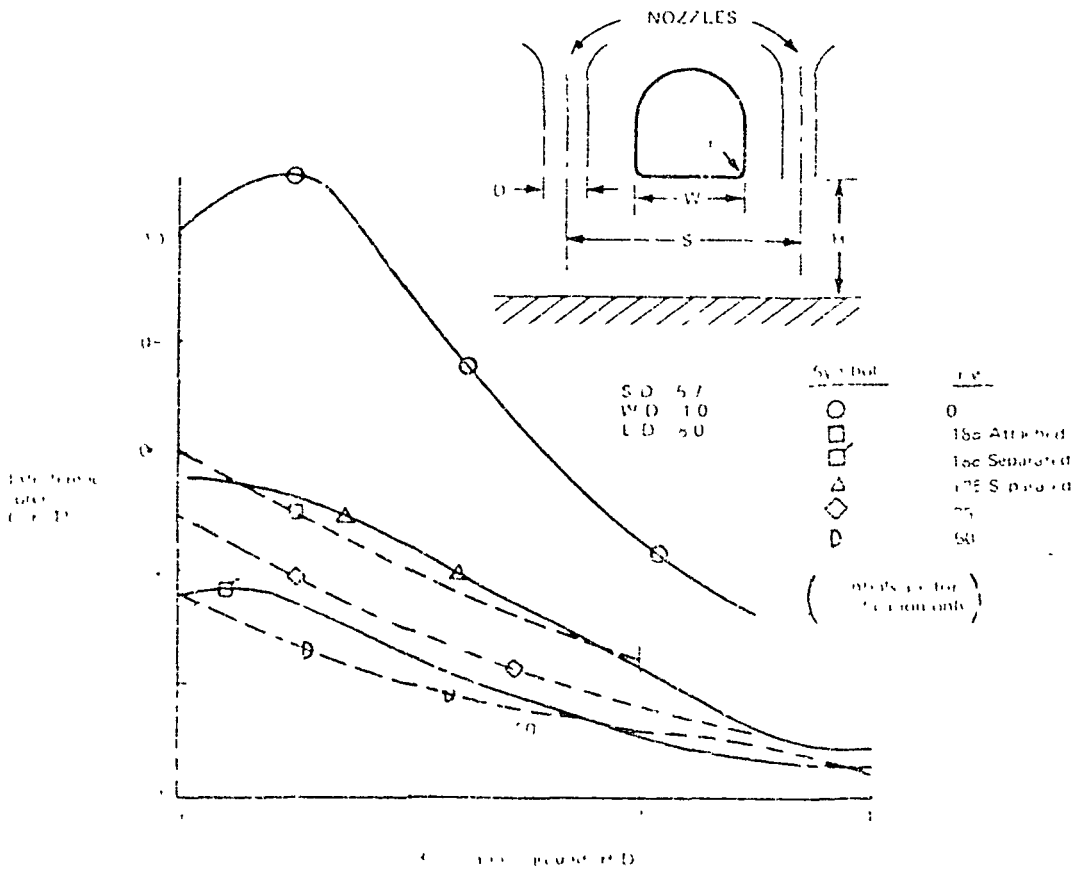

Figure 5-5. Effect of corner radius on lateral forces.

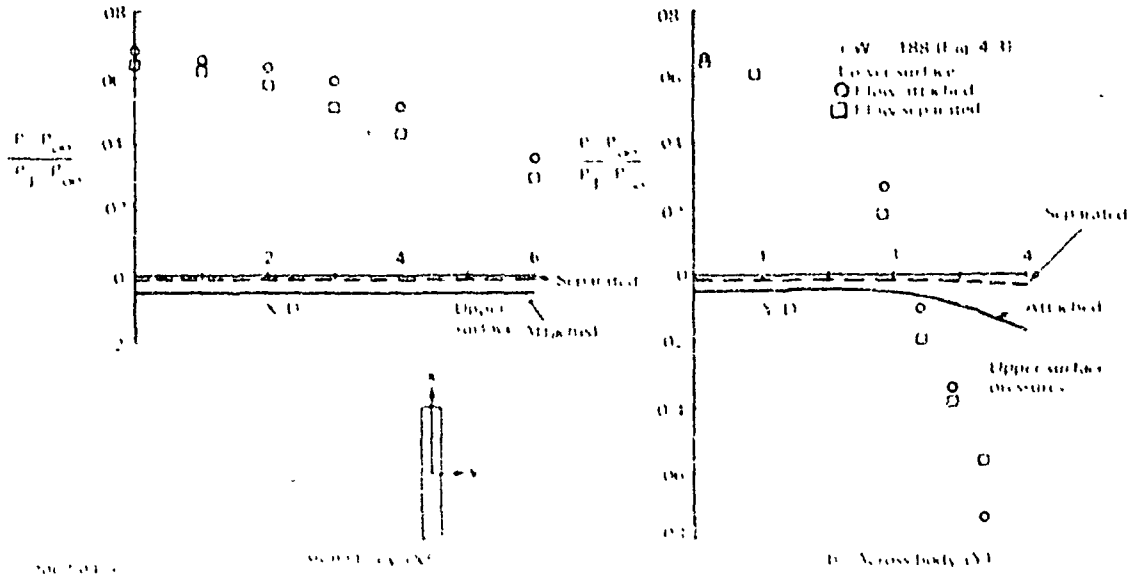

Figure 8-6. - Body pressure distribution.

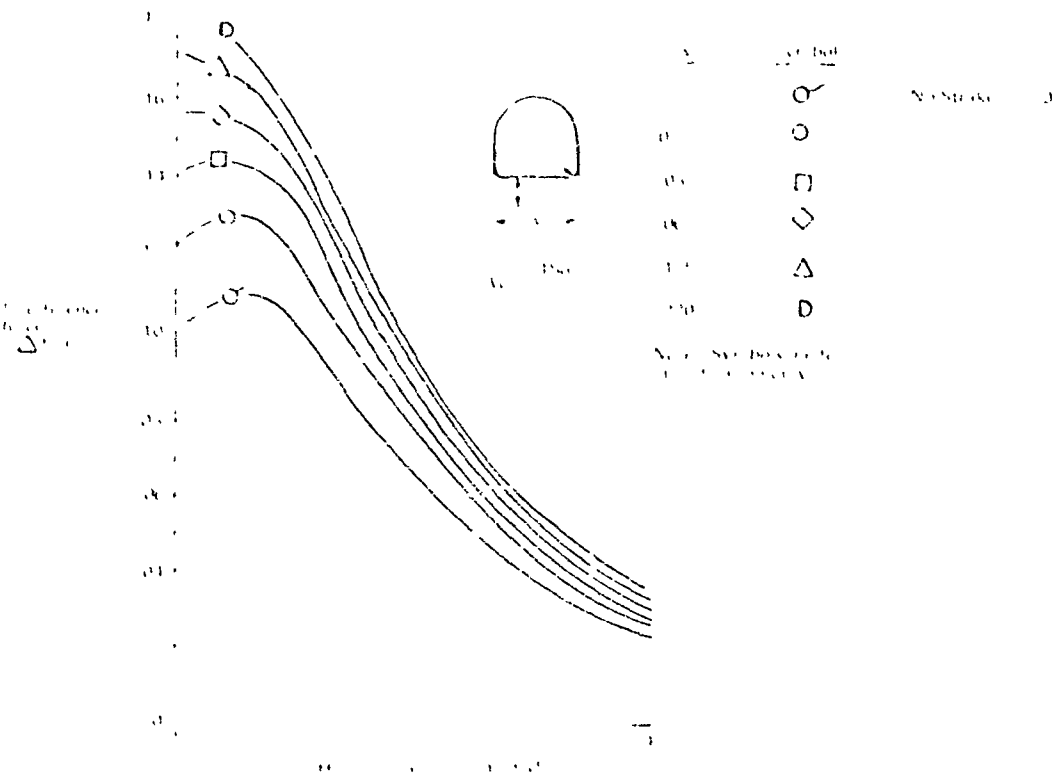

Figure 8-7. - Effect of trailing-edge flap deflection on base drag forces.

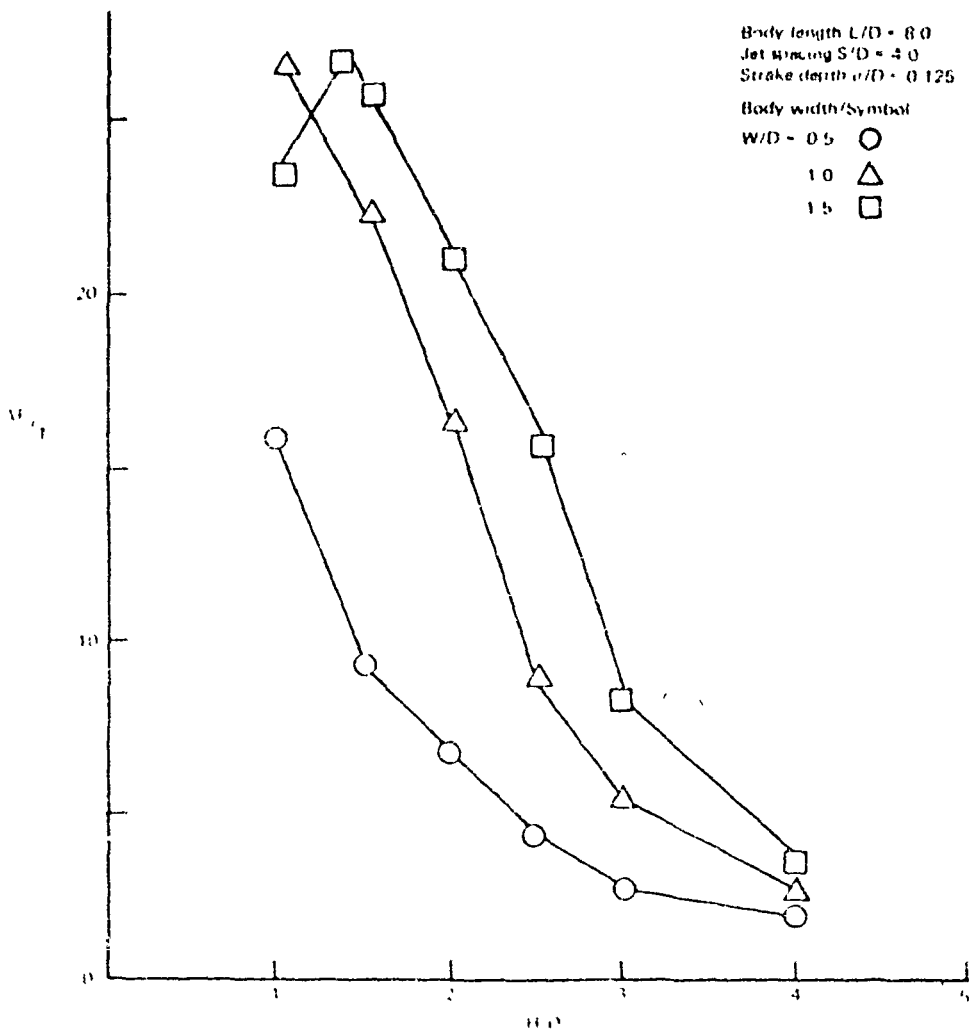

Figure 4-5. - Effect of body width on interference force.

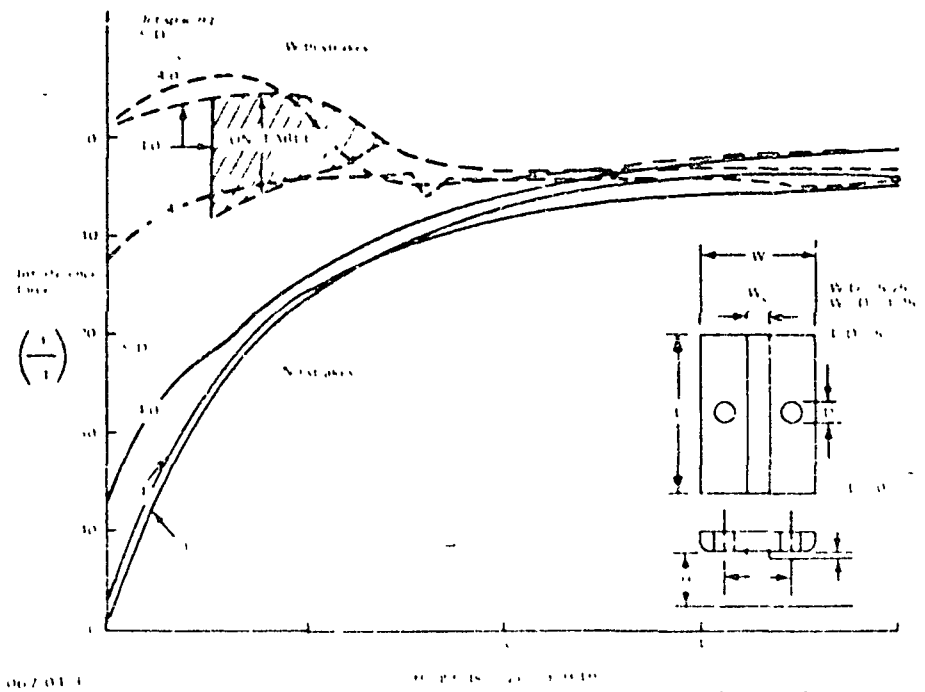

Figure S-9. - Interference forces on rectangular body.

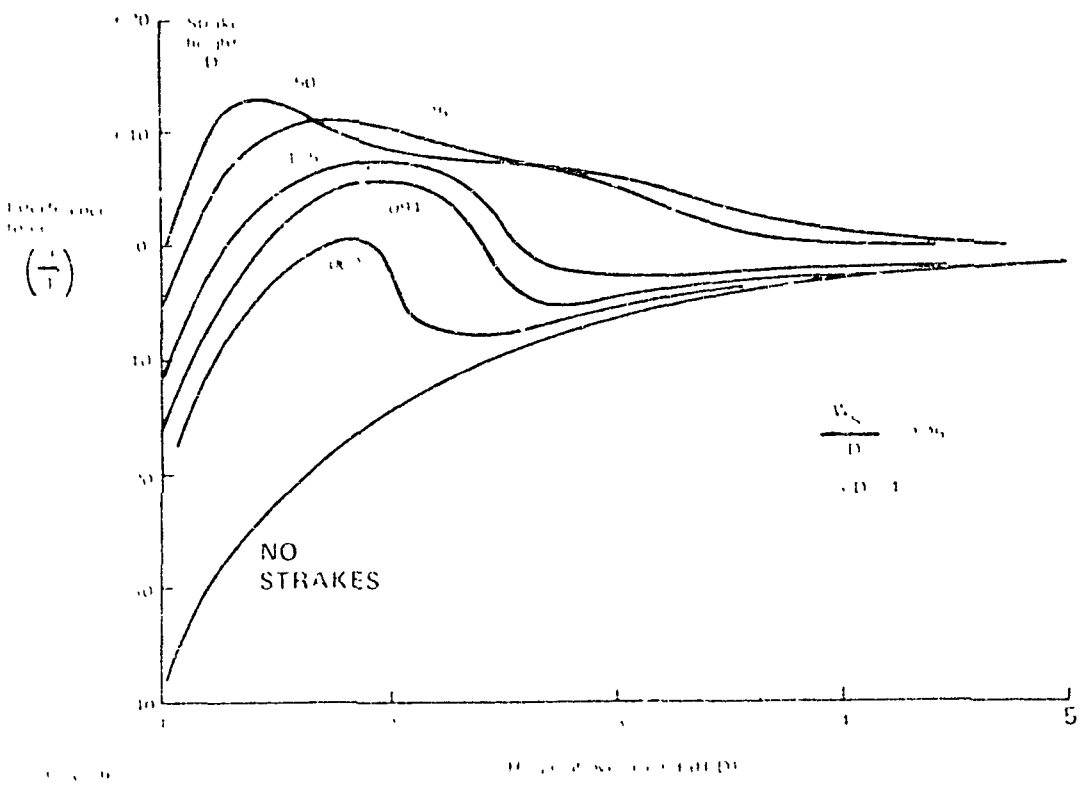

Figure S-10. - Strake height effect on rectangular body.

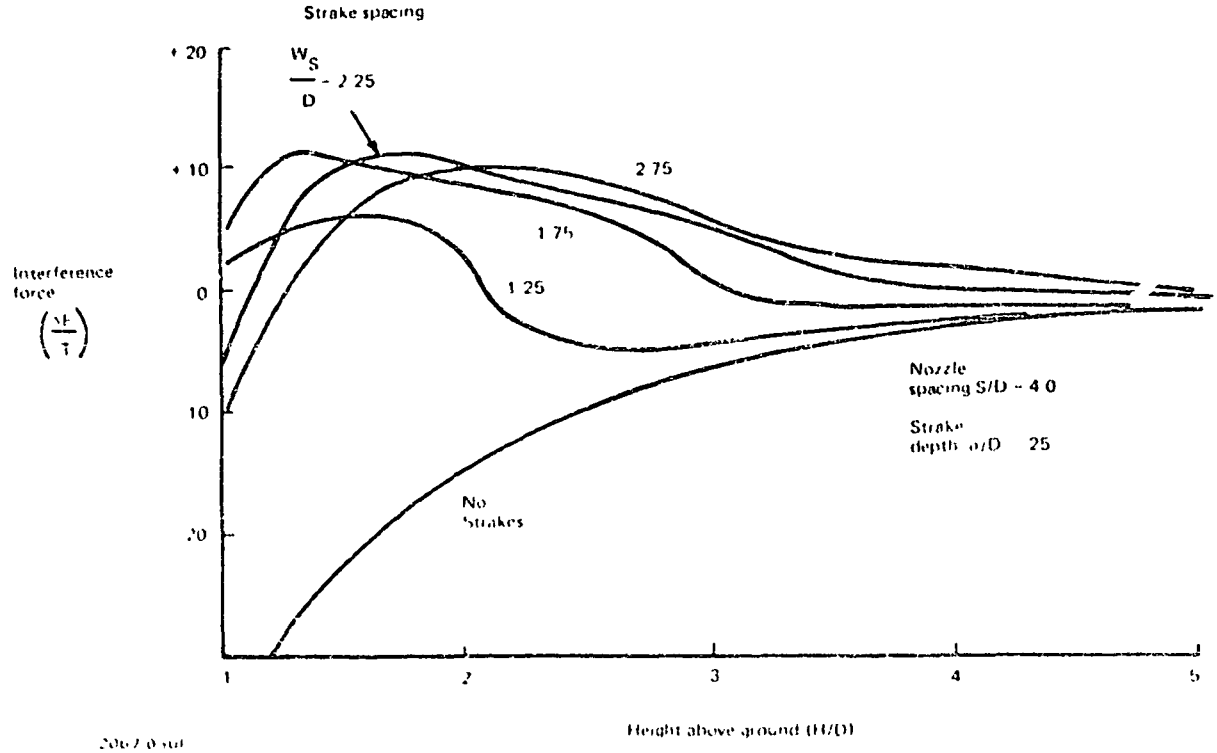

Figure 8-11. - Strake Location effect on rectangular body

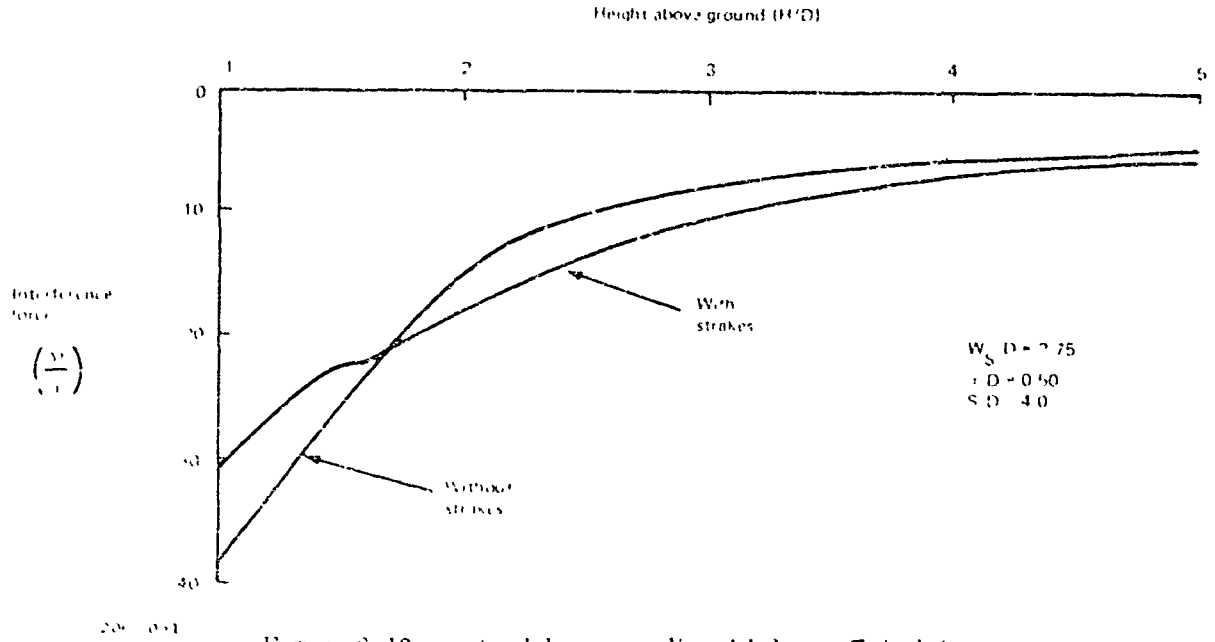

Figure 8-12. - Suckdown results with large flat plate.

9. THE DEVELOPMENT OF A THEORETICAL MODEL

The problem of single vertical axially symmetric jet impingement has been studied both experimentally and theoretically by many investigators. A survey of some of the pertinent literature can be found in Ref. 9 with a sketch of the basic flow shown in Fig. 9-1. Downstream of the nozzle there is a velocity decay region due to turbulent mixing followed by a stagnation region on the ground plane and deflection parallel to the ground plane until the pressure returns to ambient. At that point the velocity is a maximum. Turbulent mixing will then govern the behavior of the radial wall jet.

The impingement region has been treated theoretically for an inviscid irrotational or uniform incident profile (e.g., Ref. 10, 11, 12). An analytic inviscid solution (i.e., Euler Eqs.) was generated for the impingement region due to a rotational or fully developed incident profile in Ref. 13. More recently, numerical solutions have been generated for the rotational inviscid impingement problem using a frozen vorticity concept (Ref. 14). These approaches, although theoretically sound, have deficiencies when compared to experimental data even when coupled with a boundary layer analysis. For example, any inviscid solution of the impingement region will yield a wall jet growth that is inversely proportional to the radial distance from the stagnation point and a maximum velocity along the wall equal to the maximum velocity of the incident profile. This behavior is never quite achieved in the physical flow. No adequate theoretical analysis is available that couples the jet decay, impingement region, and resultant turbulent wall jet.

In the present study semi-empirical models are formulated for each region and coupled together to simulate the physical flow. Momentum is conserved and the empirical input to each region is well defined and capable of experimental verification.

The establishment of a vertical jet impingement model is the basis for the behavior of two jets impinging on a ground plane. A sketch of the flow problem is shown in Figure 9-2. Figure 9-2(a) shows the vertical plane containing the jet stagnation points and the ground plane. Each jet impinges on the ground plane and deflects to form wall jets. The wall jets then interact and form an upwash deflection zone where the wall jets collide and are turned upward leaving the ground plane. The stagnation line lies on the ground in the vertical plane of symmetry between the two impinging jets. The

maximum upwash stagnation pressure occurs at the midpoint of the line connecting the two jet stagnation points on the ground. The ground pressure then drops off with lateral distance along the stagnation line. Figure 9-2(b) shows the radial streamline pattern that has been observed (Ref. 3) both in the ground plane and in the vertical plane of symmetry between the two jets. This flow situation only exists when the jets are spaced far enough apart so that the jet impingement zone does not interact or has a negligible effect on the upwash deflection zone.

Figure 9-3 shows a sketch of the flow pattern when the jets have a spacing such that the jet impingement pressure recovery is not achieved before the upwash deflection occurs. In this situation, some of the wall jet streamlines interact with the upwash deflection zone so that ambient pressure is not achieved along the entire upwash deflection line. Hence, a boundary of minimum pressure occurs between the jet impingement and upwash deflection zones (Figure 9-3). This boundary is a result of the matching of the pressures in these two regions.

In general, the flow in the upwash sheet behaves as a free shear flow in that it exhibits typical turbulent mixing behavior for the decay of total pressure and velocity. Figure 9-4 shows a sketch based upon empirical observations of what may happen when the two jets are very close or just prior to coalescence into a merged jet with no upwash flow. Upwash flow does not exist in the vertical plane containing the jet stagnation points but does occur laterally. The streamlines are diverted about a zone of no upwash flow near the center of the upwash sheet.

It is the intent of this study to model the behavior of two closely spaced jets interacting to form an upwash sheet. Few investigators have attempted to study this problem in any detail (Ref. 3, 4, 5, 16 and 17) and little was known about the behavior of closely spaced jets prior to this study.

Although some results for the two jet impingement problem have been obtained by numerical integration of the Navier-Stokes equations, (Ref. 17), this type of approach certainly is not a practical approach at the current time. Turbulence modeling, changes in length scales, and boundary conditions, aside from computational time, pose formidable task in obtaining valid solutions of the Navier Stokes equations. Therefore a semi-empirical component modeling approach was taken as described below.

Jet Impingement Models

The jet impingement problem is subdivided into three major regions:

- Free jet decay
- Impingement or deflection
- Wall jet

Each of these finite regions are further subdivided into minor regions where the flow transitions from inviscid to turbulent behavior. For simplicity, a power function of the form,

$$f(\eta) = (1 - \eta\alpha)^{\beta}$$

is used to simulate both pressure and velocity behavior. This functional form was first used by Abramsvich (Ref. 18) for shear layers.

9.1 Free Jet Decay Model

Figure 9-5 shows a sketch of the basic jet decay model, subdivided into three regions:

- potential core
- transition
- fully turbulent

The half velocity boundary growth in each region can be determined largely from experimental data. The model assumes a simple linear boundary growth in each region.

Region I: $\frac{b_{jII}}{t_N} = a_{j_1}\left(\frac{z_j}{t_N}\right) + 1$

Region II: $\frac{b_{jII}}{t_N} = a_{j_2}\left(\frac{z_j}{t_N}\right) + b_{j_2}$

Region III: $\frac{b_{jII}}{t_N} = a_{j_3}\left(\frac{z_j}{t_N}\right)$

The constants governing the half velocity boundary growth in the transition and fully developed regions have been determined empirically. In addition, the potential core length and fully developed similarity exponent of the velocity profile must be specified.

The growth constant of the half-velocity boundary in the potential core region is determined by matching the boundaries at the end of the potential core.

$$a_{J_1} = \frac{(\omega_{J_2} - 1)}{(Z_{pc}/r_N)} + a_{J_2}$$

In addition, a linear decay in potential core radius, r_c, is assumed, or

$$\frac{r_c}{b_J} = 1 - \frac{Z_J}{Z_{pc}}$$

Further, the parameter Z_{JFD} is determined by matching the boundaries between the transition and fully developed regions.

$$\frac{Z_{FD}}{r_N} = \frac{b_{J_2}}{(a_{J_3} - a_{J_2})}$$

The static pressure in the jet at the nozzle exit is assumed to be ambient. The momentum equation can then be written as,

$$M_J = \pi\rho V_N^2 r_N^2 = \rho \int_0^{b_J} \int_0^{2\pi} V^2 r\, dr\, d\phi = \text{CONSTANT} \qquad (9\text{-}1)$$

$$\text{let} \quad \frac{V(r, Z)}{V_m(Z)} = f(\eta_J) \qquad \eta_J = \frac{r}{b_J(Z)}$$

Eq. 9-1 then reduces to:

$$\omega_J - 1 = \left(\frac{V_m}{V_N}\right)^2 \left(\frac{b_J}{r_N}\right)^2 C_{SV_J} \qquad (9\text{-}2)$$

where

$$C_{SV_J} = \int_0^1 f^2(\eta_J)\, \eta_J\, d\eta_J \qquad (9\text{-}3)$$

C_{SV_J} is an integral of the profile function. In the fully developed region this integral is assumed to be a constant.

The general form of the velocity profile is chosen as, (after Ref. 18),

$$\frac{V}{V_m} = f(\eta) = \left\{ 1 - \left(\frac{\eta_J - \eta_{JC}}{1 - \eta_{JC}} \right)^{\alpha_J} \right\}^2 \qquad (9\text{-}4)$$

where $\eta_{JC} = \frac{r_c}{b_J}$

Substituting into eq. 9-3 and integrating, yields

$$C_{SV_J}(\eta_{JC}, \alpha_J) = \frac{\eta_{JC}^2}{2} + (1 - \eta_{JC})^2 \left\{ \frac{1}{2} - \frac{4}{\alpha_J + 2} + \frac{3}{\alpha_J + 1} - \frac{4}{3\alpha_J + 2} + \frac{1}{4\alpha_J + 2} \right\}$$

$$+ \eta_{JC}(1 - \eta_{JC}) \left\{ 1 - \frac{4}{\alpha_J + 1} + \frac{6}{2\alpha_J + 1} - \frac{4}{3\alpha_J + 1} + \frac{1}{4\alpha_J + 1} \right\} \qquad (9\text{-}5)$$

which is a general expression for C_{SV_J} integral as a function of potential core radius and velocity exponent α_J.

The ratio of half velocity width to jet width can be determined from (9-4) as,

$$R_J = \frac{b_{JH}}{b_J} = \eta_{JC} + (1 - \eta_{JC}) \left(\frac{2 - \sqrt{2}}{2} \right)^{\frac{1}{\alpha_J}} \qquad (9\text{-}6)$$

9.1.1 Potential Core and Transition Region - The momentum equation 9-2, given that $V_m = V_N$, reduces to

$$\frac{R_J^2(\eta_{JC}, \alpha_J)}{2} \left(\frac{b_{JH}}{r_N} \right)^2 C_{SV_J}(\eta_{JC}, \alpha_J) \qquad (9\text{-}7)$$

where $\eta_{JC} = 1 - \frac{\ell}{\ell_{pc}}$

Thus, given η_{JC} and the half velocity boundary b_{JH}, the solution of equation (7) yields the exponent α_J governing the velocity profile in the potential core region.

The exponent α_{JPC} is known at $Z = Z_{pc}$. The fully developed exponent α_{JFD} is also given empirically for $Z \geq Z_{FD}$.

Thus, the velocity exponent α_J must vary accordingly in this region. By prescribing the condition that the jet half radius (b_J) must vary continuously from the end of the potential core region to its known value in the fully developed region, the transition exponent α_{JT} can be computed as

$$\alpha_{JT} = \frac{\ln\left(\frac{2-\sqrt{2}}{2}\right)}{\ln(b_{JH}/b_J)_T} \tag{9-8}$$

Thus, the momention equation (9-7), given $\eta_{JC} = 0$, can be used to determine the maximum velocity:

$$\frac{V_m}{V_N} = \frac{1}{\sqrt{2}} \frac{R_J(\alpha_{JT})\, C_{SV_J}(\alpha_{JT})}{(b_{JH}/r_N)} \tag{9-9}$$

9.1.2 Fully Developed Region - In this region similarity of the jet profile is assumed ($\alpha_{JFD} = 1.5$) and, thus, the ratio of half velocity width to jet radius and the similarity integral are constants. The velocity, as determined from equation (9-9), decays inversely proportional to the half width or Z.

Figure 9-6 shows a typical result for maximum velocity decay and boundary growth in the free jet compared with some test data from Ref. 19.

9.2 Jet Deflection Region

Figure 9-7 shows a sketch of the scaling parameters for the jet impingement problem. At some height, Δ_J, the incident jet "feels" the effect of the ground plane and the centerline velocity decreases and finally stagnates at the ground. The jet mixing is inhibited somewhat in the deceleration region, although the stagnation pressure is observed to be lower then the total pressure of the jet at the ground effect height Δ_J, due to the effects of mixing in the deceleration region. The impingement half velocity radius and half width will be used to further scale the wall jet regions.

The ground effect height has been determined experimentally and is given from reference 11 as,

$$\frac{\Delta_J}{d_N} = 1.2 \quad \text{for} \quad \frac{h}{d_N} < 6.8$$

$$\frac{\Delta_J}{d_N} = 0.153 \left(1 + \frac{h}{d_N}\right) \quad \text{for} \quad \frac{h}{d_N} > 6.8$$

The stagnation pressure is also given in reference 11 as,

$$\frac{\Delta P_S}{\Delta P_J} = \left(\frac{V_g}{V_N}\right)^2$$

where

$$\frac{V_g}{V_N} = \left(1.001 - .003 \frac{h}{d_N}\right) \quad \text{for} \quad \frac{h}{d_N} \leq 5.5$$

$$\frac{V_g}{V_N} = \left(1.35 - 0.066 \frac{h}{d_N}\right) \quad \text{for} \quad 5.5 \leq \frac{h}{d_N} \leq 10.0$$

and

$$\frac{V_g}{V_N} = \frac{7.37}{\left(0.67 + \frac{h}{d_N}\right)} \quad \text{for} \quad \frac{h}{d_N} > 10.0$$

The jet impingement radii are determined from the jet decay model. The impingement or deflection radius on the ground, r_o, is defined to be the location where the pressure in the ground plane reaches ambient conditions.

9.2.1 Ground Pressure Distribution. - The empirical input data requirements are. r_{JHi}, ΔP_S, r_o. The ground pressure recovery function is assumed to be of the form.

$$\frac{\Delta P}{\Delta P_S} \quad f_g(\eta) = \left(1 - (\eta_w)^{\alpha_g}\right)^4 \qquad (9\text{-}10)$$

where

$$\eta_w = \frac{r}{r_o}$$

A momentum balance is performed with the integral of the ground pressure equal to the momentum or thrust of the incident jet.

$$\frac{M_J}{4} = \int_0^{r_0} \int_0^{\pi/2} \Delta P \, r \, dr \, d\varphi$$

or $$1 \left(\frac{r_0}{r_N}\right)^2 \left(\frac{V_g}{V_N}\right)^2 \int_0^1 f_g(\eta_W)\eta_W \, d\eta_W$$

Let, $$C_{SPg}(\alpha_g) = \int_0^1 f_g(\eta_W)\eta_W \, d\eta_W$$

where $$C_{SPg}(\alpha_g) = \frac{1}{2} - \frac{1}{\alpha_g + 2} + \frac{3}{\alpha_g + 1} - \frac{4}{3\alpha_g + 2} + \frac{1}{1\alpha_g + 2}$$

$$C_{SPg}(\alpha_g) = \frac{1}{\left(\frac{r_0}{r_N}\right)^2 \left(\frac{V_g}{V_N}\right)^2} \qquad (9\text{-}11)$$

This equation yields the exponent α_g of the pressure recovery function that satisfies the momentum condition.

The deflection radius r_0 is estimated empirically and in nondimensional form

$$2.9 \simeq \frac{r_0}{r_{JH}} \simeq 3.6 \quad \text{for} \quad 1.2 \simeq \frac{h}{d_N} \simeq 3.0$$

$$\frac{r_0}{r_{JH}} \simeq 3.6 \quad \text{for} \quad \frac{h}{d_N} > 3.0$$

Figure 9-8 shows the kind of correlation achieved for the pressure distribution on the ground from this simple procedure. Unfortunately, the degree of success largely depends upon the chosen form of the pressure function, equation 9-10.

9.2.2 Wall Jet Transition Model. - The wall jet transition model consists of three subregions:

i) Inviscid deflection region where the effects of viscosity are assumed to be negligible except in a region close to the wall and near the edge of the deflected flow. In this region, the inner boundary layer is established as governed by axially symmetric stagnation flow.

ii) Transition region where the effects of viscosity are beginning to dominate and the inner boundary layer and outer shear flow transitions to the fully developed turbulent wall jet.

iii) Fully developed flow where the effects of turbulent viscosity dominate and the static pressure through the wall layer is considered ambient, or fully recovered. In this region, the nearly similar wall jet develops.

The inviscid deflection region is assumed to occur under the half velocity width (r_{JH}) of the incident jet profile. The pressure distribution on the ground was determined in a previous section as

$$\Delta P = \Delta P_S f_g(\eta_W) = \Delta P_S \left[1 - (\eta_W)^{a_g} \right]^1$$

The maximum velocity in this region can be predicted adequately from Bernoulli's equation as,

$$\frac{V_M}{V_g} = \sqrt{1 - f_g(\eta_W)} \qquad \text{where} \quad 0 \le \eta_W \le \frac{r_{JH}}{r_0} \tag{9-12}$$

The initial boundary layer thickness δ_s at the stagnation point is assumed to be both a function of nozzle height above ground and of Reynolds number. (Ref. 20). δ_s is assumed to be determined empirically. The determination of the maximum velocity variation is the only requirement of this region since the maximum total pressure is assumed constant.

A model must be established that matches the inviscid maximum velocity at the end of the inviscid region and transitions to a fully turbulent wall jet. Figure 9-9 shows a sketch of the wall jet transition boundary growth model. The model consists of two layers. The inner boundary layer flow and outer shear. The fully developed behavior of the boundary layer and half velocity width is assumed to be,

$$\frac{b_{WH}}{r_N} = a_{W_2} \left(\frac{r}{r_N} \right)^{\beta_S} \qquad (9\text{-}13)$$

and $$\frac{\delta_{bL}}{d_N} = a_{bL_2} \left(\frac{r}{d_N} - 1 \right)^{\beta_{bL}}$$

For simplicity, β_s and $\beta_{bL} \cong 1$.

The form of the boundary layer growth arises from experimental observation (Ref. 20). The thickness of the boundary layer appears to be relatively constant in the vicinity of the stagnation point or in the inviscid deflection region. The boundary layer grows relatively slowly until pressure recovery takes place and then the boundary layer grows with radial distance from the stagnation point. This delay in boundary layer growth is the reason for the choice of the above function which precludes the establishment of complete similarity in the wall jet profile.

The empirical constants for the fully developed wall layer growth are approximately, (Ref. 20)

$$a_{W_2} \cong .09$$

$$a_{bL_2} \cong .0175$$

Thus, the limit of the ratio of the boundary layer height to the half velocity point in the shear layer is,

$$\lim_{r \to \infty} K_{\delta H} = \frac{\delta_{bL}}{b_{WH}} = .1944$$

This value is in agreement with other investigators (Ref. 21).

The more ambiguous value of K_δ in the limit can be computed from,

$$K_\delta \frac{K_{\delta H} \left(\frac{r - r_N}{r} \right)^{\frac{1}{a_{WHD}}}}{1 - K_{\delta H} \left[\left(\frac{r - r_N}{r} \right)^{\frac{1}{a_{WHD}}} - 1 \right]} = .0962 \quad \text{where} \quad a_{WFd} =$$

which is slightly smaller than the often quoted value of 1/9 and may be the result of the finite form of the chosen profile.

9.2.3 Velocity and Static Pressure Profiles. - Figure 9-10 shows a sketch of the two layer model chosen to represent the velocity and static pressure profiles in the developing wall layer. The inner boundary layer velocity profile is approximated by the well known turbulent power law,

$$\frac{V(r, Z)}{V_m(r)} = \left(\frac{\zeta}{k_\delta}\right)^{\frac{1}{N}} \quad \text{where} \quad \zeta = \frac{Z}{b_W} \tag{9-14}$$

and $$k_\delta = \frac{\delta_{bL}}{b_W} \quad \text{for} \quad 0 \le \zeta \le \frac{\delta_{bL}}{b_W}$$

The static pressure across the boundary layer is assumed constant, or

$$\frac{\Delta P(r, Z)}{\Delta P_m(r)} = 1$$

The outer shear layer profiles are approximated by the functions,

$$\frac{V(r, Z)}{V_m(r)} = \left\{1 - \left(\frac{\zeta - k_\delta}{1 - k_\delta}\right)^{a_W}\right\}^{\frac{1}{2}} \tag{9-15}$$

and $$\frac{\Delta P(r, Z)}{\Delta P_m(r)} = \left\{1 - \left(\frac{\zeta - k_\delta}{1 - k_\delta}\right)^{a_W}\right\}^{1}$$

The ratio of the half velocity height to the wall layer height can be determined by,

$$R_W = \frac{b_{WH}}{b_W} = k_\delta + (1 - k_\delta)\left(\frac{\frac{1}{2} - k_\delta}{1}\right)^{\frac{1}{a_W}} \tag{9-16}$$

9.2.4 Radial Momentum Flux Equation. - The governing equation for the flow in the wall jet is formulated as a radial momentum flux equation

By an inviscid flow solution of the exact rotational equations (Ref. 14) it can be shown, from the far field analytical solution, that the maximum of the momentum

flux in any wall jet sector summed over 2π is exactly equal to the thrust of the incident jet. This is the basic principle used to construct the following equation where a pressure term has been added to account for the static pressure variation in the deflection region.

$$M_r = \frac{M_J}{2\pi} f_M(\eta_W) f_{MVIS}(r) = \int_0^{b_W} \{\rho V^2(r, Z) + \Delta P(r, Z)\} r dZ \qquad (9\text{-}17)$$

The above equation applies both to the transition region and fully developed wall jet. In the transition region, a static pressure variation exists in the wall layer due to the streamline deflection and hence the pressure term on the RHS of this equation. Because of the streamline deflection, the momentum flux in the radial direction does not achieve its constant optimum value until pressure recovery occurs. The function $f_M(\eta_W)$ on the LHS reflects the change of radial momentum in the deflection region.

Hence, the behavior of this function must be such that,

$$f_M(0) = 0$$

and $$f_M(r) = 1 \quad \text{for} \quad r \geq r_0$$

The second function $f_{M_{VIS}}$ on the LHS of this equation is a term reflecting the losses in momentum due to skin friction or shear at the wall. This term becomes important at large distances from the stagnation point. Its behavior can be approximated by,

$$f_{MVIS}(r) = \frac{1}{\left(\frac{r}{r_N}\right)^{\alpha_{VIS}}} \quad \text{where } \alpha_{VIS} \sim .15 - .25$$

In parametric form the radial momentum flux eq. (9-17) can be further expressed as,

$$f_M(\eta_W) f_{MVIS}(r) = \left(\frac{r}{r_N}\right)\left(\frac{b_W}{r_N}\right) \frac{1}{I}\left(\frac{V_M}{V_N}\right)^2 \int_0^1 I_V(\zeta, k_\delta, N, \sigma_W) d\zeta$$

$$\frac{1}{2}\left(\frac{V_s}{V_N}\right)^2 I_s(\eta_W) \int_0^1 I_P(\zeta, k_\delta, \sigma_W) d\zeta \Big] \qquad (9\text{-}18)$$

The integrals of the velocity squared and pressure profile functions vary with radial distance, or

$$C_{SWV}(r) = \int_0^1 F_V(\xi, K_\delta, N, \alpha_W)\, d\xi$$

$$C_{SWP}(r) = \int_0^1 F_P(\xi, K_\delta, \alpha_W)\, d\xi$$

Integration of the profile functions, 9-11 and 9-15 yield,

$$C_{SWV}(r) = \left(\frac{N}{2+N}\right) K_\delta + (1 - K_\delta)\, I(\alpha_W)$$

$$C_{SWP}(r) = K_\delta + (1 - K_\delta)\, I(\alpha_W) \qquad (9\text{-}19)$$

where

$$I(\alpha_W) = 1 - \frac{1}{\alpha_W + 1} + \frac{6}{2\alpha_W + 1} - \frac{4}{3\alpha_W + 1} + \frac{1}{4\alpha_W + 1}$$

In these equations α_W and K_δ are functions of r.

The momentum flux equation can then be rewritten as,

$$f_M(\eta_W) H_{MVIS}(r) = \left(\frac{2}{R_W}\right)\left(\frac{r}{r_N}\right)\left(\frac{b_{WH}}{r_N}\right)\left(\frac{V_m}{V_N}\right)^2 C_{SWV} + \frac{1}{2}\left(\frac{V_s}{V_N}\right)^2 f_g(\eta_W)\, C_{SWP} \qquad (9\text{-}20)$$

As mentioned previously, the radial momentum function $f_M(\eta_W)$ is related to the pressure recovery in the deflection region. The approximation is now introduced that the radial momentum flux is related to the pressure recovery function $f_g(\eta_W)$ by,

$$f_M(\eta_W) = 1 - f_g(\eta_W) \qquad (9\text{-}21)$$

The behavior of this function is such that when pressure recovery occurs at the wall all of the streamlines in the layer are assumed parallel to the wall.

The maximum velocity at the start of the wall jet at $r = r_{JHi}$ is given by the inviscid Bernoulli equation,

$$\left(\frac{V_m}{V_N}\right)^2_{INV} = \left(\frac{V_E}{V_N}\right)^2 (1 - f_E(\eta_i)) \text{ where } \eta_i = \frac{r_{JHi}}{r_0} \tag{9-22}$$

The initial boundary layer thickness δ_s is assumed constant throughout the inviscid region. The initial height of the wall layer is estimated to be the ground effect height Δ_J. Thus, K_δ has an initial value given by,

$$K_{\delta 1} = \frac{\delta_s}{\Delta_J} \quad \text{at} \quad r = r_{JHi}$$

Given the inviscid starting maximum velocity, the momentum flux equation can be solved for the initial half velocity width b_{WHi} of the profile as

$$\frac{b_{WHi}}{r_N} = \frac{f_M(\eta_{W1})\, R_W(\alpha_{W1})}{2\left(\frac{r_{JHi}}{r_N}\right)\left[\left(\frac{V_m}{V_N}\right)^2_{INV} C_{SW1}(\alpha_{W1}) + \frac{1}{2}\left(\frac{V_E}{V_N}\right)^2 f_E(\eta_{W1})\, C_{SWP}(\alpha_{W1})\right]} \tag{9-23}$$

where $\eta_{W1} = \frac{r_{JHi}}{r_0}$ and $f_{MVIS}(r_{JHi}) = 1$

The velocity profile expression also yields,

$$b_{WHi} = b_{W1}\left[1 + K_\delta (1 - K_\delta)\left(\frac{2 - \sqrt{2}}{2}\right)^{\frac{1}{\alpha_W}}\right] \tag{9-24}$$

Given initial values of $K_{\delta 1}$, b_{W1}, δ_s, $7 \le N_1 \le 15$, and $\left(\frac{V_m}{V_n}\right)_{INV}$; the above two equations have the two unknowns b_{WHi} and α_{Wi}. The solution of eqs. 9-23 and 9-24 yields the initial starting profile for the wall layer.

Figure 9-11 shows a comparison between the initial profile predicted by this method and the exact solution for an inviscid rotational fully developed impinging jet at some distance beyond the deflection region as given in Ref. 11. This simple procedure yields an inviscid starting profile not unlike that of the exact inviscid solution.

To compute the maximum velocity variation and boundary along the wall, a fully developed value of the exponent c_w must be prescribed. This value is chosen to be $\alpha_{wfd} = 1.5$ after Abramovich (Ref. 18). The turbulent wall exponent N must also be prescribed throughout the wall layer and has experimental values ranging from

$$7 \leq N \leq 15$$

The value of 7 is chosen to be the fully developed value at the end of the impingement region. The variation of the exponent α_w throughout the deflection region has to be prescribed with the boundary values given by,

$$\alpha_w = \alpha_{wi} \text{ at } r = r_{Jin}$$

$$\alpha_w = \alpha_{FD} \text{ at } r \geq r_o$$

Due to a lack of empirical or theoretical evidence in regard to the behavior of the profile in the deflection region, a simple linear variation of the exponent was assumed.

The half velocity height is determined for the initial profile and its behavior at the end of the deflection region is also known. Hence, the half velocity behavior assumes a simple linear variation matched to the fully developed height at the end of the deflection region.

The maximum velocity in the deflection region can then be computed as,

$$\frac{V_m}{V_\infty} = \frac{1}{C_{SW}} \left(\frac{F_W[1 - \cos(\theta_W)]_{MIS}(\alpha)}{2\left(\frac{r}{r_\infty}\right)\left(\frac{D_W}{r_\infty}\right)} - \frac{1}{2}\left(\frac{V_s}{V_\infty}\right)^2 \cos(\theta_W) C_{SW} \right)^{1/2} \quad (9\text{-}25)$$

$$\text{for } r_{Jin} \leq r \leq r_o$$

In the fully developed wall layer, this expression reduces to,

$$\frac{V_m}{V_N} = \frac{1}{\sqrt{C_{SWV}}} \left(\frac{R_W f_{MVIS}(r)}{2\left(\frac{r}{r_N}\right)\left(\frac{b_{WH}}{r_N}\right)} \right)^{1/2} \quad \text{for} \quad r > r_0 \tag{9-26}$$

Figure 9-12 shows a typical numerical result for the boundary layer thickness, as a ratio with respect to both the wall half-velocity thickness and layer height. Figure 9-13 shows a typical variation of the wall jet profile as a function of radial distance. The variation is relatively insignificant and becomes very nearly similar as the radial distance increases. Figure 9-14 shows a typical overall result from the wall jet transition model in terms of layer thicknesses, ground pressure, and maximum velocity along the wall. Figure 9-15 shows a comparison with the data of ref. 20 of the maximum velocity variation for different nozzle heights. Generally good agreement is achieved. In comparison, the level of maximum inviscid ground velocity at each nozzle height is also marked off.

9.3 Two-Jet Interaction Model

Figure 9-16 shows a sketch of the ground plane coordinate systems for the two jet impingement interaction problem. The jets stagnate on the ground, deflect into radial wall jets and collide along their plane of symmetry. The formation of an upwash stagnation zone is a result of the upward deflection of the wall jet flow. The point Su, on the line joining the jet centers, is the only true stagnation point where the flow comes to rest and deflects vertically. At points off of the center, the flow is deflected at an angle such that the pressure is representative of the stagnation of the normal component of the maximum wall jet velocity. The flow continues radially after deflection into the upwash sheet as has been observed experimentally.

9.3.1 Maximum Pressure Distribution along the Upwash Stagnation Line. To estimate the upwash stagnation line ground pressure distribution the normal velocity at the stagnation line must be computed.

$$V_{NORM} = V_{n,W} \cos\alpha_u \tag{9-26}$$

The pressure is then, simply,

$$\Delta P_{umg} = \frac{1}{2}\rho V^2_{NORM} = \frac{1}{2}\rho V^2_{mW}\cos^2\varphi_u \qquad (9\text{-}27)$$

$$\text{or} \qquad \frac{\Delta P_{umg}}{\Delta P_J} = \left(\frac{V_{mW}}{V_N}\right)^2 \cos^2\varphi_u - \left(\frac{V_{mW}}{V_N}\right)^2 \left[\frac{1}{1 + \left(\frac{X}{S_2}\right)^2}\right]$$

Figure 9-17 shows some typical results compared with test data, for the maximum stagnation point pressure on the ground (as computed from the wall jet transition model) as a function of jet spacing. Fairly good agreement is achieved down to a jet spacing of two diameters as a result of the transition model. For comparison, the fully developed wall jet decay is extrapolated back and yields much higher pressures than the test data indicate.

In general, the wall jet transition model must be used to compute the maximum velocity along the stagnation line for close jet spacing. For a jet spacing, s/d, large enough such that the wall jet is fully developed and the jet deflection regions do not interact with the upwash deflection zone, a simple expression can be derived to predict the maximum pressures along the stagnation line.

Under these conditions, the wall jet maximum velocity can be written as,

$$\left(\frac{V_{mW}}{V_N}\right)^2 \quad \frac{a_{WFD}}{\left(\frac{r}{r_N}\right)^{(2\ -\ a_{VIS})}}$$

where $a_{WFD} \quad \frac{R_W\ a_{VIS}}{2\ s_{WN}\ r_W}$

(9-28)

$$\text{or} \quad \left(\frac{V_{mW}}{V_N}\right)^2 \quad \frac{a_{WFD}}{\left(\frac{S_2}{r_N}\right)^{(2\ -\ a_{VIS})}} \left[\cos\varphi_u\right]^{(2\ -\ a_{VIS})}$$

Thus, $$\frac{\Delta P_{umg}}{\Delta P_J} = \frac{a_{WFD}}{\left(\frac{S_2}{r_N}\right)^{(2+\alpha_{VIS})}} \left|\cos\varphi_u\right|^{(1+\alpha_{VIS})}$$

or where $\alpha_{vis} \cong .24$

$$\frac{\Delta P_{umg}}{\Delta P_J} = \frac{a_{WFD}}{\left(\frac{S_2}{r_N}\right)^{(2+\alpha_{VIS})}} \frac{1}{\left[1+\left(\frac{X}{S_2}\right)^2\right]^{\left(2+\frac{\alpha_{VIS}}{2}\right)}} \qquad (9\text{-}29)$$

If this expression is further nondimensionalized by the stagnation point pressure at x = 0,

$$\frac{\Delta P_{umg}}{\Delta P_{umg}(X=0)} = \frac{1}{\left[1+\left(\frac{X}{S_2}\right)^2\right]^{\left(2+\frac{\alpha_{VIS}}{2}\right)}} \qquad (9\text{-}30)$$

or, since $S_2 = \frac{S}{2}$,

$$\frac{\Delta P_{umg}}{\Delta P_{umg}(X=0)} = \frac{1}{\left[1+\left(\frac{X}{S}\right)^2\right]^{\left(2+\frac{\alpha_{VIS}}{2}\right)}} \qquad (9\text{-}31)$$

Figure 9-18 shows the computed results in comparison with test data for several jet spacings. The above expressions correspond to the larger jet spacings. For the closer jet spacings, equation (9-27) is modified slightly to account for the static pressure variation in the deflection region, or,

$$\frac{\Delta P_{umg}}{\Delta P_{SJ}} = f_g(\eta_{WS}) \left(\frac{X_{mW}}{X}\right)^2 \cos^2\varphi_u \qquad (9\text{-}32)$$

where $$\eta_{WS} = \frac{\sqrt{X^2 - S_2^2}}{r_0}$$

For $\eta_{WS} \geq 1$, the above expression reduces to the original equation (9-27).

The correlation is very good for spacings above 3.5. For closer jet spacings, the model yields slightly higher pressures along the stagnation line.

9.3.2 Model of Upwash Deflection Zone Without Jet Deflection Zone Interaction. - In this section, a model for the ground pressure distribution of the upwash deflection zone is developed for the problem of large jet spacings. When the jet spacing is large enough, such that the jets deflect into radial wall jets prior to interaction, an upwash deflection zone of high pressures develop. This zone is demarcated by a line of ambient pressures. External to this line ambient pressures exist in the wall jet and internal to this line ($y<y_u$) the wall jet begins to deflect upward and, hence, develops the upwash deflection zone.

The ground pressures in the upwash deflection zone exert a force on the ground plane equal to the normal momentum of the entire upwash sheet. The normal momentum of the upwash sheet, assuming a radial streamline pattern emanating from the jet stagnation point, can be computed simply as

$$\frac{M_{UN}}{4} = \int_0^{\pi/2} \frac{M_J}{2\pi} \cos\varphi_u \, d\varphi_u \quad \frac{M_J}{2\pi} \tag{9-33}$$

for one quadrant of the upwash sheet. In this expression, the momentum of the incident jet is divided only per unit radian into the wall jet and finally into the upwash sheet. The normal momentum of the entire upwash sheet is then equal to $\frac{2M_J}{\pi}$

or, roughly, 64% of the momentum of one of the jets.

Equating the normal momentum of the upwash sheet to the upwash zone pressure distribution, yields the following expression:

$$M_{UN} = \frac{M_J}{2\pi} \int_0^{y_{u\infty}} \int_0^{\infty} \Delta P_{u2} \, dx \, dy \tag{9-34}$$

Relating this expression to the cylindrical ground coordinate system of an incident jet (see fig. 9-16), and noting that

$$x = S_2 \tan\varphi_u$$

$$dx = S_2 \sec^2\varphi_u \, d\varphi_u$$

the above expression becomes,

$$\frac{M_J}{2\pi} = S_2 \int_0^{y_{u\infty}} \int_0^{\pi/2} \Delta P_{ug} \sec^2\varphi_u \, d\varphi_u \, dy \tag{9-35}$$

or,

$$1 - \frac{S_2}{r_\lambda^2} \int_0^{y_{u\infty}} \int_0^{\pi/2} \left(\frac{\Delta P_{ug}}{\Delta P_{SJ}} \right) \sec^2\omega_u \, d\varphi_u \, dy$$

To develop this expression further, a pressure function must be assumed across the upwash zone at any location λ or angle ϕ_u.

$$\frac{\Delta P_{ug}}{\Delta P_{SJ}} \quad \frac{\Delta P_{umg}}{\Delta P_{SJ}} \; f(\eta_{ug}) \tag{9-36}$$

where $f(\eta_{ug}) \left[1 - (\eta_{ug})^{n_{ug}} \right]^{1}$ and $\eta_{ug} = \frac{r}{r_u(\varphi_u)}$

The expression for ΔP_{umg} along the stagnation line was developed previously, eq. 9-28. Substituting all this into eq. (9-35), and noting that

$$dy = r_u(\varphi_u) \, d\eta_{ug}, \text{ yields,}$$

$$1 - \left(\frac{S_2}{r_\lambda} \right) \frac{(W+1)}{(2 - \alpha_{VIS})} \int_0^{\pi/2} \int_0^1 (\cos\varphi_u)^{(2 - \alpha_{VIS})} \frac{r_u(\varphi_u)}{r_\lambda} f(\eta_{ug}) \, d\eta_{ug} \, d\varphi_u$$

$$\left(\frac{S_2}{r_\lambda} \right) \tag{9-37}$$

let $C_{sug} = \int_0^1 f(\eta_{ug})\, d\eta_{ug}$ be the profile integral for the ground pressure distribution.

Now,

$$1 = \left(\frac{S_2}{r_N}\right) \frac{a_{WFD}\, C_{sug}}{\left(\frac{S_2}{r_N}\right)^{(2+\alpha_{VIS})}} \int_0^{\pi/2} [\cos\varphi_u]^{(2+\alpha_{VIS})} \frac{y_u(\varphi_u)}{r_N}\, d\varphi_u \qquad (9\text{-}38)$$

An hypothesis about the behavior of the upwash zone must now be introduced into eq. (9-38), as,

$$\frac{y_u(\varphi_u)}{r_N} = \frac{C_u \left(\frac{S_2}{r_N}\right)}{\cos\varphi_u} \qquad (9\text{-}39)$$

This expression says that the upwash zone becomes infinite in width and the radial distance to the stagnation line also becomes infinite as $\phi_u \to \pi/2$. Hence, the mass in the wall jet also approaches infinity. At the same time, the stagnation line pressure approaches zero. Substituting eq. (9-39) into the integral expression eq. (9-38) yields a finite integral.

$$1 = \left(\frac{S_2}{r_N}\right)^2 \frac{a_{WFD} C_u C_{sug}}{\left(\frac{S_2}{r_N}\right)^{(2+\alpha_{VIS})}} \int_0^{\pi/2} [\cos\varphi_u]^{(1+\alpha_{VIS})}\, d\varphi_u \qquad (9\text{-}40)$$

To derive a simple expression for the upwash zone, using eq. (9-10, and making the further assumption that there are no momentum losses in the wall jet, or

$$\alpha_{VIS} = 0$$

the following expression can be used to estimate the width of the upwash zone,

$$C_u = \frac{1}{a_{WFD} C_{sug}} \frac{2 C_{SAV} a_{W2}}{R_W C_{sug}} \qquad (9\text{-}41)$$

Thus, the initial upwash width is proportional to the jet spacing and depends on the similarity constants for the velocity squared wall jet profile and upwash ground pressure profile as well as the slope of the wall jet half velocity growth. If it is further assumed that the exponent α_{ug} of the ground pressure profile is 1.5, an estimate can be made of the initial width of the upwash zone. Assuming a fully developed and nearly similar wall jet flow, or $K_\delta = .0962$, $\alpha_{WFD} = 1.5$, and $N = 7$,

$$C_{swv} = .36$$

$$a_{w2} = .09$$

$$R_w = .49481$$

$$C_{sug} = .3156$$

Hence, $C_u \cong .415$ and

$$\frac{y_u(\varphi)}{r_N} \sim 0.415 \left(\frac{S_2}{r_N}\right) \frac{1}{\cos\varphi_u} \qquad (9\text{-}42)$$

For example, at a spacing $S/d_N = 6$, the entire width of the upwash deflection zone along the line connecting the jet stagnation points is approximately 2.4 nozzle diameters. A more realistic or representative boundary for the upwash deflection zone might be the half pressure boundary which can be easily computed as,

$$\frac{y_{uHP}(\varphi)}{r_N} \sim \frac{0.122}{\cos\varphi_u} \left(\frac{S_2}{r_N}\right) \qquad (9\text{-}43)$$

9.3.3 Upwash Momentum Models for Close - Jet Interaction. - To further estimate the behavior of the upwash zone on the ground and upwash sheet for closer jet spacings, a model for the behavior of the momentum in the upwash sheet must be hypothesized. As the jets are spaced closer, their boundaries begin to merge, and a redistribution of momentum in the upwash sheet occurs until the jets coalesce. At this point, the upwash sheet ceases to exist. Hence, the normal or vertical momentum in the upwash is no longer M_d and a model must be provided

$$\frac{}{2}$$

The condition for no upwash flow, in the vertical plane of symmetry containing the jet stagnation points, is presumed to be the nozzle height above ground where the jet boundaries touch at the ground effect height Δ_J. It is assumed that the momentum per unit angle in the upwash sheet has a parametric form:

$$M_u(\varphi_u) = \frac{M_J}{2\pi} f_{Mu}(\varphi_u, h/d_N, S/d_N) \tag{9-44}$$

In the limit as $s/d \rightarrow \infty$, $f_{Mu} \rightarrow 1$. It is also assumed, that until the jets begin to coalesce, the momentum per unit angle in the upwash sheet is conserved, or equal to the jet momentum and for any quadrant of the upwash sheet,

$$\frac{M_{uT}}{4} = \int_0^{\pi/2} M_u(\varphi_u)\, d\varphi_u = \frac{M_J}{4}$$

A function that satisfies all of the above conditions can be derived as,

$$f_{Mu} = a_u + 2(1 - a_u)\sin^2\varphi_u \tag{9-45}$$

where

$$a_u = 1 - \left[\frac{r_{J1}(h/d_N)}{S_2}\right]^2$$

Thus, when the impingement radius of the jet equals the half spacing of the two jets, the above equation yields a zero momentum flux along the $\varphi_u = 0$ streamline.

Figure 9-19 shows the variation in f_{Mu} given by this model as a function of angle and the parameter a_u. Thus, this model indicates that as the spacing gets smaller or the nozzle height gets larger the momentum in the upwash sheet is redistributed away from the centerpoint between the two jets. The above expression can be further integrated to yield the normal momentum in the upwash sheet assuming that the upwash streamlines remain approximately radial.

$$\frac{M_{uN}}{4} = \frac{M_J}{2\pi} \int_0^{\pi/2} [a_u + 2(1 - a_u)\sin^2\varphi_u]\cos\varphi_u\, d\varphi_u$$

$$\frac{M_{uN}}{4} = \frac{M_J}{2\pi}\left[a_u + \frac{2}{3}(1 - a_u)\right] \tag{9-46}$$

The model then predicts that the normal momentum in the entire upwash sheet decreases from a value of $\frac{2M_J}{\pi}$ to $\frac{4}{3}\frac{M_J}{\pi}$.

At nozzle heights where the jets begin to merge, or their boundaries begin to overlap, another model must be hypothesized. In this situation, it is assumed that there is a region between the jets where no upwash flow exists. It is no longer assumed that the momentum in the entire upwash sheet equals the momentum in one of the jets. Hence, for $r_{J1} > S$, a function of the following form is assumed:

$$M_u(\varphi_u) = \frac{M_J}{\pi \sin^2\left(\frac{\pi}{2} - \varphi_{u0}\right)} \sin^2(\varphi_u - \varphi_{u0}) \quad \text{for} \quad \varphi_u \geq \varphi_{u0}$$

$$\text{and} \quad M_u(\varphi_u) = 0 \quad \text{for} \quad \varphi_u < \varphi_{u0}$$

The value of 2 at $\varphi_u = \pi/2$ has been held fixed and the angle φ_{u_o} denotes the angle at which upwash flow exists. This angle is estimated from whatever little empirical evidence that is available as,

$$a_c = \frac{S_2}{r_{J1}}$$

$$\varphi_{u0} = \cos^{-1}(a_c)^{\alpha_c} \qquad \text{where } \alpha_c \sim .30$$

and is a function of the degree of overlap of the jet boundaries at the ground effect height as reflected in the coalescence parameter a_c. In the limit, when $r_{J1} >> S_2$, the angle $\varphi_{u_o} \longrightarrow \pi/2$. The normal, or vertical upwash momentum, in general is

$$\frac{M_{uN}}{4} = \frac{M_J}{3\pi \sin^2\left(\frac{\pi}{2} - \varphi_{u0}\right)}\left\{1 + \sin\varphi_{u0}(\sin\varphi_{u0} - 2)\right\} \tag{9-47}$$

Thus, the vertical momentum in the upwash sheet vanishes rapidly as the jet boundaries overlap or as the jets coalesce as demonstrated in figure 9-19. This behavior is a result of the diverting of momentum flux into streamlines that become more parrallel to the ground. In the limit as $\varphi_{u_o} \rightarrow \pi/2$, the amount of momentum in the upwash streamline does not have any effect on the vertical upwash momentum because this streamline lies parallel to the ground.

Further improvement in these simple models entails further empirical study. Unfortunately, it is extremely difficult, if not impossible, to measure the upwash momentum. Hence, the best evidence for such models comes by way of correlation between ground upwash pressures and total pressure in the upwash sheet.

9.3.4 General Approach to the Prediction of Two - Jet Ground Pressure Distributions for Close - Jet Spacing.- Figure 9-20 shows a schematic of the ground pressure phenomena that occurs for close jet spacing where the jet impingement and upwash deflection zone interact. The upwash deflection zone now includes a portion where the upwash pressures are equal to the jet impingement zone pressures. Along this portion of the upwash boundary the jet impingement pressures do not fully recover. Hence, the impinging flow does not become entirely parallel to the ground before it begins to deflect upward and stagnate in the upwash zone.

To estimate the behavior of such a flow, it is assumed that the jet impingement or deflection region is perturbed due to the closeness of the two jets. The ambient pressure boundary is assumed to have the form:

$$r_p(\varphi) = r_0 \cdot \epsilon(1 + \cos\varphi) \tag{9-48}$$

The upwash boundary is assumed to keep the same form except for the perturbation parameter σ, or

$$r_u(\varphi_u) = \frac{\sigma C_u S_u}{\cos\varphi_u} \tag{9-49}$$

Referring to figure 9-20, it can be seen that the pressure at the mutual boundary between the upwash zone and impingement zone is above ambient until the intersection of the two boundaries where the pressure returns to ambient. The jet impingement radius to the upwash boundary is given by,

$$r_u(\varphi) = X^2(\varphi_u) + [S_2 - y_u(\varphi_u)]^2 \tag{9-50}$$

The relationship between the two angles φ and φ_u is such that,

$$\tan\varphi = \frac{X(\varphi_u)}{S_2 - y(\varphi_u)}$$

and

$$\tan\varphi_u = \frac{X}{S_2}$$

Hence, given, φu,

$$\varphi = \tan^{-1}\left[\frac{S_2 \tan\varphi_u}{S_2 - y_u(\varphi_u)}\right]$$

For a given ϵ and σ, the intersection of the two boundaries can be found from the solution of the following equations:

$$X^2(\varphi_{u_0}) + [S_2 - y_u(\varphi_{u_0})]^2 = r_0^2 + 2\epsilon r_0(1+\cos\varphi_0) + \epsilon^2(1+\cos\varphi_0)^2$$

$$\tan\varphi_0 = \frac{X(\varphi_{u_0})}{S_2 - y(\varphi_{u_0})} \tag{9-51}$$

This gives the two angles φ_{uo} and φo which completely define the intersection of the two boundaries.

9.3.4.1 Jet Deflection Region. - To develop the analysis, it is assumed that the integral of the pressure in the jet impingement zone is still equal to the jet thrust, or

$$\frac{M_j}{2} = \int_0^{\varphi_0}\int_0^{r_u(\varphi_0)} \Delta P_1 \, dr\,d\varphi + \int_{\varphi_0}^{\pi}\int_0^{r_p(\varphi)} \Delta P_1 \, r\,dr\,d\varphi \tag{9-52}$$

The pressure integral is divided into two parts. The first integral represents the pressure in the region of interaction between the two deflection zones where

a minimum pressure boundary exists.

$$\Delta P_l(\varphi) - \Delta P_{JS} f_g(\eta_\omega)$$

$$\eta_w = \frac{r}{r_p(\varphi)}$$

Substituting into eq. 9-52,

$$\frac{M_J}{2} = \Delta P_{JS} \left\{ \int_0^{\varphi_0} \int_0^{\eta_{min}(\varphi)} r_p^2(\varphi) f_g(\eta_w) \eta_w \, d\eta_w d\varphi \right. \tag{9-53}$$

$$\left. + \int_{\varphi_0}^{\pi} \int_0^1 r_p^2(\varphi) f_g(\eta_w) \eta_w d\eta_w d\varphi \right\}$$

Let $$G_{min}(\varphi) = \int_0^{\eta_{min}(\varphi)} f_g(\eta_w) \eta_w d\eta_w \quad \text{where } \eta_{min}(\varphi) = \frac{r_u(\varphi)}{r_p(\varphi)}$$

and $$I_g = \int_0^1 f_g(\eta_w) \eta_w d\eta_w = C_{spg}(\alpha_g)$$

Then the above expression reduces to, upon non dimensionalization,

$$\pi = \left(\frac{V_g}{V_N}\right)^2 \left\{ \int_0^{\varphi_0} r_p^2(\varphi) G_{min}(\varphi) d\varphi + I_g \int_{\varphi_0}^{\pi} r_p^2(\varphi) d\varphi \right\} \tag{9-54}$$

where

$$I_g = \frac{1}{2} - \frac{4}{\alpha_g + 2} + \frac{3}{\alpha_g + 1} - \frac{4}{3\alpha_g + 2} + \frac{1}{4\alpha_g + 2} \tag{9-55}$$

and $$G_{min}(\varphi) = \frac{\eta_{min}^2}{2} - \frac{4\eta_{min}^{a_g+2}}{a_g+2} + \frac{3\eta_{min}^{2a_g+2}}{a_g+1} - \frac{4\eta_{min}^{3a_g+2}}{3a_g+2} + \frac{\eta_{min}^{4a_g+2}}{4a_g+2}$$

Unfortunately, the first part of this integral does not lend itself to analytical integration. Aside from its complexity, the implicit nature of $r_u(\varphi)$ with respect to φu makes numerical integration a necessity.

The second integral in eq. 9-54 can be carried out and is equal to:

$$\int_{\varphi_0}^{\pi} r_p^2(\varphi)\, d\varphi = (\pi - \varphi_0)\left[r_0(r_0+2\epsilon) + \frac{3}{2}\epsilon^2\right]$$

$$-2\epsilon(r_0+\epsilon)\sin\varphi_0 - \frac{c^2}{4}\sin 2\varphi_0$$

9.3.4.2 Upwash Deflection Zone. - In the upwash deflection zone, the normal component or vertical momentum in the upwash sheet is assumed given by the momentum models described in section 9.3.3.

Hence, for a quadrant of the upwash zone,

$$\frac{M_{uZ}}{1} = S_2 \int_0^{\pi/2}\int_0^{y_u} \Delta P_u \sec^2\varphi_u\, d\varphi_u\, dy$$

This integral is also divided into two parts, being

$$\frac{M_{uZ}}{4} = S_2 \int_0^{\varphi_{u_0}}\int_0^{y_u} \Delta P_u \sec^2\varphi_u\, d\varphi_u\, dy + S_2 \int_{\varphi_{u_0}}^{\pi/2}\int_0^{y_u} \Delta P_u \sec^2\varphi_u\, d\varphi_u\, dy \qquad (9\text{-}56)$$

In the interaction region of the upwash zone, the upwash pressures are assumed given by,

$$\Delta P_u(\varphi_u) = \Delta P_{u_{ming}}(\varphi_u) + [\Delta P_{umg}(\varphi_u) - \Delta P_{umingg}(\varphi_u)]\,[1-\eta_u^{a_{ug}}]^4$$

$$\text{for } 0 \le \varphi_u \le \varphi_{u_0} \qquad (9\text{-}57)$$

and for $\varphi_u > \varphi_{vo}$,

$$\Delta P_u(\varphi_u) = \Delta P_{umg}(\varphi_u)\,[1 - \eta_u^{\alpha_{ug}}]^4 \tag{9-58}$$

where $$\eta_u = \frac{y}{y_u(\varphi_u)}$$

Substituting into eq. (9.56),

$$\frac{M_{uZ}}{4} = S_2 \int_0^{\varphi_{u_0}} y_u\,[\Delta P_{umng} + (\Delta P_{umg} - \Delta P_{umng})\,C_{sug}]\sec^2\varphi_u\,d\varphi_u$$

$$+ S_2 C_{sug} \int_{\varphi_{u_0}}^{\pi/2} y_u \Delta P_{umg} \sec^2\varphi_u\,d\varphi_u \tag{9-59}$$

$$\text{where}\quad C_{sug} = \int_0^1 f(\eta_u)\,d\eta_u$$

Now, letting $$\frac{\Delta P_{umg}}{\Delta P_J} = \Delta P_{wall}(\varphi_u)$$

Eq. (9-59) becomes,

$$\lambda_Z = \sigma C_u \left(\frac{S_2}{r_N}\right)^2 \left\{ \int_0^{\varphi_{u_0}} \frac{1}{\cos^3\varphi_u} \left[\left(\frac{V_g}{V_N}\right)^2 f_g(\eta_{min}) \right.\right.$$

$$\left.\left. + \left\{ \Delta P_{wall}(\varphi_u) - \left(\frac{V_g}{V_N}\right)^2 f_g(\eta_{min}) \right\} C_{sug} \right] d\varphi_u \right. \tag{9-60}$$

$$\left. + C_{sug} \int_{\varphi_{uo}}^{\pi/2} \frac{1}{\cos^3\varphi_u} \Delta P_{wall}(\varphi_u)\,d\varphi_u \right\}$$

$$\text{where}\quad \frac{M_{uZ}}{4} = \lambda_Z \left(\frac{M_J}{2\pi}\right)$$

Unfortunately, these integrals also do not lend themselves to analytical integration and must be numerically evaluated.

9.3.4.3 Overall Solution. - To obtain the solution for the ground pressure patten for a given spacing and nozzle height, the following two simultaneous equations are solved iteratively for ϵ and σ,

$$F_{J_i}(\epsilon, \sigma) = \pi - I_{J_1} - I_{J_2} = 0$$

and $$F_{u_i}(\epsilon, \sigma) = \lambda_Z - I_{u_1} - I_{u_2} = 0 \qquad (9\text{-}61)$$

where I_{J1} and I_{J2} are the two integral expressions for the jet impingement region and I_{u1} and I_{u2} correspond to the integrals for the upwash zone.

The Newton iterative scheme consists of,

$$\Delta\epsilon = \frac{1}{D}\left\{ F_{J_1}(\epsilon_0, \sigma_0) \frac{\partial F_{u_i}}{\partial \sigma} - F_{u_1}(\epsilon_0, \sigma_0) \frac{\partial F_{J_i}}{\partial \sigma} \right\} \qquad (9\text{-}62)$$

and $$\Delta\sigma = \frac{1}{D}\left\{ F_{u_1}(\epsilon_0, \sigma_0) \frac{\partial F_{J_1}}{\partial \epsilon} - F_{J_1}(\epsilon_0, \sigma_0) \frac{\partial F_{u_1}}{\partial \epsilon} \right\}$$

where $$D = \frac{\partial F_{u_1}}{\partial \epsilon} \frac{\partial F_{J_1}}{\partial \sigma} - \frac{\partial F_{J_1}}{\partial \epsilon} \frac{\partial F_{u_1}}{\partial \sigma}$$

and the function and its partial derivatives are evaluated at the value ϵ_0, σ_0 which may be an initial guess. Further iterates are defined as

$$\epsilon_{i+1} = \epsilon_i + F_R \Delta\epsilon$$

$$\sigma_{i+1} = \sigma_i + F_R \Delta\sigma \qquad (9\text{-}63)$$

where a relaxation factor F_R may be necessary to speed up convergence.

Figures 9-21 and 9-22 show a comparison with test data of the computed ground pressure distribution along the line of the jet stagnation points (X = 0) for various jet spacings and a nozzle height of $4 d_N$. Reasonable good agreement is

achieved down to a spacing of two diameters. The assumed form of the jet deflection zone pressure function seems to differ somewhat from the test data but the maximum upwash pressures and widths seem to be in good agreement.

In addition, the predicted minimum pressures between the jet and upwash zone are in good agreement. Figure 9-23 shows some extreme situations for a close jet spacing of $2d_n$ and nozzle heights up to $10d_N$. At approximately $8d_N$ the upwash momentum model predicts no upwash between the jets. As the nozzle height is increased, the upwash width decreases significantly at this spacing. The test data is in fair agreement with the predicted pressures.

In general, the exponent α_{ug} of the upwash ground pressure function is assumed to be

$$\alpha_{ug} > \alpha_{ugFD} \quad \text{for} \quad \varphi_u < \varphi_{uo}$$

and $$\alpha_{ug} = \alpha_{ugFD} \quad \text{for} \quad \varphi_u \geq \varphi_{uo}$$

Further, the exponent α_{ug} is assumed to be a function of the minimum pressure in the deflection zone for $\varphi_u < \varphi_{uo}$. To determine α_{ug}, for $P_{min} > 0$, an equivalent profile for the upwash pressure function is assumed to exist whose integral force per unit length is equal to the partial integral or partial force of the fully developed pressure function ($\alpha_{ugFD} = 1.5$)

Let, $$\bar{P}_{min} = \frac{P_{min}}{P_{max}}$$

$$I(\alpha_{ugFD}, \eta_{min}(\bar{P}_{min})) = \int_0^{\eta_{min}} (1 - \eta^{\alpha_{ugFD}})^4 \, d\eta$$

and $$I'(\alpha_{ug}) = \int_0^1 (1 - \eta'^{\alpha_{ug}})^4 \, d\eta'$$

where $$\eta_{min} = (1 - \bar{P}_{min})^{\frac{1}{4}})^{\frac{1}{\alpha_{ugFD}}}$$

Then,

$$\bar{P}_{min} + (1 - \bar{P}_{min}) I'(\alpha_{ug}) = I(\alpha_{ugFD}, \eta_{min}) \qquad (9\text{-}64)$$

Given any $\overline{P}min$ value along the upwash, equation 9-64 can be solved to find the exponent α_{ug}. When Pmin = 0 at $\varphi_u = \varphi_{uo}$, or at the intersection of the impingement and upwash deflection zone, equation (9-64) reduces to an identity and, hence, $\alpha_{ug} = \alpha_{ugFD}$.

It can be seen both in the test data and in the predicted pressures that negligible interaction between the deflection zones occures at spacings greater than 6 dN. Significant interaction does not take place until a spacing of 3dN for this nozzle height as is reflected by the minimum upwash pressure level.

Figures 9-24 and 9-25 show a sample of the entire ground isobar pattern for a range of spacings and nozzle heights. Figure 9-26 shows the kind of corelation achieved for one case.

9.3.5 Upwash Decay Model. - Figure 9-27 shows a schematic of the upwash sheet model and the characteristic scaling parameters. The upwash sheet is assumed to be a reflection of the wall jet flow into the vertical plane of symmetry lying between the jets. The radial streamline pattern of the wall layer is assumed to continue into the upwash sheet and to a first approximation unperturbed by the turning region. The wall jet flow is assumed to enter the upwash deflection region with a characteristic profile, half velocity width and maximum velocity or total pressure. The characteristic length scale in the upwash sheet is the half velocity width of the incident wall jet layer estimated at the wall location. The pressure recovery region in the upwash sheet is assumed to be approximately 3 times the half velocity width of the incident wall jet profile. The magnitude of the momentum flux in the resulting upwash streamline is assumed equal to that of the incident wall jet. Hence, the upwash sheet is treated in a similar fashion as the wall jet with a few exceptions.

Due to the high turbulence levels typically measured in the upwash sheet the flow is considered to be fully turbulent and similar. The upwash velocity profile is taken to be that of a free shear profile with no internal momentum defect due to the wall layer. The upwash sheet growth rate is assumed to be constant without any initial transition phase. It is also assumed that the magnitude of the momentum flux distribution in the upwash sheet is given by the previously discussed momentum models. An expression analogous to that derived for the wall jet can now be derived for the upwash sheet:

$$f_{Mu}(\varphi_u)[1 - f_{Pu}(\zeta)] = 2\left(\frac{r_w(\varphi_u) + Z_S}{r_N}\right)\left(\frac{R_u b_{uH}(Z, \varphi_u)}{r_N}\right) C_{su}$$

$$\cdot\left\{\left(\frac{V_{mu}}{V_N}\right)^2 + \frac{1}{2}\left(\frac{\Delta P_{wall}(\varphi_u)}{\Delta P_J}\right)^2 f_{Pu}(\zeta)\right\} \qquad (9\text{-}65)$$

where $\zeta = \dfrac{Z_S}{Z_{Sou}}$, $R_u = \dfrac{b_{uH}}{b_u}$, and $f_{Pu} = [1 - \zeta^{1.5}]^4$

$$R_u = .441 \text{ for } \alpha_u = 1.5$$

The velocity squared profile is assumed to be identical in shape to the static pressure profile and as a result only one similarity constant is required:

$$C_{Su} = \int_0^1 (1 - \eta_u^{\alpha_u})^4 \, d\eta_u = .31558 \text{ for } \alpha_u = 1.5 \text{ where } \eta_u = \frac{y}{b_u}$$

The procedure for starting the upwash flow is similar to that of the wall jet where an initial upwash half width (bu_{H_0}) is determined from eq. 9-64 given an inviscid starting maximum velocity. A model for the upwash sheet growth must then be provided based upon empirical observation.

$$b_{uH}(\varphi_u, Z) = b_{uH_0}(\varphi_u) + a_{bu}(Z_S - b_{WH}(r_w))(\cos\varphi_u)^{\alpha_{bu}} \qquad (9\text{-}66)$$

where

$$a_{b_u} \sim .30 \quad \text{and} \quad Z_s = \frac{Z}{\cos\varphi_u}$$

$$\alpha_{b_u} \sim .50$$

The value of $a_{b_u} = .30$ is consistent with empirical observations that the upwash flow decays at a rate approximately three times that of a free jet.

An approximate expression can be derived for the upwash decay. Assume that the region of interest is beyond the turning region of the upwash sheet such that $f_{pu} = 0$. Then eq. 9-65 reduces to,

$$f_{Mu}(\varphi_u) = 2\left(\frac{r_w(\varphi_u) + Z_S}{r_N}\right)(R_u C_{Su})\left(\frac{b_{uH}}{r_N}\right)\left(\frac{V_{mu}}{V_N}\right)^2$$

Hence, the maximum velocity squared is equal to

$$\left(\frac{V_{mu}}{V_N}\right)^2 = \frac{f_{Mu}(\varphi_u)}{2\left(\frac{r_w + Z_s}{V_N}\right)\left(\frac{b_{uH}}{r_N}\right) R_u C_{su}} \tag{9-67}$$

Now, if the approximation that

$$b_{uH} \sim \frac{\dot{a}_{bu}\bar{Z}}{(\cos\varphi)^{\alpha_{bu}}} \quad \text{is introduced}$$

Noting that

$$r_w + Z_s = \sqrt{X_u^2 + (S_2 + Z_u)^2}$$

$$\sin\varphi_u = \frac{X_u}{\sqrt{X_u^2 + (S_2 + Z_u)^2}}$$

$$\cos\varphi_u = \frac{S_2 + Z}{\sqrt{X_u^2 + (S_2 + Z_u)^2}}$$

and

$$f_{Mu}(\varphi_u) = a_u + 2(1 - a_u)\sin^2\varphi_u \text{ for } a_u > 0$$

Then,

$$\left(\frac{V_{mu}}{V_N}\right)^2 = \frac{[a_u + 2(1 - a_u)\sin^2\varphi_u][\cos\varphi_u]^{(1+a_{bu})}}{2a_{bu} R_u C_{Su} Z_u (S_2 + Z_u)} \tag{9-68}$$

or, equivalently,

$$\left(\frac{V_{mu}}{V_N}\right)^2 = \frac{(S_2 + Z_u)^{(1+a_{bu})}}{[X_u^2 + (S_2 + Z_u)^2]^{\frac{1+a_{bu}}{2}}} \left[\frac{a_u + \frac{2(1-a_u)X_u^2}{X_u^2 + (S_2+Z_u)^2}}{2a_{bu} R_u C_{Su} (S_2 + Z_u) Z_u}\right] \tag{9-69}$$

Nondimensionalizing both of these expressions by the value at $\varphi_u = 0$ or $X_u = 0$:

$$\left(\frac{V_{mu}}{V_{mu_0}}\right)^2 = \frac{\left(\frac{V_{mu}}{V_N}\right)^2}{\left(\frac{V_{mu}}{V_N}\right)^2_{\varphi_u = 0}} = \left[1 + \frac{2}{a_u}(1 - a_u)\sin^2\varphi_u\right] [\cos\varphi_u]^{(1+\alpha_{bu})} \tag{9-70}$$

or

$$\left(\frac{V_{mu}}{V_{mu_0}}\right)^2 = \left[1 + \frac{2(1-a_u)X_u^2}{a_u[X_u^2 + (S_2 + Z_u)^2]}\right] \frac{1}{\left[1 + \frac{X_u^2}{(S_2+Z_u)^2}\right]^{\frac{1+\alpha_{bu}}{2}}}$$

where $a_u > 0$ (9-71)

The more general procedure was used to generate comparisons with test data. Figure 9-28 shows the upwash centerline ($X_u = 0$) decay and half velocity boundary growth characteristics in comparison with some test data. The model predicts higher initial total pressures for the closer jet spacings along with a smaller turning region. The decay curves tend to merge with increasing height above ground. The model half velocity boundary growth starts off at a smaller value closer to the ground for closer spacings and then grows at the same rate.

Figure 9-29 shows the predicted lateral variation in the upwash pressures for H/dn = 4.0, S/dn = 6.0 for several heights in the upwash sheet. The total pressure in the upwash sheet drops off more rapidly compared to the centerline value for greater heights due to the radial spreading of the upwash streamlines. Figure 9-30 shows a comparison of the lateral total pressure decay with some test data at $h/d_N = 3$, $S/d_N = 4$. Figure 9-31 demonstrates the small influence that nozzle height above ground has on the lateral characteristics of the upwash sheet at a fixed Z_u plane. Figure 9-32 shows the lateral decay characteristics for a close jet spacing of $2d_N$ just prior to significant coalescence effects. At greater heights above

ground significant upwash flow does not exist along the centerline between the jets. Figure 9-33 demonstrates this effect where the upwash total pressure now has to be nondimensionalized by the jet stagnation point pressure. Figure 9-34 shows an even more extreme condition with some test data plotted for comparison.

9.4 Model for the Prediction of Upwash Forces on Slender Bodies

It is a well known fact that when an upwash flow field impacts on the underside of an aircraft an upward lift force can be generated on the aircraft. This upwash lift force is sometimes negated at heights close to the ground by negative interference forces (suckdown) caused by the secondary induced flow field generated by the entrainment action of the primary jet and wall jet flows. It is the intent of this section to develop a method for the prediction of the upwash lift on a slender fuselage where the suckdown force has a minor effect in comparison to the upwash force.

9.4.1 Upper Limit of Upwash Forces from a Momentum Capture Model. Figure 9-36 shows a sketch of the flow model to be used for momentum capture.

The height above ground of the fuselage and nozzles are assumed equal. It will be assumed that the entire vertical momentum included in the upwash sheet by the length of the fuselage can be converted into a lift force. Accordingly, this lift force can be computed as:

$$\frac{L_u}{2T_J} = \frac{1}{\pi} \int_0^{\varphi_f} [a_u + 2(1-a_u)\sin^2\varphi_u] \cos\varphi_u \, d\varphi_u$$

$$\frac{L_u}{2T_J} = \frac{1}{\pi} \left(a_u \sin\varphi_f + \frac{2}{3}(1-a_u)\sin^3\varphi_f \right) \qquad (9\text{-}72)$$

where $a_u = 1 - \left(\frac{r_J}{S_2}\right)^2$ $\varphi_f = \tan^{-1}\left(\frac{f}{S_2+h}\right)$

In the above expression, the lift force has been nondimensionalized by the thrust of the two jets. Hence, the maximum lift force attainable for an infinite length body with $a_u = 1$ is

$$\frac{L_u}{2T_J} = \frac{1}{\pi}$$

This expression, in the limit as $\ell \longrightarrow \infty, \varphi_\ell \longrightarrow \frac{\pi}{2}$ tells us that only 31.8% of the thrust can be achieved as the optimum ideal lift force neglecting jet coalescence effects. In reality, for a finite length body, the lift force will be markedly less than this optimum value. Eq. (9-72) is plotted versus nozzle height for several jet spacings in figure 9-37 for a typical Type A fan jet V/STOL fuselage length of 8 d_N. The jets are also placed at the midpoint of the fuselage. The figure shows that the maximum upwash force on this finite length body is about .25 T_J. The upwash force also drops off rapidly for a closely spaced jet configuration due to the rapid coalescence of the jets. The momentum capture model neglects any finite width or fuselage shape effects.

This type of calculation is most representative of a fuselage fitted with strakes which is capable of approaching the force as predicted by a momentum capture model.

9.4.2 General Approach to the Prediction of Upwash Force on Arbitrary Slender Bodies. In general, the finite width of a fuselage will have a marked effect on the amount of momentum transferred to the body as a lift force. In addition, the shape of the fuselage cross section will determine the local pressure distribution around the body and thus also effect the drag or upwash force. A general approach to a prediction model for the upwash force on slender bodies is developed in this section.

9.4.2.1 Maximum Stagnation Pressure Distribution Along Centerline of Fuselage Underbody. Figure 9-38 shows a schematic of the fuselage, the pertinent coordinate systems, and geometrical parameters. The centerpoint or centerline of the body is located at an arbitrary height Z_p relative to the ground and the nozzles are located at a height h above the ground. The fuselage depth is given by the equation

$$Z_B = f(X_B)$$

The fuselage half width is also defined as

$$W_{B_2} = g(X_B)$$

The nozzles are placed at the midpoint of the body. The angle in the upwash sheet included by the half length of the fuselage is then given by

$$\varphi_{\ell} = \tan^{-1}\left(\frac{\ell_2}{S_2 + Z_p - Z_B(\ell_2)}\right)$$

The underside fuselage centerline coordinate relative to the upwash sheet at any position X_B is given by

$$Z_u = S_2 + Z_p - Z_B(X_B)$$

To determine the maximum pressure distribution on the underside of the body, it is assumed that the local stagnation pressure on the body is representative of the stagnation of the cross flow component of the upwash velocity. The cross flow upwash velocity is just the normal component of the upwash relative to the underside of the body.

$$V_N = V_{mu}(\varphi_{uB}, Z_B)\cos(\varphi_{uB} + \Theta_B)$$

where

$$\Theta_B = \tan^{-1}\left(\frac{dZ_B}{dX_B}\right)$$

and

$$\varphi_{uB} = \tan^{-1}\left(\frac{X_B}{S_2 + Z_p - Z_B(X_B)}\right)$$

Hence

$$\frac{\Delta P_{usB}}{\Delta P_J} = \left(\frac{V_{mu}}{V_N}\right)^2 \cos^2(\varphi_{uB} + \Theta_B) \qquad (9\text{-}73)$$

9.4.2.2 General Force Integral. If $F_u(X)$ is defined to be the upwash force per unit length of the body, then the entire force on the body can be defined as

$$F_T = 2\int_0^{\ell_2} F_u(X_B)\, dX_B \qquad (9\text{-}74)$$

Converting this integral to the upwash coordinate system entails,

$$\tan \varphi_{uB} = \frac{X_B}{S_2 + Z_p - Z_B(X_B)}$$

Thus,

$$dX_B = \frac{(S_2 + Z_p - Z_B)^2}{(S_2 + Z_p - Z_B - X_B Z'_B)} \sec^2 \varphi_{uB} \, d\varphi_{uB}$$

where

$$Z'_B = \frac{dZ_B}{dX_B}$$

Hence, the integral eq. (9-74) for the total force becomes,

$$F_T = 2 \int_0^{\varphi_\ell} \frac{(S_2 + Z_p - Z_B)^2}{(S_2 + Z_p - Z_B - X_B Z'_B)} F_u(\varphi_{uB}) \sec^2 \varphi_{uB} \, d\varphi_{uB} \tag{9-75}$$

Now, it is assumed that the force on any cross section is proportional to the local cross flow stagnation pressure, or

$$F_u(\varphi_{uB}) = 2\Delta P_{uS}(\varphi_{uB}) \int_0^{y = W_{B_2}(\varphi_{uB})} G_p(y) \, dy \tag{9-76}$$

where $G_p(y)$ is the pressure function representing the local flow around the cross section.

Upon substitution of this expression into eq. (9-75) and using eq. (9-73) for the stagnation pressure, eq. (9-75) becomes,

$$F_T = 2 \int_0^{\varphi_\ell} \frac{(S_2 + Z_p - Z_B)^2}{(S_2 + Z_p - Z_B - X_B Z'_B)} \left\{ \frac{\rho V_{mu}^2 \cos^2(\varphi_{uB} + \alpha_B)}{\cos^2 \varphi_{uB}} \int_0^{y = W_{B_2}(\varphi_{uB})} G_p(y) \, dy \right\} d\varphi_{uB} \tag{9-77}$$

If the integral over the body width is identified as the drag, and a sectional drag coefficient C_{Dp} is introduced as,

$$C_{D_P}(\varphi_{uB}) \equiv \frac{D_{rag}}{W_{B_2}(\varphi_{uB})} = \frac{1}{W_{B_2}(\varphi_{uB})} \int_0^{y = W_{B_2}(\varphi_{uB})} G_p(y)\, dy \qquad (9\text{-}78)$$

and eq. (9-77) is nondimensionalized by the thrust of the two jets, the final expression for the total force becomes,

$$\frac{F_{uT}}{2T_J} = \left(\frac{1}{\pi}\right) \int_0^{\varphi_\ell} \frac{(S_2 + Z_P - Z_B)^2}{(S_2 + Z_P - Z_B - X_B Z'_B)}$$

$$\times W_{B_2} C_{DP} \left(\frac{V_{mu}}{V_N}\right)^2 \frac{\cos^2(\varphi_{uB} + \Theta_B)}{\cos^2(\varphi_{uB})}\, d\varphi_{uB} \qquad (9\text{-}79)$$

where the above lengths are nondimensional.

For a cylindrical body (i.e., constant width and depth) whose underside is located at the nozzle height, or

$$Z_p - Z_B = h$$

the above expression reduces to,

$$\frac{F_{uT}}{2T_J} = \frac{(S_2 + h)}{\pi} W_{B_2} C_{DP} \int_0^{\varphi_\ell} \left(\frac{V_{mu}}{V_N}\right)^2 d\varphi_{uB} \qquad (9\text{-}80)$$

9.1.2.3 Estimation of the Drag For Different Cross Sectional Shapes. Figure 9-39 shows approximate drag models corresponding to a circular and rectangular shaped cross section body. The models for the drag for the upwash problem are markedly different than conventional aerodynamics. A cylinder immersed in an infinite stream will exhibit zero drag if the flow is attached and inviscid. The viscous flow,

on the other hand, will separate at some point and a base pressure will result causing a drag on the cylinder. In the upwash problem, the viscous flow will impact the body, flow around it and also separate at some point. The difference being that the pressures aft of the separate point will be the result of secondary induced flow. Hence, resulting in base pressures much closer to ambient as compared to the body immersed in an already energized infinite stream. These considerations were the basis for the drag models. This is also the primary reason for consideration of slender bodies because these small secondary induced pressures acting over a large area will result in a significant suckdown force. For the present time they are neglected.

Figure 9-39 b shows the model for a flat bottom body. In this model, a finite width upwash flow impinges on the underside of the fuselage. The model assumes that the flow separates at the bottom corner of the fuselage and continues without curvature away from the body. In reality, the flow would have a tendency to follow the body after separation. The force can then be easily estimated as the portion of the force that would be exerted on an infinite flat plate but taking into account the finite width of the underbody.

If the pressure recovery zone for the stagnating flow is estimated to be approximately,

$$y_o = a_o b_{uH} \text{ where } a_o \sim 3.6$$

in terms of the half velocity width of the incident upwash stream.

Now, let $C_{P_{FLAT}}(\eta) = [1 - \eta^{\alpha}]^4$

where $\eta = \frac{y}{y_0} = \frac{y}{a_o b_{uH}}$ and $\alpha \sim 1.5$.

Substituting these expressions into eq. (9-77) yields for the cross-sectional drag function,

$$\eta_B = \frac{W_{B_o}}{a_o b_{uH}}$$

$$D_F = a_o b_{uH} \int_0^{\eta_B} C_{PF}(\eta)\, d\eta$$

$$\text{or } C_{D_{PF}} = \frac{D_F}{W_{B_2}} = 1 - \frac{4\eta_B^{\alpha}}{\alpha+1} + \frac{6\eta_B^{2\alpha}}{2\alpha+1} - \frac{4\eta_B^{3\alpha}}{3\alpha+1} + \frac{\eta_B^{4\alpha}}{4\alpha+1} \tag{9-81}$$

where $\eta_B \leq 1.$

The drag coefficient for the flat bottom fuselage is thus totally dependent upon the relative size of the incident upwash flow and body width. In the limit of $b_{u_H} \rightarrow \infty$ or $\eta_B \rightarrow 0$, the maximum drag coefficient is 1. This can be interpreted as in the limit the stagnation pressure acts over the entire width of the body (analogous to a pitot tube). On the other hand, the minimum drag coefficent will be obtained when $\eta_\beta = 1$ and yields a value of .3156. The drag coefficient behavior versus the parameter η_B is shown in figure 9-40.

For the cirular cross section, the potential flow solution for the pressure distribution around the cylinder immersed in an infinite stream is used. The flow is assumed to separate at some body angle Θ_s and the base pressures are taken to be ambient. Thus, for the circular cylinder,

$$C_{P_c}(\Theta_c) = (1 - 4\sin^2\Theta_c)\cos\Theta_c \tag{9-82}$$

and

$$C_{D_{FC}} = \frac{D_C}{W_{B_2}} = \sin\Theta_s \left(- \frac{4}{3} \sin^2\Theta_s \right) \tag{9-83}$$

It is assumed that the flow separates anywhere between 120° and 160°. The drag coefficient as a function of separation angle is shown in figure 9-41. The maximum value of the drag coefficient for a circular cross section occurs when the flow separates at $\Theta_s = 150°$ and is $C_{DPC} = .333$.

To see how well these models work, some correlation with test data was carried out for cylindrical bodies whose underbody was placed at the nozzle height. Figure 9-42 shows the correlation achieved for two such bodies for circular and rectangular shapes and a cross sectional width equal to one diameter or half width of one nozzle radius. For the simple models used, the correlation achieved is quite remarkable especially since the suckdown effect was neglected. The test data drops

off at a slightly higher rate than that predicted probably because of the suckdown effect. Thus, the mysterious sensitivity to body curvative observed in past experiments can now be logically explained.

Figure 9-43 shows some parametric curves generated for the flat bottom cylindrical body as a function of body width. As expected, the predicted force increases proportionately to the width. Unfortunately, this trend is an ideal one and at some body width the suckdown forces will predominate. Figure 9-44 further shows the predicted trend for a parabolic body of maximum cross section equal to that of a cylindrical flat bottom body. As expected, the force on the parabolic body is somewhat less than that on the cylindrical body.

These models could further be improved by including the suckdown effect and also extending the estimate of the drag coefficient to arbitrary cross sectional shapes.

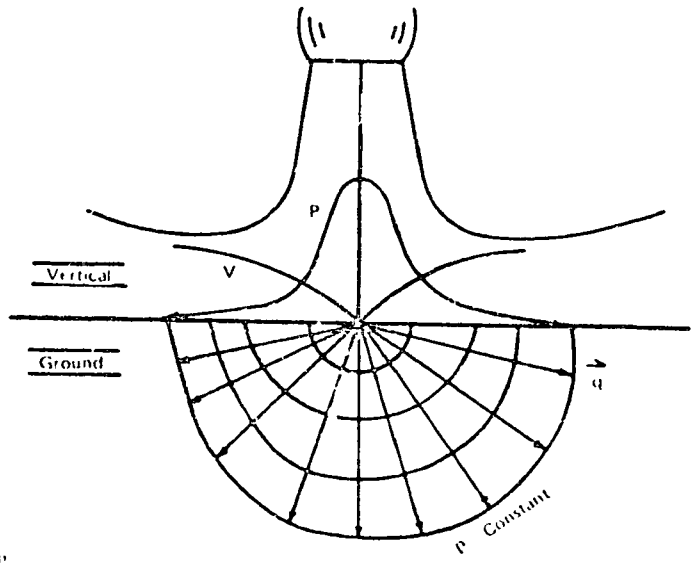

Figure 9-1. - Jet impingement region.

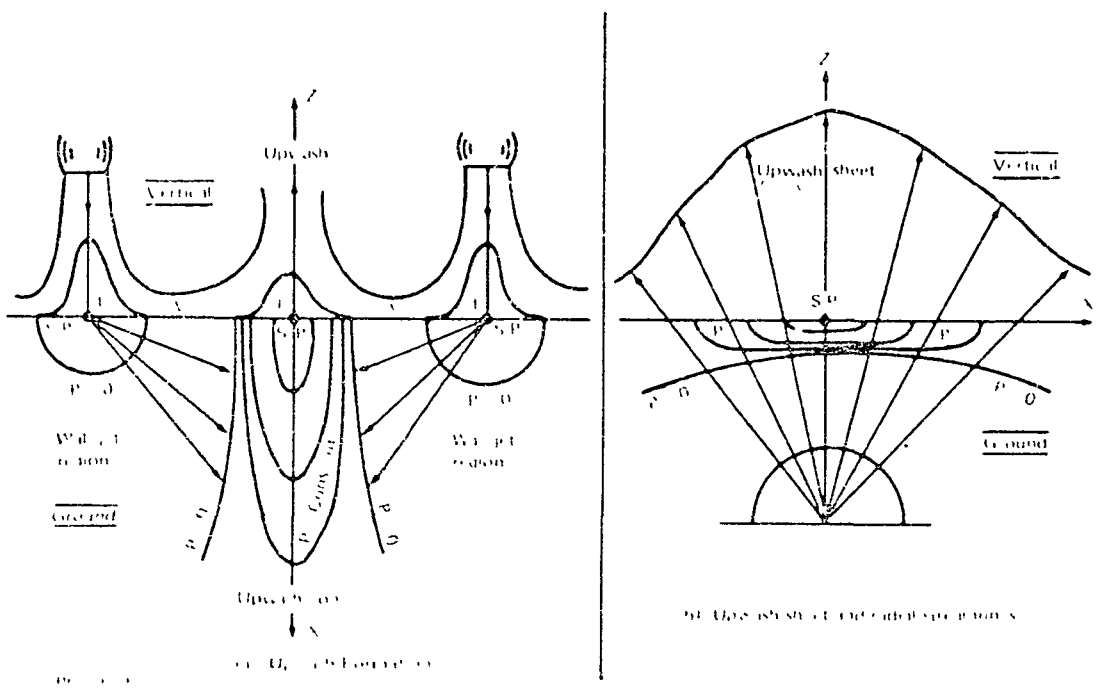

Figure 9-2. Two-jet interacting flows - negligible deflection zone interaction.

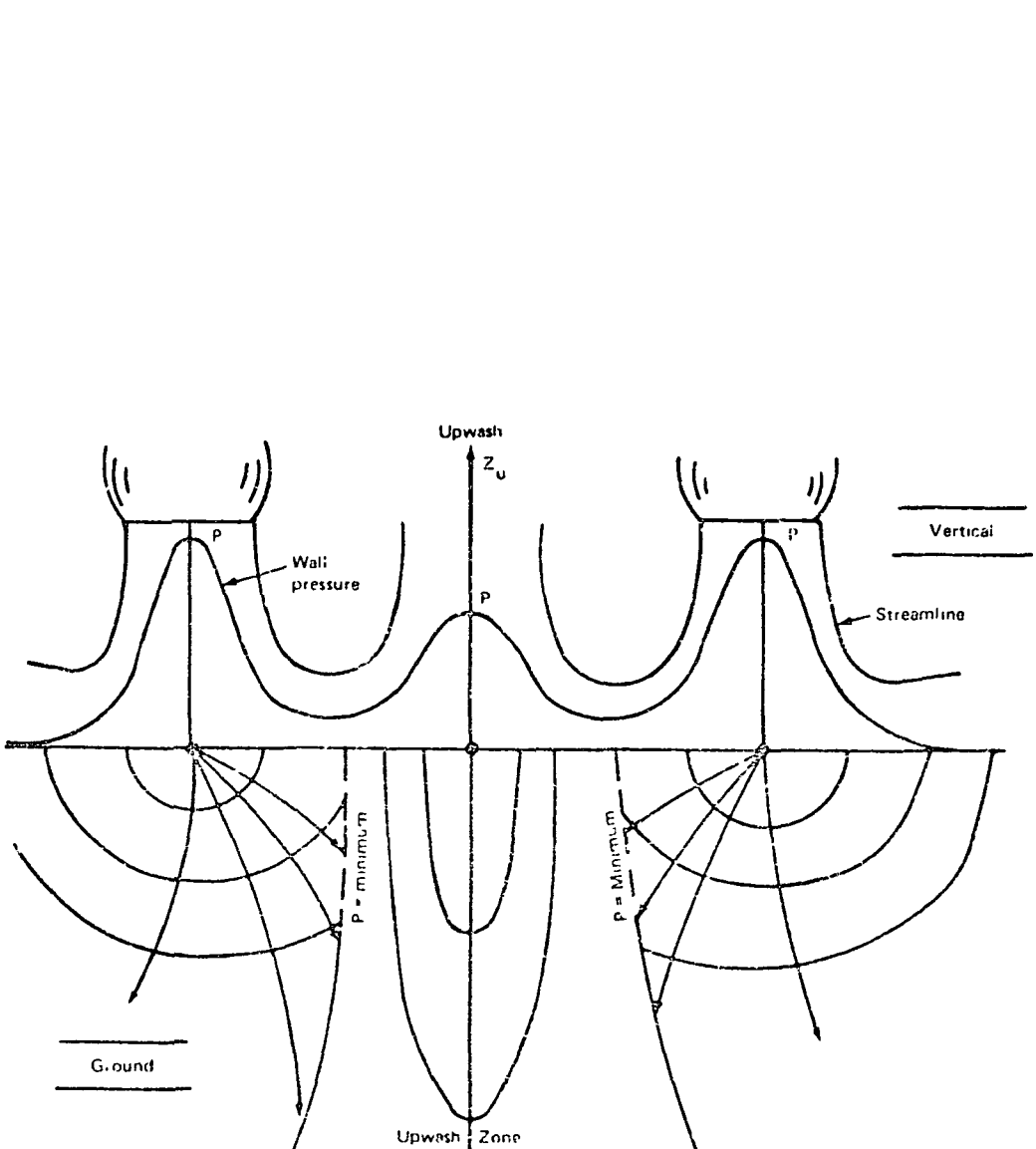

2067 055P

Figure 9-3. - Two-jet interacting flow with deflection zone interaction.

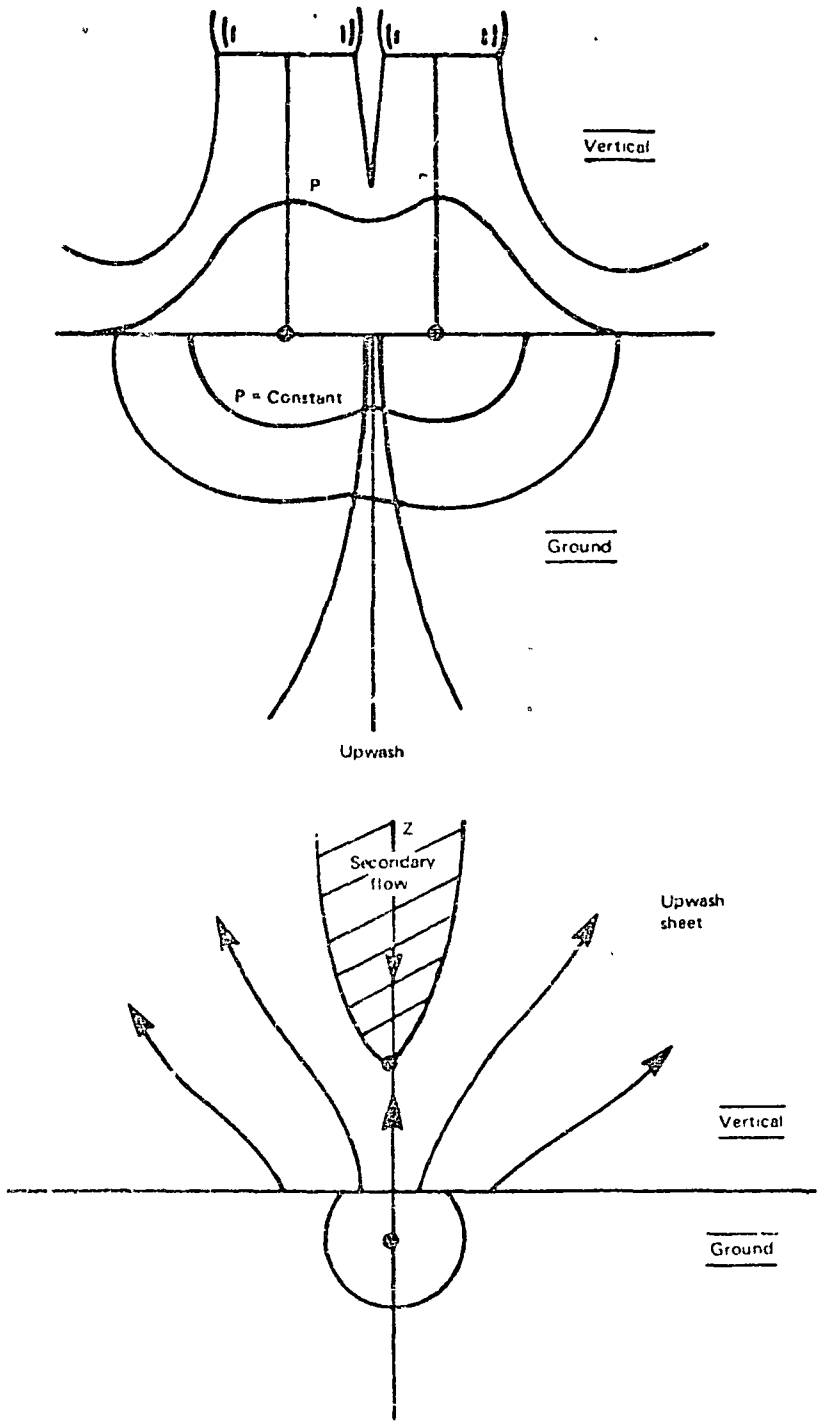

2067 056F

Figure 9-4. - Flow behavior just prior to coalescence.

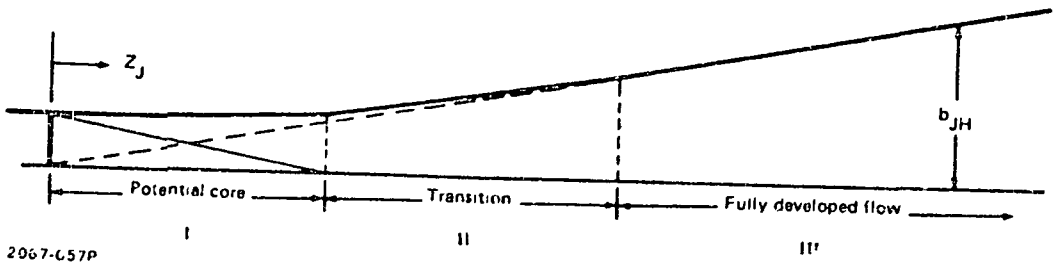

Figure 9-5. - Jet half-velocity width model

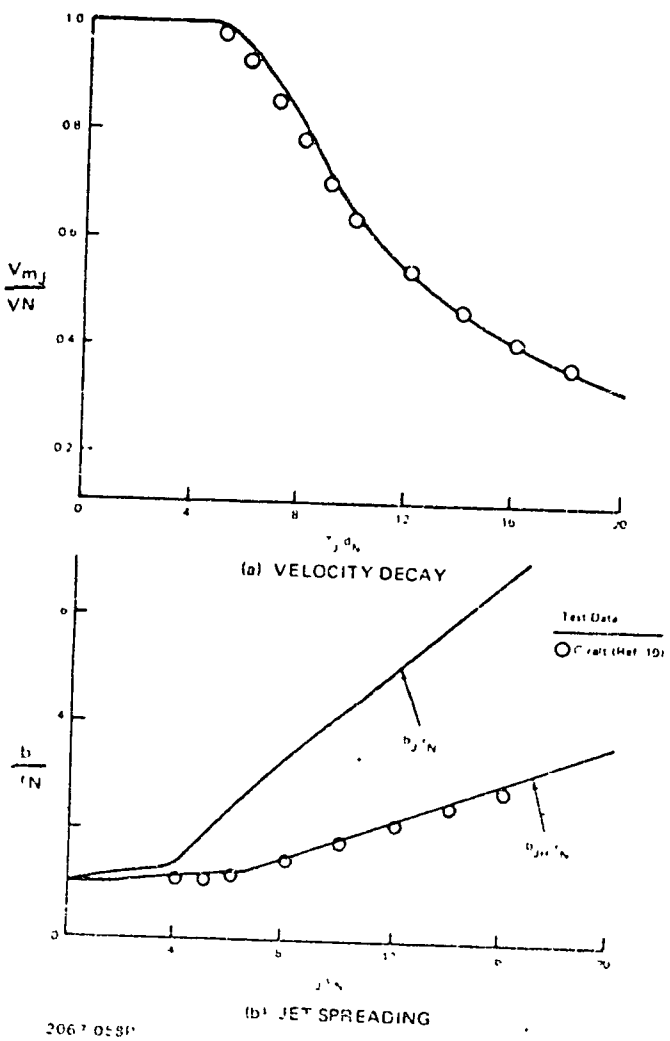

Figure 9-6. - Jet decay model.

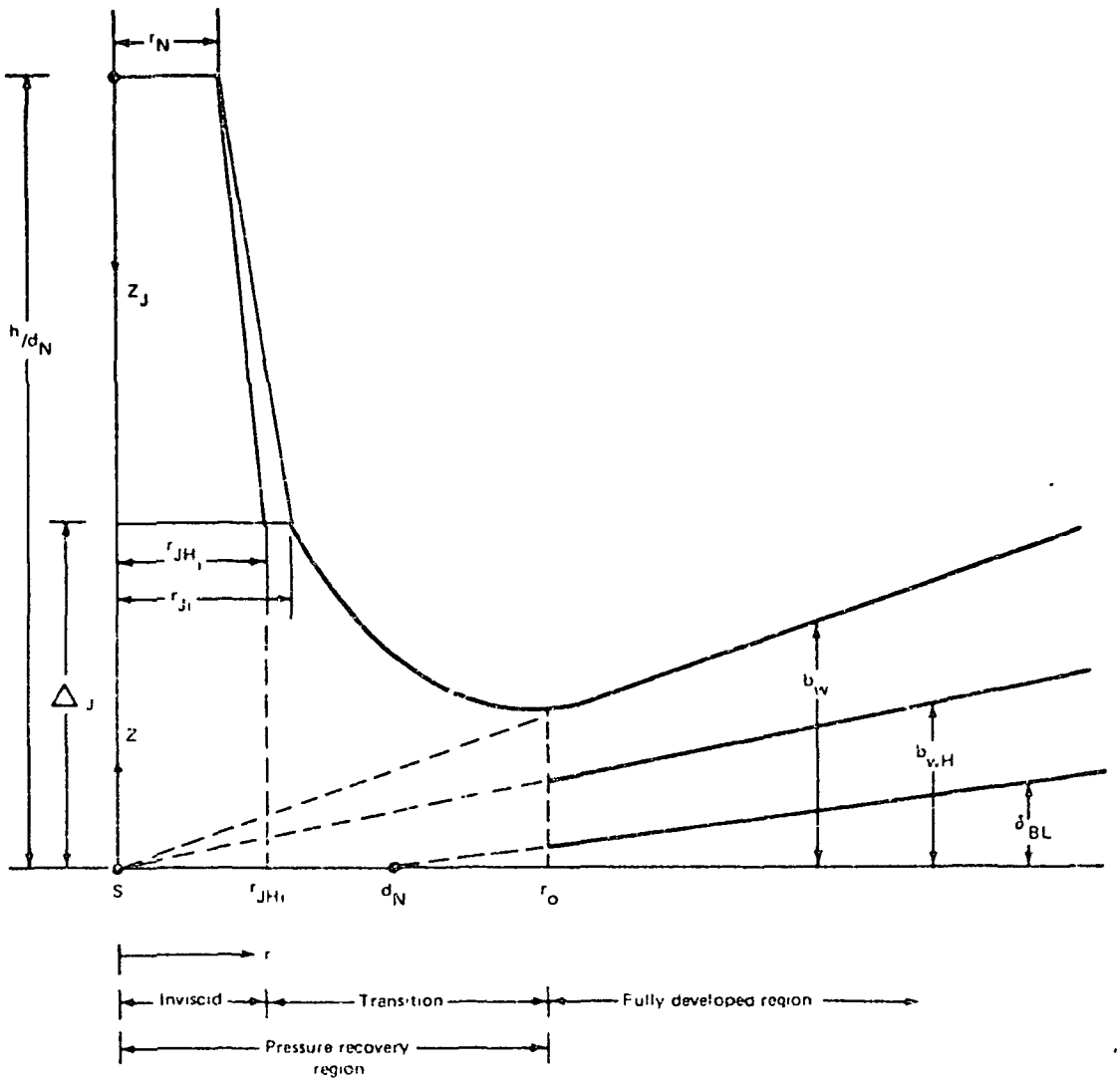

Figure 9-7. - Definition of scaling parameters for jet impingement and wall jet regions.

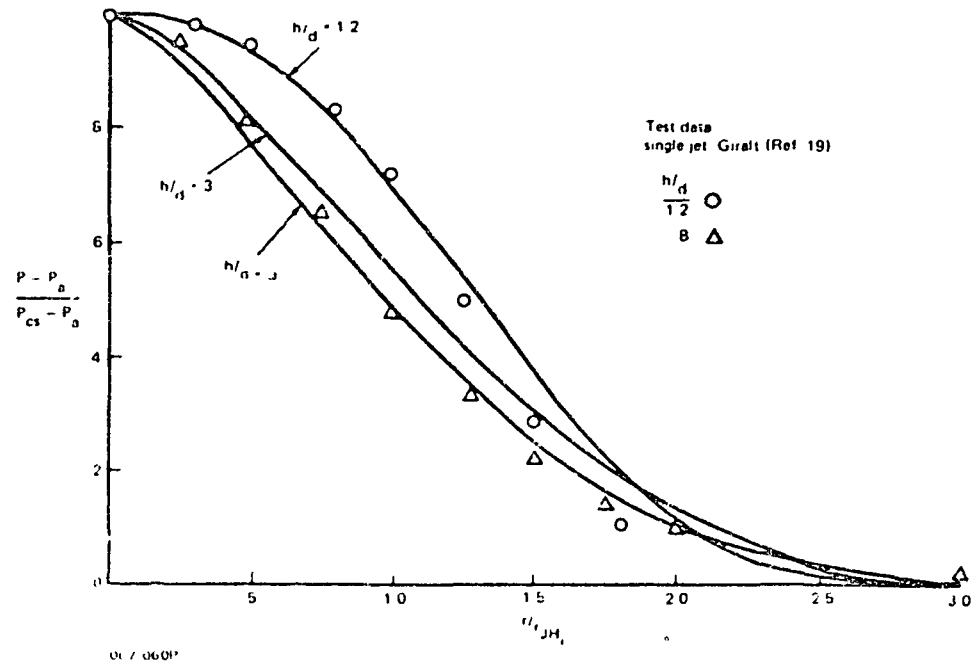

Figure 9-8. - Jet impingement region - ground plane pressure distribution.

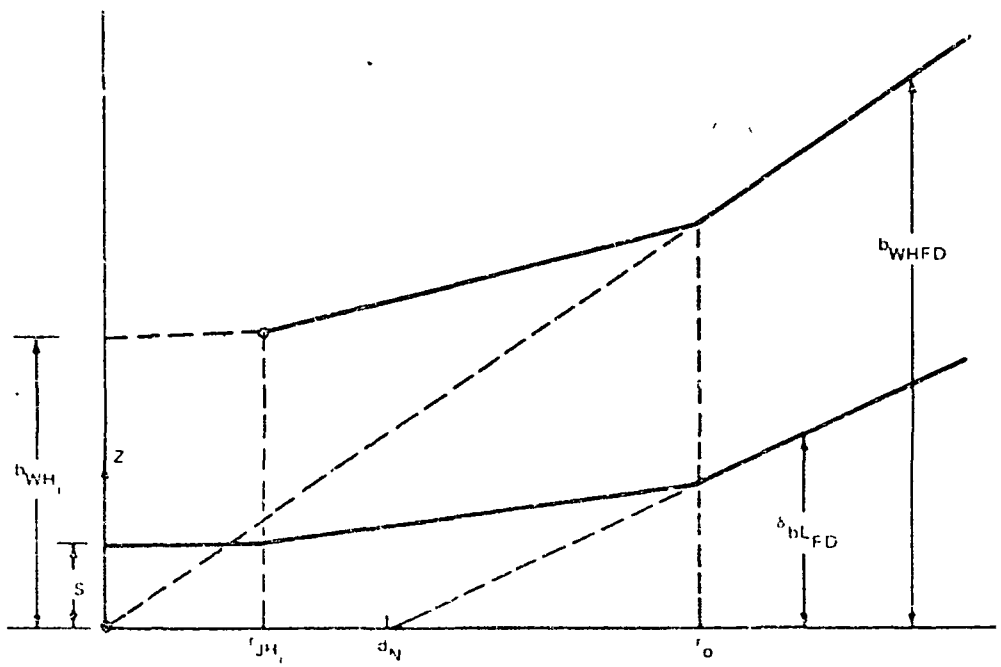

Figure 9-9. - Wall half-velocity and boundary layer thickness models.

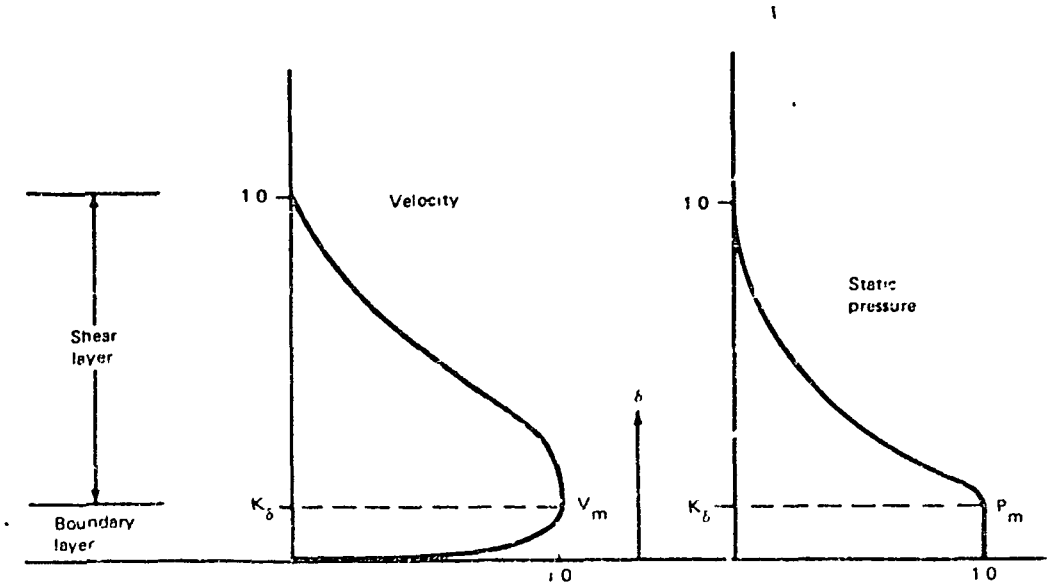

2057 062P

Figure 9-10. - Wall jet profile models.

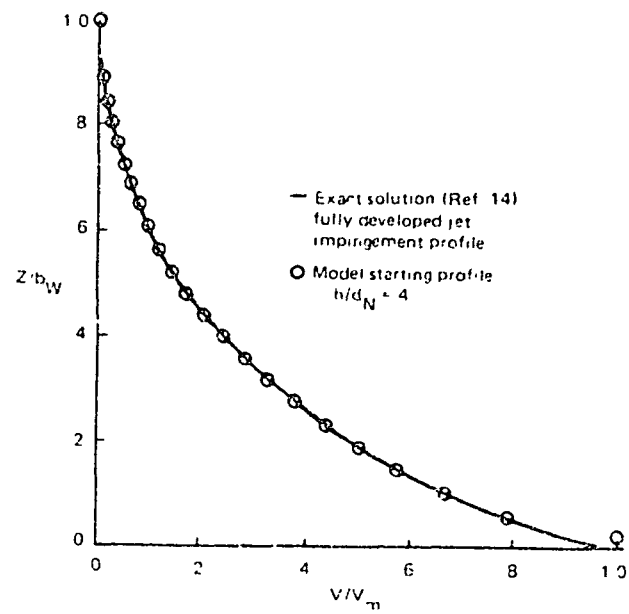

2057 063P

Figure 9-11. - Comparison of a typical inviscid starting profile with an exact inviscid rotational solution (Ref. 14).

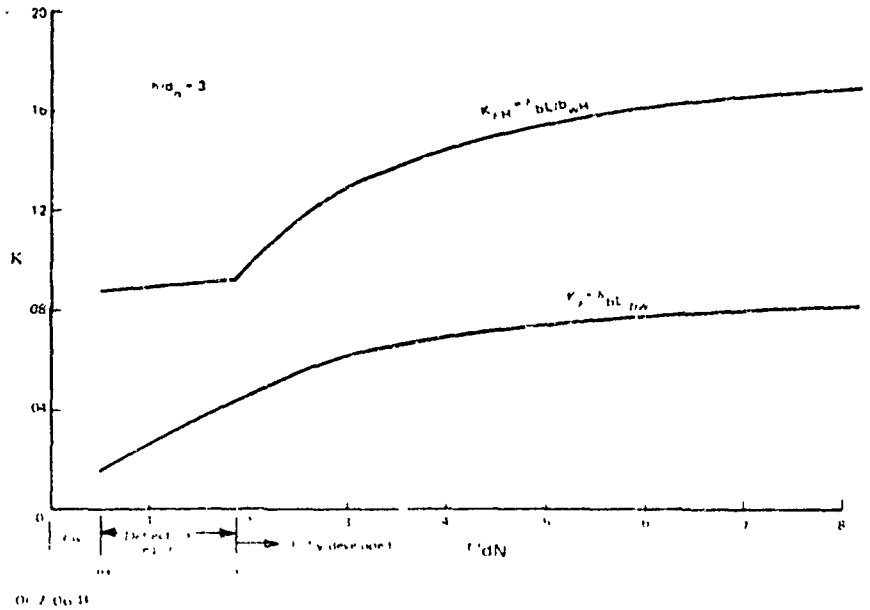

Figure 9-12. - Typical Behavior of wall jet model of boundary layer to shear layer thickness

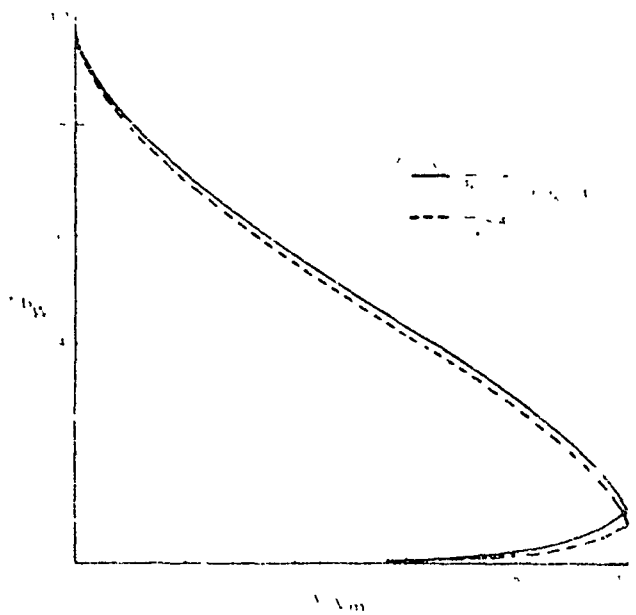

Figure 9-13. - Variation of wall layer profile with distance from stagnation point.

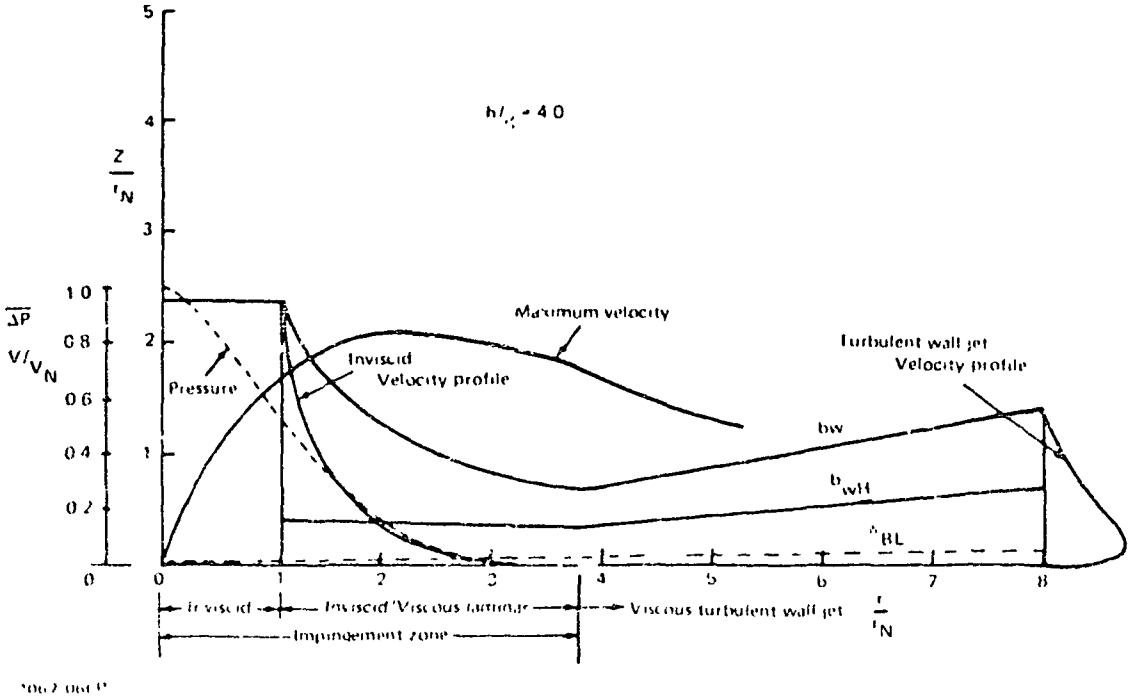

Figure 9-14. - Turbulent wall jet transition model.

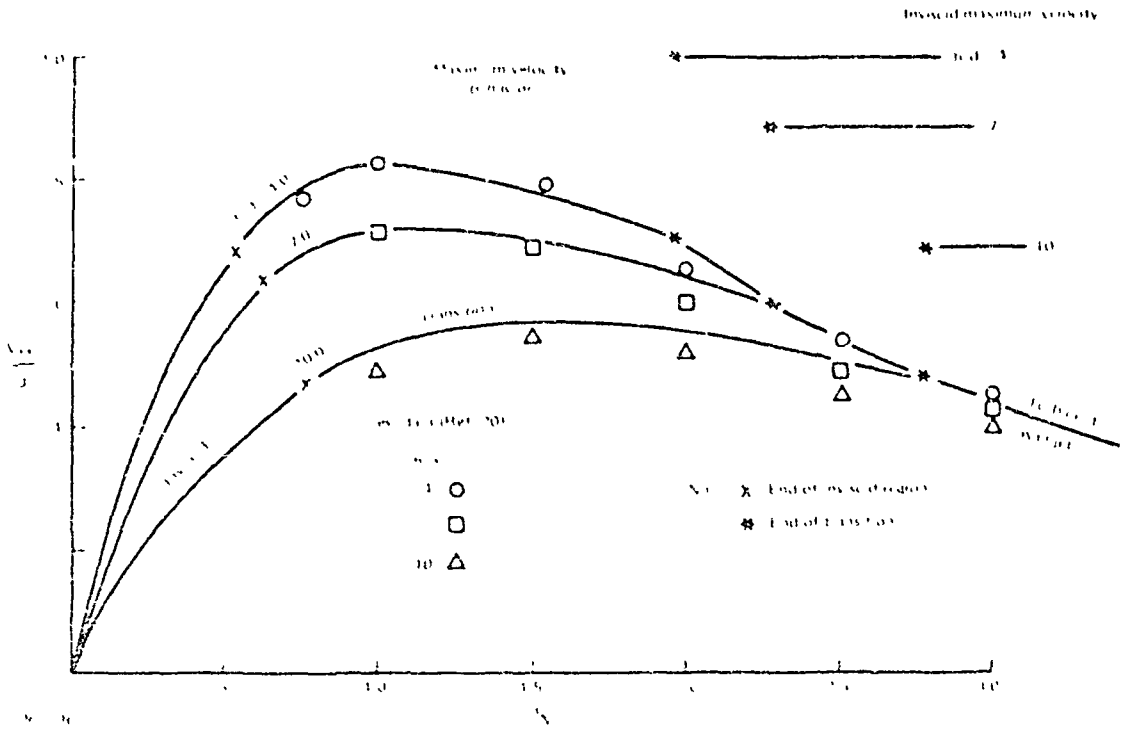

Figure 9-15. Wall jet transition model maximum velocity.

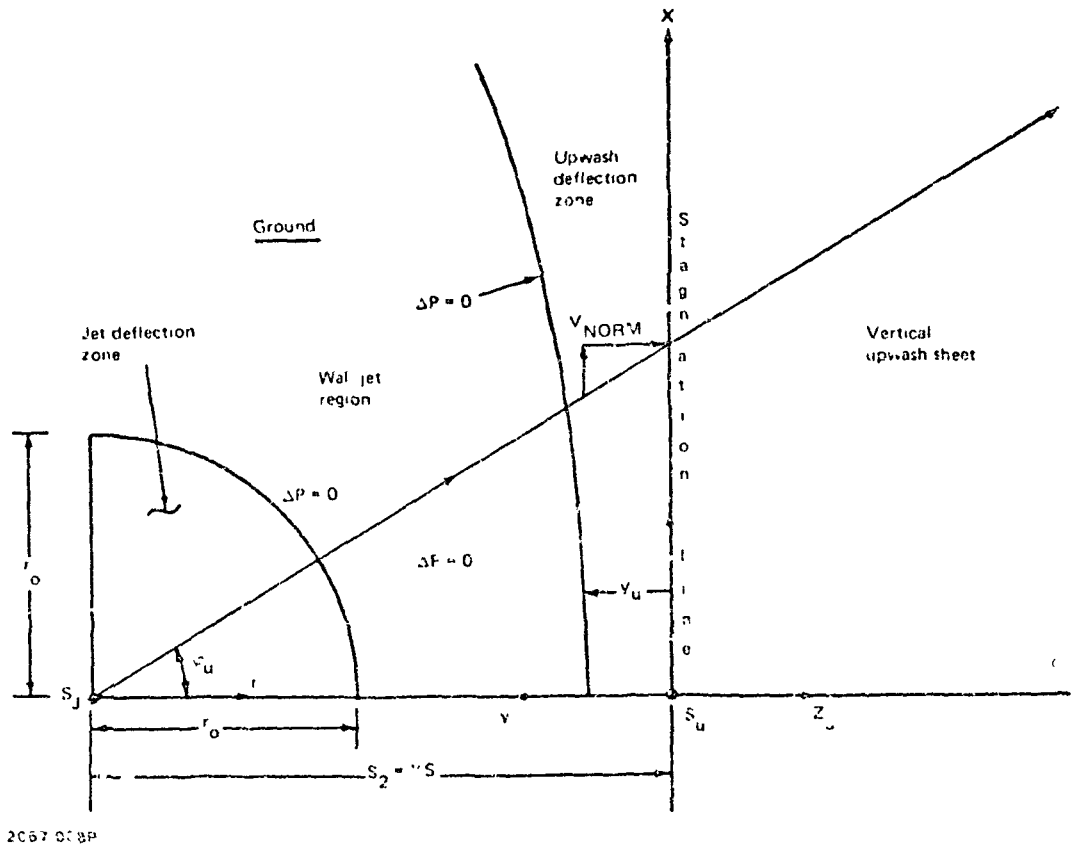

Figure 9-16. - Two-jet impingement without deflection zone interaction.

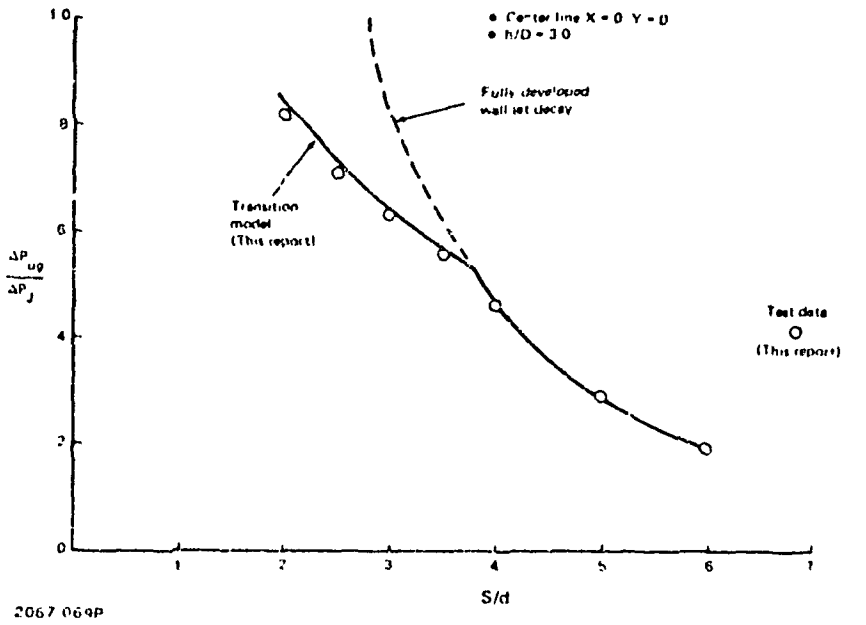

Figure 9-17. - Upwash maximum ground pressure.

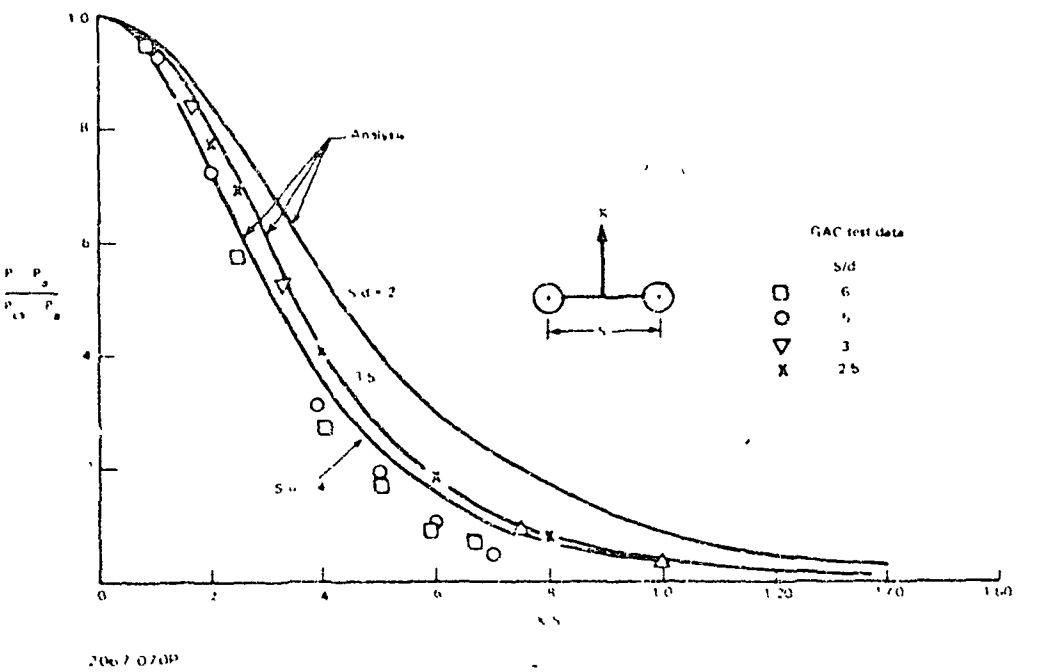

Figure 9-18. - Maximum ground pressure distribution along upwash stagnation line.

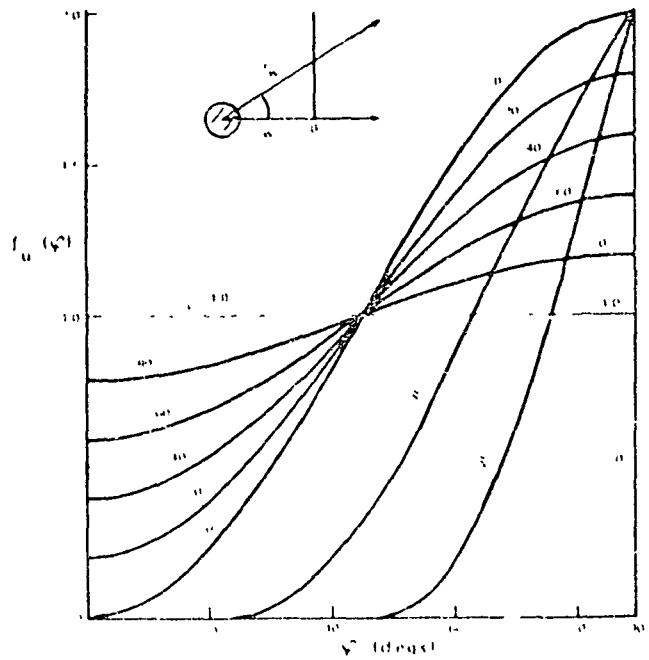

Figure 9-19. - Upwash momentum model.

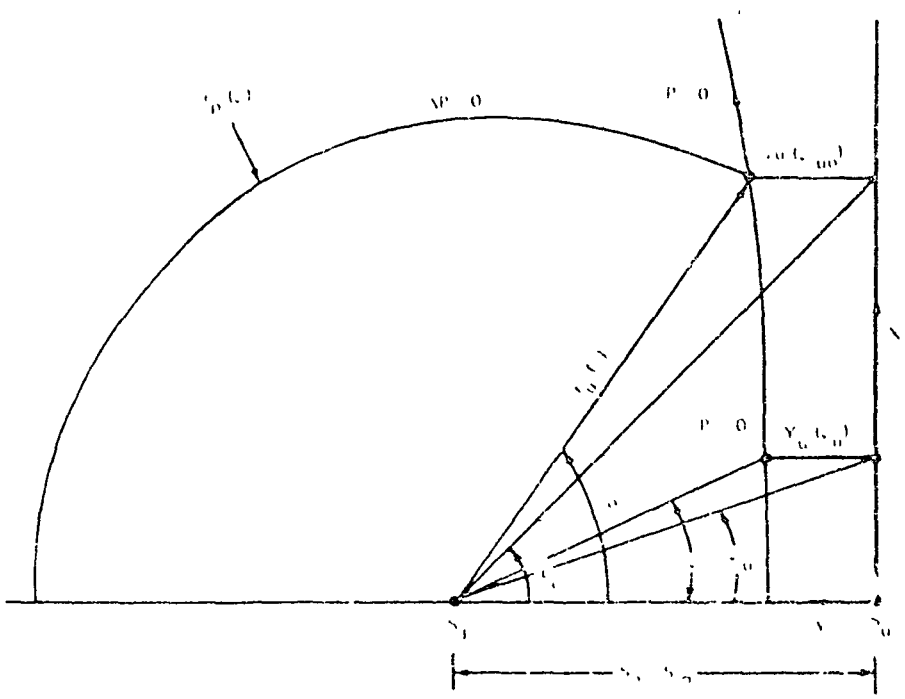

Figure 9-20. - Schematic representation of two-set impingement problem with deflection zone interaction.

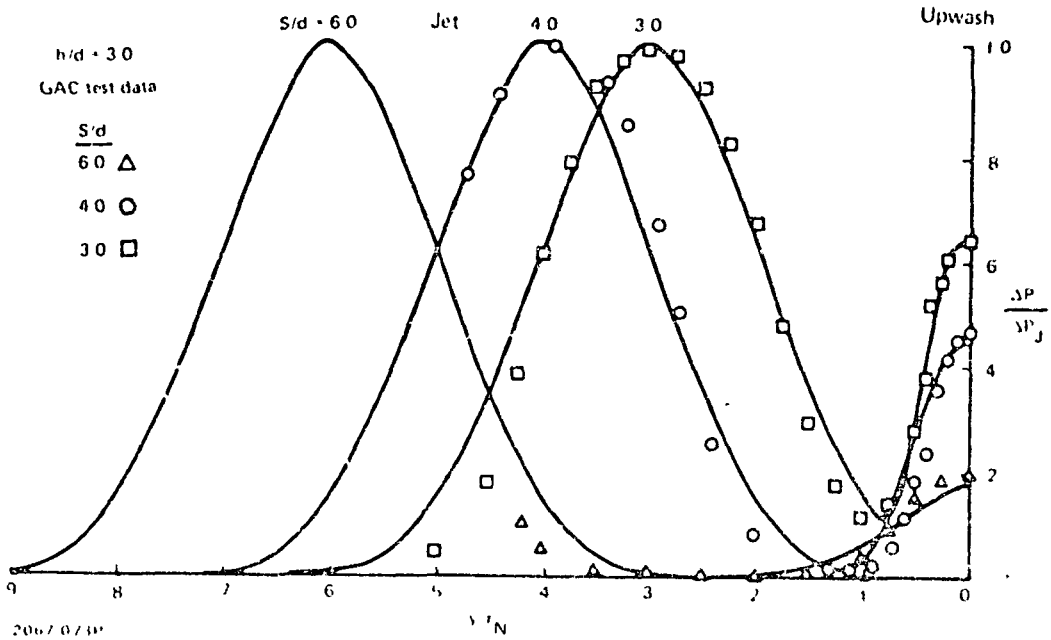

Figure 9-21. - Ground plane pressure distributions (X = 0).

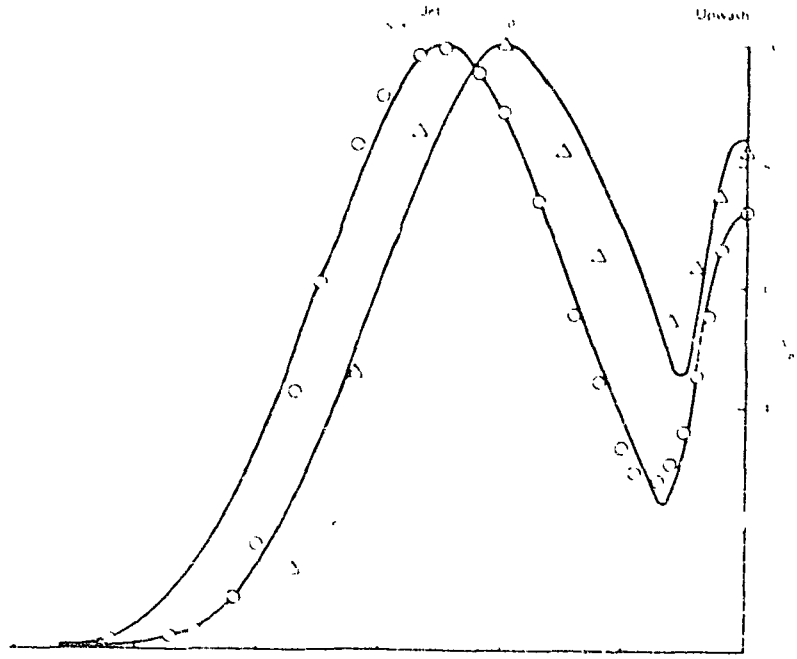

Figure 9-22. - Ground plane pressure distribution.

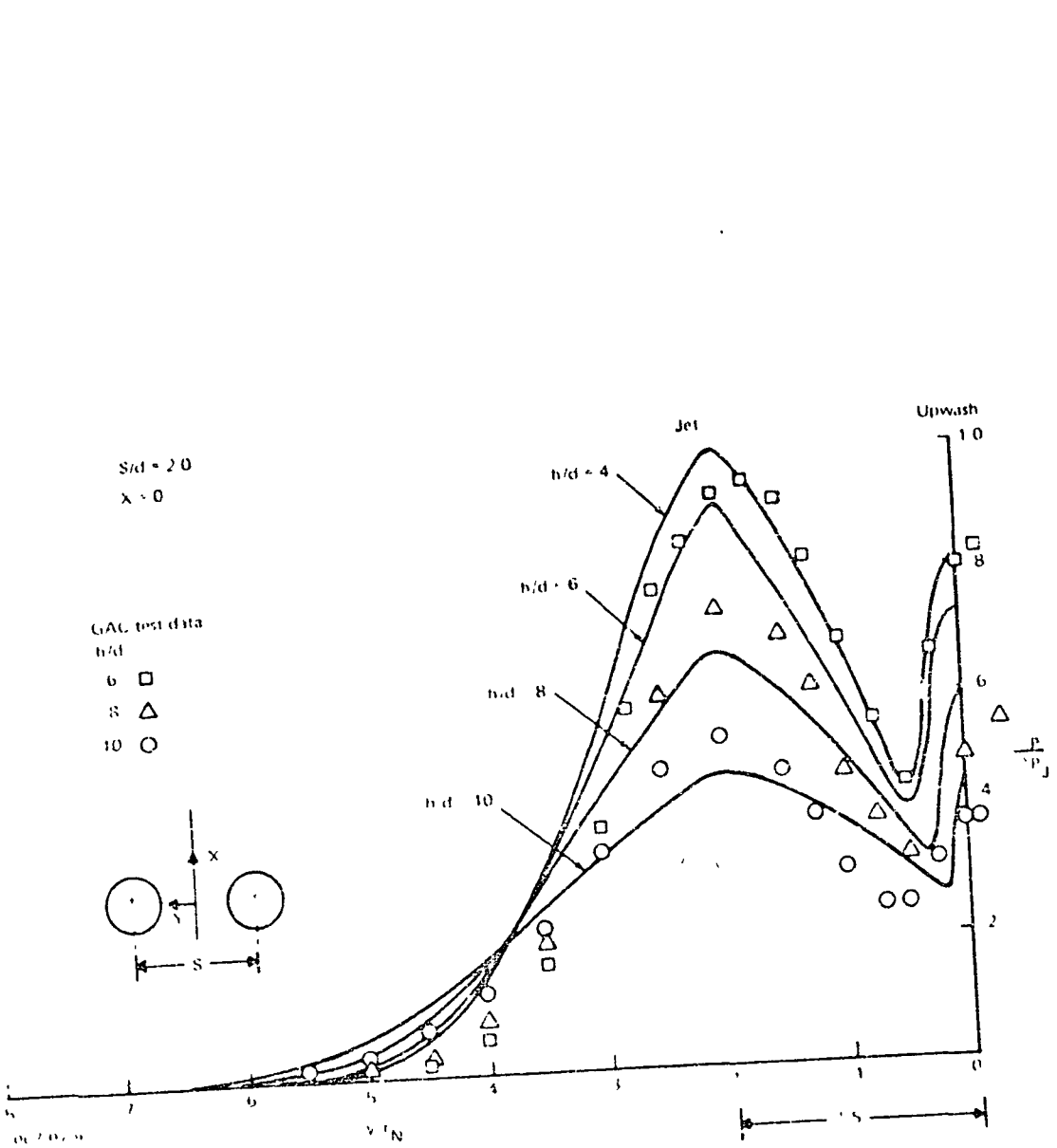

Figure 9-23. - Ground plane pressure distribution.

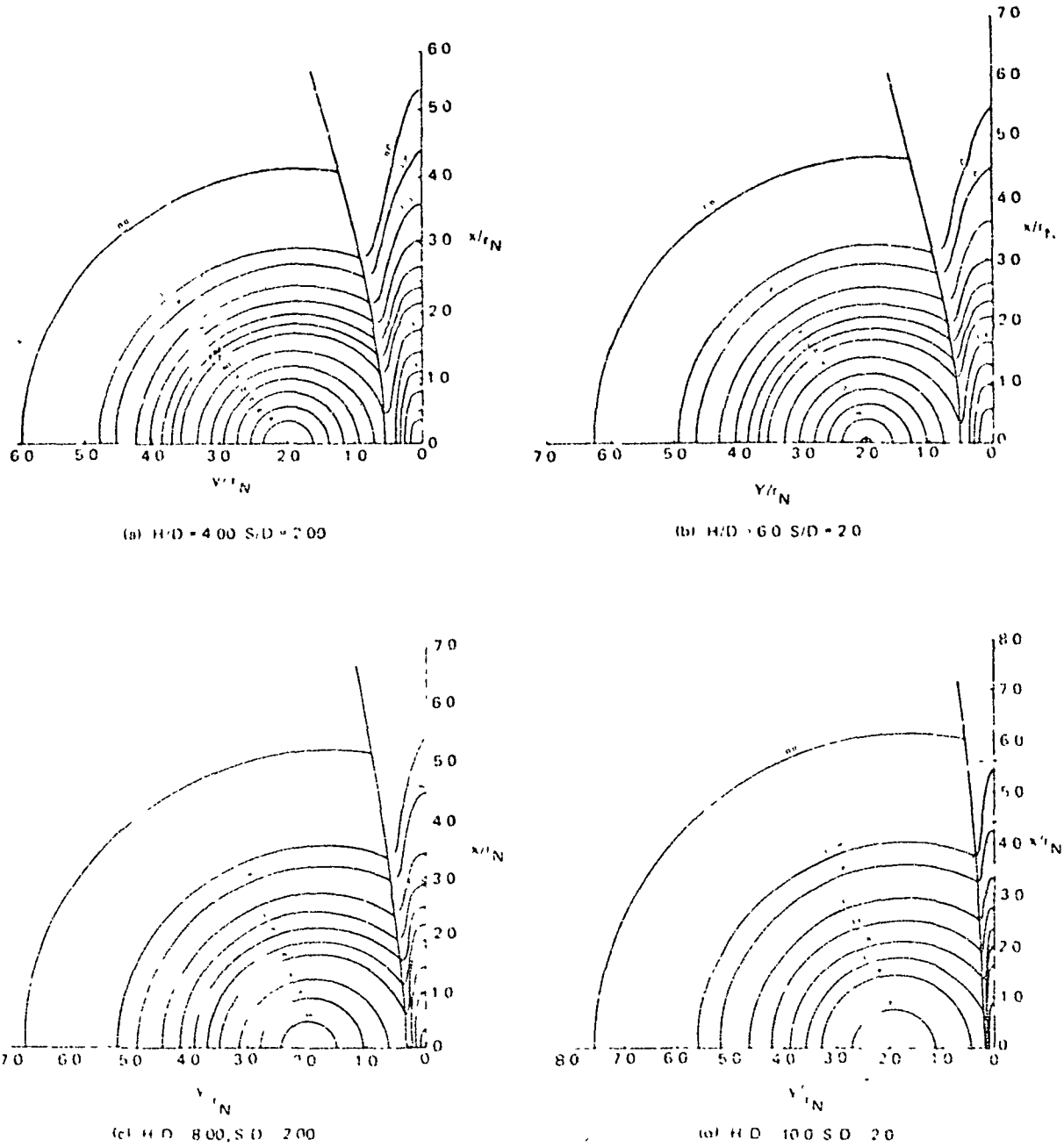

(a) H/D = 4.00 S/D = 2.00

(b) H/D = 6.0 S/D = 2.0

(c) H/D = 8.00, S/D = 2.00

(d) H/D = 10.0 S/D = 2.0

Figure 9-21. - Computed ground isobars.

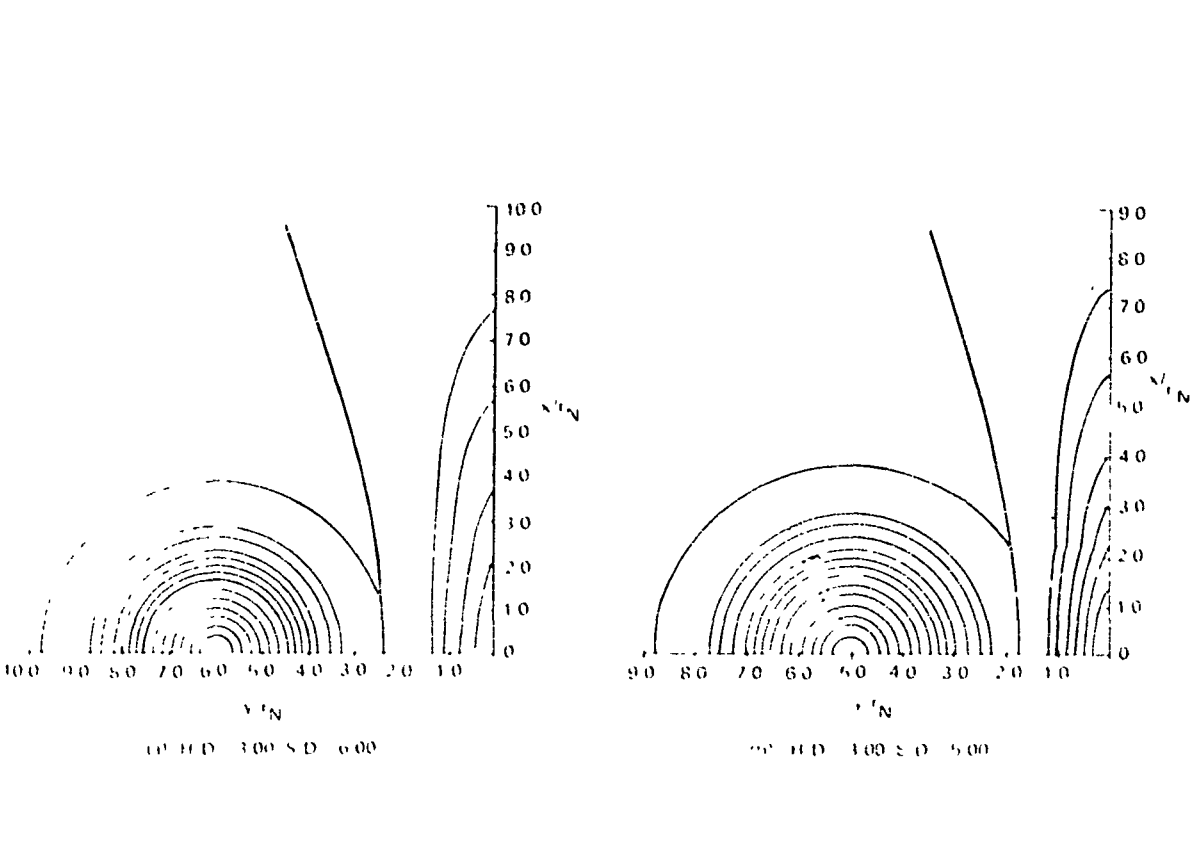

Figure 9-25. - Ground isobars (S.P. = 0.0).

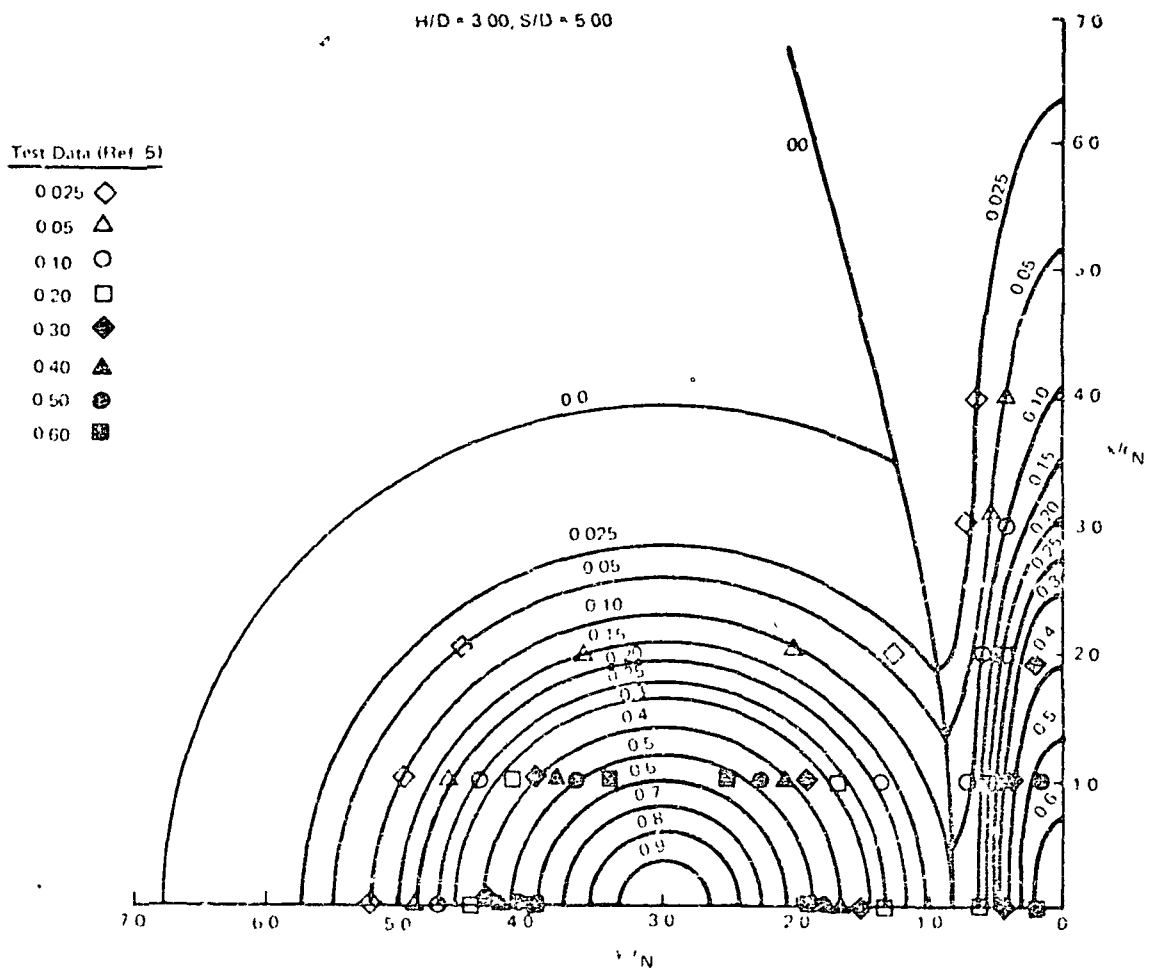

Figure 9-20. - Comparison of measured ground pressures with predictions.

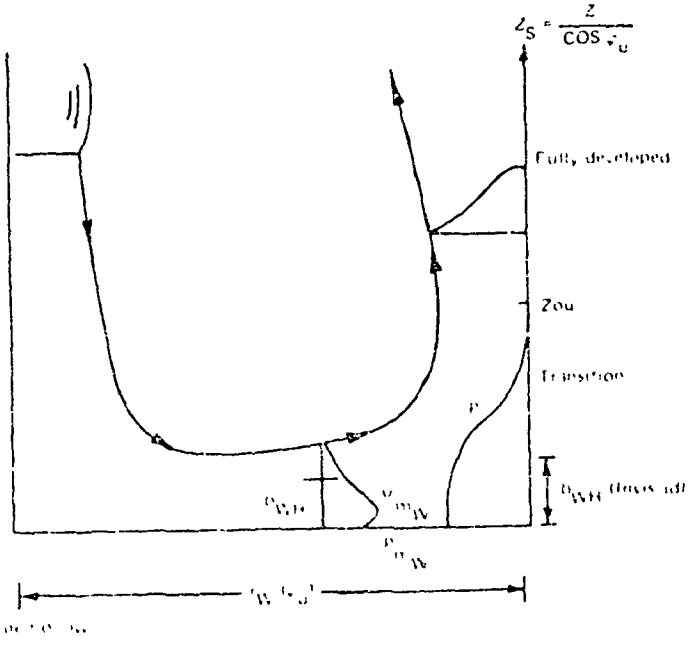

Figure 9-27. - Characteristic scaling parameters for upwash model.

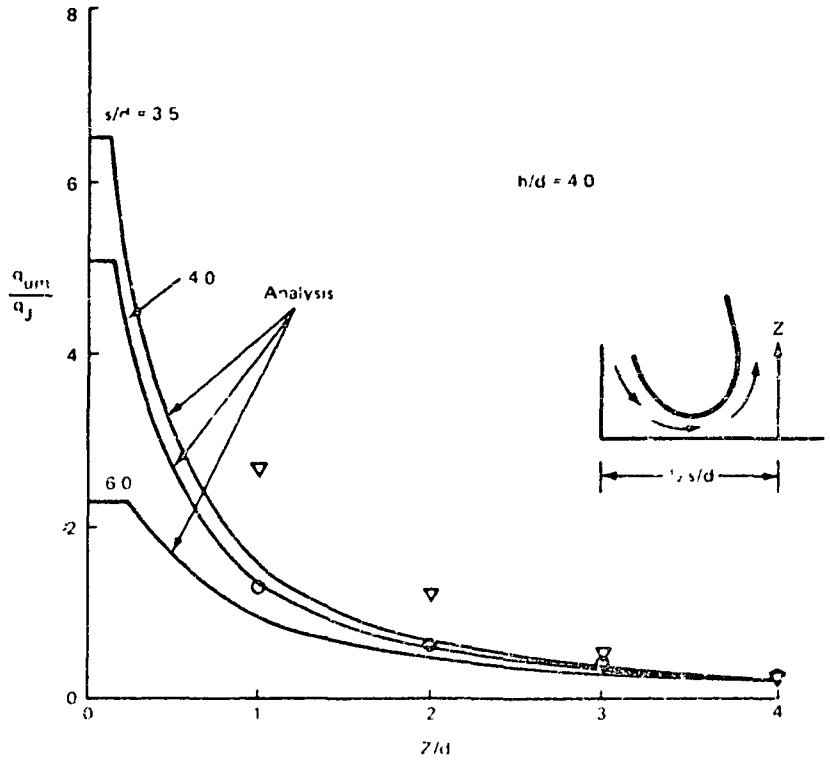

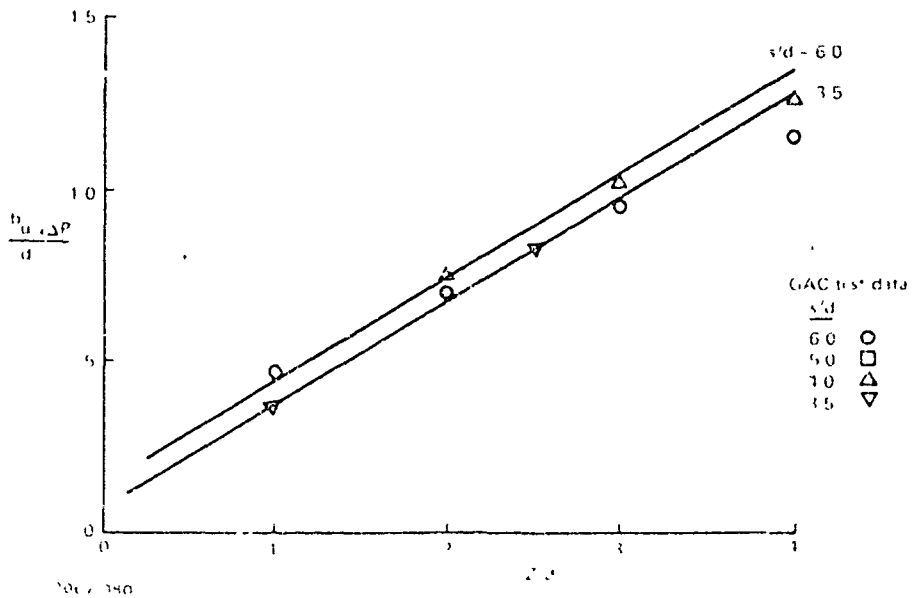

Figure 9-25. - Upwash centerline (X - O) characteristics.

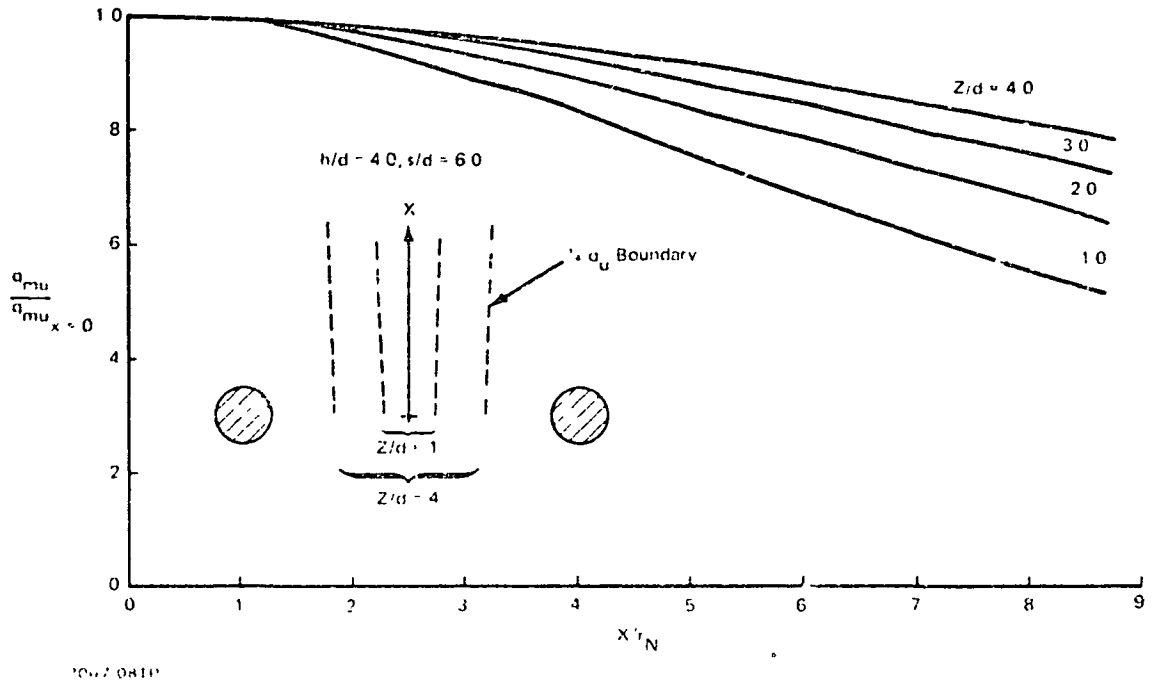

Figure 9-29. - Upwash dynamic pressures.

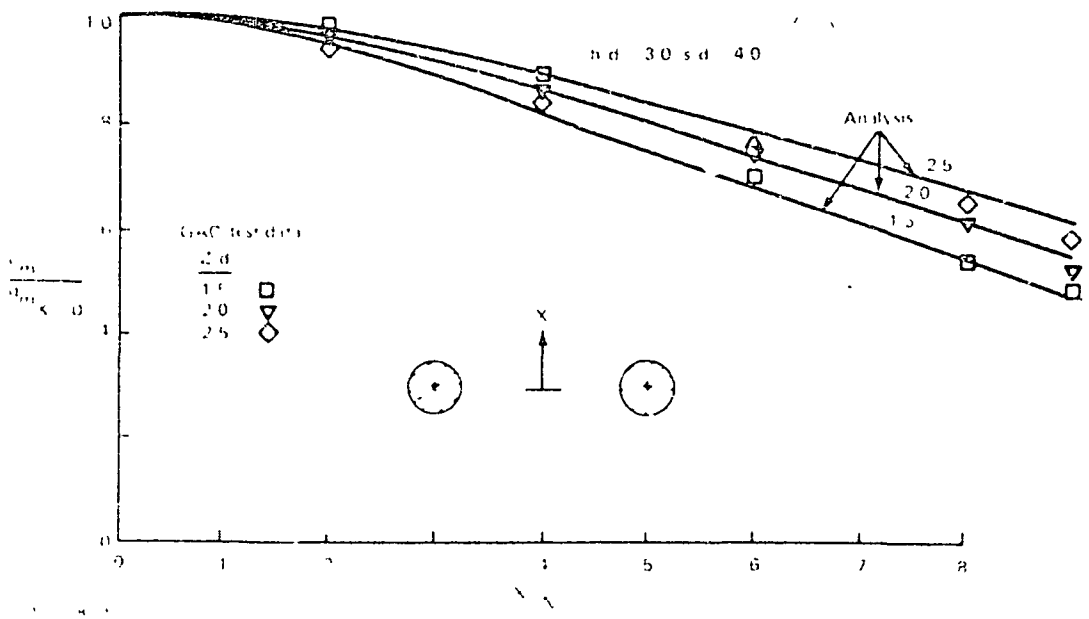

Figure 9-30. - Upwash dynamic pressures.

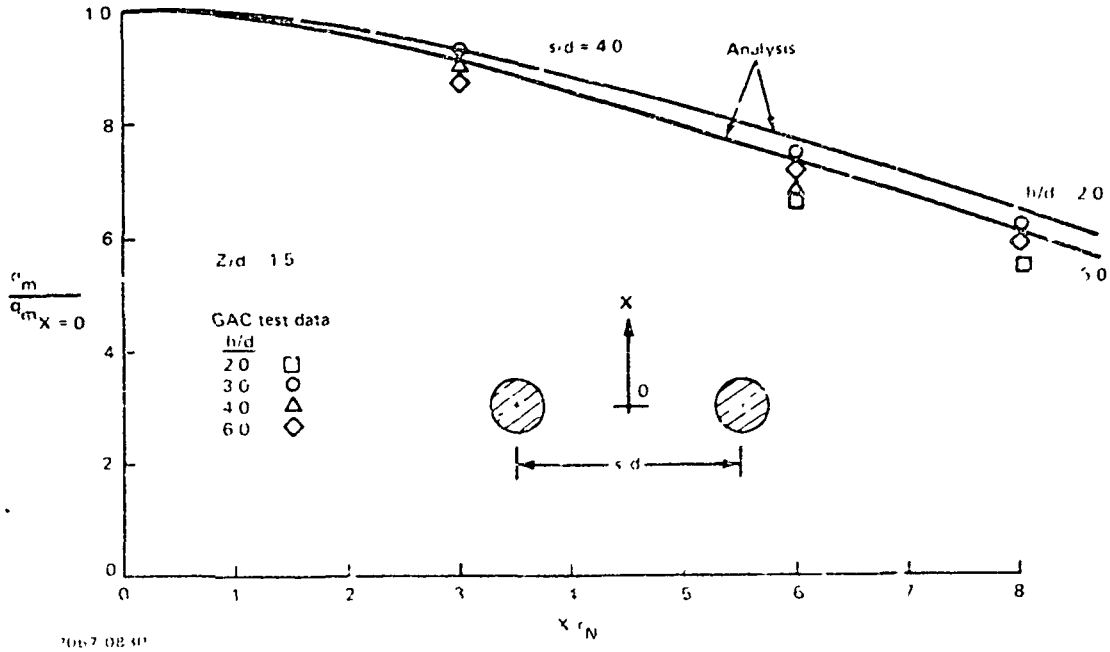

Figure 9-31. - Upwash dynamic pressures at nozzle height.

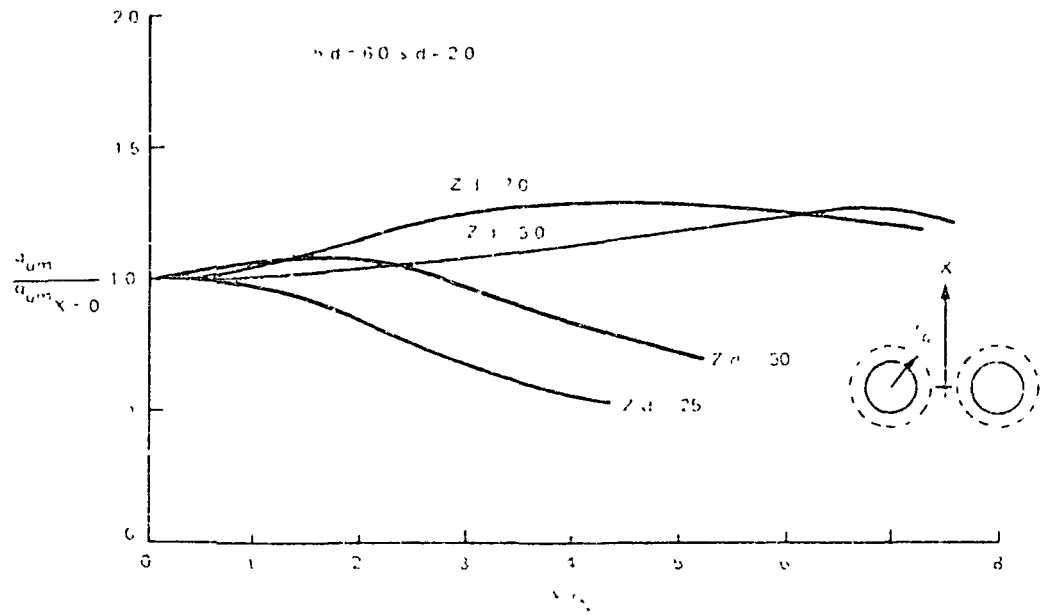

Figure 9-32. - Upwash dynamic pressure.

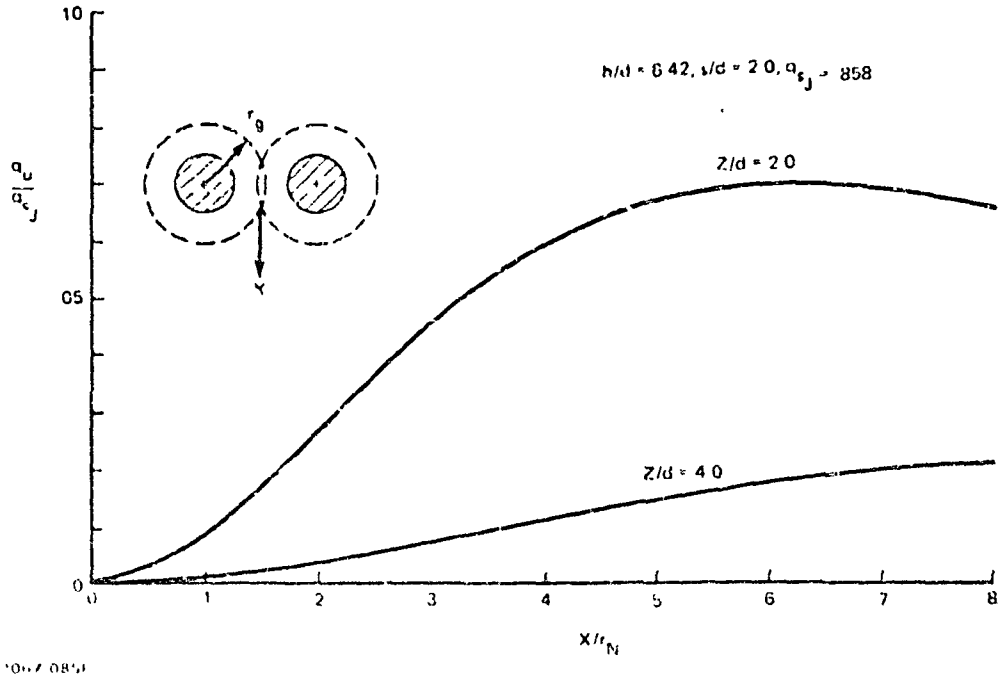

Figure 9-33. - Upwash dynamic pressures.

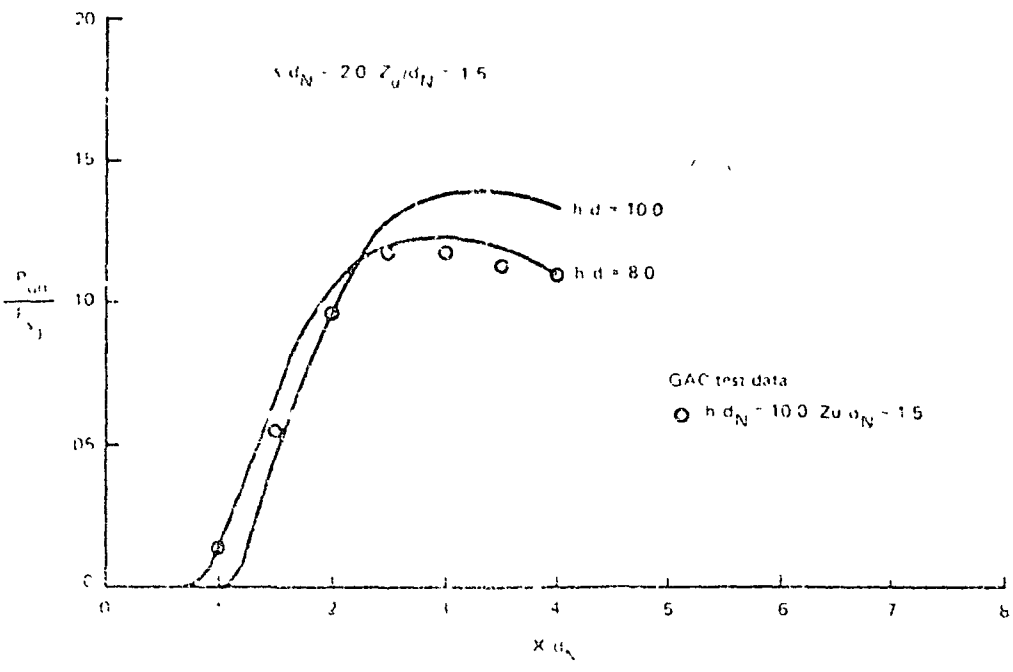

Figure 9-34. - Upwash total pressure.

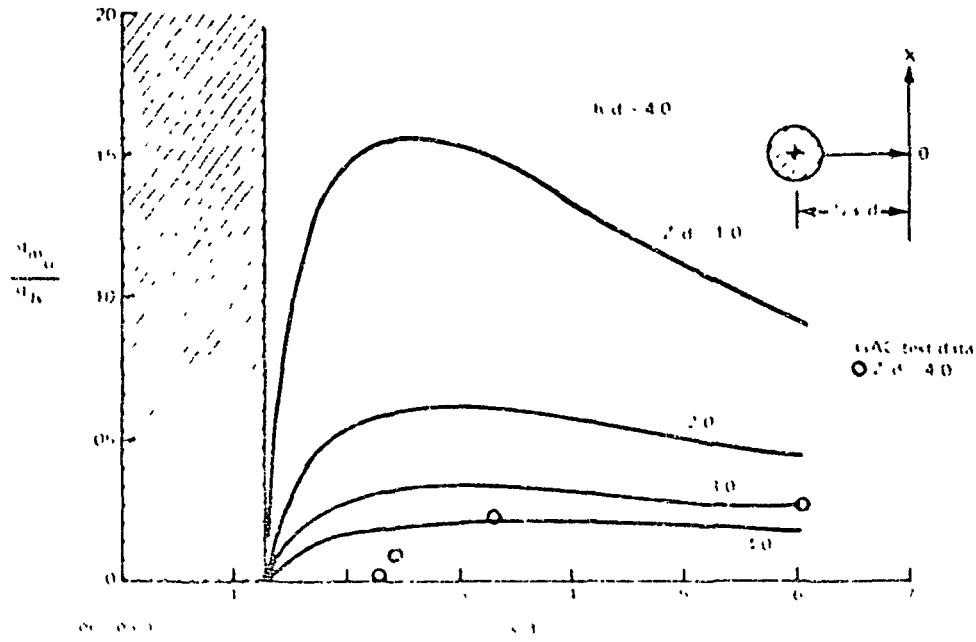

Figure 9-35. - Upwash dynamic pressures at centerline Y = 0.

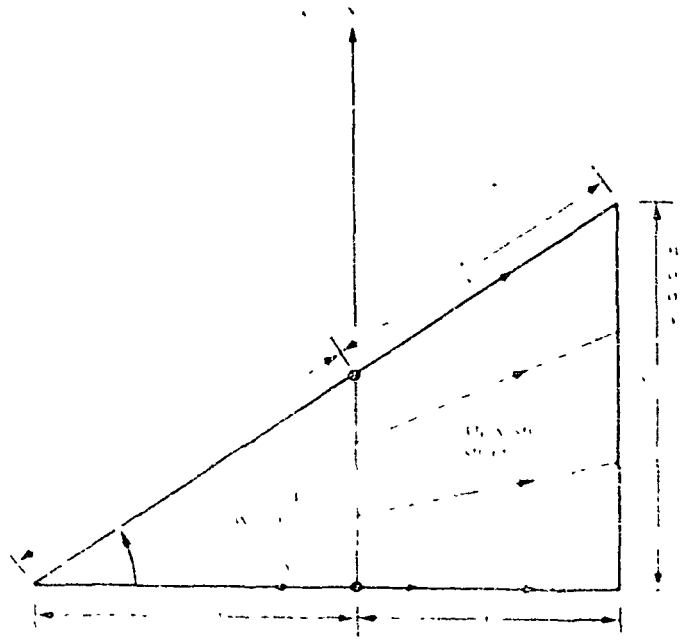

Figure 9-36. Schematic of momentum capture model.

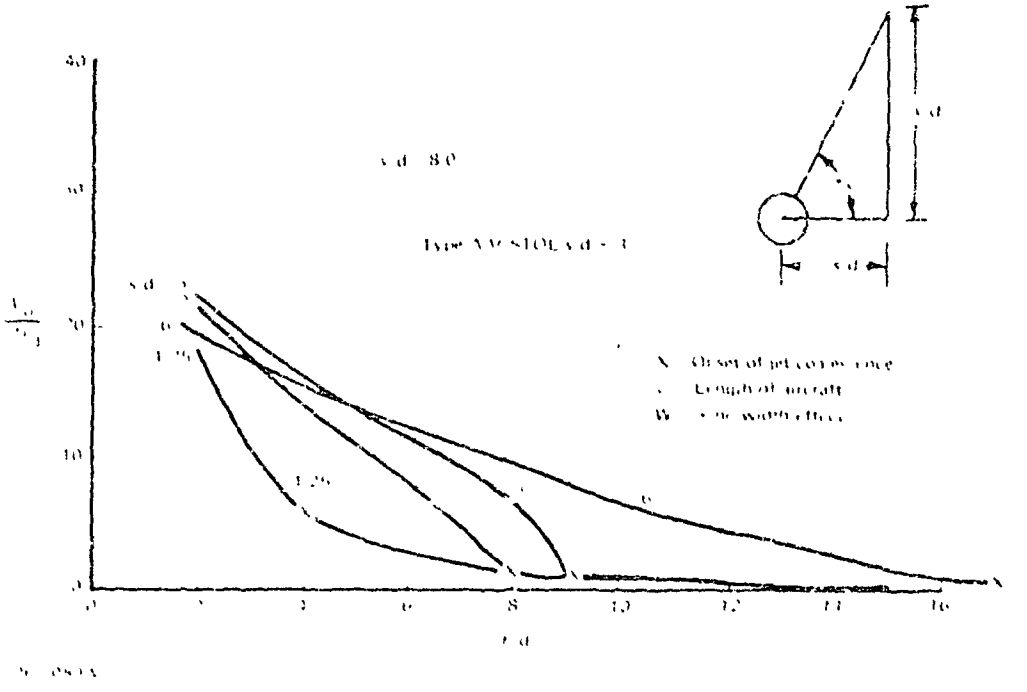

Figure 6-7. - Typical Results using momentum capture model.

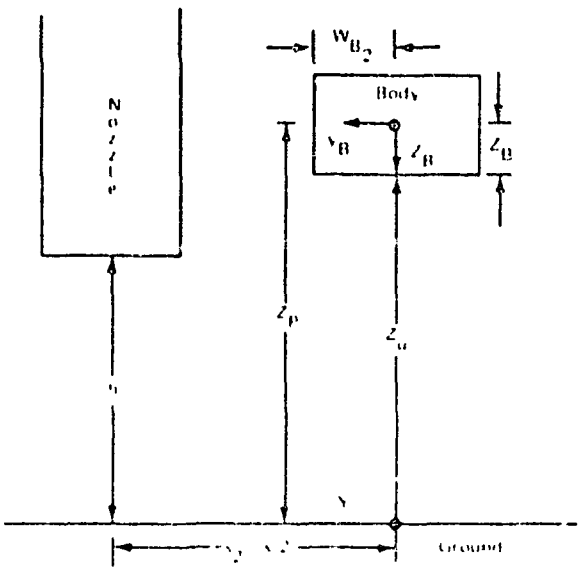

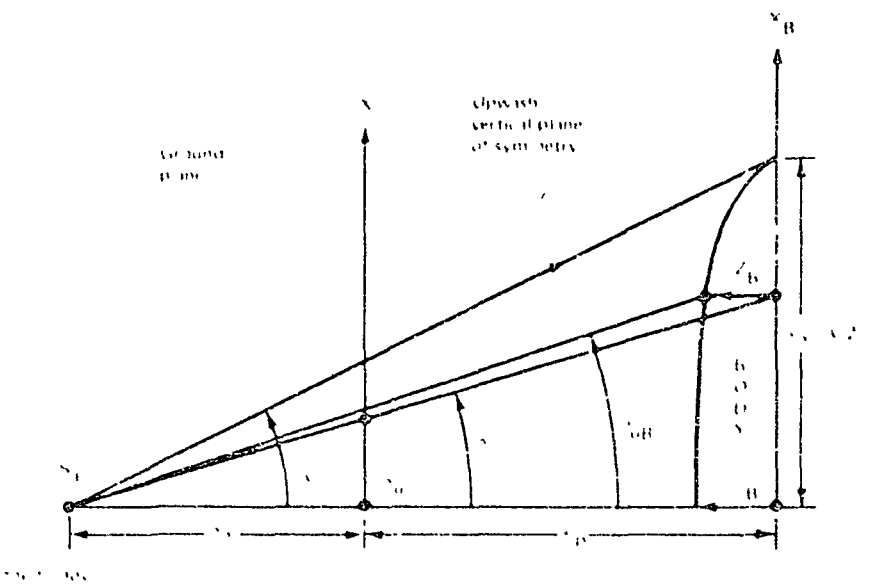

Figure 9-38. - Sketch of upwash force prediction parameters.

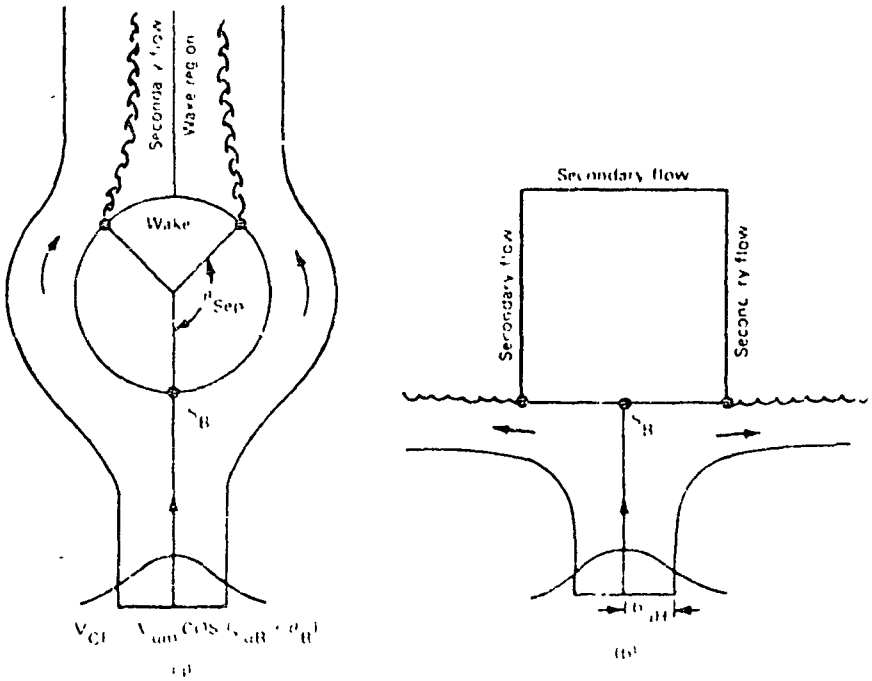

Figure 9-39. - Approximate drag models: a) circul. r, b) rectangular cross sectional shape.

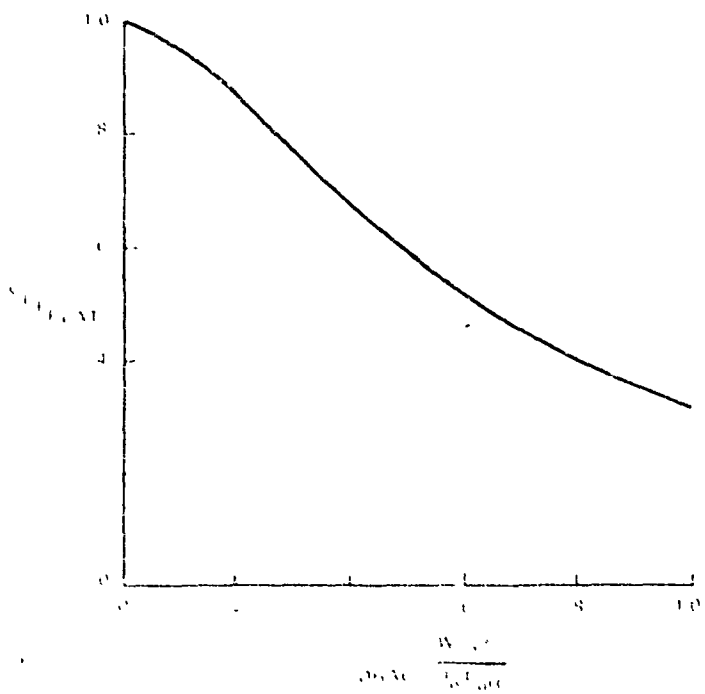

Figure 9-40. - Flat bottom or rectangular cross section drag coefficient.

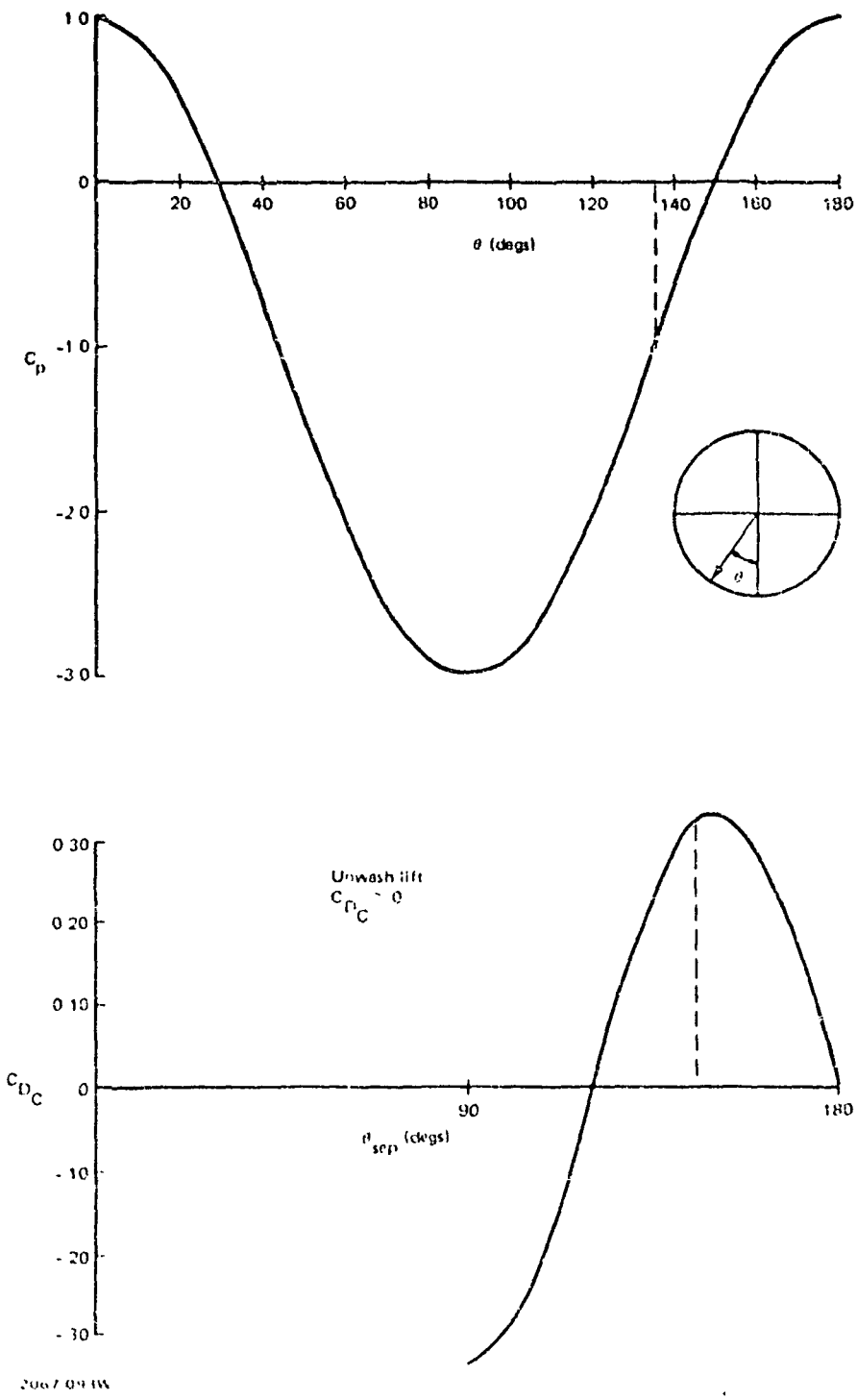

Figure 9-41. - Circular cross section drag model.

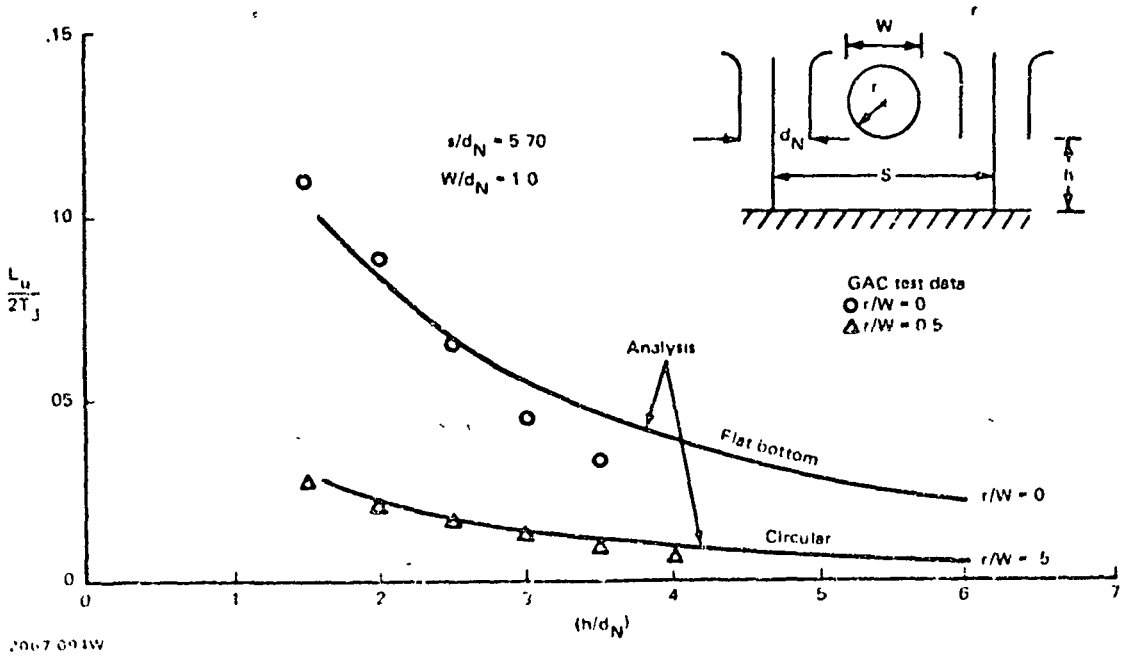

Figure 9-42. - Upwash force on cylindrical (2D) bodies.

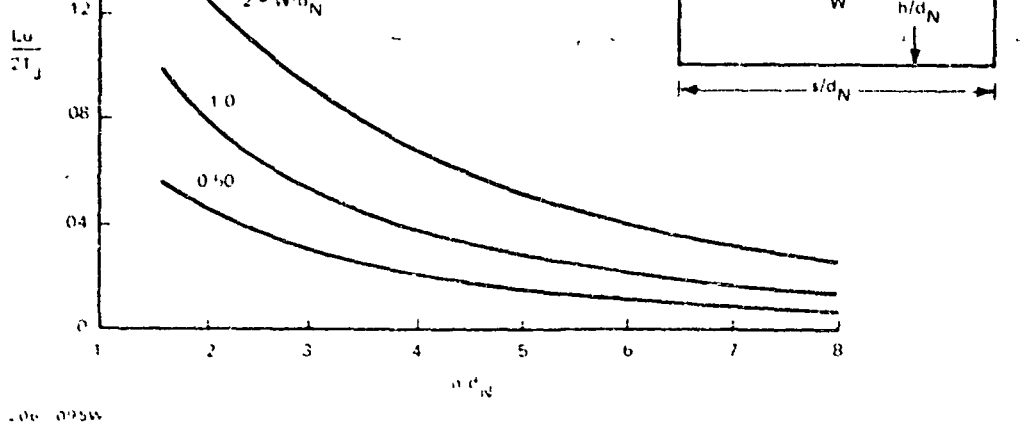

Figure 9-43. - Upwash force on flat bottom cylindrical (2D) body.

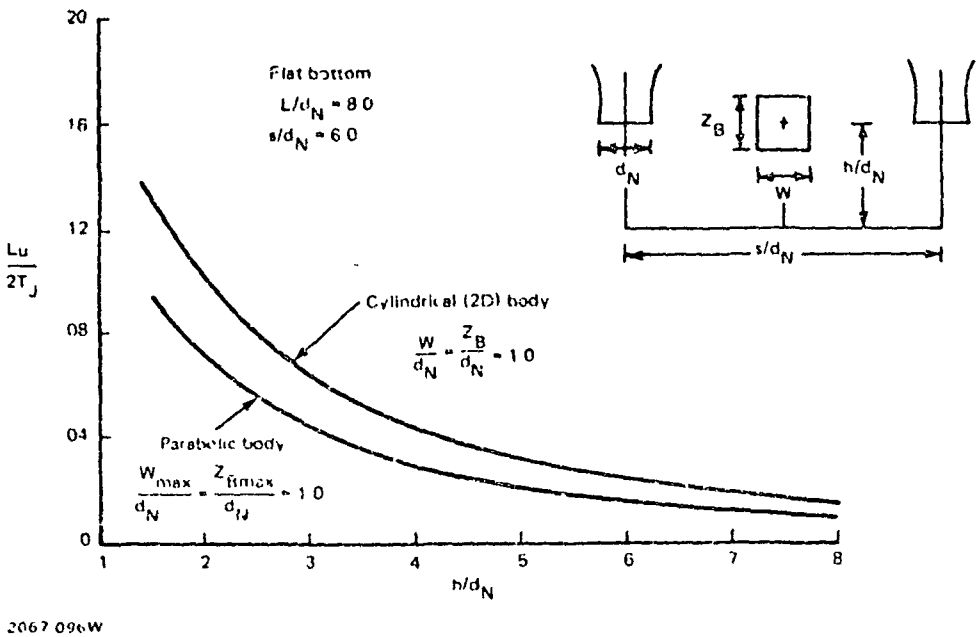

Figure 9-41. - Effect of body longitudinal shape on upwash force.

10. CONCLUSIONS

In ground effect twin jet tests were conducted to determine the general features of the resulting flow field and to ascertain whether such flows are amenable to a mathematical model. Some of the general features looked for were instabilities, basic flow structure as the jet spacing was decreased or height increased (causing jet merging), types of measurements, the deflection zone which results from the collision of wall jets and the resulting upwash sheet, and the effects of bodies placed in the upwash sheet.

The isolated twin jet tests revealed unstable upwash flow over a narrow range of jet spacing in the vicinity of three jet diameters and jet heights around 1 1/2 to 3 diameters. Instabilities were observed in pressure measurements on the ground plane in upwash pressures, and in force measurements on bodies placed in this flow field.

Regions of below ambient pressure were noted in many areas of the isolated two jet flow field. These included both static pressure measurements made by traversing probes across the upwash sheet and measuring surface pressures from the stagnation line on the ground plane. The low pressures in the upwash sheet appear to be a characteristic of the two jet ground impingement flow and were obtained for all values of height and spacing that were tested (from 2-6 diameters). The lowest static pressures occur in the center of the upwash sheet and not at the edges.

Three types of bodies placed in the resulting two jet upwash sheets as well as a 1/10th scale aircraft model with strakes of various depth produced markedly different jet induced forces. Net lift forces over 20% of the jet thrust were measured due to the upwash sheet impinging on fuselage-type surfaces. Strakes were beneficial on simulated fuselage surfaces but not on large flat plate surfaces.

A thorough investigation was made of the flow field that results when the jets are closely spaced and merging of the outer boundaries occurs prior to impingement on the ground plane. It was concluded that the upwash sheet continues to be formed even at close spacings and that if separate peaks appear in the free jet pressure profiles without a ground plane, separate impingement and upwash formation will occur with a ground plane.

A new flow model was developed for close jet spacings which accounts for non fully formed wall jets prior to the development of an upwash sheet. It includes a jet impingement zone wall-jet transition region which adequately predicts the effects of jet spacing and height above ground on the flow field pressures and upwash flow field. Integration of the upwash sheet pressures were used to compare with the test data on fountain lift. Good correlation was obtained with simple two-dimensional bodies of varying cross section.

11. APPENDIX

Appendix A

Computer Program Description

Program

Name: GRUMJET2

Purpose: VTOL Two - Jet Impingement Interaction Problem

The program is designed to estimate the flow characteristics associated with two vertically impinging and equal strength incompressible jets. This program is specifically oriented towards the closely spaced jet interaction problem where the deflection regions interact until eventually jet coalescence occurs.

Aside from the basic flow characteristics, the program assumes the symmetrical placement of a slender fuselage in the upwash flow. The upwash lift force is then computed for a cylindrical fuselage of constant cross-sectional shape. The body parameters, in terms of width and depth, do not vary longitudinally. The program estimates the force based on a rectangular and circular cross section. Two planes of symmetry are assumed and all output applies to one quadrant of the flow field (ie. equal jets and nozzles located at the midpoint of the fuselage). Jet entrainment effects may be significant but are neglected in this program. Hence, the force is only that due to upwash impingement. Some residual programming exists in the code for a parabolic body of revolution. These cards have been commented out but may be used if desired.

Input Description

Note: All input parameters are in terms of nozzle diameters.

Card No.	Code Names	Format
1	HD, SD, ZPLD, DZPL, ZFINAL	5F10.5

Name	Definition
HD	Nozzle height above ground
SD	Nozzle spacing

Note The program will compute one or several positions of the fuselage relative to the ground for a fixed nozzle height above ground.

ZPLD	Initial fuselage height above ground
DZPL	Increment in fuselage ΔZ above ground
ZFINAL	Final Z coordinate of fuselage height relative to ground plane.

Card No.	Code Names	Format
2	XL2, WCON, ZCON	3F10.5

Names	Definition
XL2	Fuselage Length
WCON	Fuselage Width
ZCON	Fuselage Depth

Note: ZCON determines position of fuselage underside relative to its ZPLD location. Bottom of fuselage will be located at ZPLD-ZCON at first computed location. The upwash sheet properties are also computed at this Z location.

Card No.	Code Names	Format
3	IPBAR	I1

Name	Definition
IPBAR	Integer controlling the output of ground pressure pattern. IPBAR = 0, no pressure pattern output IPBAR = 1, pressure pattern output is desired

Note Card No. 4 is not required if IPBAR = 0.

Card No.	Code Name	Format
4	NU	I2

Name	Definition
NU	Number of pressure values to be input for computation of ground isobar pattern NU < 25

Note Card No. 5 is repeated NU times.

Card No.	Code Name	Format
5	PU	F10.5

Name	Definition
PU	Nondimensional pressure for isobar pattern $0.0 \leq PU < 1.0$

Figure A-1 shows a typical input set.

Printed Output Description

Figure A-2 shows a typical computer printout. Most of the geometrical output quantities are nondimensionalized by the nozzle radius. All velocities and pressure are initially nondimensionalized by the nozzle exit velocity and stagnation pressure. All pressures are relative to ambient conditions.

Note: RN and D refer to nozzle exit radius and diameter. VN refers to nozzle exit velocity.

Input Parameters

The first set of output echoes the input parameters.

Output Titles	Definitions
H/D	Nozzle height above ground
S/D	Nozzle spacing distance between jet centerlines
Z/D	Initial fuselage height
DZ/D	Increment in fuselage position
ZFINAL/D	Final location of fuselage
L/D	Body length
W/D	Body width
ZB/D	Location of underside of body relative to specified fuselage location

Note If ZB = 0, underside location is coincident with specified fuselage position.

Jet Decay Region .

Output Titles	Definitions
DELG/D	Jet ground effect height relative to ground plane
ZPC/RN	Length of potential core
ZFD/RN	Length of potential core and transition regions
Z/RN	Jet axial location measured from nozzle exit
RJH/RN	Half-velocity radius of jet measured from jet centerline
RJ/RN	Half width of jet
ALP	Exponent of velocity profile
CV2	Momentum flux integral
VJ/VN	Centerline velocity
RCORE/RN	Potential core radius

Jet Deflection Region

Single jet impingement characteristics are printed.

Output Titles	Definitions
RGH/RN	Half velocity radius of jet at ground effect height
RG/RN	Jet half width at ground effect height
RO/RN	Deflection zone or pressure recovery radius
VG/VN	Square root of jet ground stagnation pressure
DPS/DPTJ	Jet ground stagnation pressure nondimensionalized by nozzle stagnation pressure
ALPG	Exponent of ground pressure distribution
R/RGH	Radial location in deflection region relative to ground stagnation point. Nondimensionalized by ground effect half velocity radius of jet
DPS/DPTG	Ground pressure nondimensionalized by ground stagnation pressure

Output Titles	Definitions
R/RN	Radial location in deflection region nondimensionalized by nozzle radius
DPS/DPTJ	Ground pressure nondimensionalized by nozzle stagnation pressure

Wall Jet Region

Isolated wall jet properties are printed in this set of output.

Output Titles	Definitions
DELS/RN	Boundary layer thickness at stagnation point
VM/VG	Inviscid maximum velocity at jet half width (RGH) radial location or start of transition to turbulent wall jet
ALPWO	Exponent of velocity profile at start of wall jet
BWOH/RN	Half velocity thickness at start of wall jet
BWO/RN	Initial thickness of wall layer
R/RN	Radial location on wall jet measured from ground stagnation point
VM/VG	Maximum velocity in wall layer nondimensionalized by square root of ground stagnation pressure
VM/VN	Maximum velocity in wall layer referenced to nozzle exit velocity
BWH/RN	Half velocity thickness of wall layer
BW/RN	Thickness of wall layer
DELBL/RN	Boundary layer thickness
DLTPJ	Maximum stagnation pressure in wall layer
KDELL	Ratio of boundary layer to total wall layer thickness
NPOWER	Exponent of boundary layer profile

Two Jet Impingement Interaction Output

Maximum Ground Pressures along Upwash Ground Stagnation Line

Output Titles	Definitions
XW/RN XW/S	Coordinate along stagnation line measured from upwash stagnation point
PMAX/PJ	Stagnation line pressure nondimensionalized by nozzle stagnation pressure
PMAX/PMAXO	Stagnation line pressure nondimensionalized by upwash stagnation point pressure

Upwash Momentum Function

Output Titles	Definitions
RG/RN	Radius of jet at ground effect height
ACON	Constant in momentum function
XMOMZ	Total vertical momentum in upwash sheet nondimensionalized by the optimum value of $M_J/2\pi$.
PHIO	Coalescence angle used in upwash momentum model If PHIO = 0 jets are not coalesced If PHIO > 0 jets have begun to coalesce

Note: Depending on the value of PHIO (i.e. zero or non-zero) the constant RCON applies to the appropriate upwash momentum model.

CU Nondimensional upwash deflection region width constant

Note: There are two possible outputs that can occur at this point. If the jets are spaced far enough apart the comment:

JET AND UPWASH DEFLECTION REGIONS DO NOT
INTERACT, CU ESTIMATE IS CORRECT

In this case the value of CU is correct and the jet impingement and upwash deflection regions are independent. The perturbation parameters are then defined as:

EPS = 0.0

SIG = 1.0

PHIUO = 0.0

PHIO = 0.0

PMIN = 0.0 along upwash line

ALPUG = 1.50

If the nozzle spacing and height above ground are such that the deflection regions interact, the subroutine INTERG will be called and

CALL INTERG

will be displayed. The following output will be printed.

Output Titles	Definitions
Iteration cycle	Number of iterations required to find solution using Newton's method
EPS or EPI	Perturbation parameter for jet impingement pressure distribution
SIGMA or SIG	Perturbation parameter for upwash deflection region pressure distribution
CU or CUI	Upwash width estimate prior to iterative solution
PHIUO PHIO	Angles defining the intersection of jet and upwash deflection regions

Note The following values apply along the line connecting the jet stagnation points on the ground (i.e. x = 0).

DELPWO	Pressure at upwash stagnation point nondimensionalized by nozzle stagnation pressure
PMIN	Minimum pressure between jet and upwash deflection regions nondimensionalized by nozzle stagnation pressure
ALPUG	Exponent of upwash ground pressure distribution function
(CU) x (SIGMA)	Final value of upwash thickness constant

Note: If IPBAR ≠ 0, the following output will occur.

Computation of Two - Jet Ground Isobar Pattern

Output Titles	Definitions
PBAR	Input values of pressure, nondimensionalized by nozzle stagnation pressures, will be echoed.

Note: The following will be repeated NU times.

Output Titles	Definitions
IJET	Number of points on jet impingement region isobar
IU	Number of points on upwash deflection region isobar

If IJET = 0 or IU = 0, the specified value of PBAR was not found in ground pressure distribution

Note: The following coordinates are referenced to the jet stagnation point on the ground.

XISOJ	X coordinate of jet isobar
YISOJ	Y coordinate of jet isobar
XISOU	X coordinate upwash region isobar
YISOU	Y coordinate of upwash region isobar

The final set of output in this section is the upwash deflection zone line. If the deflection zones do not interact, ambient conditions exist along this line.

XUP	X coordinate of upwash line
YUP	Y coordinate of upwash line

Computation of Upwash Flow Field

Upwash Streamline Properties

Note Two streamlines are printed

Output Titles	Definitions
PHID	Azimuthal angle of upwash streamline referenced to jet ground coordinate system
INV . VEL.	Inviscid turning region maximum velocity

DELPWJ	Maximum pressure on upwash stagnation line on the ground where upwash streamline orginated
BWGH/RN	Half velocity width of incident wall jet streamline
ZOU/RN	Upwash turning region height above ground
BUO/RN	Initial upwash width
BUOHN/RN	Initial upwash half velocity width

Upwash Streamline Decay Properties

Z/RN	Upwash streamline coordinate (ZS)
VMU/VN	Upwash maximum or centerline velocity
BUH/RN	Half velocity width
BU/RN	Half-width
DELPU/DELPJ	Upwash centerline or maximum total pressure nondimensionalized by nozzle stagnation pressure

Upwash Properties Computed At Z Location of Underside of Body

If ZB = 0, the output will yield the upwash properties at Z = constant plane above ground.

Output Titles	Definitions
ZU/RN	Upwash coordinate measured from ground plane
RW/RN	Radial coordinate from jet ground stagnation point to upwash stagnation line
PHIB	Azimuthal location of upwash streamline referenced to jet coordinate system
X/RN	X coordinate in upwash sheet or X coordinate on fuselage
VMU/VN	Maximum or centerline upwash velocity
PU/PN	Maximum or centerline upwash total pressure nondimensionalized by nozzle stagnation pressure
BUH/RN	Half-velocity width of upwash

PU/PUO	Upwash total pressure nondimensionalized by total pressure on streamline originating from upwash stagnation point (X = 0, Y = 0)
PU/PJS	Upwash total pressure nondimensionalized by jet ground stagnation pressure
PBS/PN	Stagnation pressure on underside of fuselage placed in upwash sheet

Upwash Lift Force

Two values are printed:

FLAT BOTTOM VEHICLE WITH SHARP CORNERS

BODY WITH CIRCULAR CROSS SECTION

Output Title	Definition
LU/2TJ	Upwash lift force nondimensionalized by the total thrust of the two jets

Computer Program Listing

Figure A-3 shows a fortran listing of the computer program.

```
4.00        4.00        2.00        1.00        4.00
8.00        1.00        0.0
1
 4
.60
.3
.2
.05
```

Figure A-1. Sample Input Data Set

```
DMSI 10740I EXECUTION BEGINS...

                    ***   INPUT PARAMETERS   ***

          H/D=   4.00000  S/D=   4.00000  Z/D=    .00000

          Z/H=   2.00000  DZ/D=   1.00000  ZFINAL/D=   4.00000

          BODY LENGTH L/D=   8.00000  WIDTH W/D=   1.00000  DEPTH ZB/D=   0.0


                    *****      JET DECAY REGION      *****

JET DEFLECTION HEIGHT DEFG/D =   1.19340
JET RN=   8.00000  ZFD,RN=  15.20913
      Z RN        RJH RN        RJ RN          ALF          CV2          VJ/VN        RCORE/RN

     0.0          1.00000      1.00000      0.0          0.50000      1.00000      1.00000
     0.7 369      1.00535      1.03047      4.07761      0.47096      1.00000      0.95013
     1.24738      1.01871      1.06045      4.1 1106     0.44462      1.00000      0.89510
      .87107      1.03807      1.09022      4.39[illegible]      0.42067      1.00000      0.83523
     2.4.475      1.07142      1.11988      4.55906      0.39868      1.00000      0.77065
     3.11344      1.04628      1 11953      4 71406      0 37818      1.00000      0.70144
     3.74,13      1.05813      1.17927      4 84081      0.35953      1.00000      0.62765
     4.36782      1.06549      1.20917      5.00033      0 34197      1.00000      0.54929
     4.98951      1 07403      1. 3929      5.13302      0 32551      1.00000      0.46636
     5 61170      1.08420      1 26970      5.25635      0.31015      1.00000      0.37882


                    *****      JET DEFLECTION REGION      *****

RJH RN=   1.08420  RJ/RN=   1.26770  RJ/RJH=   1.90311  VJ/VN=   1.00000

STAGNATION PRESSURE, DELTA PT/Q=   1.00000
Z =   1.48760

                    SINGLE JET GROUND PRESSURES

          Z RGH          P/DELTA Q          X/RN          DELTA PT/Q

          .,             1 00000          0.0          1.00000
          0.0734         0.98763          0 01356      0.93763
          1 14014        0.96569          0.15931      0.08569
          1.  941        0.93906          0.23897      0.93906
          1  9789        0.90628          0 31862      0.90628
          2 3 75         0 87136          0 39820      0 87136
          2 84063        0 83406          0.47793      0.83406
          3.51429        0 79498          0.55759      0.79498
          4 18776        0 75464          0.63714      0.75464
          4 86123        0 71349          0.71690      0 71348
          5 5345         0 + 190          0.79655      0.67190
          6.80814        0.53024          0 87621      0.53024
          7 48151        0.58866          0.95586      0 58881
          8 15500        0 [illegible]          1 03552      0.54782
          8 82847        0 [illegible]          1 11517      0 50769
          9 50194        0 [illegible]          1 19483      0 46865
          10 [illegible]         0 [illegible]          1 27448      0 43031
          10 [illegible]         0 [illegible]          1 35414      0 39360
```

Figure A-2. Sample Computer Printout

1.32245	0.35827	1.43370	0.35827
1.39592	0.32452	1.51345	0.32452
1.46939	0.29244	1.59310	0.29244
1.54286	0.26209	1.67276	0.26209
1.61632	0.23355	1.75241	0.23355
1.68979	0.20686	1.83207	0.20686
1.76326	0.18207	1.91172	0.18207
1.83673	0.15906	1.99138	0.15906
1.91020	0.13796	2.07103	0.13796
1.98367	0.11869	2.15069	0.11869
2.05714	0.10134	2.23034	0.10134
2.13061	0.08551	2.31000	0.08551
2.20408	0.07148	2.38965	0.07148
2.27755	0.05907	2.46931	0.05907
2.35102	0.04820	2.54896	0.04820
2.42449	0.03877	2.62862	0.03877
2.49795	0.03068	2.70827	0.03068
2.57142	0.02385	2.78793	0.02385
2.64489	0.01816	2.86758	0.01816
2.71836	0.01349	2.94724	0.01349
2.79183	0.00975	3.02689	0.00975
2.86530	0.00681	3.10655	0.00681
2.93877	0.00457	3.18620	0.00457
3.01224	0.00292	3.26586	0.00292
3.08571	0.00175	3.34551	0.00175
3.15918	0.00096	3.42517	0.00096
3.23265	0.00047	3.50482	0.00047
3.30612	0.00020	3.58448	0.00020
3.37958	0.00006	3.66413	0.00006
3.45305	0.00001	3.74379	0.00001
3.52652	0.00000	3.82345	0.00000
3.59999	0.00000	3.90310	0.00000

***** WALL JET REGION *****

TRANSITION POINT BOUNDARY LAYER THICKNESS DELS/X= 0.03735
VELOCITY AT START OF TURBULENT WALL JET, UM/UC= 0.69010
START OF WALL JET REGION, X/EMOD= 0.41473 RWJ/RN= 0.41473 RWJ RN= 2.38637

WALL JET PROPERTIES

X RN	UM/UO	UM UN	RWJ RN	RW RN	DELRI/RN	DELS	RDEL	MFLOWER
0.0	0.0	0.0	0.41473	2.38632	0.03734	1.00000	0.01565	14.00000
0.07347	0.18859	0.18859	0.41473	2.38632	0.03734	1.00000	0.01565	14.00000
0.14694	0.31151	0.31152	0.41473	2.38632	0.03734	1.00000	0.01565	14.00000
0.22041	0.41417	0.41417	0.41473	2.38632	0.03734	1.00000	0.01565	14.00000
0.29388	0.50347	0.50347	0.41473	2.38632	0.03734	1.00000	0.01565	14.00000
0.36735	0.58176	0.58176	0.41473	2.38632	0.03734	1.00000	0.01565	14.00000
0.44082	0.65071	0.65071	0.41473	2.38632	0.03734	1.00000	0.01565	14.00000
0.51429	0.70883	0.70883	0.41473	2.38632	0.03734	0.99636	0.01559	13.95433
0.58776	0.75097	0.75097	0.40923	2.35468	0.03703	0.97955	0.01532	13.74891
0.66123	0.77221	0.77221	0.40606	2.33639	0.03680	0.96985	0.01517	13.63349
0.73470	0.78437	0.78437	0.40239	2.31523	0.03654	0.95865	0.01499	13.49696
0.80817	0.79145	0.79145	0.39913	2.29649	0.03630	0.94874	0.01484	13.37944
0.88164	0.79534	0.79534	0.39704	2.28447	0.03609	0.93814	0.01467	13.27771
0.95511	0.79734	0.79734	0.39536	2.27479	0.03586	0.93128	0.01456	13.21379
1.02858	0.79834	0.79834	0.39420	2.26809	0.03568	0.92677	0.01449	13.17186
1.10205	0.79884	0.79884	0.39364	2.26487	0.03557	0.92386	0.01444	13.13836
1.17552	0.79909	0.79909	0.39334	2.26314	0.03550	0.92205	0.01441	13.11674

Figure A-2. Continued

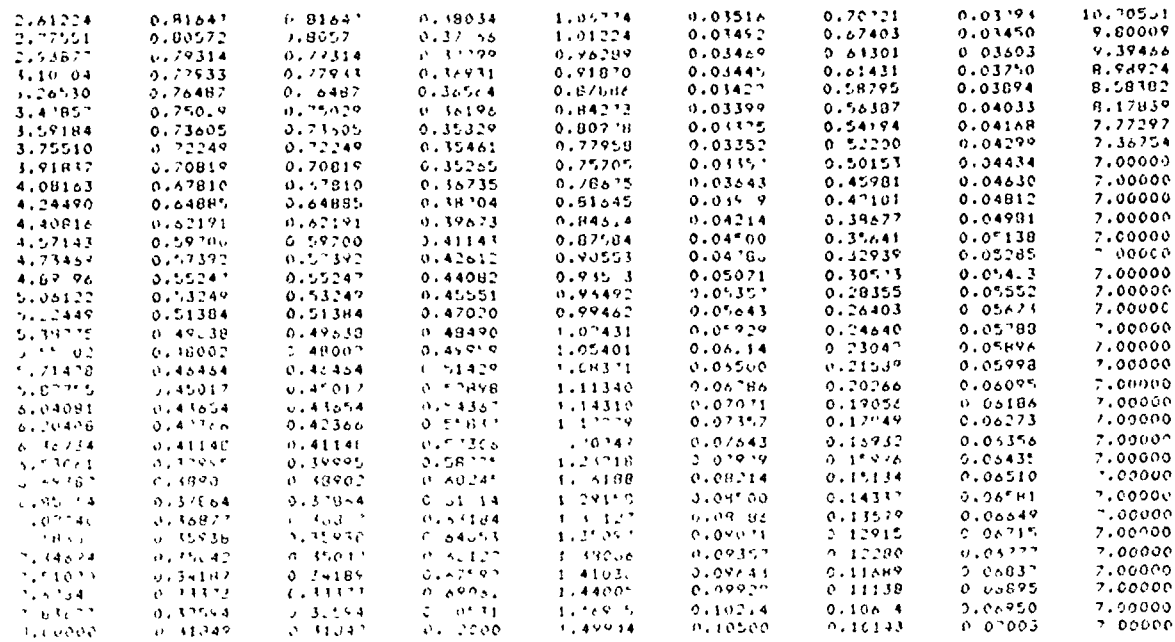

Figure A-2. Continued

```
   6.08169     0.76021     0.03786     0.07868
   6.92818     0.86602     0.02536     0.05270
   7.96461     0.99558     0.01603     0.03332
   9.22298     1.15912     0.00943     0.01961
  10.98930     1.37372     0.00506     0.01052
  13.36074     1.67009     0.00240     0.00498
  16.87698     2.10962     0.00095     0.00198
  22.66445     2.83556     0.00029     0.00059

UFWASH MOMENTUM FUNCTION: JET RADIUS, INTERACTION  CONSTANT, VERTICAL UFWASH SHEET MOMENTUM,
AND COALESCENCE ANGLE

          KG/RN=   1.26970  ACON=   0.89924  XMOM/=   0.96641  PHIO(DEGS)=   0.0

                UFWASH WIDTH CONSTANT ESTIMATE , CU=   0.29801

*** CALL INTERG ***

          SOLUTION OF GROUND PRESSURE DISTRIBUTION HAS BEEN FOUND
       ITERATION CYCLE= 12  EPS=   0.00346  SIGMA=   0.99063
       EPI=   0.00346  CUI=   0.29801  PHIUO=  36.70523  PHIO=  49.71178  DEGREES
                       PHI=0.0, DELPWO=   0.48118
                       PHI=0.0, PMIN=   0.02186
                       PHI=0.0, ALPOG=   2.74955
            UFWASH THICKNESS CONSTANT, (CU) X (SIGMA)=   0.29522

                    *** COMPUTATION OF TWO-JET GROUND ISOBAR PATTERN ***

                       4 VALUES OF PRESSURE SPECIFIED FOR PATTERN

      PBAR=   0.60000     0.30000     0.20000     0.05000

                    GROUND PATTERN IN JET CENTERED COORDINATE SYSTEM


                                    PBAR=   0.60000

      JET IMPINGEMENT REGION, IJET=  58          UFWASH DEFLECTION REGION, IU=   0

          XISOJ       YISOJ       XISOU       YISOU

        0.93593     0.0
        0.93543     0.01038
        0.93395     0.02071
        0.93149     0.03095
        0.92802     0.04106
        0.92356     0.05100
        0.91810     0.06072
        0.91200     0.07018
        0.90468     0.07934
        0.89665     0.08816
```

Figure A-2. Continued

```
0.88764     0.29662
0.87776     0.32466
0.86704     0.35226
0.85551     0.37930
0.84319     0.40600
0.83011     0.43209
0.81640     0.45761
0.80179     0.48256
0.78661     0.50690
0.77080     0.53062
0.75437     0.55370
0.73737     0.57612
0.71983     0.59787
0.70177     0.61894
0.68323     0.63931
0.66424     0.65901
0.64484     0.67798
0.62505     0.69625
0.60489     0.71380
0.58469     0.73060
0.56497     0.74648
0.54145     0.76213
0.52149     0.77649
0.50023     0.79059
0.47545     0.80566
0.45486     0.81931
0.43206     0.83293
0.41037     0.84513
0.38745     0.85741
0.36498     0.86933
0.34587     0.87946
0.32370     0.89140
0.30023     0.91359
0.27545     0.92676
0.25486     0.93781
0.23206     0.94871
0.21037     0.95945
0.18745     0.96992
0.16498     0.97997
0.14587     0.98864
0.12370     0.99664
0.10023     1.00727
0.07545     1.01813
0.05486     1.02741
0.03206     1.03733
0.01037     1.04816
-0.01255    1.05846
-0.03498    1.06826
-0.05587    1.07778
-0.07809    1.08709
-0.09981    1.09581
-0.12409    1.10409
-0.14587    1.11227
-0.16745    1.12030
-0.18983    1.12837
-0.21255    1.13643
-0.23498    1.14319
-0.25587    1.14927
-0.27809    1.15509
-0.30119    1.16080
-0.32427    1.16601
```

```
EDGE=   0.350000
```

```
... MEASUREMENT REGION, NET= 48          DRAIN REFLECTION REGION, NU= 22

   X(50)        Y(50)        X(100)       Y(100)

 1.5[illegible]  [illegible]  3.[illegible]  0.
 [illegible]  0.[illegible]  3.[illegible]  0.00453
 [illegible]  [illegible]  3.[illegible]  0.18312
 [illegible]  [illegible]  3.[illegible]  0.27499
 [illegible]  [illegible]  3.[illegible]  0.36[illegible]
```

Figure A-2. Continued

1.55606	0.25436	3.55292	0.49960
1.54703	0.30415	3.57897	0.55258
1.53642	0.35403	3.60621	0.60616
1.52476	0.40321	3.57505	0.74043
1.51056	0.45177	3.58532	0.83591
1.49538	0.49970	3.59734	0.93149
1.47874	0.54694	3.61121	1.02847
1.46068	0.59344	3.62727	1.17667
1.44125	0.63913	3.64582	1.22611
1.42050	0.68398	3.66728	1.37695
1.39847	0.72792	3.69220	1.42933
1.37520	0.77093	3.72139	1.53334
1.35076	0.81296	3.75604	1.63932
1.32519	0.85396	3.79824	1.74724
1.29854	0.89392	3.85226	1.85771
1.27087	0.93280	3.93959	1.96981
1.24223	0.97058	4.00000	1.99644
1.21767	1.00722		
1.18825	1.04272		
1.15102	1.07705		
1.11903	1.11021		
1.08634	1.14218		
1.05300	1.17295		
1.01915	1.20253		
1.01505	1.20753		
0.98109	1.23115		
0.81109	1.35132		
0.79876	1.37257		
0.53184	1.46450		
0.46109	1.50677		
0.37257	1.53910		
0.31135	1.56178		
0.08400	1.57317		
0.04308	1.57468		
0.01745	1.56582		
0.29796	1.54664		
0.42284	1.51726		
0.54399	1.47792		
0.66203	1.42881		
0.77670	1.37013		
0.88825	1.30261		
0.99696	1.22672		
1.10316	1.14255		
1.20721	1.05087		
1.30953	0.95216		
1.37659	0.84742		
1.39091	0.73659		
1.44606	0.62172		
1.49126	0.50236		
1.52750	0.37969		
1.55324	0.25453		
1.56875	0.12776		
1.57394	0.00002		

FRAC= 0.70000

JET IMPINGEMENT REGION, IJET= 50 DOWNWASH DEFLECTION REGION, IU= 29

1.500 1.501 1.500 1.500

Figure A-2. Continued

1.85676	0.0	1.40526	0.0
1.85578	0.06026	3.40594	0.09123
1.85285	0.12044	3.40663	0.18716
1.84799	0.18043	3.40934	0.27499
1.84135	0.24017	3.41075	0.36710
1.83242	0.29956	3.41396	0.45960
1.82179	0.35852	3.41791	0.55258
1.80930	0.41697	3.42267	0.64616
1.79497	0.47482	3.42834	0.74043
1.77884	0.53201	3.43494	0.83551
1.76096	0.58845	3.44253	0.93149
1.74135	0.64408	3.45133	1.02851
1.72010	0.69883	3.46132	1.12667
1.69722	0.75264	3.47268	1.22611
1.67276	0.80545	3.48558	1.32695
1.64684	0.85720	3.50019	1.42932
1.61944	0.90785	3.51672	1.53341
1.59066	0.95734	3.53545	1.63932
1.56054	1.00563	3.55664	1.74724
1.52916	1.05268	3.58065	1.85734
1.49653	1.09847	3.60799	1.96981
1.46274	1.14295	3.63880	2.08484
1.42804	1.18611	3.67397	2.20264
1.39222	1.22791	3.71410	2.32345
1.35544	1.26834	3.76013	2.44750
1.31778	1.30738	3.81362	2.57511
1.27936	1.34502	3.87790	2.70652
1.24021	1.38122	3.96936	2.84206
1.20003	1.41610	4.00000	2.98185
1.20003	1.41610		
1.16125	1.45069		
0.92425	1.55137		
0.88226	1.66381		
0.84051	1.77469		
0.79928	1.87438		
0.75878	1.96745		
0.71923	2.05385		
0.68089	2.13355		
0.64396	2.20655		
0.60866	2.27284		
0.57521	2.33243		
0.54381	2.38533		
0.51465	2.43154		
0.48792	2.47107		
0.46380	2.50390		
0.44247	2.53004		
0.42410	2.54950		
0.40885	2.56227		
0.39687	2.56835		
0.38829	2.56775		
0.38324	2.56045		
0.38183	2.54648		
0.38416	2.52581		
0.39033	2.49846		
0.40042	2.46443		
0.41450	2.42371		
0.43263	2.37631		
0.45485	2.32223		
0.48120	2.26147		
0.51170	2.19403		
0.54636	2.11990		
0.58518	2.03910		
0.62813	1.95161		
0.67516	1.85744		
0.72618	1.75659		
0.78107	1.64906		
0.83966	1.53485		
0.90172	1.41396		
0.96693	1.28639		
1.03490	1.15214		
1.10513	1.01121		
1.17697	0.86360		
1.24961	0.70931		
1.32199	0.54834		
1.39270	0.38069		
1.45973	0.20636		
1.52000	0.02535		

Figure A-2. Continued

x[50]	y[50]	x[50]	y[50]
2.51941	0.0	4.17002	0.0
2.53813	0.00242	4.17926	0.00153
2.53411	0.16472	4.17900	0.18116
2.52744	0.24608	4.17822	0.27499
2.51811	0.32040	4.17190	0.35710
2.50611	0.40970	4.17404	0.45960
2.49163	0.49034	4.17462	0.55058
2.47475	0.57620	4.17961	0.64616
2.45592	0.64940	4.1780[illegible]	0.74043
2.43289	0.72762	4.14690	0.83551
2.40844	0.80481	4.15099	0.93149
2.38164	0.88090	4.15557	1.07851
2.35256	0.95578	4.16056	1.17867
2.32127	1.02918	4.16599	1.2[illegible]611
2.28784	1.10160	4.17189	1.32695
2.25236	1.17438	4.17830	1.4[illegible]931
2.21489	1.24165	4.18530	1.53341
2.17552	1.30934	4.19297	1.61912
2.13433	1.37518	4.20140	1.74724
2.09141	1.43774	4.21071	1.85734
2.04685	1.50336	4.22106	1.96981
2.00077	1.56320	4.23261	2.09406
1.95331	1.62227	4.24556	2.20264
1.90461	1.67935	4.26014	2.31335
1.85483	1.73405	4.27659	2.44252
1.80430	1.78804	4.29519	2.57511
1.75265	1.83978	4.31620	2.70672
1.69988	1.88914	4.33981	2.84206
1.64611	1.93617	4.36649	2.98708
1.64611	1.93617	4.36649	2.98708
1.59206	1.98241	4.39[illegible]	3.05000
1.53654	2.02764	4.41242	3.11526
1.47942	2.07237	4.43648	3.18929
1.42110	2.11581	4.46598	3.25075
1.36163	2.15679	4.49196	3.31147
1.30131	2.19436	4.51347	3.40753
1.24040	2.23458	4.54075	3.49196
1.17859	2.27513	4.61376	3.59982
1.11618	2.31617	4.62165	3.68819
1.05367	2.35230	4.63[illegible]9	3.78[illegible]1
0.99104	2.39101	4.64576	3.89465
0.92850	2.42431	4.65[illegible]	3.98280
0.86614	2.4631	4.67[illegible]2	4.06790
0.80416	2.49[illegible]	4.68[illegible]1	4.15[illegible]7
0.74284	2.52703	4.69[illegible]	4.24354
0.68236	2.56[illegible]9	4.70[illegible]	4.33411
0.62295	2.59513	4.71[illegible]	4.42124
0.56487	2.64318	4.74148	4.51134
0.50835	2.68[illegible]	4.76143	4.61[illegible]
0.45368	2.71[illegible]3	4.78[illegible]	4.71[illegible]
0.40125	2.76[illegible]	4.81150	4.82192
0.35139	2.80699	4.84111	4.93[illegible]2
0.30457	2.86114	4.87464	5.03[illegible]0
0.26129	2.90[illegible]9	4.91231	5.14539
0.22207	2.95[illegible]1	4.95[illegible]2	5.27911
0.18751	3.00[illegible]5	4.99696	5.41[illegible]4
0.15827	3.04[illegible]5	5.04[illegible]0	5.59[illegible]1
0.13504	3.09[illegible]4	5.09[illegible]6	5.78045

Figure A-2. Continued

```
UPWASH DEFLECTION ZONE LINE, FBAR=0 OUTSIDE INTERACTION REGION

                      XUF          YUF

                    2.81913      0.0
                    2.81777      0.22464
                    2.81166      0.45069
                    2.80220      0.67963
                    2.78876      0.91[illegible]
                    2.77110      1.15230
                    2.74892      1.39966
                    2.72183      1.65685
                    2.68933      1.92630
                    2.65078      2.21072
                    2.60536      2.51336
                    2.55307      2.83815
                    2.48961      3.18969
                    2.41630      3.57461
                    2.33000      4.00000
                    2.22784      4.47599
                    2.10603      5.01583
                    1.95914      5.63246
                    1.76045      6.36594
                    1.55877      7.23741

        *****      COMPUTATION OF UPWASH FLOW FIELD      *****


               COMPUTATION OF UPWASH STREAMLINE PROPERTIES


        [illegible]  0.0    DEGS

 INV VEL/A   0.5258   DELTAW/A   0.48118  RWCH/RN=   0.32000
 DUU/RN    1.08303  RUU/RN=   1.43570  RUUUN/RN=   0.21962

   Z/RN       VMU/VN       RUM/RN       RU/RN       DELTU/DELTJ

 [illegible]  0.[illegible]    0.71867      0.49[illegible]0    0.48118
 [illegible]  0.60[illegible]  0.7441[illegible]   0.59985      0.4561
 0.[illegible]333  0.62[illegible]  0.50962  0.[illegible]703   0.4[illegible]111
 0.81[illegible]  0.[illegible]910  0.[illegible]512  0.80520    0.35569
 [illegible]  [illegible]   0.400[illegible]  0.[illegible]     0.31575
 [illegible]11833  [illegible]  0.4461     1.01153      0.[illegible]18
 [illegible]  0.4[illegible]4   0.4[illegible]   1.[illegible]0   0.24253
 [illegible]  [illegible]51   0.[illegible]12   [illegible]86   [illegible]
 [illegible]  0.41090    [illegible]     [illegible]     0.19351
 [illegible]  [illegible]41[illegible]2  0.[illegible]12   1.4[illegible]420  0.[illegible]474
 [illegible]  [illegible]64   0.[illegible]3[illegible]2  [illegible]52[illegible]  0.150[illegible]3
 2.0[illegible]  [illegible]   [illegible]191   1.[illegible]   0.14495
 [illegible]  [illegible]   [illegible]   [illegible]33[illegible]   0.1[illegible]29
 [illegible]  [illegible]   [illegible]   1.[illegible]     0.[illegible]
 [illegible]  [illegible]   [illegible]55[illegible]   1.54[illegible]   [illegible]
 [illegible]  [illegible]   [illegible]   [illegible]    [illegible]
 [illegible]  [illegible]   [illegible]   14.[illegible]   [illegible]
 [illegible]  [illegible]   [illegible]   [illegible]    [illegible]
 [illegible]  [illegible]   [illegible]   [illegible]    0.[illegible]541
 [illegible]  [illegible]   [illegible]   [illegible]    [illegible]
```

Figure A-2. Continued

3.39333	0.22441	1.12062	2.55902	0.07530
3.54500	0.16633	1.17412	2.66219	0.07093
3.69667	0.25822	1.21962	2.76516	0.06894
3.84833	0.25156	1.26512	2.86852	0.06328
4.00000	0.24480	1.31062	2.97169	0.05993

PHIB= 60.0000 DEGS

I =.VEL.= 0.24143 DELPWJ= 0.10143 RWGH/RN= 0.00000
ZOU/RN= 0.16000 RUO/RN= 1.37335 RUOHN/RN= 0.40569

Z/RN	VRU/VN	RUH/RN	RU/RN	DELPU/DELPJ
0.00000	0.24145	0.40569	1.37335	0.10143
1.02333	0.29308	0.67004	1.51925	0.10682
1.17666	0.30541	0.73439	1.56515	0.10307
1.33000	0.30555	0.79873	1.81104	0.09479
1.93333	0.29246	0.86308	1.95694	0.08559
2.24666	0.27805	0.92743	2.10284	0.07731
2.54999	0.26498	0.99177	2.24874	0.07021
2.84333	0.25316	1.05612	2.39464	0.06409
3.14666	0.24242	1.12047	2.54054	0.05877
3.44999	0.23260	1.18481	2.68644	0.05410
3.75332	0.22359	1.24916	2.83234	0.04993
4.05666	0.21528	1.31351	2.97823	0.04615
4.35999	0.20760	1.37785	3.12414	0.04310
4.66332	0.20047	1.44220	3.27003	0.04019
4.96665	0.19383	1.50655	3.41593	0.03757
5.26999	0.18764	1.57089	3.56183	0.03521
5.57332	0.18185	1.63524	3.70773	0.03307
5.87665	0.17641	1.69958	3.85363	0.03112
6.17998	0.17130	1.76393	3.99953	0.02934
6.48331	0.16649	1.82828	4.14543	0.02772
6.78665	0.16195	1.89262	4.29132	0.02623
7.08998	0.15765	1.95697	4.43722	0.02485
7.39331	0.15357	2.02132	4.58312	0.02359
7.69664	0.14973	2.08566	4.72902	0.02242
7.99998	0.14607	2.15001	4.87491	0.02134

UFWASH PROPERTIES COMPUTED AT 2 LOCATION OF UNDERSIDE OF BODY

BODY CENTERLINE LOCATION AT Z RN= 4.00000

U RN	RW/RN	PHIB	X RN	VRU/VN	RU/RN	RUH/RN	RU RUO	RU/RJS	RBS/RN
4.00000	4.00000	0.0	0.0	0.24480	0.05993	1.31062	1.00000	0.05993	0.05993
4.00000	4.00083	1.16914	0.16333	0.24477	0.05991	1.31081	0.99974	0.05991	0.05986
4.00150	4.00333	1.33731	0.32653	0.24468	0.05987	1.31139	0.99896	0.05987	0.05977
4.00349	4.00749	1.50153	0.48980	0.24451	0.05979	1.31233	0.99766	0.05979	0.05961
4.00600	4.01330	1.66586	0.65306	0.24430	0.05968	1.31367	0.99585	0.05968	0.05938
4.00900	4.0223	1.82633	0.81633	0.24401	0.05954	1.31541	0.99353	0.05954	0.05893
4.01250	4.03251	1.98702	0.97959	0.24366	0.05941	1.31746	0.99071	0.05941	0.05849
4.01650	4.04421	2.14806	1.14286	0.24326	0.05927	1.31979	0.98739	0.05927	0.05799
4.02099	4.05744	2.30957	1.30612	0.24279	0.05905	1.32236	0.98359	0.05905	0.05741

Figure A-2. Continued

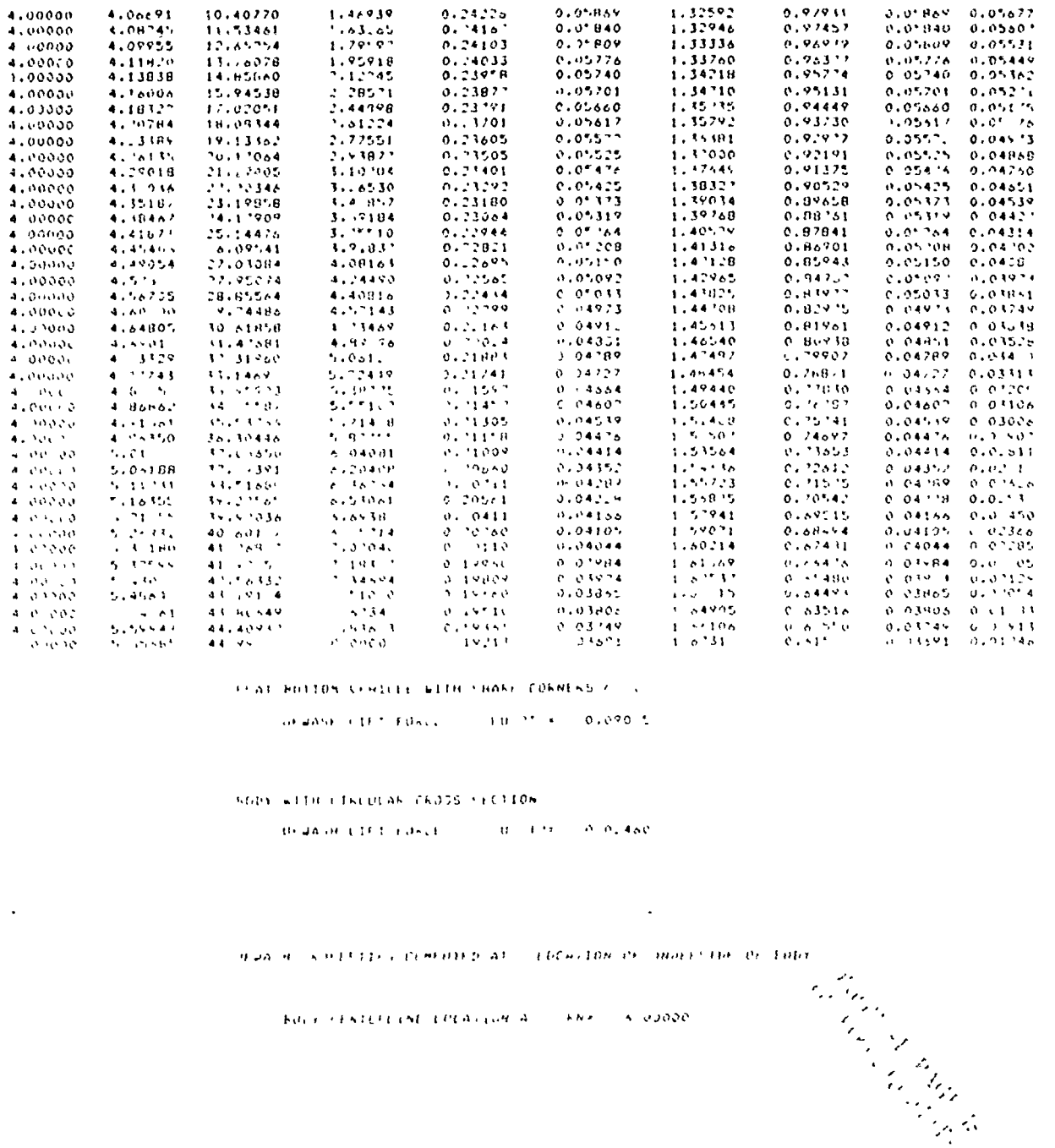

Figure A-2. Continued

TU/KN	KU/KN	FRIB	X/KN	VHU/VN	PU/PN	BUH/KN	PU FUO	FU/F 15	FBG/FN
6.00000	4.00000	0.0	0.0	0.18135	0.03289	1.91062	1.00000	0.03289	0.03289
6.00000	4.00053	0.93536	0.16[illegible]	0.18133	0.03288	1.91078	0.99984	0.03288	0.03287
6.00000	4.00213	1.87022	0.32653	0.18129	0.03287	1.91126	0.99937	0.03287	0.03283
5.00000	4.00479	2.80408	0.48980	0.18122	0.03284	1.91207	0.99858	0.03284	0 03276
6.00000	4.00852	3.73645	0.65306	0.18112	0.03280	1.91321	0.99747	0.03280	0.03266
6.00000	4.01330	4.66684	0.81633	0.18099	0.03276	1.91466	0.99605	0.03276	0.03254
6.00000	4.01915	5.59479	0.97959	0.18083	0.03270	1.91643	0 99431	0 03270	0.03239
5.00000	4.02604	6.51980	1.14286	0.18065	0.03263	1.91851	0.99210	0.03263	0.03221
6.00000	4 03397	7.44140	1.30612	0.18044	0.03256	1.92090	0.98996	0.03254	0.03201
5.00000	4.04295	8.35915	1.46939	0.18020	0.03247	1.92346	0 98737	0.03247	0.03178
6.00000	4.05296	9.27259	1.63265	0.17993	0.03237	1.92669	0.98440	0.03237	0.03154
5.00000	4 06399	10.18131	1.79592	0.17963	0 03227	1.91003	0.98118	0.03227	0.03126
6.00000	4.07604	11.08488	1.95918	0.17931	0.03215	1.93368	0 97767	0.03215	0.03096
6.00000	4.08910	11.98290	2.12245	0.17897	0.03203	1.93762	0.97389	0.03203	0.03065
6.00000	4.10316	12.87499	2.28571	0.17859	0.03190	1.94187	0.96986	0.03190	0.03031
6.00000	4.11820	13.76078	2.44898	0.17820	0.03175	1.94640	0.96553	0.03175	0.02996
6.00000	4.13421	14.63990	2.61224	0.17777	0.03160	1.95123	0.96096	0.03160	0.02958
6.00000	4.15121	15.51204	2.77551	0.17733	0.03144	1.95633	0.95614	0.03144	0 02920
6.00000	4 16 15	16.37685	2 93877	0.17686	0.03128	1.9617	0.95108	0.03128	0.02879
6.00000	4.18903	17.23409	3.10204	0.17637	0.03110	1.96738	0.94579	0.03110	0.02837
6.00000	4.20904	18.08344	3.26530	0.17585	0.03092	1.97332	0 94028	0.03092	0 02794
6.00000	4.22957	18 92462	3.42857	0 17531	0.03073	1 97951	0 93454	0.03073	0.02750
6.00000	4.25110	19 75745	3.59.84	0 17476	0.03054	1.98597	0.9.861	0.03054	0.02705
6.00000	4.27363	20.58165	3 75510	0 17418	0.03034	1.99267	0 93248	0.03034	0.02659
6.00000	4. 9711	21.39705	3 91837	0.17358	0.03013	1.99963	0.91616	0 03013	0.02612
6.00000	4.32081	22.20346	4.08163	0.17296	0.02992	2.00684	0.90956	0.02992	0.02564
6.00000	4.34 44	23.000 0	4 24490	0.17233	0.02970	2.01428	0.90300	0.02970	0.02515
6.00000	4.37140	23 78865	4 40816	0.17168	0.0294	2.0 194	0.89619	0.02947	0.0 465
6.00000	4.39814	24.56 14	4.57143	0 1 131	0.02924	2.02988	0.88922	0 02924	0.02419
6.00000	4.42569	25.33611	4 73469	0.17031	0.02901	2.03796	0.88211	0.02501	0.02370
6.00000	4.4 401	26 09541	4 89796	0 16963	0 0287	0 8430	0 87487	0.0287	0 0 371
6.00000	4 48314	26 84457	5 06122	0.16891	0.0284	2.05484	0.86752	0.0_853	0 0 1
6.00000	4 51431	27 58335	5 22448	0 16818	0 0.8	2.06318	0.86006	0.02819	0 02 .
6.00000	4 54626	28 31147	5 38 5	0 1 744	0 02804	2 07153	0.85250	0 02804	0 02175
6.00000	4 . 4	29 034 1	5 5 0	0 1 6	0 02 8	2.0816	0.844 4	0.02778	0.02 4
6.00000	4 60 00	29. 44 5	5 7 4	0 16599	0 02 58	2.09100	0.83 1.	0 0 25	0 0 75
6.00000	4.64	30 44 07	5 87 5	0 1 1	0 02731	2 10251	0 82 35	0 0 2.	0 0 2.
6.00000	4.67 310	31 13570	6 04081	0.16415	0 0 701	2.11015	0 8 14	0 0 701	0.01 5
6.00000	4 7 8	31 8 8	6.20408	0.1	0 026	2 1 30	0 81250	0.02679	1 1 1
6.00000	4 4 04	2.48630	6 36 34	0.162 6	0.02644	2.1300	0.80553	0 02649	0 01 1
6.00000	4 7 45	33 14697	6 53061	0 1615	0 0 65	140 6	0. 1	0 3 67	0 01 9
6.00000	4.71 4	33. 9 04	6 69387	0.16113	0 02596	2.14069	0 7824	0.02596	0 01 53
6.00000	4 8 00	34.43696	6 5 14	0.16031	0 0 50	1 1	0 8140	0.02570	0.01 40
6.00000	4 58 3	35 0 0 2	7 0 49	0 15945	0 0 43	1 1	0.7 31	0 02544	0 01 04
6.00000	4 . 1	35 55210	7.1 6	0 15864	0 1 1	2 1 5	0 1 1	0 0 1	3 01 6
6.00000	4 56 0	35 50446	7 46 4	0.15780	0 0 49	2 15 43	0 5 12	0.0 450	0 0161
6.00000	00 4	35.70 1	7 0 3	0.156 5	0.0 4 3	2 20450	0 73902	0 0 463	3.015
6.00000	5.04154	1 0 0	7 14	0 15610	0 0 4	1 68	0.760 5	0 0 43	0.01534
6.00000	5 0 6	36 0 484	8 3 3	0.1 1	0 0 410	2 69	0 72 4	0 0 410	0.01453
6.00000	5 1 0	36.65	8 00 0	0 15439	0 0 364	2 3041	0 2481	0 0 364	0.01 43

FLAT BOTTOM VEHICLE WITH SHORT CORNERS

[illegible]

[illegible]

Figure A-2. Continued

UPWASH LIFT FORCE LU/2TJ= 0.01512

UPWASH DERIVATIVES COMPUTED AT Z LOCATION OF UNDERSIDE OF BODY

BODY CENTERLINE LOCATION AT Z/RN= 8.00000

LU/RN	BW/RN	THIB	X/RN	VMU/VN	FU/RN	BUH/RN	FU/FUO	FU/FJS	FBS/RN
8.00000	4.00000	0.0	0.0	0.14447	0.02086	2.51062	1.00000	0.02086	0.02086
8.00000	4.00017	0.77949	0.14327	0.14441	0.02085	2.51025	0.99989	0.02085	0.02085
8.00000	4.00148	1.55868	0.57653	0.14439	0.02085	2.51118	0.99957	0.02085	0.02083
8.00000	4.00333	2.33731	0.48980	0.14435	0.02084	2.51168	0.99904	0.02084	0.02080
8.00000	4.00592	3.11504	0.65306	0.14429	0.02082	2.51286	0.99829	0.02081	0.02076
8.00000	4.00924	3.89167	0.81633	0.14423	0.02080	2.51412	0.99731	0.02080	0.02071
8.00000	4.01330	4.66686	0.97959	0.14414	0.02078	2.51546	0.99616	0.02078	0.02064
8.00000	4.01810	5.44031	1.14286	0.14404	0.02075	2.51748	0.99476	0.02075	0.02056
8.00000	4.02362	6.21181	1.30612	0.14393	0.02071	2.51957	0.99319	0.02071	0.02047
8.00000	4.02988	6.98106	1.46939	0.14380	0.02068	2.52193	0.99141	0.02066	0.02037
8.00000	4.03685	7.74776	1.63265	0.14365	0.02064	2.52456	0.98941	0.02064	0.02026
8.00000	4.04454	8.51167	1.79592	0.14349	0.02059	2.52746	0.98721	0.02059	0.02014
8.00000	4.05296	9.27259	1.95918	0.14332	0.02054	2.53065	0.98482	0.02054	0.02001
8.00000	4.06208	10.03028	2.12245	0.14313	0.02049	2.53409	0.98213	0.02049	0.01986
8.00000	4.07191	10.78429	2.28571	0.14293	0.02043	2.53780	0.97944	0.02043	0.01971
8.00000	4.08245	11.53461	2.44898	0.14271	0.02037	2.54176	0.97647	0.02037	0.01955
8.00000	4.09366	12.28084	2.61224	0.14248	0.02030	2.54596	0.97331	0.02030	0.01938
8.00000	4.10560	13.02307	2.77551	0.14223	0.02023	2.55042	0.96992	0.02023	0.01920
8.00000	4.11824	13.76078	2.93877	0.14197	0.02016	2.55520	0.96645	0.02016	0.01902
8.00000	4.13157	14.49386	3.10204	0.14170	0.02008	2.56019	0.96276	0.02008	0.01882
8.00000	4.14564	15.22212	3.26530	0.14142	0.02000	2.56541	0.95889	0.02000	0.01862
8.00000	4.16042	15.94538	3.42857	0.14112	0.01991	2.57088	0.95481	0.01992	0.01841
8.00000	4.17594	16.66347	3.59184	0.14081	0.01983	2.57659	0.95068	0.01984	0.01820
8.00000	4.19217	17.37619	3.75510	0.14049	0.01974	2.58253	0.94633	0.01974	0.01798
8.00000	4.20913	18.08334	3.91837	0.14015	0.01964	2.58871	0.94183	0.01964	0.01775
8.00000	4.22685	18.78450	4.08163	0.13981	0.01955	2.59511	0.93719	0.01955	0.01752
8.00000	4.24532	19.48000	4.24490	0.13945	0.01945	2.60172	0.93241	0.01945	0.01728
8.00000	4.26455	20.17014	4.40816	0.13908	0.01934	2.60852	0.92749	0.01934	0.01704
8.00000	4.28457	20.85473	4.57143	0.13870	0.01924	2.61564	0.92244	0.01924	0.01680
8.00000	4.30539	21.53320	4.73469	0.13831	0.01913	2.62293	0.91726	0.01913	0.01655
8.00000	4.32704	22.20546	4.89796	0.13791	0.01902	2.63040	0.91197	0.01902	0.01630
8.00000	4.34952	22.87084	5.06122	0.13750	0.01891	2.63809	0.90655	0.01891	0.01605
8.00000	4.37286	23.52934	5.22449	0.13709	0.01879	2.64597	0.90103	0.01879	0.01580
8.00000	4.39707	24.18090	5.38775	0.13668	0.01868	2.65405	0.89541	0.01868	0.01554
8.00000	4.42216	24.82454	5.55102	0.13626	0.01856	2.66233	0.88969	0.01856	0.01528
8.00000	4.44815	25.46031	5.71428	0.13583	0.01845	2.67079	0.88387	0.01843	0.01503
8.00000	4.47506	26.08741	5.87755	0.13539	0.01833	2.67943	0.87797	0.01831	0.01477
8.00000	4.50291	26.70584	6.04081	0.13496	0.01819	2.68826	0.87198	0.01819	0.01451
8.00000	4.53172	27.31525	6.20408	0.13452	0.01806	2.69726	0.86591	0.01806	0.01425
8.00000	4.56152	27.91494	6.36734	0.13351	0.01793	2.70644	0.85976	0.01793	0.01399
8.00000	4.59233	28.50455	6.53061	0.13343	0.01780	2.71576	0.85358	0.01780	0.01373
8.00000	4.62419	29.08376	6.69387	0.13294	0.01767	2.72526	0.84732	0.01767	0.01348
8.00000	4.65709	29.65214	6.85714	0.13244	0.01754	2.73491	0.84100	0.01754	0.01322
8.00000	4.69106	30.20932	7.02041	0.13194	0.01741	2.74472	0.83463	0.01741	0.01297
8.00000	4.72613	30.75504	7.18367	0.13143	0.01727	2.75468	0.82819	0.01727	0.01272
8.00000	4.76231	31.28894	7.34694	0.13091	0.01714	2.76480	0.82169	0.01714	0.01247
8.00000	4.79963	31.81064	7.51020	0.13040	0.01700	2.77507	0.81513	0.01700	0.01222

8.00000	4.74787	33.59709	7.67347	0.12938	0.01687	2.78545	0.80074	0.01687	0.01191
8.00000	4.77744	33.14697	7.83673	0.12935	0.01673	2.79598	0.80219	0.01673	0.01173
8.00000	4.80740	34.69003	8.00000	0.12882	0.01659	2.80664	0.79561	0.01659	0.01149

FLAT BOTTOM VEHICLE WITH SHARP CORNERS

UPWASH LIFT FORCE [illegible] 0.04130

BODY WITH CIRCULAR CROSS SECTION

UPWASH LIFT FORCE [illegible] 0.01029

Figure A-2. Concluded

```
C*******************************************************************************GRU00010
C                                                                               GRU00020
C      VTOL TWO-JET IMPINGEMENT INTERACTION COMPUTER PROGRAM                    GRU00030
C                  FOR CLOSELY SPACED JETS                                      GRU00040
C                    BY M.J.SIRLARI                                             GRU00050
C                     516 575-2207                                              GRU00060
C              GRUMMAN AEROSPACE CORPORATION                                    GRU00070
C                BETHPAGE,NEW YORK 11714                                        GRU00080
C                                                                               GRU00090
C*******************************************************************************GRU00100
C                                                                               GRU00110
C    PROGRAM GRUMJET2                                                           GRU00120
C                                                                               GRU00130
      REAL KDELFD,KDELO,NFD,NO,N,KDEL                                           GRU00140
      COMMON/WALL/DELS,NO,KDELO,ALFG,ALFWD,ALFWFD,RO,RGH,VG,BWHO                GRU00150
      COMMON/JET/SD,KGU                                                         GRU00160
      COMMON/HEIGHT/ HD,IFBAR                                                   GRU00170
      FETAWR(ETA,A)=ETA-(4./(A+1.))*ETA**(A+1.)+(6./(2.*A+1.))*ETA**(2.*AGRU00180
     1A+1.) (4./(3.*A+1.))*ETA**(3.*A+1.)+(1./(4.*A+1.))*ETA**(4.*A+1.) GRU00190
C                                                                               GRU00200
C    BODY SHAPE FUNCTIONS FOR FOSCE INJECTION                                   GRU00210
C      W2...HALF WIDTH IN NOZZLE RADII                                          GRU00220
C      ZBODY...HALF DEPTH IN NOZZLE RADII                                       GRU00230
C      DZDXR...AXIAL SLOPES                                                     GRU00240
C      THNOSE...NOSE ANGLE OF PARABOLIC BODY                                    GRU00250
C                                                                               GRU00260
C                                                                               GRU00270
C   PARABOLIC BODY WITH CONSTANT CROSS SECTIONAL SHAPE                          GRU00280
C                                                                               GRU00290
C      W2(XB)=.5*TAN(THNOSE)*(XL2**2-XB**2)/XL2                                 GRU00300
C      ZBODY(XB)=.5*TAN(THNOSE)*(XL2**2-XB**2)/XL2                              GRU00310
C      DZDXR(XB)=TAN(THNOSE)*XB/XL2                                             GRU00320
C                                                                               GRU00330
C   CYLINDRICAL BODY WITH CONSTANT CROSS SECTIONAL SHAPE                        GRU00340
C                                                                               GRU00350
C      W2(XB)=WCON                                                              GRU00360
C      ZBODY(XB)=ZCON                                                           GRU00370
C      DZDXR(XB)=ZCON                                                           GRU00380
C                                                                               GRU00390
C   CYLINDRICAL BODY PARAMETERS IN TERMS OF NOZZLE DIAMTERS                     GRU00400
C                                                                               GRU00410
C                                                                               GRU00420
      ZCON 0.0                                                                  GRU00430
      THNOSE=14.036*PI/180.                                                     GRU00440
C                                                                               GRU00450
C   CIRCULAR CROSS SECTION                                                      GRU00460
C      POINT OF FLOW SEPARATION                                                 GRU00470
C                                                                               GRU00480
      PI=3.141592654                                                            GRU00490
      PHISEP=139.*PI/180.                                                       GRU00500
      READ (5,1) HD,SD,ZFLD,DZFL,ZFINAL                                         GRU00510
    1 FORMAT (5F10.5)                                                           GRU00520
      READ (5,1) XL2,WCON,ZCON                                                  GRU00530
      WRITE (6, 1)                                                              GRU00540
   21 FORMAT (1 ,// 50X, ***    INPUT PARAMETERS    ***'//)                     GRU00550
      WRITE (6,2) HD,SD,ZFLD                                                    GRU00560
    2 FORMAT (/50X, 'HD= ',F10.5,2X, 'SD= ',F10.5,2X, 'ZD=',F10.5)             GRU00570
      WRITE (6,22) ZFLD,DZFL,ZFINAL                                             GRU00580
   22 FORMAT (/50X, 'ZD= ',F10.5,2X, 'DZ/D= ',F10.5,2X, 'ZFINAL/D=',F10.5/)   GRU00590
      WRITE (6,208) XL2,WCON,ZCON                                               GRU00600
  208 FORMAT (/ 50X, 'BODY LENGTH/ D  ',F10.5,2X, 'WIDTH W/D= ',F10.5,2X,'DEGRU00610
     1TH Z/D  ',F10.5)                                                          GRU00620
      ZFINAL = ZFLD                                                             GRU00630
C                                                                               GRU00640
```

Figure V-3. Computer Listing

```
C  COMPUTE JET STANDOFF DISTANCE AND EFFECTIVE JET DECAY HEIGHT          GRU00650
C  (GIRALT ET AL)                                                       GRU00660
C                                                                       GRU00670
      IF (HD.LE.6.8) DELG=0.153*7.8                                     GRU00680
      IF (HD.GT.6.8) DELG=0.153*(1.+HD)                                 GRU00690
      ZEND=(HD-DELG)*2.                                                 GRU00700
      WRITE (6,22)                                                      GRU00710
   22 FORMAT (///30X,'*****      JET DECAY REGION      *****'//)        GRU00720
      WRITE (6,7) DELG                                                  GRU00730
    7 FORMAT (10X,'JET DEFLECTION HEIGHT DELG/D =',F10.5)               GRU00740
C                                                                       GRU00750
C  COMPUTE JET DECAY                                                    GRU00760
C                                                                       GRU00770
C  ALL DIMENSIONS NONDIMENSIALIZED BY NOZZLE RADIUS                     GRU00780
C                                                                       GRU00790
C   SET EMPIRICAL CONSTANTS FOR HALF-WIDTH BEHAVIOR AND LENGTH OF       GRU00800
C  POTENTIAL CORE (HRYCAN,ET AL)                                        GRU00810
C                                                                       GRU00820
      A2=.04                                                            GRU00830
      B2=.800                                                           GRU00840
      A3=.0926                                                          GRU00850
      B3=0.                                                             GRU00860
      ZFC=0.                                                            GRU00870
      A1=A2*(B2-1.)/ZFC                                                 GRU00880
      ZFD=B2/(A3-A2)                                                    GRU00890
      ALFD=1.5                                                          GRU00900
      WRITE (6,23) ZFC,ZFD                                              GRU00910
   23 FORMAT (10X,'ZFC/RN=',F10.5,2X,'ZFD/RN=',F10.5)                   GRU00920
      WRITE (6,12)                                                      GRU00930
   12 FORMAT (16X, Z/RN',6X,'RJH/RN',6X,'RJ/RN',7X,'ALP',9X,'CV2',8X,'VJGRU00940
     1/VN',6X,'RCORE/RN'/)                                              GRU00950
C                                                                       GRU00960
C  REGION I...POTENTIAL CORE REGION OF JET..                            GRU00970
C                                                                       GRU00980
      NJPC=10                                                           GRU00990
      DNPC=NJPC-1                                                       GRU01000
      IF (.ZEND.GE.ZFC) DZFC=ZFC/DNPC                                   GRU01010
      IF (ZEND.LT.ZFC) DZFC=ZEND/DNPC                                   GRU01020
      Z=0.                                                              GRU01030
      DO 100 I=1,NJPC                                                   GRU01040
      IF (I.GT.1) GO TO 102                                             GRU01050
      GO TO 103                                                         GRU01060
  102 VJ=1.                                                             GRU01070
      RJH=1.                                                            GRU01080
      RJ=1.                                                             GRU01090
      ALFC=0.                                                           GRU01100
      CV2=.5                                                            GRU01110
      RJPC=1.                                                           GRU01120
      RC=1.                                                             GRU01130
      GO TO 104                                                         GRU01140
  103 ETAC=1.-Z/ZFC                                                     GRU01150
      RJH=A1*Z+1.                                                       GRU01160
      CALL ALFC (ETAC,RJH,ALFC,K,CV2)                                   GRU01170
      RJ=RJH/K                                                          GRU01180
      RJPC=RJ                                                           GRU01190
      RJFC=(RJPC-RJPC0)/DZFC                                            GRU01200
      VJ=1.                                                             GRU01210
      RC=ETAC*RJ                                                        GRU01220
  104 WRITE (6,11) Z,RJH,RJ,ALFC,CV2,VJ,RC                              GRU01230
   11 FORMAT (11X,7(F10.5,2X))                                          GRU01240
      Z=Z+DZFC                                                          GRU01250
      RJPC0=RJPC                                                        GRU01260
  100 CONTINUE                                                          GRU01270
C                                                                       GRU01280
C  TRANSITION REGION II AND FULLY DEVELOPED REGION OF JET               GRU01290
C                                                                       GRU01300
```

Figure A-3. Continued

```
      IF (ZEND.LE.ZPC) GO TO 998                                        GRU01310
      NJFD=50                                                           GRU01320
      DNFD=NJFD-1                                                       GRU01330
      CALL SIM(0.,ALFFD,RFD,DUM)                                        GRU01340
      RJZFD=A3/RFD                                                      GRU01350
      RJFD=(A3*ZFD+B3)/RFD                                              GRU01360
      DZ=(ZEND-ZPC)/DNFD                                                GRU01370
      Z=ZPC+DZ                                                          GRU01380
      DO 200 I=2,NJFD                                                   GRU01390
      IF (Z.LT.ZFD) RJ=AAJ*(Z-ZPC)**3+BBJ*(Z-ZPC)**2+CCJ*(Z-ZPC)+DDJ    GRU01400
      RCON=(2.-SQRT(2.))/2.                                             GRU01410
      DZPCF=ZFD-ZPC                                                     GRU01420
      CCJ=RJZPC                                                         GRU01430
      DDJ=RJPC                                                          GRU01440
      AAJ=(2.*DDJ+CCJ*DZPCF+RJZFD*DZPCF-2.*RJFD)/DZPCF**3               GRU01450
      BBJ=.5*(RJZFD-C-3.*AAJ*DZPCF**2)/DZPCF**2                         GRU01460
      IF (Z.LT.ZFD) RJ=RJPC+((RJFD-RJPC)/(ZFD-ZPC))*(Z-ZPC)             GRU01470
      IF (Z.GE.ZFD) ALFT=ALFFD                                          GRU01480
      IF (Z.LE.ZFD) RJH=A2*Z+B2                                         GRU01490
      IF (Z.GT.ZFD) RJH=A3*Z+B3                                         GRU01500
      IF (Z.LT.ZFD) R=RJH/RJ                                            GRU01510
      IF (Z.LT.ZFD) ALFT=ALOG(RCON)/ALOG(R)                             GRU01520
      CALL SIM(0.,ALFT,R,CV2)                                           GRU01530
      VJ=RJ/(RJH*SQRT(2.*CV2))                                          GRU01540
      R=RJH/RJ                                                          GRU01550
      WRITE (6,11) Z,RJH,RJ,ALPT,CV2,VJ                                 GRU01560
      Z=Z+DZ                                                            GRU01570
  200 CONTINUE                                                          GRU01580
C                                                                       GRU01590
C  JET DEFLECTION REGION                                                GRU01600
C  JET IMPINGEMENT PRESSURES                                            GRU01610
C                                                                       GRU01620
  998 AGCON=-.032026                                                    GRU01630
      EGCON=.3354248                                                    GRU01640
      CGCON=2.8                                                         GRU01650
      IF (HD.GT.3.) AD=3.6                                              GRU01660
      ADSLP=(3.6-2.5)/(3.-1.2)                                          GRU01670
      IF (HD.LE.3.) AD=2.5+ADSLP*(HD-1.2)                               GRU01680
      WRITE (6,29)                                                      GRU01690
   29 FORMAT (///30X,'*****      JET DEFLECTION REGION      *****'/)    GRU01700
   80 FORMAT (10X,'KGH/KN=',F10.5,2X,'KG/KN =',F10.5,2X,'KD/KN=',F10.5,2XGRU01710
     1,'VG/VN=',F10.5/)                                                 GRU01720
C                                                                       GRU01730
C  SET CHARACTERISTIC SCALE LENGTHS FOR IMPINGEMENT REGION              GRU01740
C                                                                       GRU01750
      KGH=KJH                                                           GRU01760
      KG=KJ                                                             GRU01770
      KD=AD*KGH                                                         GRU01780
      ETAWG=KGH/KD                                                      GRU01790
      VG=1.                                                             GRU01800
      IF (2.*HD.LE.ZFD) GO TO 454                                       GRU01810
C                                                                       GRU01820
C  DETERMINE STAGNATION POINT PRESSURE                                  GRU01830
C                                                                       GRU01840
      IF (2.*HD.LE.ZFD) RJHD=A2*2.*HD+B2                                GRU01850
      IF (2.*HD.GT.ZFD) RJHD=A3*2.*HD+B3                                GRU01860
      Z=2.*HD-.2*RJHD                                                   GRU01870
      IF (Z.LT.ZFD) ALFT=ALPHA+((ALFFD-ALFA)/(ZFD-ZPC))*(Z-ZFD)         GRU01880
      IF (Z.GE.ZFD) ALFT=ALFFD                                          GRU01890
      CALL SIM(0.,ALFT,R,CV2)                                           GRU01900
      VG=R/(RJHD*SQRT(2.*CV2))                                          GRU01910
      IF (HD.LE.3.5) VG=1.004-.003*HD                                   GRU01920
      IF (HD.LE.10..AND.HD.GT.3.5) VG=1.35-0.066*HD                     GRU01930
      IF (HD.GT.10.) VG=.7+(3.6/HD)                                     GRU01940
  454 WRITE (6,80) KGH,KG,KD,VG                                         GRU01950
                                                                        GRU01960
```

Figure V-3. Continued

```
C  STAGNATION PRESSURE NONDIMENSIONALIZED BY JET TOTAL PRESSURE          GRU01970
C                                                                       GRU01980
      RGU=RG                                                            GRU01990
      DELFS=VG**2                                                       GRU02000
      WRITE (6,81) DELFS                                                GRU02010
   81 FORMAT (10X,'STAGNATION PRESSURE, DPS/DPTJ=',F10.5)               GRU02020
      CALL GPRFS(RO,VG,ALFG,R,CV2)                                      GRU02030
      WRITE (6,82) ALPG                                                 GRU02040
   82 FORMAT (10X,'ALPG=',F10.5)                                        GRU02050
      NG=50                                                             GRU02060
      RNGM=NG-1                                                         GRU02070
      DR=RO/(RNGM*RGH)                                                  GRU02080
      DELTA=1./(RNGM)                                                   GRU02090
      ETA=0.                                                            GRU02100
      R=0.                                                              GRU02110
      WRITE (6,83)                                                      GRU02120
   83 FORMAT (30X,'SINGLE JET GROUND PRESSURES'//5X,'R/RGH',6X,'DPS/DPTGRU02130
     1G ',8X,'R/RN',7X,'DPS/DPTJ //)                                    GRU02140
      DO 300 I=1,NG                                                     GRU02150
      DPTG=(1.-ETA**ALFG)**4                                            GRU02160
      DPTJ=DPTG*DELFS                                                   GRU02170
      RRN=R*RGH                                                         GRU02180
      WRITE (6,84) R,DPTG,RRN,DPTJ                                      GRU02190
   84 FORMAT (20X,4(F10.5,5X))                                          GRU02200
      R=R+DR                                                            GRU02210
      ETA=ETA+DELTA                                                     GRU02220
  300 CONTINUE                                                          GRU02230
C                                                                       GRU02240
C  INITIALIZE WALL JET REGION                                           GRU02250
C                                                                       GRU02260
      AW3=.09                                                           GRU02270
      ALFWO=1.5                                                         GRU02280
      RDELFO=.0962                                                      GRU02290
      ALFWG=1.5                                                         GRU02300
      NCR=2.                                                            GRU02310
      CALL SIMW(RDELFO,NFO,ALFWFO,RATW,CSV2W,CFW)                       GRU02320
      CALL SIMWG(ALFWG,RATWG,CSFWG)                                     GRU02330
      CW=.5*AW3*CSV2W/(RATW*CSFWG)                                      GRU02340
      AS1=-.015638                                                      GRU02350
      AS2=-.128045                                                      GRU02360
      DELS=2.*A31*(HO)**AS2                                             GRU02370
      WRITE (6,26)                                                      GRU02380
   26 FORMAT (///30X, *****      WALL JET REGION      *****'//)        GRU02390
      WRITE (6,86) DELS                                                 GRU02400
   86 FORMAT (5X,'STAGNATION POINT BOUNDARY LAYER THICKNESS, DELS/RN=',  GRU02410
     1F10.5)                                                            GRU02420
      NO=14                                                             GRU02430
      RDELO=DELS/(2.*RELG)                                              GRU02440
      CALL GMATCH(RGH,VG,ALFG,RDELO,NO,ETAWG,DELS,ALFWO,R)              GRU02450
      CALL SIMW(RDELO,NO,ALFWO,R,CV2,CF)                                GRU02460
      RATWO=R                                                           GRU02470
      FETAG=(1.-ETAWG**ALFG)**4                                         GRU02480
      DEN=(RGH*VG**2)*(2.*CV2*(1.-FETAG)+CF*FETAG)                      GRU02490
      BWO=(1.-FETAG)/DEN                                                GRU02500
      BWRO=R*BWO                                                        GRU02510
      DELTM=BWO*RDELO                                                   GRU02520
      XLAM=(1.-FETAG)                                                   GRU02530
      VMG1=SQRT(XLAM)                                                   GRU02540
      WRITE (6,91) VMG1                                                 GRU02550
   91 FORMAT (5X,'VELOCITY AT START OF TURBULENT WALL JET, VM/VG=',F10.5GRU02560
     1)                                                                 GRU02570
      WRITE (6,85) ALFWO,BWRO,BWO                                       GRU02580
   85 FORMAT (10X,'START OF WALL JET REGION, ALFWO=',F10.5,2X,'BWOR/RN=GRU02590
     1',F10.7,2X,'BWO/RN=',F10.5)                                       GRU02600
C                                                                       GRU02610
C  MAXIMUM OF G IS THE DISTRIBUTION IN DEFLECTION REGION                GRU02620
```

Figure V-3. Continued

```
C                                                                       GRU02630
      NWFT=50                                                           GRU02640
      XNWFT=NWFT-1                                                      GRU02650
      REND=2.*SD                                                        GRU02660
      DR=REND/XNWFT                                                     GRU02670
      BW3RO=AW3*RO                                                      GRU02680
      DELBRH=(BW3RO-BWRO)/(RO-RGH)                                      GRU02690
      DELRR=(NFD-NO)/(RO-RGH)                                           GRU02700
      DELAR=(ALFWFD-ALFWO)/(RO-RGH)                                     GRU02710
      ADELBT=.0175                                                      GRU02720
      ADELBL=(ADELBT*(RO-2.)-DELS)/(RO-RGH)                             GRU02730
      R=0.                                                              GRU02740
      WRITE (6,107)                                                     GRU02750
  107 FORMAT(//45X,'WALL JET PROPERTIES'//)                             GRU02760
      WRITE (6,97)                                                      GRU02770
   97 FORMAT (//15X,'R/RN',6X,'VM/VG',6X,'VM/VN',6X,'BWH/RN',6X,        GRU02780
     1'BW/RN',6X,'DELBL/RN',6X,'DELF',6X,'NDEL',6X,'NPOWER'/)           GRU02790
      DO 400 I=1,NWFT                                                   GRU02800
      IF (R.LE.RO) ETA=(1.-(R/RO)**ALFG)**4                             GRU02810
      IF (R.GT.RO) ETA=0.0                                              GRU02820
      IF (R.LE.RGH) VMG=SQRT(1.-ETA)                                    GRU02830
      IF (R.LE.RGH) VMN=VMG*VG                                          GRU02840
      IF (R.LE.RGH) DELF=DELFS                                          GRU02850
      IF (R.LE.RGH) DELTA=NDELO*BWO                                     GRU02860
      IF (R.LE.RGH) N=14                                                GRU02870
      IF (R.LE.RGH) NDEL=NDELO                                          GRU02880
      IF (R.LE.RGH) BW=BWO                                              GRU02890
      IF (R.LE.RGH) BWH=RATWO*BWO                                       GRU02900
      IF (R.LE.RGH) GO TO 401                                           GRU02910
      IF (R.LE.RO) BWH=BWHO+DELBRH*(R-RGH)                              GRU02920
      IF (R.GT.RO) BWH=AW3*R                                            GRU02930
      IF (R.LE.RO) ALFW=ALFWO+DELAR*(R-RGH)                             GRU02940
      IF (R.LE.RO) DELBL=DELS+ADELBL*(R-RGH)                            GRU02950
      IF (R.GT.RO) DELBL=ADELBT*(R-2.)                                  GRU02960
      IF (R.LE.RO) N=NO+DELNR*(R-RGH)                                   GRU02970
      IF (R.GT.RO) N=NFD                                                GRU02980
      IF (R.GT.RO) ALFW=ALFWFD                                          GRU02990
      ALAM=(2.**(N+1.))/2.)**(1./ALFW)                                  GRU03000
      RDEL=DELBL/(DELBL+(BWH-DELBL)/ALAM)                               GRU03010
      CALL SIMW(FDEL,N,ALFW,RAT,CV2,F)                                  GRU03020
      IF (R.LE.4.) VISMOM=1.0                                           GRU03030
      IF (R.GT.4.) VISMOM=1./(R/4.)**.24                                GRU03040
      FI=VISMOM*RAT*(1.-ETA)/(R*BWH)                                    GRU03050
      F=(1.+ETA*SQ)**2                                                  GRU03060
      VMN=SQRT((F-1.)/(2.*CV2))                                         GRU03070
      VMG=VMN/VG                                                        GRU03080
      DELF=DELFS*(1.+ETA)*VMN**2                                        GRU03090
      RW=BWH/RAT                                                        GRU03100
      DELTA=NDEL*BW                                                     GRU03110
  401 WRITE (6,99) R,VMG,VMN,BW,RW,DELTA,DELBL,NDEL,N                   GRU03120
      R=R+DR                                                            GRU03130
   99 FORMAT (10X,9(F10.5,2X))                                          GRU03140
  400 CONTINUE                                                          GRU03150
C                                                                       GRU03160
C   DEWASH GROUND MAXIMUM EXPOSURE DISTRIBUTION                         GRU03170
C                                                                       GRU03180
      WRITE (6,24)                                                      GRU03190
   24 FORMAT (1H1,30X,'*****     TWO JET INTERACTION PROBLEM     *****'//GRU03200
     1)                                                                 GRU03210
      WRITE (6,460)                                                     GRU03220
  460 FORMAT (//9X,'MAXIMUM GROUND EXPOSURES ALONG DEWASH   (WIND STAGNAGRU03230
     1TION LINE)')                                                      GRU03240
      WRITE (6,470)                                                     GRU03250
  470 FORMAT (13X,'XW/RN',7X,'XW',7X,'EMAX/E',7X,'EMAX/EMAXO'//)        GRU03260
      FACT=1.                                                           GRU03270
      EMAXO=0.                                                          GRU03280
```

Figure A-3. Continued

```
      DPHI=PHIM/24.                                                     GRU03290
      DO 450 IL=1,25                                                    GRU03300
      XW=SD*TAN(PHI)                                                    GRU03310
      RW=SQRT(XW**2+SD**2)                                              GRU03320
      XWS=XW/(2.*SD)                                                    GRU03330
      CALL WALLJ (RW,VMN,DUM2,DUM3,DUM4,DELPW)                          GRU03340
      IF (IL.EQ.1) DELPWO=DELPW                                         GRU03350
      PMAXG=DELPW-VMN**2+(VMN*COS(PHI))**2                              GRU03360
      PMAXND=PMAXG/DELPWO                                               GRU03370
      WRITE (6,455) XW,XWS,PMAXG,PMAXND                                 GRU03380
  455 FORMAT (10X,4(F10.5,2X))                                          GRU03390
      PHI=PHI+DPHI                                                      GRU03400
  450 CONTINUE                                                          GRU03410
      ACON=1.-(RG/SD)**2                                                GRU03420
      PHIOD=0.0                                                         GRU03430
      IF (ACON.GE.0.) PHIO=0.0                                          GRU03440
      IF (ACON.GE.0.) GO TO 667                                         GRU03450
      PHIO=ARCOS((SD/RG)**.20)                                          GRU03460
      PHIOD=PHIO*180./PI                                                GRU03470
      ACON=2./(SIN(.5*PI-PHIO)**2)                                      GRU03480
      XMOMZ=ACON*(1.0+SIN(PHIO)*(SIN(PHIO)-2.0))/3.                     GRU03490
      GO TO 668                                                         GRU03500
  667 XMOMZ=ACON+2.*(1.-ACON)/3.                                        GRU03510
  668 WRITE (6,553)                                                     GRU03520
  553 FORMAT (//5X,'UPWASH MOMENTUM FUNCTION: JET RADIUS, INTERACTION   GRU03530
     1CONSTANT, VERTICAL UPWASH SHEET MOMENTUM, AND COALESCENCE ANGLE'/)GRU03540
      WRITE (6,551) RG,ACON,XMOMZ,PHIOD                                 GRU03550
  551 FORMAT ('0',5X,'RG/RN=',F10.5,2X,'ACON=',F10.5,2X,'XMOMZ=',F10.5,2X,'GRU03560
     1PHIO(DEGS)=',F10.5/)                                              GRU03570
      CALL WALLJ(SD,DUM1,DUM2,DUM3,DUM4,DELFW)                          GRU03580
      CALL FGUMAT(CU,DELFS,DELFW,RO,SD,ALFG,ALFUG)                      GRU03590
      CALL SIMW(NDELFD,NFD,ALFWFD,RATW,CSV2W,CPW)                       GRU03600
      CALL SIMUG(ALFUG,RATUG,CSFUG)                                     GRU03610
      CU=2.*AW3*CSV2W/(RATW*CSFUG)                                      GRU03620
      WRITE (6,557) CU                                                  GRU03630
  557 FORMAT (25X,'UPWASH WIDTH CONSTANT ESTIMATE = CU=',F10.5)         GRU03640
      READ (5,661) IFBAK                                                GRU03650
  661 FORMAT (I1)                                                       GRU03660
C                                                                       GRU03670
C   TEST FOR INTERACTION OF DEFLECTION REGIONS                          GRU03680
C                                                                       GRU03690
      IF (CU*SDIRO.LE.SD) GO TO 222                                     GRU03700
C                                                                       GRU03710
C  COMPUTATION OF DEFLECTION REGION INTERACTION                         GRU03720
C                                                                       GRU03730
      CALL INTERG(XMOMZ,DELFS,SD,RO,ALFG,EPS,CU,SIG)                    GRU03740
C                                                                       GRU03750
      GO TO 223                                                         GRU03760
  222 EPS=0.0                                                           GRU03770
      SIG=1.0                                                           GRU03780
      PHIUD=0.                                                          GRU03790
      PHIO=0.0                                                          GRU03800
      WRITE (6,28) EPS,SIG,PHIUD,PHIO                                   GRU03810
   28 FORMAT (//20X,'JET AND UPWASH DEFLECTION REGIONS DO NOT INTERACT, GRU03820
     1 CU ESTIMATE IS CORRECT '/                                        GRU03830
     1/35X,'EPS=',F10.5,2X,'SIG=',F10.5,2X,'PHIUD=',F10.5,2X,'PHIO=',F10GRU03840
     1.5)                                                               GRU03850
      WRITE (6,29) ALFUG                                                GRU03860
   29 FORMAT (30X,'PHI=0.0 ALONG UPWASH  LINE, ALFUG=',F8.4,1X,' IN UPWGRU03870
     1ASH DEFLECTION REGION ')                                          GRU03880
      IF (IFBAK.NE.0) CALL GPLOT (ALFG,DELFS,SD,RO,EPS,CU,SIG,PHIUD,PHIOGRU03890
     1)                                                                 GRU03900
C                                                                       GRU03910
C                                                                       GRU03920
  223 WRITE (6,111)                                                     GRU03930
  111 FORMAT (//30X,'*****     COMPUTATION OF UPWASH FLOW FIELD     *****GRU03940
```

Figure A-3. Continued

```
     1*'//)                                                                  GRU03950
      WRITE (6,112)                                                          GRU03960
  112 FORMAT (//35X,'COMPUTATION OF UPWASH STREAMLINE PROPERTIES'/)          GRU03970
      DPHI=60.*PI/180.                                                       GRU03980
      PHI=0.                                                                 GRU03990
  114 FORMAT (//30X,'PHID=',F8.4,' DEGS'//)                                  GRU04000
      DO 600 I=1,2                                                           GRU04010
      PHID=PHI*180./PI                                                       GRU04020
      WRITE (6,114) PHID                                                     GRU04030
      ZEND=ZFLANE/COS(PHI)                                                   GRU04040
      Y=SD*TAN(PHI)                                                          GRU04050
      RW=SQRT(SD**2+Y**2)                                                    GRU04060
      IF (RW.LE.RO) BWH=BWHO+DELBRN*(RW-RGH)                                 GRU04070
      IF (RW.GT.RO) BWH=AW3*RW                                               GRU04080
      CALL WAKEJ(RW,VUGN,BWHG,RWO,CPWG,DELPWS)                               GRU04090
      IWR=1                                                                  GRU04100
      CALL UPWASH(KO,RW,PHI,ZEND,BWHG,BWG,VWGN,DELPWS,CFWG,ALPG,DELPS,       GRU04110
     1VUN,DELFUS,RGH,ZOUS,IWR)                                               GRU04120
      END PRECEDING                                                          GRU04130
  600 CONTINUE                                                               GRU04140
      NUPT=50                                                                GRU04150
      XNUPT=NUPT-1                                                           GRU04160
      ALFU=1.5                                                               GRU04170
C                                                                            GRU04180
C  CIRCULAR CYLINDER DRAG FUNCTION                                           GRU04190
C                                                                            GRU04200
      DRAG=SIN(PHISEP)*(1.-(4./3.)*(SIN(PHISEP/8*2)))                        GRU04210
      DO 700 I=1,25                                                          GRU04220
      SUMF=0.0                                                               GRU04230
      SUMFC=0.0                                                              GRU04240
      XI=0.                                                                  GRU04250
      DX=FLOAT/XNUPT                                                         GRU04260
      WRITE (6,116)                                                          GRU04270
  116 FORMAT (//,//,35X,' UPWASH PROPERTIES COMPUTED AT Z LOCATION OF UNDEGRU04280
     1R SIDE OF BODY //)                                                     GRU04290
      WRITE (6,118) ZFLANE                                                   GRU04300
  118 FORMAT (/,5X,' BODY CENTERLINE LOCATION AT Z/RN=',F10.5//)             GRU04310
      WRITE (6,20)                                                           GRU04320
   20 FORMAT (/,2X,'X/RN',7X,'RW/RN',7X,'PHIR',7X,'X/RN',7X,'VRL/VN',       GRU04330
     1 6X,'FU/FN',7X,'FUR/RN',7X,'FU/FUPUO',6X,'FU/FUS',4X,'FUS/FN'/)        GRU04340
      IWR=0                                                                  GRU04350
      DO 500 I=1,NUPT                                                        GRU04360
      FACT=1.0                                                               GRU04370
      IF (I.EQ.1) FACT=1.0                                                   GRU04380
      IF (I.EQ.NUPT) FACT=1                                                  GRU04390
      XB=ZEDGY(XB)                                                           GRU04400
      PHIR=ATAN(XB/(SD+ZFLANE-ZB))                                           GRU04410
      RW=SD*TAN(PHIR)                                                        GRU04420
      RW=SQRT(SD**2+RW**2)                                                   GRU04430
      CALL WAKEJ(RW,VWGN,BWHG,BWG,CVZWG,DELFWS)                              GRU04440
      Q=ZFLANE-ZB                                                            GRU04450
      ZEND=ZB-COS(PHIR)                                                      GRU04460
      CALL UPWASH(KO,RW,PHIR,ZEND,BWHG,BWG,VWGN,DELFWS,CFWG,ALFG,DELFS,GRU04470
     1VUN,DELFUS,RGH,ZOUS,IWR)                                               GRU04480
      IF(XB.GT.(XMAX/2.0)) GO TO 500                                         GRU04490
      FACT=SQRT(1.-(Q/RGH)**2)                                               GRU04500
      IF(FACT.GT.1.) FACT=1.                                                 GRU04510
      IF(FACT.LT.0.) FACT=0.                                                 GRU04520
      DFU=(1.-VUN)*DX                                                        GRU04530
      SUMF=SUMF+DFU*FACT                                                     GRU04540
      SUMFC=SUMFC+DFU*FACT*DRAG*(VUN**2)*(COS(PHIR)*COS(PHIR))**2            GRU04550
      DRAG=SUMFC/(SUMF*FACT*DRAG*(VUN**2)*(COS(PHIR)*COS(PHIR))**2)          GRU04560
      XB=XB+DX                                                               GRU04570
      IF(I.EQ.1) FI=SUMF                                                     GRU04580
      IF(I.EQ.NUPT) FACT=.5*DELFUS                                           GRU04590
      IF(I.EQ.NUPT) WRITE(6,500)                                             GRU04600
```

Figure A-3. Continued

```
      IF (DELFM.EQ.0.) DELFM=DELFUJ                                     GRU04610
      DELFUS=DELFUJ-DELFS                                               GRU04620
      FBS=(VUN*COS(PHI*THETA))**2                                       GRU04630
      WRITE (6,77) ZU,RW,PHID,XB,VUN,DELFUJ,BWH,DELFB,DELFUS,FBS        GRU04640
   77 FORMAT (1X,9(F10.5,2X),F8.5)                                      GRU04650
      XB=XB+DXB                                                         GRU04660
  500 CONTINUE                                                          GRU04670
C                                                                       GRU04680
C  FLAT BOTTOM LIFT FORCE                                               GRU04690
C                                                                       GRU04700
      XLUT=(1./PI)*SUMT                                                 GRU04710
      WRITE (6,778)                                                     GRU04720
  778 FORMAT (//30X,'FLAT BOTTOM VEHICLE WITH SHARP CORNERS'/)          GRU04730
      WRITE (6,771) XLUT                                                GRU04740
  771 FORMAT (35X, 'UPWASH LIFT FORCE',5X,'(LU/2T)=',F10.5//)           GRU04750
C                                                                       GRU04760
C  UPWASH LIFT FORCE FOR CIRCULAR CROSS SECTION                         GRU04770
C                                                                       GRU04780
      XLUT=(1./PI)*SUMFL                                                GRU04790
      WRITE (6,773)                                                     GRU04800
  773 FORMAT (//30X,'BODY WITH CIRCULAR CROSS SECTION'/)                GRU04810
      WRITE (6,771) XLUT                                                GRU04820
      ZPLANE=ZPLANE+2.*DZPL                                             GRU04830
      IF (ZPLANE.GT.2.*ZFINAL) STOP                                     GRU04840
  700 CONTINUE                                                          GRU04850
      END                                                               GRU04860


      SUBROUTINE WALLJ(R,VMN,BWH,RW,CV2,DELFW)                          WAL00010
      REAL KDELO,KO,KDELFD,NFD,N,KDEL                                   WAL00020
C                                                                       WAL00030
C   THIS COMPUTES THE WALL JET PROPERTIES GIVEN A WALL RADIUS           WAL00040
C                                                                       WAL00050
      COMMON/WALL/ DELS,KO,KDELO,ALFO,ALFWO,ALFWFD,RO,RGH,VG,BWHO       WAL00060
C                                                                       WAL00070
C  MAXIMUM VELOCITY DISTRIBUTION IN DEFLECTION REGION                   WAL00080
C                                                                       WAL00090
      AW3=.09                                                           WAL00100
      NFD=7.                                                            WAL00110
      KDELFD=1./9.                                                      WAL00120
      BW3HO=AW3*KO                                                      WAL00130
      DELBRH=(BW3HO-BWHO)/(RO-RGH)                                      WAL00140
      ALFWFD=1.5                                                        WAL00150
      DELAR=(ALFWFD-ALFWO)/(RO-RGH)                                     WAL00160
      DELNF=(NFD-NO)/(RO-RGH)                                           WAL00170
      ADELBT=.0175                                                      WAL00180
      ADELBL=(ADELBT*(RO-2.)-DELS)/(RO-RGH)                             WAL00190
      DKDELR=(KDELFD-KDELO)/(RO-RGH)                                    WAL00200
      IF (R.LE.KO) ETA=(1.-(R/RO)**ALFO)**4                             WAL00210
      IF (R.GT.KO) ETA=0.0                                              WAL00220
      IF (R.LE.RGH) VMG=SQRT(1.-ETA)                                    WAL00230
      IF (R.LE.RGH) VMN=VMG*VG                                          WAL00240
      IF (R.LE.RGH) GO TO 402                                           WAL00250
      IF (R.LE.KO) BWH=BWHO+DELBRH*(R-RGH)                              WAL00260
      IF (R.GT.KO) BWH=AW3*R                                            WAL00270
      IF (R.LE.KO) ALFW=ALFWO+DELAR*(R-RGH)                             WAL00280
      IF (R.GT.KO) ALFW=ALFWFD                                          WAL00290
      IF (R.LE.KO) N=NO+DELNF*(R-RGH)                                   WAL00300
      IF (R.GT.KO) N=NFD                                                WAL00310
      IF (R.LE.KO) DELBL=DELS+ADELBL*(R-RGH)                            WAL00320
      IF (R.GT.KO) DELBL=ADELBT*(R-2.)                                  WAL00330
      ALAM=((2.-SQRT(2.))/2.)**(1./ALFW)                                WAL00340
      KDEL=DELBL/(DELBL+(BWH-DELBL)/ALAM)                               WAL00350
      CALL SINW(KDEL,N,ALFW,.AT,CV2,LP)                                 WAL00360
         IF (.LE..4.) VISMLH=1.0                                        WAL00370
```

Figure A-1. Continued

```
      IF (R.GT.4.) VISNOM=1./(R/4.)**0.24                                WAL00380
      F1=VISNOM*KAT*(1.-FETA)/(K*BWH)                                    WAL00390
      F2=CF*BETA*VG**2                                                   WAL00400
      VMN=SQRT((F1-F2)/(2.*F2))                                          WAL00410
      VMG=VMN/VG                                                         WAL00420
      DELPW=FETA*VG**2*VMN**2                                            WAL00430
      BW=BWH/RAT                                                         WAL00440
      DELTA=RGL*BW                                                       WAL00450
  401 CONTINUE                                                           WAL00460
      IF (R.LT.RGH) DELPW=VG**2                                          WAL00470
      IF (R.LT.RGH) BW=BWH                                               WAL00480
      RETURN                                                             WAL00490
      END                                                                WAL00500


      SUBROUTINE UFWASH (RO,RWALE,PHIE,ZEND,BWGH,BWG,VWGN,DELPW,CFWG,    UFW00010
     1ALFG,DELF,VMUN,DELPWJ,BWH,ZGO,IWR)                                 UFW00020
      COMMON /JET/ SO,KGH                                                UFW00030
      REAL MUMU                                                          UFW00040
C                                                                        UFW00050
C  THIS ROUTINE COMPUTES THE UFWASH STREAMLINE PROPERTIES                UFW00060
C                                                                        UFW00070
      AOU=5.                                                             UFW00080
      PI=3.1415926                                                       UFW00090
      ALFUF=1.5                                                          UFW00100
      ALFUM=1.5                                                          UFW00110
      ACON=1.-(RGH/RO)**2                                                UFW00120
      IF (ACON.GT.0.) GO TO 20                                           UFW00130
      PHIO=ASIN(SQRT(1.-RGH/RO)**2.5)                                    UFW00140
      ACON=1.-(SIN(.9*PHIE-PHIO))**2                                     UFW00150
      PHIOD=PHIO*180./PI                                                 UFW00160
      IF (PHIE.GE.PHIO) MUMU=ACON**SIN(PHI-PHIO)**2                      UFW00170
      IF (PHIE.LT.PHIO) MUMU=1.                                          UFW00180
      GO TO 30                                                           UFW00190
   20 MUMU=(1.-(1.-ACON)**SIN(PHIE))**2                                  UFW00200
   30 CONTINUE                                                           UFW00210
C  30 WRITE (6,*) ACON,MUMU                                              UFW00220
      AOS=.50                                                            UFW00230
      ALFS=1.5                                                           UFW00240
      AOU=.8                                                             UFW00250
      IF(AOU.GE.BWGH/ZGO) AOU=BWGH/ZGO                                   UFW00260
      IF(ZGO.LE.0.0) AOU=.8                                              UFW00270
      ALFU=1.5                                                           UFW00280
      ALFO=1.5                                                           UFW00290
      CALL UWIDTH(ALFU,ALFO,AOU)                                         UFW00300
C                                                                        UFW00310
C   DETERMINE DELTA FROM INTERCEPT DEFLECTION                            UFW00320
C  DETERMINE INITIAL UFWASH WIDTH                                        UFW00330
C                                                                        UFW00340
      DELPW=VWGN**2                                                      UFW00350
      DELPWJ=DELPW                                                       UFW00360
      ETAOO=BWGH/ZGO                                                     UFW00370
      ETAO=ETAOO+ALFUF*AOU**4                                            UFW00380
      ETA=ETAO+ALFUM*AOU**4                                              UFW00390
      VMNUI=SQRT(DELPW/(2.*ETAO))                                        UFW00400
      IF (IWR.NE.2) WRITE (6,20) VMNUI,DELPWJ,BWGH                       UFW00410
C  20 FORMAT (1X,'UFW PRE ',F10.5,3X,'DELPWJ= ',F10.5,2X,'BWGH/ZKN=',F10.UFW00420
     1,/)                                                                UFW00430
      FUMM=(ETA-ETAOM)*MUMU/2.*(RWALE+BWGH)*(U20)**2                     UFW00440
     1*SQRT(2.*DELPW/(ETAO))                                             UFW00450
      BWGH=RWALE+BWGH                                                    UFW00460
      IF (MUMU.EQ.1.0) BWGH=BWGH+.5                                      UFW00470
      IF (MUMU.NE.1.0) BWGH=BWGH+.5*(1.-MUMU)                            UFW00480
      IF (IWR.NE.2) WRITE (6,30) BWGH,BWGH                               UFW00490
C  30 FORMAT (1X,'UFW BWGH= ',F10.5,3X,'BWGH/ZKN= ',F10.5               UFW00500
```

Figure A-3, Continued

```
     1,2X,'BUOHN/RN=',F10.5/)                                          UPW00510
      NUPT=25                                                          UPW00520
      XNUPT=NUPT-1                                                     UPW00530
      DZ=(ZEND-BWGH)/XNUPT                                             UPW00540
      Z=BWGH                                                           UPW00550
      IF (IWR.NE.0) WRITE (6,12)                                       UPW00560
   12 FORMAT (16X,'Z/RN',6X,'VMU/VN',6X,'BUH/RN',6X,'BU/RN',6X,        UPW00570
     1'DELPU/DELPJ'/)                                                  UPW00580
      DO 100 I=1,NUPT                                                  UPW00590
      BUH=BUOHN*AU3*(Z-BWGH)*(COS(PHI)**ALU1)                          UPW00600
      BU=BUH/RAT                                                       UPW00610
      ZETA=Z/ZOU                                                       UPW00620
      IF (Z.GE.ZOU) ZETA=1.                                            UPW00630
      FETAF=(1.-ZETA**ALPUF)**4                                        UPW00640
      FETAM=(1.-ZETA**ALPUM)**4                                        UPW00650
      F1=.5*MOMU*(1.-FETAM)/(BU*(RWALL+Z)*CV2U)                        UPW00660
      F2=.5*DELFWJ*FETAF                                               UPW00670
      IF (F1.LT.F2) VMUN=0.                                            UPW00680
      IF (F1.LT.F2) GO TO 905                                          UPW00690
      VMUN=SQRT(F1-F2)                                                 UPW00700
  905 DELPUJ=VMUN**2+DELFWJ*FETAF                                      UPW00710
      IF (IWR.EQ.0) DELPUJ=DELPUJ/DELFS                                UPW00720
      IF (IWR.NE.0) WRITE (6,11) Z,VMUN,BUH,BU,DELPUJ                  UPW00730
   11 FORMAT (10X,5(F10.5,2X))                                         UPW00740
      Z=Z+DZ                                                           UPW00750
  100 CONTINUE                                                         UPW00760
      RETURN                                                           UPW00770
      END                                                              UPW00780
```

Figure A-3. Continued

```
      SUBROUTINE INTERG (XLAM,DELFS,SD,RO,ALFG,EFS,CU,SIG)                  INT00010
C                                                                           INT00020
C  MAIN ROUTINE FOR COMPUTING GROUND PRESSURE DISTRIBUTION                  INT00030
C   THIS ROUTINE FINDS THE SOLUTION FOR THE DEWASH THICKNESS AND            INT00040
C   JET IMPINGEMENT PERTURBATION PARAMETERS SIGMA AND EFS BY                INT00050
C   MATCHING PRESSURE INTEGRALS                                            INT00060
C                                                                           INT00070
      COMMON /WEIGHT/ WD,IFBAR                                              INT00080
      DIMENSION EE(200),C(200),PHIU(200),PHI(200),CSJ(200),FUI(4),FJI(4)INT00090
      CSP1(ETA,A)=.5*ETA**2 (4. (A12.))*ETA**(A12.))+(3./(A11.))*ETA**(2.INT00100
     1*A,2.))-(4./(3.*A12.))*ETA**(3.*A12.))(1.,(4.*A12.))*ETA**(4.*A(2.))INT00110
      FETA(ETA,A)=(1. ETA**A)**4                                            INT00120
      EE(1)=.0                                                              INT00130
      WRITE (6,777)                                                         INT00140
  777 FORMAT (///1X, *** CALL  INTERG *** ///)                              INT00150
      IFLAG=0                                                               INT00160
      C(1)=1.                                                               INT00170
      PI=3.141592654                                                        INT00180
      SIGI 1.0                                                              INT00190
      FUI=1.0                                                               INT00200
      ALG=1.0                                                               INT00210
      FAKM=.01                                                              INT00220
      DO 900 I=1,100                                                        INT00230
      EEI EE(I)                                                             INT00240
      SIGI C(I)                                                             INT00250
      DO 1000 ITK=1,4                                                       INT00260
      IF (ITK.EQ.2) EEI=EE(I)*FAKM                                          INT00270
      IF (ITK.EQ.3) EEI EE(I)                                               INT00280
      IF (ITK.EQ.4) SIGI C(I)*FAKM                                          INT00290
C                                                                           INT00300
C   SOLVE FOR INTERSECTION OF PRESSURE BOUNDARIES                           INT00310
C                                                                           INT00320
      DO 100 I=1,99                                                         INT00330
      IF (I.EQ.1) PHIU(1) 1.42                                              INT00340
      XU SD*TAN(PHIU(I))                                                    INT00350
      XUI SD/(COS(PHIU(I))**2)                                              INT00360
      YU (FUI*SIGI**3 (COS(PHIU(I)))**ALG)                                  INT00370
      YUI  (FUI*SIGI**3*ALG/((COS(PHIU(I))**(ALG+1.))                       INT00380
      RUSQ XU**2+(SD YU)**2                                                 INT00390
      RU  SQRT(RUSQ)                                                        INT00400
      FOR  ROTEFI=(1.+(SD YU) RU))                                          INT00410
      ROPSQ R**2                                                            INT00420
      1 RUSQ RUPSQ                                                          INT00430
      EE  *.*XU*XUI  2.*( D YU)*YUI  *.*EFI*RUI*(SD YU)*                    INT00440
     1(YUI*(1.+(  *XU*XUI  _  *(SD YU)*YUI))/RUPSQ)                         INT00450
      EE(I+1) EE(I)  EI                                                     INT00460
      IF (ABS(PHIU(I+1) PHIU(I)).LT.1.E 5) GO TO 101                        INT00470
  100 CONTINUE                                                              INT00480
        IF                                                                  INT00490
  101 PHIUO PHIU(I+1)                                                       INT00500
      PHIUDG PHIUO*180. /PI                                                 INT00510
      YUO CUI*SIGI**3 (COS(PHIUO)**ALG)                                     INT00520
      PHIO ATAN(SQRT(TAN(PHIUO))*SD YUO)                                    INT00530
      PHIOD PHIO*180. PI                                                    INT00540
      IF (IFLAG.EQ.1) WRITE (6,10) EE,CUI,PHIUOG,PHIOD                      INT00550
   10 FORMAT (1X,* EE= *E15.7,* CUI= *E10.3,* PHIUOG= *E10.5              INT00560
     1,* PHIOD= *E10.5                                                      INT00570
C                                                                           INT00580
C  DETERMINE MOMENTUM INTEGRAL FOR IMPINGEMENT REGION                       INT00590
C                                                                           INT00600
      NP1=I 99                                                              INT00610
      IF (I.EQ. 99) NP1=I+1                                                 INT00620
```

Figure A-3. Continued

```
      XPTS=NUPTS-1.                                                     INT00630
      DFHIU=FHIUO/XPTS                                                  INT00640
      PHIU(1)=0.                                                        INT00650
      SUMU1=0.                                                          INT00660
      DO 200 IJ=1,NUPTS                                                 INT00670
      FACT=2.0                                                          INT00680
      IF (IJ.EQ.1) FACT=1.0                                             INT00690
      IF (IJ.EQ.NUPTS) FACT=1.0                                         INT00700
      RW=SD/COS(PHIU(IJ))                                               INT00710
      CALL WALLJ (RW,VMN,DUM2,DUM3,DUM4,DELFW)                          INT00720
      IF (IJ.EQ.1.AND.IFLAG.EQ.1) WRITE (6,111) DELFW                   INT00730
  111 FORMAT (35X, PHI=0.0, DELFW0= ,F10.5)                             INT00740
      YU=FUI*SIGI*SD/COS(PHIU(IJ))                                      INT00750
      XU=SD*TAN(PHIU(IJ))                                               INT00760
      PHI(IJ)=ATAN2(XU,SD-YU)                                           INT00770
      RU=(SD-YU)/COS(PHI(IJ))                                           INT00780
      ROF=ROHEFI*(1.+COS(PHI(IJ)))                                      INT00790
      ETAM=RU/ROF                                                       INT00800
      IF (ETAM.GT.1.) ETAG=0.0                                          INT00810
      IF (ETAM.GT.1.) GO TO 1011                                        INT00820
      ETAG=ETA(ETAM,ALPG)                                               INT00830
 1011 FMIN DELFS*ETAG                                                   INT00840
      IF (IJ.EQ.1.AND.IFLAG.EQ.1) WRITE (6,775) FMIN                    INT00850
  775 FORMAT (3*X, PHI 0 0, FMIN  ,F10.5)                               INT00860
      FMAX DELFW VMN**2*(VMN*COS(PHIU(IJ)))**2                          INT00870
      CALL FMATCH (FMIN,FMAX,ALFUG)                                     INT00880
      IF (IJ.EQ.1.AND.IFLAG.EQ.1) WRITE (6,1055) ALFUG                  INT00890
 1055 FORMAT (35X, PHI=0.0, ALFUG  ,F10.5)                              INT00900
      CALL SIMUG(ALFUG,RATU,SFUG)                                       INT00910
      FMAX DELFW VMN**2*(VMN*COS(PHIU(IJ)))**2                          INT00920
      FU=DELFS*ETAG+SFUG*(FMAX DELFS)*ETAG)                             INT00930
      FUT SIGI*FU/( OS(PHIU(IJ))**3)                                    INT00940
      SUMU1= SUMU1+.5*DFHIU*FACT*FUT                                    INT00950
      IF (ETAM.GT.1.) ETAM=1.0                                          INT00960
      CALL ETF(ETAM,ALFG)                                               INT00970
      PHIU(IJ+1) PHIU(IJ)+DFHIU                                         INT00980
  200 CONTINUE                                                          INT00990
      XIUG=FUI*SUMU1*.0**2                                              INT01000
      SUMI=0.                                                           INT01010
      NUPTSM=NUPTS-1                                                    INT01020
      DO 300 IJ=1,NUPTSM                                                INT01030
      ROFF ROHEFI*(1.+COS(PHI(IJ+1)))                                   INT01040
      ROFFSQ=ROFF**2                                                    INT01050
      ROFM=ROHEFI*(1.+COS(PHI(IJ)))                                     INT01060
      ROFMSQ ROFM**2                                                    INT01070
      FM ROFMSQ*SIGI(IJ)                                                INT01080
      FF ROFFSQ*SIGI(IJ+1)                                              INT01090
      DFHI PHI(IJ+1) PHI(IJ)                                            INT01100
      SUMI SUMI+.5*DFHI*(FM+FF)                                         INT01110
  300 CONTINUE                                                          INT01120
      XIUG DELFS*SUMI                                                   INT01130
      CALL SIMCO,0,ALFG,RATUG,SFUG)                                     INT01140
      XIUG (SFUG*DELFS*(FI FHI)**(KOH*(KOH+2.*FI)+1.5*FI**2)            INT01150
     1 -2.*FI**(KOH+1.)*SIN(FHI)   **SIN(2.*FHI)*FI**2)                 INT01160
      XII=XIUG+XIPG                                                     INT01170
      FII(IIK) XII FI                                                   INT01180
      DFHIU (.5*FI FHIUO)/XPTS                                          INT01190
      SUMU2 0.0                                                         INT01200
      DO FHIUO                                                          INT01210
      XI UG  IGI*(1  SIN(FHIUO))                                        INT01220
      FHI(IIK) XIUG+XIPG XIAM                                           INT01230
      IF (FHIAG.EQ.1) (0 TO 502                                         INT01240
       F (IIK.EQ.1) GO TO 1000                                          INT01250
      KE=2                                                              INT01260
      DFI FAFM                                                          INT01270
      DFHI FAFM                                                         INT01280
```

Figure A-3. Continued

```
      IF (ITR.EQ.2) FUIE=(FUI(ITR)-FUI(ITR-1))/DEPI                    INT01290
      IF (ITR.EQ.4) FUIC=(FUI(ITR)-FUI(ITR-1))/DCUI                    INT01300
      IF (ITR.EQ.2) FJIE=(FJI(ITR)-FJI(ITR-1))/DEPI                    INT01310
      IF (ITR.EQ.4) FJIC=(FJI(ITR)-FJI(ITR-1))/DEPI                    INT01320
 1000 CONTINUE                                                         INT01330
      DET=FUIE*FJIC-FJIE*FUIC                                          INT01340
      DELE=(FJI(1)*FUIC-FUI(1)*FJIC)/DET                               INT01350
      DELC=(FUI(1)*FJIE-FJI(1)*FUIE)/DET                               INT01360
      EP(J+1)=EP(J)+RELAX*DELE                                         INT01370
      C(J+1)=C(J)+RELAX*DELC                                           INT01380
  905 FORMAT (15X,'ITERATION CYCLE=',I3,2X,'EPS=',F10.5,2X,'SIGMA=',F10.INT01390
     1 5)                                                              INT01400
      IF (ABS(DELE).LT.1.E-5.AND.ABS(DELC).LT.1.E-5) IFLAG=1           INT01410
      IF (IFLAG.EQ.1) WRITE (6,909)                                    INT01420
  909 FORMAT (20X,'SOLUTION OF GROUND PRESSURE DISTRIBUTION HAS BEEN FOU;INT01430
     1ND')                                                             INT01440
      IF (IFLAG.EQ.1) WRITE (6,905) J,EP(J+1),C(J+1)                   INT01450
  900 CONTINUE                                                         INT01460
      STOP                                                             INT01470
  907 SIG=C(J)                                                         INT01480
      EPS=EP(J)                                                        INT01490
      CUU=SIG*CUI                                                      INT01500
      WRITE (6,13) CUU                                                 INT01510
   13 FORMAT (20X,'UPWASH THICKNESS CONSTANT, (CU) X (SIGMA)=',F10.5)  INT01520
      IF (IPBAR.NE.0) CALL GPLOT(ALFG,DELFS,SD,RO,LPS,CU),SIG,PHIUO,PHIOINT01530
     1)                                                                INT01540
      RETURN                                                           INT01550
      END                                                              INT01560
```

Figure A-3. Continued

```
      SUBROUTINE GPLOT (ALPG,DELPS,SD,RO,EPS,CUI,SIGI,FKIUO,PHIO)        GPL00010
      DIMENSION PU(25),RWALL(102),ERR(102),XPLOTU(202),YPLOTU(           GPL00020
     1202),XPLOTJ(202),YPLOTJ(202),XAXIS(30),YAXIS(30),XDATA(10),YDATA(1GPL00030
     20)                                                                 GPL00040
      COMMON /HEIGHT/ HD,IPDAR                                           GPL00050
C                                                                        GPL00060
C   THIS ROUTINE COMPUTES THE GROUND ISOBAR PATTERN FOR THE TWO-JET      GPL00070
C    IMPINGEMENT FLOW FIELD                                             GPL00080
C                                                                        GPL00090
      FETA(ETA,A)=(1.-ETA$**A)$**4                                       GPL00100
C                                                                        GPL00110
C    INPUT NUMBER OF ISOBAR VALUES                                      GPL00120
C                                                                        GPL00130
      READ(5,51) NU                                                      GPL00140
   51 FORMAT (I2)                                                        GPL00150
      WRITE (6,53) NU                                                    GPL00160
   53 FORMAT ( 1H1,///30X,'***  COMPUTATION OF TWO-JET GROUND ISOBAR PATTEGPL00170
     1RN ***'///32X,I2,' VALUES OF PRESSURE SPECIFIED FOR PATTERN'       GPL00180
     2//)                                                                GPL00190
C                                                                        GPL00200
C    INPUT NU ISOBAR VALUES FOR GROUND PATTERN                          GPL00210
C                                                                        GPL00220
      READ(5,1) (PU(I),I=1,NU)                                           GPL00230
    1 FORMAT (F10.5)                                                     GPL00240
      WRITE (6,112) (PU(I),I=1,NU)                                       GPL00250
  112 FORMAT (10X,'PBAR=',8(F10.5,2X))                                   GPL00260
      WRITE (6,121)                                                      GPL00270
  121 FORMAT (///20X,'GROUND PATTERN IN JET CENTERED COORDINATE SYSTEM'//GPL00280
     1)                                                                  GPL00290
      NOPTS=29                                                           GPL00300
C     CALL PLOT(6.,0.,-3)                                              GPL00310
      XLMAX=ROUND                                                        GPL00320
C     XSC=XLMAX/8.                                                     GPL00330
      XSC=1.0                                                            GPL00340
      XMIN=0.                                                            GPL00350
      DXMIN=-1.                                                          GPL00360
      DO 801 IP=1,100                                                    GPL00370
      IF (XMIN.LT.-.60) GO TO 802                                        GPL00380
      XMIN=XMIN+DXMIN                                                    GPL00390
  801 CONTINUE                                                           GPL00400
  802 XMAX=SD                                                            GPL00410
      DXAXIS=SD-XMIN                                                     GPL00420
      NAPTS=DXAXIS+1                                                     GPL00430
      XAXIS(1)=XMIN/XSC                                                  GPL00440
      YAXIS(1)=0.                                                        GPL00450
      DO 803 IP=2,NAPTS                                                  GPL00460
      XAXIS(IP)=XAXIS(IP-1)+1./XSC                                       GPL00470
      YAXIS(IP)=YAXIS(IP-1)                                              GPL00480
  803 CONTINUE                                                           GPL00490
      DYAX=1./XSC                                                        GPL00500
      XAXIS(NAPTS+1)=SD/XSC                                              GPL00510
      YAXIS(NAPTS+1)=0.                                                  GPL00520
      DO 804 IP=1,NAPTS                                                  GPL00530
      XAXIS(NAPTS+IP+1)=SD/XSC                                           GPL00540
      YAXIS(NAPTS+IP+1)=YAXIS(NAPTS+IP-1)+DYAX                           GPL00550
  804 CONTINUE                                                           GPL00560
      NPLOT=2*NAPTS                                                      GPL00570
C     CALL LINE (XAXIS,YAXIS,NPLOT,1,1,3,1.,1)                         GPL00580
C     CALL SYMBOL (-.5,0.,.2,10HD/D=14.0, 5/8=2.00 ,0.,18)             GPL00590
      IF (.NOT.IPDAR) GO TO 1                                            GPL00600
      XSC=.NOPTS-1                                                       GPL00610
      RETURN                                                             GPL00620
```

Figure A-3. Continued

```
      DO 500 I=1,NU                                                    GPL00630
      WRITE (6,66) PU(I)                                               GPL00640
   66 FORMAT (///45X,'PBAR=',F10.5)                                    GPL00650
      IFLAG=1                                                          GPL00660
      XPUF=0.                                                          GPL00670
      IJET=1                                                           GPL00680
      IU=1                                                             GPL00690
      RW=SD                                                            GPL00700
      ALPUG=1.5                                                        GPL00710
      CALL WALLJ (RW,VMN,DUM2,DUM3,DUM4,DELPW)                         GPL00720
      PMAXO=DELPW                                                      GPL00730
      IF (PMAXO.LT.PU(I)) IFLAG=0                                      GPL00740
      RW=SD/COS (PHIUO)                                                GPL00750
      CALL WALLJ (RW,VMN,DUM2,DUM3,DUM4,DELPW)                         GPL00760
      PMAXF=DELPW-VMN**2*(VMN*COS(PHIUO))**2                           GPL00770
      IF (IFLAG.EQ.0) GO TO 502                                        GPL00780
      RWALL(1)=SD                                                      GPL00790
      RWALL(2)=SD+.1                                                   GPL00800
      DO 400 K=1,100                                                   GPL00810
      CALL WALLJ(RWALL(K),VMN,DUM2,DUM3,DUM4,DELPW)                    GPL00820
      XU=SQRT(RWALL(K)**2-SD**2)                                       GPL00830
      PHIU=ATAN2(XU,SD)                                                GPL00840
      PMAX=DELPW-VMN**2*(VMN*COS(PHIU))**2                             GPL00850
      ERR(K)=PU(I)-PMAX                                                GPL00860
      IF (K.EQ.1) GO TO 400                                            GPL00870
      IF (ABS(ERR(K)).LT.1.E-5) GO TO 501                              GPL00880
      DRDE=(RWALL(K)-RWALL(K-1))/(ERR(K)-ERR(K-1))                     GPL00890
      RWALL(K+1)=RWALL(K)-RELAX*DRDE*ERR(K)                            GPL00900
  400 CONTINUE                                                         GPL00910
      STOP                                                             GPL00920
  501 RW=RWALL(K)                                                      GPL00930
      XPUF=SQRT(RW**2-SD**2)                                           GPL00940
      PUF=ATAN2(XPUF,SD)                                               GPL00950
      YUF=CUI*SIGI*SD/COS(PUF)                                         GPL00960
      PUFD=PUF*180./PI                                                 GPL00970
  502 DPHIU=PHIUO/XFTS                                                 GPL00980
      IF (PHIUO.EQ.0.) GO TO 201                                       GPL00990
      PHIU=0.                                                          GPL01000
      DO 200 I=1,NUFTS                                                 GPL01010
      RW=SD/COS(PHIU)                                                  GPL01020
      CALL WALLJ (RW,VMN,DUM2,DUM3,DUM4,DELPW)                         GPL01030
      YU=CUI*SIGI*SD/COS(PHIU)                                         GPL01040
      XU=SD*TAN(PHIU)                                                  GPL01050
      PHI=ATAN2(XU,SD-YU)                                              GPL01060
      RU=(SD-YU)/COS(PHI)                                              GPL01070
      ROE=ROEPS*(1.+COS(PHI))                                          GPL01080
      ETAM=RU/ROE                                                      GPL01090
      IF (ETAM.GT.1.) PTAG=0.0                                         GPL01100
      IF (ETAM.GT.1.) GO TO 1011                                       GPL01110
      PTAG=PTAG*ETAM**ALPG)                                            GPL01120
 1011 PMIN=DELPS*PTAG                                                  GPL01130
      PMAX=DELPW-VMN**2*(VMN*COS(PHIU))**2                             GPL01140
      CALL PMATCH (PMIN,PMAX,ALPUG)                                    GPL01150
      PRAT=(PU(I)-PMIN)/(PMAX-PMIN)                                    GPL01160
      IF (PMIN.GT.PU(I)) GO TO 509                                     GPL01170
      PRAT=PU(I)/DELPS                                                 GPL01180
      IF (PRAT.GT.1.) GO TO 509                                        GPL01190
      ETA=(1.-PRAT**.25)**(1./ALPG)                                    GPL01200
      XPUF=XPUF+ROE*ETA*COS(PHI)                                       GPL01210
      YPUF=YPUF+ROE*ETA*SIN(PHI)                                       GPL01220
      XPUF(IJET)=XPUF(IJET)/XSC                                        GPL01230
      YPUF(IJET)=YPUF(IJET)/XSC                                        GPL01240
      IJET=IJET+1                                                      GPL01250
  509 IF (PRAT.GT.1..OR.PRAT.LT.0.) GO TO 506                          GPL01260
      PTAG(I)=PRAT**(1./ALPG)                                          GPL01270
      XPUF(IJET)=XU*ETA                                                GPL01280
```

Figure A-3. Continued

```
      YFLOTU(IU)=XU                                                    GFL01290
      XFLOTU(IU)=XFLOTU(IU)/XSC                                        GFL01300
      YFLOTU(IU)=YFLOTU(IU)/XSC                                        GFL01310
      IU=IU+1                                                          GFL01320
  506 PHIU=PHIU+DPHIU                                                  GFL01330
  200 CONTINUE                                                         GFL01340
  201 DPHI=(PI-PHIO)/XPTS                                              GFL01350
      PHI=PHIO                                                         GFL01360
      DO 600 IN=1,NUPTS                                                GFL01370
      PBARJ=PU(I)/DELPS                                                GFL01380
      IF (PBARJ.GT.1.) GO TO 600                                       GFL01390
      ETAJ=(1.-PBARJ**.25)**(1./ALPG)                                  GFL01400
      ROP=RO+EPS*(1.+COS(PHI))                                         GFL01410
      XFLOTJ(IJET)=ROP*ETAJ*COS(PHI)                                   GFL01420
      YFLOTJ(IJET)=ROP*ETAJ*SIN(PHI)                                   GFL01430
      XFLOTJ(IJET)=YFLOTJ(IJET)/XSC                                    GFL01440
      YFLOTJ(IJET)=YFLOTJ(IJET)/XSC                                    GFL01450
      IJET=IJET+1                                                      GFL01460
      PHI=PHI+DPHI                                                     GFL01470
  600 CONTINUE                                                         GFL01480
      IF (IFLAG.EQ.0) GO TO 513                                        GFL01490
      IF (FU(I).EQ.0.) GO TO 513                                       GFL01500
      IF(FUF.LT.PHIUO) GO TO 510                                       GFL01510
      GO TO 511                                                        GFL01520
  510 XFLOTU(IU)=SD                                                    GFL01530
      YFLOTU(IU)=XFUF                                                  GFL01540
      XFLOTU(IU)=XFLOTU(IU)/XSC                                        GFL01550
      YFLOTU(IU)=YFLOTU(IU)/XSC                                        GFL01560
      GO TO 800                                                        GFL01570
  511 DPHIU=(FUF-PHIUO)/XPTS                                           GFL01580
      PHIU=PHIUO                                                       GFL01590
      DO 700 IU=1,NUPTS                                                GFL01600
      YU=CUR*SIGI*SD/COS(PHIU)                                         GFL01610
      XU=SD*TAN(PHIU)                                                  GFL01620
      RW=SD/COS(PHIU)                                                  GFL01630
      CALL WALL(RW,VMN,DUM2,DUM3,DUM4,DELPW)                          GFL01640
      PMAX=DELPW-VMN**2)*(VMN*COS(PHIU))**2                            GFL01650
      PBAR=PU(I)/PMAX                                                  GFL01660
      ETAU=(1.-PBAR**.5)**(1./ALPUG)                                   GFL01670
      XFLOTU(IU)=SD-YU*ETAU                                            GFL01680
      YFLOTU(IU)=XU                                                    GFL01690
      XFLOTU(IU)=XFLOTU(IU)/XSC                                        GFL01700
      YFLOTU(IU)=YFLOTU(IU)/XSC                                        GFL01710
      IU=IU+1                                                          GFL01720
      PHIU=PHIU+DPHIU                                                  GFL01730
  700 CONTINUE                                                         GFL01740
  513 IU=IU-1                                                          GFL01750
  800 IJET=IJET-1                                                      GFL01760
      WRITE (6,11) IJET,IU                                             GFL01770
   11 FORMAT (//10X,' JET IMPINGEMENT REGION,  IJET=',I4,10X,'UPWASH DEFLGFL01780
     1ECTION REGION, IU =',I4//)                                       GFL01790
      IF (IJET.GT.0.OR.IU.GT.0) WRITE (6,552)                          GFL01800
  552 FORMAT (//3X,' XISOJ ',6X,' YISOJ ',8X,'XISOU',8X,' YISOU /)     GFL01810
      IMIN=IU                                                          GFL01820
      IMAX=IJET                                                        GFL01830
      IF (IU.GT.IJET) IMAX=IU                                          GFL01840
      IF (IU.GT.IJET) IMIN=IJET                                        GFL01850
      DO 903 IM=1,IMAX                                                 GFL01860
      IF (IM.LE.IMIN) WRITE(6,12) XFLOTJ(IM),YFLOTJ(IM),XFLOTU(IM),YFLOTGFL01870
     1U(IM)                                                            GFL01880
   12 FORMAT (5X,4(F10.5,2X))                                          GFL01890
      IF (IM.GT.IMIN.AND.IMIN.EQ.IU) WRITE (6,15) XFLOTJ(IM),YFLOTJ(IM) GFL01900
   15 FORMAT (5X,,(F10.5,2X))                                          GFL01910
      IF (IM.GT.IMIN.AND.IMIN.EQ.IJET) WRITE (6,16) XFLOTU(IM),YFLOTU(IMGFL01920
     1)                                                                GFL01930
   16 FORMAT (54X,,2(F10.5,2X))                                        GFL01940
```

Figure A-3. Continued

```
  803 CONTINUE                                                          GFL01950
C     CALL LINE (XFLOTU,YFLOTU,IU,1,1,1,1,.1)                         GFL01960
C     CALL LINE (XFLOTJ,YFLOTJ,IJET,1,1,1,1,.1)                       GFL01970
  900 CONTINUE                                                          GFL01980
      DPHIU=.5*PI/XPTS                                                GFL01990
      PHIU=0.                                                         GFL02000
      DO 900 I=1,NUPTS                                                GFL02010
      YU=CUI*SIGI*SD/COS(PHIU)                                        GFL02020
      XU=SD*TAN(PHIU)                                                 GFL02030
      IF (XU.GT.XLMAX) GO TO 901                                      GFL02040
      XFLOTU(I)=SD-YU                                                 GFL02050
      YFLOTU(I)=XU                                                    GFL02060
      XFLOTU(I)=XFLOTU(I)/XSC                                         GFL02070
      YFLOTU(I)=YFLOTU(I)/XSC                                         GFL02080
      PHIU=PHIU+DPHIU                                                 GFL02090
  900 CONTINUE                                                          GFL02100
  901 IU=I-1                                                            GFL02110
      WRITE (6,807)                                                   GFL02120
  807 FORMAT (///1X, DEWASH DEFLECTION ZONE LINE, PHAR=0 OUTSIDE INTERAGFL02130
     1CTION REGION ///)                                               GFL02140
      WRITE (6,808)                                                   GFL02150
  808 FORMAT (5X,'XUP',8X,'YUP'//)                                    GFL02160
      DO 811 IM=1,IU                                                  GFL02170
      WRITE (6,811) XFLOTU(IM),YFLOTU(IM)                             GFL02180
  811 CONTINUE                                                          GFL02190
  811 FORMAT (30X,2(F10.5,2X))                                        GFL02200
C     CALL LINE (XFLOTU,YFLOTU,IU,1,1,1,1,.1)                         GFL02210
C     CALL ADRAW                                                      GFL02220
C     CALL PLOT (-99.,99.,-3)                                         GFL02230
C     READ (5,101) PAUSE                                              GFL02240
  101 FORMAT (1X,F10.5)                                               GFL02250
      RETURN                                                          GFL02260
      END                                                             GFL02270


      SUBROUTINE JETEC (ETAC,KJH,ALEC,K,CV2)                          JET00010
      DIMENSION ALE(100),ERR(100)                                     JET00020
C                                                                     JET00030
C     THI  ROUTINE COMPUTES THE EXPONENT OF THE JET VELOCITY PROFILE  JET00040
C     IN THE POTENTIAL CORE REGION                                    JET00050
C                                                                     JET00060
      ALE(1)=1.5                                                      JET00070
      ALE(2)=10.                                                      JET00080
      DO 100 I=1,99                                                   JET00090
      CALL SIM(ETAC,ALE(I),K,CV2)                                     JET00100
      ERR(I)=CV2-.5*(K/K0)**2                                         JET00110
      IF (I.GE.2) ALE(I+1)=ALE(I)-(ALE(I)-ALE(I-1))/(ERR(I)-ERR(I-1))*JET00120
     1ERR(I)                                                          JET00130
      ALE=ALE(I)                                                      JET00140
      IF (ABS(ERR(I)).LT.1.E-5) GO TO 101                             JET00150
  100 CONTINUE                                                        JET00160
      STOP                                                            JET00170
  101 RETURN                                                          JET00180
      END                                                             JET00190


      SUBROUTINE SIM(ETAC,ALE,K,CV2)                                  SIM00010
C                                                                     SIM00020
C     INTEGRAL OF  JET VELOCITY EXPONENT FUNCTION (2*                 SIM00030
C     K RATIO OF (0 TO 1)                                             SIM00040
C                                                                     SIM00050
      A1 = 1. /(ALE+2.)*(1.-(ALE+1.)/4. +(3.*ALE+11.)/(4.*ALE+2.)     SIM00060
      A2 = 1. /(ALE+1.)*(1.-(3.*ALE+1.)/4. +(3.*ALE+11.)/(4.*ALE+2.)  SIM00070
      CV2 = ETAC**2)*A1*(1.-ETAC)**2)*(1.-ETAC**2                     SIM00080
```

Figure A-2, Continued

```
      R=ETAC+(1.-ETAC)*((2.-SQRT(2.))/2.)**(1./ALF)                    SIM00090
      RETURN                                                           SIM00100
      END                                                              SIM00110


      SUBROUTINE GPRES (PO,VG,ALPG,R,CV2)                              GPR00010
      DIMENSION ALP(100),ERR(100)                                      GPR00020
C                                                                      GPR00030
C  THIS ROUTINE SOLVES GROUND PRESSURE INTEGRAL FOR GROUND PRESSURE     GPR00040
C   EXPONENT                                                           GPR00050
C                                                                      GPR00060
      ALP(1)=1.5                                                       GPR00070
      ALP(2)=5.                                                        GPR00080
      DO 100 I=1,99                                                    GPR00090
      CALL SIM(0.0,ALP(1),R,CV2)                                       GPR00100
      ERR(I)=RO-1./(VG*SQRT(CV2))                                      GPR00110
      IF (I.GE.2) ALP(I+1)=ALF(I)-((ALP(I)-ALP(I-1))/(ERR(I) ERR(I-1)))*GPR00120
     1ERR(I)                                                           GPR00130
      ALPG=ALP(I)                                                      GPR00140
      IF (ABS(ERR(I)).LT.1.E-5) GO TO 101                              GPR00150
  100 CONTINUE                                                         GPR00160
      STOP                                                             GPR00170
  101 RETURN                                                           GPR00180
      END                                                              GPR00190


      SUBROUTINE SIMW(KDEL,N,ALFW,R,CV2,CP)                            SIM00010
C                                                                      SIM00020
C   THIS ROUTINE COMPUTES THE INTEGRAL OF THE VELOCITY SQUARED PROFILE SIM00030
C   AND STATIC PRESSURE PROFILE FOR WALL JET FUNCTIONS                 SIM00040
C     CV2=VELOCITY SQUARED INTEGRAL                                    SIM00050
C     CP=STAIC PRESSURE INTEGRAL                                       SIM00060
C     R=RATIO OF BWH TO BW                                             SIM00070
C                                                                      SIM00080
      REAL KDEL,N                                                      SIM00090
      XN=N                                                             SIM00100
      XI1=1.-4./(ALFW+1 )+6./(2.*ALFW+1.)-4./(3.*ALFW+1.)+1./(4.*ALFW+1.SIM00110
     1)                                                                SIM00120
      CV2=(XN/(2.+XN))*KDEL+(1.-KDEL)*XI1                              SIM00130
      CP=KDEL+(1. KDEL)*XI1                                            SIM00140
      F=((2.-SQRT(2.))/2.)**(1./ALFW)                                  SIM00150
      R=KDEL+(1.-KDEL)*F                                               SIM00160
      RETURN                                                           SIM00170
      END                                                              SIM00180


      SUBROUTINE SIMUG(ALFU,R,CV2U)                                    SIM00010
C                                                                      SIM00020
C   THIS ROUTINE COMPUTES VELOCITY SQUARED INTEGRAL FOR UPWASH         SIM00030
C                                                                      SIM00040
      CV2U=1.-4./(ALFU+1.)+6./(2.*ALFU+1.)-4./(3.*ALFU+1.)+1./(4.*ALFU+1SIM00050
     1.)                                                               SIM00060
      F=(SQRT(2.)-1.)/SQRT(_ )                                         SIM00070
      R=F**(1./ALFU)                                                   SIM00080
      RETURN                                                           SIM00090
      END                                                              SIM00100


      SUBROUTINE GMATCH (RG,VG,ALPG,KDEL,N,ETAWG,DELS,ALFW,R)          GMA00010
C                                                                      GMA00020
C   THIS ROUTINE IS USED FOR INITIATING WALL JET REGION                GMA00030
```

Figure A-3. Continued

```
C      COMPUTES THE INTIAL INVISCID EXPONENT FOR WALL JET PROFILE          GMA00040
C                                                                         GMA00050
       REAL KDEL,N                                                        GMA00060
       DIMENSION ALP(100),ERR(100)                                        GMA00070
       ALP(1)=.1                                                          GMA00080
       RELAX=.5                                                           GMA00090
       ALP(2)=1.5                                                         GMA00100
       DO 100 I=1,100                                                     GMA00110
       CALL SIMW(KDEL,N,ALP(I),R,CV2,CP)                                  GMA00120
       FETAG=(1.-ETAWD**ALPG)**4                                          GMA00130
       DEN=(RG*VG**2)*(2.*CV2*(1.-FETAG)+CP*FETAG)                        GMA00140
       RWD=(1.-FETAG)/DEN                                                 GMA00150
       RWDN=R**RWD                                                        GMA00160
       DELSM=RWD*KDEL                                                     GMA00170
       ERR(I)=DELSM-DELS                                                  GMA00180
       IF (ABS(ERR(I)).LT.1.E-5) GO TO 101                                GMA00190
       IF (I.GE.2) ALP(I+1)=ALP(I)-((ALP(I)-ALP(I-1))/(ERR(I)-ERR(I-1)))*GMA00200
      1ERR(I)*RELAX                                                       GMA00210
  100 CONTINUE                                                           GMA00220
       STOP                                                              GMA00230
  101 ALPW=ALP(I)                                                        GMA00240
       RETURN                                                            GMA00250
       END                                                               GMA00260


       SUBROUTINE SIMW(ALPW,R,CV2W)                                      SIM00010
       CV2W=1. 4./(ALPW+1.)+6./(2.*ALPW+1.)-4./(3.*ALPW+1.)+1./(4.*ALPW+1SIM00020
      1.)                                                                SIM00030
       F=(SQRT(2.) 1.)/SQRT(2.)                                          SIM00040
       R=F**(1./ALPW)                                                    SIM00050
       RETURN                                                            SIM00060
       END                                                               SIM00070


       SUBROUTINE FGUMAT(CUPD,DELFS,DELFW,RD,SD,ALPG,ALFUG)              FGU00010
       DIMENSION ERR(101),SIG(101)                                       FGU00020
C                                                                        FGU00030
C    THIS ROUTINE COMPUTES EXPONENT OF UPWASH GROUND PRESSURE PROFILE    FGU00040
C                                                                        FGU00050
       SIG(1) .10                                                        FGU00060
        SIG(2) 1.0                                                       FGU00070
       ALFUG 1.5                                                         FGU00080
       DO 100 I=1,100                                                    FGU00090
       FR=(DELFS/DELFW)**(.25)                                           FGU00100
       ETAG=SD*(1. SIG(I))/RD                                            FGU00110
       ETAU=SIG(I)/CUPD                                                  FGU00120
       F1=FR*(1.-ETAG**ALPG)                                             FGU00130
       F2=1. ETAU**ALFUPD                                                FGU00140
       ERR(I)=F1-F2                                                      FGU00150
       IF (I.EQ.1) GO TO 100                                             FGU00160
       S=(SIG(I)-SIG(I-1))/(ERR(I) ERR(I-1))                             FGU00170
       IF (ABS(ERR(I)) LT. E 5) GO TO 101                                FGU00180
       SIG(I+1) SIG(I)-S*ERR(I)                                          FGU00190
  100 CONTINUE                                                           FGU00200
       STOP                                                              FGU00210
  101 SIGUP SIG(I)                                                       FGU00220
       ETAM SIGUP/CUPD                                                   FGU00230
       IF (ETAM GT 1.0) ETAM 1.0                                         FGU00240
       FMIN DELFW*(1. ETAM**ALFUPD)**4                                   FGU00250
       CALL FMATCH (FMIN,DELFW,ALFUG)                                    FGU00260
       RETURN                                                            FGU00270
       END                                                               FGU00280
```

Figure A-3. Continued

```
      SUBROUTINE PMATCH (PMIN,PMAX,ALPUG)                               PMA00010
      DIMENSION ERR(101),AL(101)                                        PMA00020
                                                                        PMA00030
     THIS ROUTINE COMPUTES THE EXPONENT OF THE PRESSURE PROFILE FOR     PMA00040
     THE UPWASH DEFLECTION ZONE                                         PMA00050
                                                                        PMA00060
      ALPUFD=1.5                                                        PMA00070
      PB=PMIN/PMAX                                                      PMA00080
      ETAM=(1.-PB**.25)**(1./ALPUFD)                                    PMA00090
      CALL SIMUF(ALPUFD,ETAM,CSPUFD)                                    PMA00100
      AL(1)=1.5                                                         PMA00110
      AL(2)=3.0                                                         PMA00120
      DO 100 I=1,100                                                    PMA00130
      CALL SIMUF(AL(I),1.0,CSPU)                                        PMA00140
      X1=ETAM*(PB+(1.-PB)*CSPU)                                         PMA00150
      X2=CSPUFD                                                         PMA00160
      ERR(I)=X1-X2                                                      PMA00170
      IF (ABS(ERR(I)).LT.1.E-5) GO TO 101                               PMA00180
      IF (I.EQ.1) GO TO 100                                             PMA00190
      S=(AL(I)-AL(I-1))/(ERR(I)-ERR(I-1))                               PMA00200
      AL(I+1)=AL(I)-S*ERR(I)                                            PMA00210
  100 CONTINUE                                                          PMA00220
      STOP                                                              PMA00230
  101 ALPUG=AL(I)                                                       PMA00240
      RETURN                                                            PMA00250
      END                                                               PMA00260
```

Figure A-3. Concluded

12. References

1. Platzer, M.F. and Margason, R.J., "Prediction Methods for Jet V/STOL Propulsion Aerodynamics", Jr. of Aircraft, Vol. 15, No. 2, pp. 69-77, Feb. 1978.

2. Siclari, M.J., Migdal, D., and Palcza, J.L., "The Development of Theoretical Models for Jet-Induced Effects on V/STOL Aircraft", AIAA Paper No. 75-1216, AIAA/SAE 11th Propulsion Conference, Anaheim, Cal. Sept. 29 - Oct. 1, 1975.

3. Siclari, M.J., Hill, W.G., Jr., and Jenkins, R.C., "Investigation of Stagnation Line and Upwash Formation", AIAA Paper No. 77-615, AIAA/NASA, Ames V/STOL Conference, June 1977.

4. Siclari, M.J., Aidala, P., Wohlfeb, F., and Palcza, J.L., "Development of Prediction Techniques for Multi-Jet Thermal Ground Flow Fields and Fountain Formation", AIAA Paper No. 77-616, AIAA/NASA AMES V/STOL Conference, Palo Alto, Calif. June 6-8, 1977.

5. Hill, W.G., Jr. and Jenkins, R.C., "Effect of Nozzle Spacing on Ground Interference Forces for a Two-Jet V/STOL Aircraft" AIAA Paper No. 79-1856, AIAA Aircraft Systems and Technology Conference, New York City, N.Y., Aug. 20-22 1979.

6. Wohlfeb, F.A. and Migdal, D. "Some Basic Test Results of V/STOL Jet-Induced Lift Effects in Hover", AIAA Paper No. 79-0339, Jan. 1979.

7. Kline, S.J., "On The Nature of Stall", Trans. ASME, Series D, Journal of Engineering, Vol. 81, pp. 305-320, 1959.

8. Hall, G.R. and Rogers, K.H., "Recirculation Effects Produced by a Pair of Heated Jets Impinging on a Ground Plane", NASA CR 1307, May 1969.

9. Gauntner, J.W., Livingood, J.N.B., and Hrycok, P., "Survey of Literature on Flow Characteristics of a Single Turbulent Jet Impinging on a Flat Plate", NASA TN D-5642, Feb. 1970.

10. Strand, T., "On the The Theory of Normal Ground Impingement of Axisymmetric Jets in Inviscid Incompressible Flow", AIAA Paper No. 64-424, 1964.

11. Schach, W., "Umlenkung eines Kreisformigen Flüssigkeitsstrales an einer ebenon Platte senkrecht Zur Strömungsrichtung," Ingenieur Archiv, p. 51, Vol. 6, 1935.

12. Shen, Y.C., "Theoretical Analysis of Jet-Ground Plane Interaction", IAS Paper No. 62-144, June 1962.

13. Barnes, D.A., and Sullivan, R.D., "Rotational Solutions of the Euler Equations", AGAP Report No. 79., AFOSR Scientific Report No. AFOSR 65-2656.

14. Rubel, A., "Computations of Jet Impingement on a Flat Surface", AIAA J., Vol. 18, No. 2, 1980 (to be published) or AIAA Paper No. 73-207.

15. Bower, W.W., Agarwal, R.K., and Peters, G.R., "A Theoretical Study of Two and Three Dimensional Impinging Jets", Presented at Navy Workshop on V/STOL Aerodynamics, Monterey, Calif., May 1979.

16. Kotansky, D.R., Duramlo, N.A., Bristow, D.R., and Saundres, P.W., "Multi-Jet Induced Forces and Moments on VTOL Aircraft Hovering In and Out of Ground Effect", Naval Air Development Center, Report No. NADC-77-229-30, June 1977.

17. Karemaa, A., Smith, C.W., Weber, H.A., and Garner, J.E., "The Aerodynamic and Thermodynamic Characteristics of Fountains and Some Far-Field Temperature Distributions", Office of Naval Research Report No. ONR-CR212-237-1F.

18. Abramovich, G.N., "The Theory of Turbulent Jets", MIT Press, 1963.

19. Giralt, F.G., Chia, C-J., and Trass, O., "Characterization of the Impingement Region in an Axisymmetric Turbulent Jet", Ind. Eng. Chem, Fundam., Vol 16, No. 1, 1977.

20. Hrycak, P., Lee, D.T., Gauntner, J.W., and Livingood, J.N.B., "Experimental Flow Characteristics of a Single Turbulent Jet Impinging on a Flat Plate", NASA TN-D 5690, March 1970.

21. Glauert, M.B., "The Wall Jet", J. Fluid Mech, Vol. 1, (1956) 625-643.